Tunnel stability with special reference to the shear strain energy criterion

Paul N. Michelis

TUNNEL STABILITY

WITH

SPECIAL REFERENCE TO THE

SHEAR STRAIN ENERGY

CRITERION

b y

PAUL N. MICHELIS, B.Sc.

being a thesis presented to the University of Durham in fulfilment of requirements for the degree of M.Sc. by research in Engineering Geology

OCTOBER 1975

ABSTRACT

A comparison of the results of the application of the finite element method and of a modified KIRSCH's solution for the calculation of stress around an unlined tunnel in London Clay is undertaken.

Some conventional methods and the finite element method for the calculation of stress and displacement around a tunnel are referred to.

An estimate of the reduction of the shear strength parameters along fissures is obtained by laboratory tests on fissured and intact samples of London Clay.

On the basis of the MOHR-COULOMB criterion of failure and by the use of a computer technique a delimitation of potentially unstable orientation zones on equal area projections is obtained for all the elements around a tunnel in London Clay.

The shear strain energy stored around the discontinuities, which fall in the potentially unstable zones, is computed for the case of a non-random discontinuity fabric of London Clay and the values are normalized to the values corresponding to an equivalent isotropically discontinuous fabric. Then the instability of each area around the tunnel is defined in terms of the principal stresses σ_1, σ_2, σ_3, the shear strength characteristics of the material and the discontinuity fabric.

CONTENTS

Notation

Most symbols are defined each time they occur, but the following are commonly used

a	tunnel radius
$\hat{C}$	peak values of cohesion
$\hat{C}_d$	peak values of cohesion along discontinuities
C_r	residual values of cohesion
C_{rd}	residual values of cohesion along discontinuities
C_u	uniaxial compressive strength
E	Young's modulus
h	depth of a point or tunnel axis
K	stiffness matrix
K_o	ratio of horizontal and vertical pressure
p_v	rock pressure
r	distance from the centre of a tunnel
T_o	uniaxial tensile strength
u	radial displacement
v	tangential displacement
W_d	shear strain energy generated by a non-random discontinuity fabric
W_{dI}	shear strain energy generated by a random discontinuity fabric
γ	weight per unit of volume
ε	strain
θ	angle between a direction and the horizontal axis
μ	coefficient of friction
ν	Poisson's ratio
σ_1, σ_2, σ_3	principal stresses
σ_h	horizontal stress

σ_r radial stress

σ_t tangential stress

σ_v vertical stress

τ shear stress

$\hat{\phi}$ peak values of friction angle

$\hat{\phi}_d$ peak values of friction angle along discontinuities

ϕ_r residual values of friction angle

ϕ_{rd} residual values of friction angle along discontinuities

ψ angle between σ_1 and the horizontal axis

I. INTRODUCTION

Any study for the design of a tunnel consists mainly on the exploration of geological conditions along and around the proposed line of the tunnel, the subsurface geotechnical exploration, the determination of the original and secondary state of stresses, the determination of the displacement during the construction and, much later , the influence of the discontinuities on the stability of the proposed tunnel, the determination of the stresses in the lining, the interaction of the lining and surrounding ground, the analysis of economical factors and so on.

At first, in this thesis, a brief presentation of the main conventional methods and the finite element method is undertaken for the calculation of stress and displacement around an unlined tunnel. This is followed by the application of a modified KIRSCH(1898) solution and the finite element method to the case of a tunnel in London Clay. The results of the applications are compared.

The emphasis in the consideration of the states of stress is pursued on account of the fact that the disturbance of the stress, during the excavation, is the cause of many phenomena connected with tunnel stability.

However it is mainly the influence of discontinuities on the stability of the tunnel that has been studied.

The discontinuities may reduce the strength of the material, increase the permeability, accelerate the weathering and change the modulii of elasticity.

Generally, the stability of a discontinuous mass depends more directly on the shear strength characteristics of the discontinuities than on the strength of the intact elements.

An estimation of the reduction of the shear strength characteristics along small structural discontinuities, fissures, is obtained by laboratory tests on samples of London Clay.

The stability of a discontinuous mass, under polyaxial stress systems, around a tunnel in London Clay, is considered in the third part of the thesis.

On the basis of MOHR - COULOMB criterion of failure and by the use of a computer a delimitation of potentially unstable orientation zones on equal area projections is obtained. The shear strain energy stored around the discontinuities, which fall in the potentially unstable zones , is computed for the case of a non-random discontinuity fabric of London Clay and the values are normalized to the values corresponding to an equivalent isotropic discontinuity fabric.

In this manner, more and less stable areas around the tunnel are defined in terms of the principal stresses, the shear strength characteristics and the discontinuity fabric.

2. STRESS DISTRIBUTION AND DISPLACEMENT AROUND A TUNNEL. CRITICISM OF RESULTS.

General

When an underground excavation is made, the natural stress situation which exists in the material before any work has been started changes.

The material around the proposed opening must be under compression because of its own weight, the weight of any overburden upon it and the influence of the geological phenomena. Consequently the mass contains elastic energy stored in a latent state. The creation of an underground opening causes the release of potential energy and it is this released energy which exerts pressure upon the lining or contributes to the convergence of the surface of a self-supporting excavation.

N.G.W.COOK (1966) examines the changes in the energy stored in a rock mass during excavation operations for two extreme cases of material behaviour between which the actual behaviour of mass must lie.

The first case is the excavation in a fluid (zero shear stresses) in which stress concentrations cannot exist and the forces across any plane are the same before and after the excavation. In that case the released energy by excavation will be equal to the change in gravitational energy due to the downward movement of the fluid above the excavation. This case probably approximates to the situation of an excavation after an infinitely long time or at great

depths under hydrostatic pressure.

The second case is the excavation in an elastic rock in which the sum of the released energy, of the energy stored in stress concentrations and of the strain energy originally stored in the excavated rock must be equal to the sum of the change in gravitational potential and of the change in the potential of the horizontal stresses. The released energy is equal to the work which could be extracted from the rock mass by controlling the convergence of the surfaces of the excavation from their initial positions.

In both cases the total change in potential energy is the same.

Therefore, when any underground excavation is made, a change in potential energy occurs, strain energy is stored in the surrounding material and excess energy is released. The stress concentrations maintain force equilibrium and produce strain energy stored in the surrounding mass.

It is proposed further to consider these energy components of the mass.

The fundamental assumption on which this thesis is based is that the state of stress around the tunnel does not exceed the limiting stress condition for elastic behaviour of the surrounding mass. This assumption is probably a little unrealistic in view of the high stress differences that must exist at the free boundary, but it is nevertheless a necessary assumption if the analysis is to be reasonably tractable.

2.a. Stress and displacement calculation derived from the equations of theory of elasticity and calculation based on various displacement and equilibrium assumptions.

Stress and displacement calculation derived from the equations of theory of elasticity.

(Circular tunnel in an elastic infinite and semi-infinite mass).

Any elastic material must satisfy the following requirements:

i)Linearity between stress and strain.

ii)Homogeneity

iii)Isotropy

iv)Perfect elasticity

These properties are defined by two independent constants,the modulus of elasticity E and Poisson's ratio ν.

The theoretical equations specifying the stress distribution are extracted by the acceptance of plane stress or plane strain conditions.

For simplicity the problem will be discussed in polar coordinates.

L.OBERT and W.DUVALL (I967) adopt a theoretical approach to the problem.They consider an infinite plate of thickness t with a circular hole of radius a.The applied

stress field at infinity is S_x, S_z as illustrated in figure 2.a.I. and it is assumed that the AIRY stress function ϕ_o is of the form:

$$\phi_o = A \log r + Br^2 + (Cr^2 + Dr^4 + E'r^{-2} + F)\cos 2\theta \qquad \text{equ2.a.I}$$

For the conditions of no body forces the stress components are:

$$\sigma_r = \frac{\partial \phi_o}{r \partial r} + \frac{\partial^2 \phi_o}{r^2 \partial \theta^2}$$

$$\sigma_t = \frac{\partial^2 \phi_o}{\partial r^2} \qquad \text{equs. 2.a.2}$$

$$\tau_{r\theta} = \frac{\partial \phi_o}{r^2 \partial \varphi_o} - \frac{\partial^2 \phi_o}{r \partial r \partial \theta}$$

where σ_r = radial stress, σ_t = tangential stress, $\tau_{r\theta}$ = shear stress.

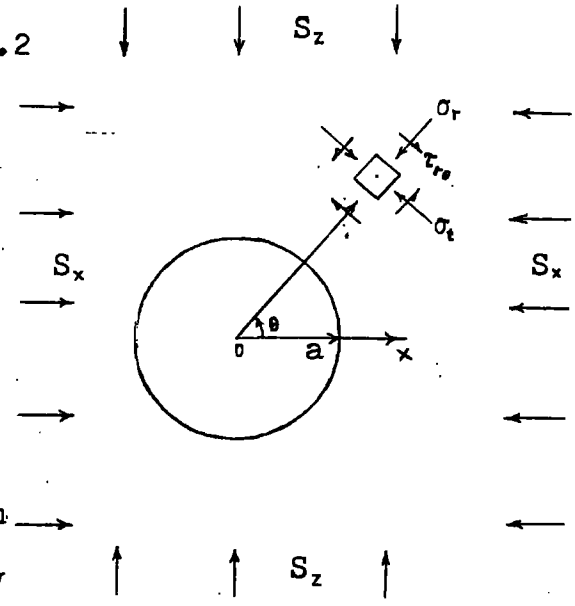

Fig. 2.a.1

Now the constants A, B, C, D, E', F have to be determined from the boundary conditions. By the use of the known stress transformation correlation equations the boundary conditions at $r = \infty$ are

$$(\sigma_r)_{r=\infty} = \frac{1}{2}(S_x + S_z) + \frac{1}{2}(S_x - S_z)\cos 2\theta$$

$$(\tau_{r\theta})_{r=\infty} = -\frac{1}{2}(S_x - S_z)\sin 2\theta \qquad \text{equs. 2.a.3}$$

Substitution of equation 2.a.1 into equation 2.a.2 and calculation of the partial derivatives gives

$$\sigma_r = \frac{\partial \phi_o}{r \partial r} + \frac{\partial^2 \phi_o}{r^2 \partial \theta^2} = \frac{A}{r^2} + 2B + (-2C - 6E'r^{-4} - 4Fr^{-2})\cos 2\theta$$

$$\sigma_t = \frac{\partial^2 \phi_o}{\partial r^2} = -\frac{A}{r^2} + 2B + (2C + 12Dr^2 + 6E'r^{-4})\cos 2\theta \qquad \text{equs. 2.a.4}$$

$$\tau_{r\theta} = \frac{\partial \phi_o}{r^2 \partial \theta} - \frac{\partial^2 \phi_o}{r \partial r \partial \theta} = (2C + 6Dr^2 - 6E'r^{-4} - 2Fr^{-2})\sin 2\theta$$

When r =∞, equations 2.a.3 and 2.a.4 give

$$(\sigma_r)_{r=\infty} = \frac{1}{2}(S_x + S_z) + \frac{1}{2}(S_x - S_z)\cos 2\theta = 2B - 2C\cos 2\theta$$

$$(\tau_{r\theta})_{r=\infty} = -\frac{1}{2}(S_x - S_z)\sin 2\theta = \left[2C + 6D(\infty)^2\right]\sin 2\theta \qquad \text{equs.2.a.5}$$

Consequently,

$$D = 0$$

$$-2C = \frac{1}{2}(S_x - S_z) \qquad \text{equs.2.a.6}$$

$$2B = \frac{1}{2}(S_x + S_z)$$

When r = a,

$$(\sigma_r)_{r=a} = 0, \quad (\tau_{r\theta})_{r=a} = 0 \qquad \text{equs.2.a.7}$$

When r=a, equations 2.a.4 and 2.a.7 give

$$(\sigma_r)_{r=a} = \frac{A}{a^2} + 2B + (-2C - 6Ea^{-4} - 4Fa^{-2})\cos 2\theta = 0$$

$$(\tau_{r\theta})_{r=a} = (2C + 6Da^2 - 6Ea^{-4} - 2Fa^{-2})\sin 2\theta = 0 \qquad \text{equs.2.a.8}$$

Consequently

$$\frac{A}{a^2} + 2B = 0$$

$$-2C - 6Ea^{-4} - 4Fa^{-2} = 0 \qquad \text{equs.2.a.9}$$

$$2C - 6Ea^{-4} - 2Fa^{-2} = 0$$

Solving the equations 2.a.6 and 2.a.9, the constants are determined and by substitution into 2.a.4 the solution is obtained (after G.KIRSCH):

$$\sigma_r = \frac{1}{2}(S_x + S_z)\left(1 - \frac{a^2}{r^2}\right) + \frac{1}{2}(S_x - S_z)\left(1 + \frac{3a^4}{r^4} - \frac{4a^2}{r^2}\right)\cos 2\theta \qquad \text{equ.2.a.10}$$

$$\sigma_t = \frac{1}{2}(S_x + S_z)\left(1 + \frac{a^2}{r^2}\right) - \frac{1}{2}(S_x - S_z)\left(1 + \frac{3a^4}{r^4}\right)\cos 2\theta \qquad \text{equ.2.a.11}$$

$$\tau_{r\theta} = -\frac{1}{2}(S_x - S_z)\left(1 - \frac{3a^4}{r^4} + \frac{2a^2}{r^2}\right)\sin 2\theta \qquad \text{equ.2.a.12}$$

In the case where $S_x = S_z = -p$, σ_r, σ_t and $\tau_{r\theta}$ become

$$\sigma_r = -p\left(1 - \frac{a^2}{r^2}\right)$$

$$\sigma_t = -p\left(1 + \frac{a^2}{r^2}\right) \qquad \text{equ.2.a.13}$$

$$\tau_{r\theta} = 0$$

When $S_x=0$ then σ_r, σ_t, $\tau_{r\theta}$ become

$$\sigma_r = \frac{S_z}{2}\left(1 - \frac{a^2}{r^2}\right) - \frac{S_z}{2}\left(1 + \frac{3a^4}{r^4} - \frac{4a^2}{r^2}\right)\cos 2\theta$$

$$\sigma_t = \frac{S_z}{2}\left(1 + \frac{a^2}{r^2}\right) + \frac{S_z}{2}\left(1 + \frac{3a^4}{r^4}\right)\cos 2\theta \qquad \text{equs.2.a.14}$$

$$\tau_{r\theta} = \frac{S_z}{2}\left(1 - \frac{3a^4}{r^4} + \frac{2a^2}{r^2}\right)\sin 2\theta$$

From the equations 2.a.I0, 2.a.II , 2.a.I2 we have that the radial stress is zero at the tunnel surface while the tangential stress is a maximum and the shear stress is zero.

The DISPLACEMENTS are obtained by the relationships between stress and displacement for plane stress or plane strain.

For a plane stress condition the relative equations are

$$\frac{\partial u}{\partial r} = \frac{1}{E}(\sigma_r - \nu\sigma_t) \qquad \text{equ.2.a.I5}$$

$$\frac{u}{r} + \frac{\partial u}{r\partial\theta} = \frac{1}{E}(\sigma_t - \nu\sigma_r) \qquad \text{equ.2.a.I6}$$

$$\frac{1}{r}\frac{\partial u}{\partial\theta} + \frac{\partial v}{\partial r} - \frac{v}{r} = \frac{2(1+\nu)}{E}\tau_{r\theta} \qquad \text{equ.2.a.I7}$$

where u= radial displacement

v = tangential displacement

ν = Poisson's ratio

By substitution of the equations 2.a.I0, 2.a.II, 2.a.I2 into equations 2.a.I5 , 2.a.I6 , 2.a.I7 and by integration the displacements are

$$u = \frac{1}{E}\left[\left(\frac{S_x+S_z}{2}\right)\left(r + \frac{a^2}{r}\right) + \left(\frac{S_x-S_z}{2}\right)\left(r - \frac{a^4}{r^3} + \frac{4a^2}{r}\right)\cos 2\theta\right] -$$

$$- \frac{\nu}{E}\left[\left(\frac{S_x+S_z}{2}\right)\left(r - \frac{a^2}{r}\right) - \left(\frac{S_x-S_z}{2}\right)\left(r - \frac{a^4}{r^3}\right)\cos 2\theta\right] \qquad \text{equ.2.a.I8}$$

$$v = \frac{1}{E}\left[-\left(\frac{S_x-S_z}{2}\right)\left(r + \frac{2a^2}{r} + \frac{a^4}{r^3}\right)\sin 2\theta\right] - \frac{\nu}{E}\left[\left(\frac{S_x-S_z}{2}\right)\left(r - \frac{2a^2}{r} + \frac{a^4}{r^3}\right)\sin 2\theta\right]$$

equ.2.a.I9

For a plane strain condition, the stress displacement equations are

$$\frac{\partial u}{\partial r} = \frac{1}{E}\left[(1-\nu^2)\sigma_r - \nu(1+\nu)\sigma_t\right]$$

$$\frac{u}{r} + \frac{\partial v}{r\partial\theta} = \frac{1}{E}\left[(1-\nu^2)\sigma_t - \nu(1+\nu)\sigma_r\right] \qquad \text{equ. 2.a.20}$$

$$\frac{\partial u}{r\partial\theta} + \frac{\partial v}{\partial r} - \frac{v}{r} = \frac{2(1-\nu)}{E}\tau_{r\theta}$$

Again by substitution of the equations 2.a.10, 2.a.11, 2.a.12 into equations 2.a.20 and by integration, the displacement are given

$$u = \frac{1-\nu^2}{E}\left[\left(\frac{S_x+S_z}{2}\right)\left(r+\frac{a^2}{r}\right) + \left(\frac{S_x-S_z}{2}\right)\left(r-\frac{a^4}{r^3}+\frac{4a^2}{r}\right)\cos 2\theta\right] -$$

$$-\frac{\nu(1+\nu)}{E}\left[\left(\frac{S_x+S_z}{2}\right)\left(r-\frac{a^2}{r}\right) - \left(\frac{S_x-S_z}{2}\right)\left(r-\frac{a^4}{r^3}\right)\cos 2\theta\right] \qquad \text{equ. 2.a.21}$$

$$v = \frac{1-\nu^2}{E}\left[-\left(\frac{S_x-S_z}{2}\right)\left(r+\frac{2a^2}{r}+\frac{a^4}{r^3}\right)\sin 2\theta\right] - \frac{\nu(1+\nu)}{E}\left(\frac{S_x-S_z}{2}\right)\left(r-\frac{2a^2}{r}+\frac{a^4}{r^3}\right)\sin 2\theta \qquad \text{equ. 2.a.22}$$

The calculation of the stresses for the case of Fleet Line Tunnel in London Clay-a subject of the present work- has been based on the above equations and will be discussed later.

R.MINDLIN (1940) succeeded in an important contribution to the solution of the problem by considering a tunnel as a horizontal cylindrical hole of circular cross-section situated in a semi-infinite elastic solid under the action of gravity.

By making use of the elasticity equations he has managed to obtain such a solution as to satisfy the boundary conditions at both the upper free surface of the solid and the surface of the hole. It is assumed that the solid has a uniform weight per unit of volume, γ, (constant body force) and the length of the tunnel is large in comparison with its diameter (Figure 2.a.2).

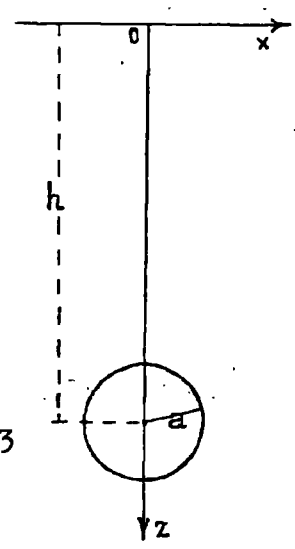

Fig.2.a.2

If the body-force potential is Ω and the AIRY's stress function Φ_0, then in rectangular co-ordinates the stresses σ_x, σ_z τ_{xz} are given by the equations

$$\sigma_x = \frac{\partial^2 \Phi_0}{\partial z^2} + \Omega, \qquad \sigma_z = \frac{\partial^2 \Phi_0}{\partial x^2} + \Omega, \qquad \tau_{xz} = -\frac{\partial^2 \Phi}{\partial x \partial z}$$

equ.2.a.23

If the components of the body force per unit of volume are X, Z then they must be

$$X = -\frac{\partial \Omega}{\partial x}, \qquad Z = -\frac{\partial \Omega}{\partial z} \qquad \text{equ.2.a.24}$$

$$\nabla^4 \Phi_0 = -\frac{1-2\nu}{1-\nu} \nabla^2 \Omega \qquad (\nabla = \text{Laplace's operator}) \qquad \text{equ. 2.a.25}$$

In the present case X=0, and from 2.a.24 $\Omega = -\gamma z$ and so $\nabla^2 \Omega = 0$. Therefore from 2.a.25, $\nabla^4 \Phi_0 = 0$ equ.2.a.26

The problem then is of finding a solution to equation 2.a.26 which satisfies four boundary conditions.

The solution is in terms of curvilinear or bipolar coordinates. In the system of bipolar coordinates, a' and b are related to the Cartesian x and z as follows

$$x = \frac{A \sin b}{\cosh a' - \cos b}, \qquad z = \frac{A \sinh a'}{\cosh a' - \cos b} \qquad \text{equs.2.a.27}$$

where $A = h\tanh a_1 = a' \sinh a_1$, $\frac{h}{a'} = \cosh a_1$

a_1 = the value of a' corresponding to the boundary of the tunnel

Long before the boring of the tunnel three initial states are assumed to exist.

Case I Each element of the material is under a state of isotropic pressure. Therefore at depth z the vertical pressure σ_v and the horizontal σ_h are: $\sigma_v = \gamma z$, $\sigma_h = \gamma z$. That state is approached at great depths. The tangential stress σ_t on the boundary is given by the equation

$$(\sigma_t)_{a'=a_1} = \frac{2\gamma A(\cosh a_1 - \cos b)}{\sinh a_1}\left[\frac{1-\cos a_1 \cos b}{(\cosh a_1 - \cos b)^2} - \coth a_1 - \right.$$

$$\left. - \frac{(7-8\nu)\cos b}{4(1-\nu)\sinh a_1} + 2e^{-a_1}\cos b - \sum_{n=2}^{\infty} R_n \cos nb\right] \qquad \text{equ.2.a.28}$$

where $R_n = N_n - ne^{-na_1}$

$$N_n = \frac{ne^{-na_1}(\sinh na_1 \cosh a_1 - n\sinh a_1 \cosh na_1)}{\sinh^2 na_1 - n^2 \sinh^2 a_1}$$

The stress on the boundary of the tunnel is greatest at the lowest point of the tunnel cross-section except when a_1 is very small.

Case II The material is restrained from lateral displacement into a gravitational field. Again at depth z $\sigma_v = \gamma z$, $\sigma_h = \frac{\nu}{1-\nu} z$

$$(\sigma_t)_{a'=a_1} = \frac{2\gamma A(\cosh a_1 - \cos b)}{\sinh a_1}\left[\frac{1-\cosh a_1 \cos b}{(\cosh a_1 - \cos b)^2} - \coth a_1 - \right.$$

$$\left. - \frac{(7-8\nu)\cos b}{4(1-\nu)\sinh a_1} + 2e^{-a_1}\cos b - \sum_{n=2}^{\infty} R_n \cos nb\right] + \gamma G' A(\cosh a_1 -$$

$$- \cos b)\left[6\coth a_1 \operatorname{csch} a_1 + 6\operatorname{csch}^2 a_1 \cos b + 4\sinh a_1 \sum_{n=2}^{\infty} T_n \cos nb\right] +$$

$$6\gamma G' A \operatorname{csch} a_1 (\cos\psi' + 2\cosh a_1 \cos 2\psi' + \cos 3\psi') \qquad \text{equ.2.a.29}$$

where

$$T_n = S_n - 2n(n^2-1)e^{-na_1}$$

$$S_n = \frac{n(n^2-1)\sinh na_1}{\sinh^2 na_1 - n^2\sinh^2 a_1}, \qquad \psi' = \sin^{-1}\frac{\sinh a_1 \sin b}{\cosh a_1 - \cos b}$$

$$G' = \frac{1-2\nu}{6(1-\nu)}$$

In that case, a significant change occurs in the stress field with a variation of Poisson's ratio.

Case III No lateral stress exists in the material. Again at depth z,

$$\sigma_v = \gamma z, \quad \sigma_h = 0$$

The tangential stress $(\sigma_t)_{a=a_1}$ is equal to the case II where $G' = \frac{1}{6}$.

K. TERZAGHI and F.RICHARD (1952) obtained a calculation of the tangential stress at the roof and at the walls of an unlined tunnel, circular cross section, situated in an elastic mass with a two-dimensional stress field.

It is also assumed that the depth of the tunnel is large compared to its diameter.

According to SAINT VENANT's principle "if a system of forces acting on one portion of the boundary is replaced by a statically equivalent system of forces, acting on the

same portion of the boundary,the stresses,strains and nonrigid body displacements remain approximately the same in the parts of the body sufficiently far moved from this portion of the boundary".The authors basing themselves upon this principle admit that the significant changes in the state of stress generated by the boring of tunnel do not extend beyond a distance equal to two or three times the largest dimension of the cross-section of a tunnel.

If now the above mentioned distance is relatively small as compared to the depth(h) of the centre of the tunnel,can be assumed (without serious error) that the initial state of stress in the material located inside the entire zone where the tunnel has an influence on the state of stress,is indentical with the initial state of stress at the centre of the tunnel itself.

A two-dimensional stress field is developed as follows.Long before the excavation of the tunnel at any depth z below the horizontal surface of the mass, the vertical gravity stress is $\sigma_v = z\gamma$.

The expansion of above mass in the horizontal direction is prevented by the resistance of the adjacent mass while horizontal forces of tectonic origin may act upon the mass tending to compress the rock in horizontal directions. Consequently a horizontal stress exists and is given by the equation $\sigma_h = K_o z\gamma$ equ.2.a.30

The tangential stress σ_t at the roof (point C) is (Figure 2.a.3) $\sigma_t = \sigma_v(3K_o - 1)$ equ.2.a.3I

The tangential stress at the walls (at point A) is

$$\sigma_t = \sigma_v (3 - K_o) \quad \text{equ.2.a.32}$$

(for $K_o = 1$ the tangential stresses are equal to two times the vertical stress).

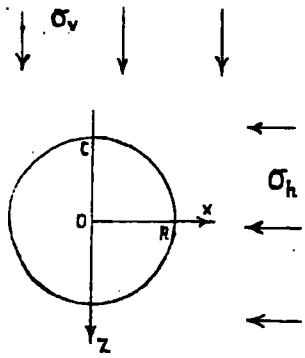

Fig.2.a.3

As a result of the above equations the state of stress in the mass around a tunnel depends to a large extent on the ratio K_o (Figure 2.a.4) which depends on the geological origin and the subsequent history of the mass formation.

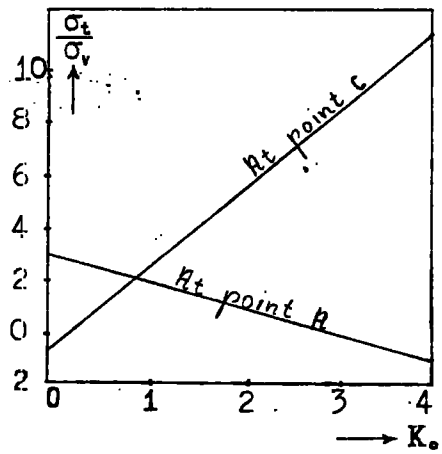

Fig. 2.a.4

Stress and displacement calculation based on various displacement and equilibrium assumptions.

In the foregoing exposition only a theoretical approach to the problem of the calculation of the stress and displacement around an unlined circular cross-section tunnel was undertaken with the assumption that the material under consideration is an elastic material, that plane stress or plane strain conditions prevailed, and that the calculations are based upon a theoretically infinite time.

In fact the geologic materials are not elastic and no true plane stress or plane strain conditions exist.

The formations in nature are affected by the weight of the overlying strata,by their own weight and by the forces generated from the geological phenomena.These forces act as a uniformly distributed load on the deeper strata and consequently on the roof of the opening which probably permits the confined mass to move downwards in the form of "plastic flow" or "rock bursts" (popping).In that way, a reduction in the state of stress very close to the tunnel occurs and usually secondary discontinuities are generated.

The displacements are elastic if the elastic limit of the mass is not exceeded by the residual stresses.When the excavation begins,the ratio between the major and the minor principal stress increases in the adjacent rock and the new state of stress depends on the shape and the dimensions of the tunnel,the initial state of stress in the rock ,the natural properties of the mass,the strength and

various other factors.If the mass is too weak to sustain the modified state of stress it starts to move from the roof and walls in a radial direction and to develop a looseness zone (protective zone)until the state of stress becomes compatible with the strength.The creation of such a zone is of fundamental importance in tunnelling and the time required for its development depends on the nature of the rock,the magnitude and depth of tunnel and the rigidity and installation time of supports.The purpose of the lining is to sustain that protective zone and not to prevent the primary displacements which is impossible for tunnels at great depths.

Rock pressure (according K.TERZAGHI) is the weight of a rock mass of a certain height above the tunnel,which, when left unsupported would gradually drop out of the roof. The magnitude of the rock pressure which acts upon the tunnel lining after the development of the protective zone varies between full geostatic pressure and zero in very solid and strong rocks.According to RABCEWICZ (I944) the reasons for the development of rock pressure are the loosening of the rock mass,the weight of the overlying rock mass, the tectonic forces,the volume expansion of the rock mass and swelling due to physical or chemical action.

Some known theories which present the above phenomena and calculate the rock pressure will be discussed.

K.TERZAGHI (I946) developed a theory for dry, granular soils at moderate overburden depths ($h_1 \leq 3B$)only.

The mass around the tunnel begins to move and the displacements lead to the development of a set of sliding planes which define the width B of the affected displacement mass.The inclination of the sliding planes are $45° + \frac{\varphi}{2}$ (active state).The width B is given as

$$B = 2\left[\frac{b}{2} + h' \tan\left(45° - \frac{\varphi}{2}\right)\right] \qquad \text{equ. 2.a.33}$$

The displacements are counteracted by friction developing on the vertical shear planes.

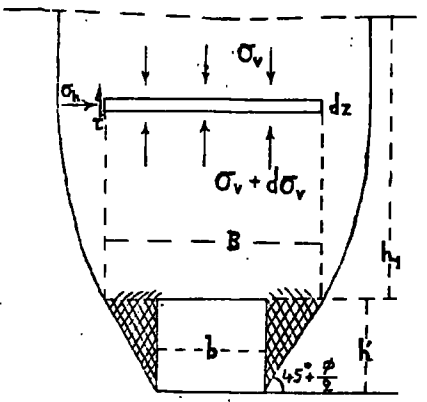

Fig. 2.a.5

By the study of the equilibrium on the prism of width B and height dz the rock pressure p_u for cohesionless soils is derived

$$p_u = \frac{B\gamma}{2K_o \tan\varphi}\left(1 - e^{-K_o \tan\varphi \frac{2h_1}{B}}\right) \qquad \text{equ. 2.a.34}$$

The displacements of the lower layers did not affect stress conditions in the upper layers in the case of heights greater than 2.5B and furthermore in the case of very great depths the rock pressure is totally unaffected by overburden depth.

$$p_{u_{max}} = \frac{B\gamma}{2K_o \tan\varphi} \qquad \text{equ.2.a.35}$$

For the cohesive soils (cohesion C)the rock pressure is

$$p_u = \frac{B(\gamma - \frac{2c}{B})}{2K_o \tan\varphi}\left(1 - e^{-K_o \tan\varphi \frac{2h_1}{B}}\right) \qquad \text{equ.2.a.36}$$

For $\gamma = \frac{2c}{B}$ $p_u = 0$ and where $B \geq \frac{2c}{\gamma}$ the cavity must be supported.

PROTODYAKONOV (1958) developed a theory for granular materials assuming the development of an arch ACB above the tunnel at which the stresses along it are purely compressive and are not associated with bending.

The arch ACB is a parabolic line and its equilibrium is investigated. The forces acting on any section DC of the arch are the horizontal resultant T of reactions acting from the right at the crown M, the resultant P of vertical pressures, the tangential reaction R' at point D of forces acting from the left on the lower half of the arch. By using the equation of the parabola taking the moment about D and the pressures at the point A, we obtain as a result that the load acting on the tunnel is equal to the weight of the rock mass confined within the parabola and thus the pressure is equal to

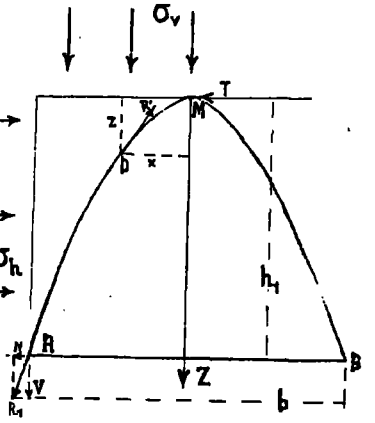

Fig. 2.a.6

$$P_v = \frac{1}{3}\gamma\frac{b^2}{\tan\varphi} \qquad \text{equ. 2.a.37}$$

For cohesive soils the pressure is given as

$$P_v = \frac{1}{3}\gamma\frac{b^2}{\tan\varphi+\frac{c}{c_u}} \qquad \text{equ. 2.a.38}$$

where $\tan\varphi+\frac{c}{c_u}$ is the strength coefficient, C_u is the unconfined compressive strength.

According to K. SZECHY (1967) this theory gives satisfactory results at depths from $\frac{b}{2\tan\varphi}$ to $\frac{b}{\tan\varphi}$ and it has two disadvantages: i) from the equations of this theory results that the height of the arch is a linear function of width ($h_1=\frac{b}{2\tan\varphi}$) although this relation should be more involved. 2) the determination of the strength coefficient, by the use of empirical values is not accurate.

K.SZÉCHY (I967)determined the height of the over-break of a rock mass,its shape and the loading upon the lining,assuming that the tensile strength will define the over-break above a rectangular cavity.

Basing himself upon a statical analogy he makes the assumption that a three hinged arch is developed whose two lower sidewards, mutually supported hinges (R_A, R_B) transmit compression stresses while its third uppermost hinge is developed in the centre line at such a height where the stresses set up by the overbridging no longer exceed the strength of the rock material.

Figure 2.a.7 shows in a cross-section the redistribution of the stresses,the lower hinges pressed by compressive stresses and the interior mass pulled by a tensile stress. The maximum tensile stress at the bottom of this cross-section should be equal to the tensile strength of the mass.From the assumption that this mass acts as a quadrangular disc-like beam K. SZECHY was able to determine the height h_1 as

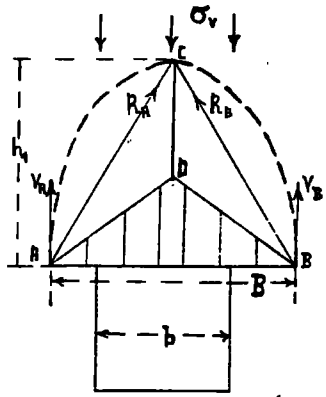

Fig.2.a.7

$$h_1 = \left[1.3I\left(1 + \frac{d}{2}\right)^2 - 0.39\right] b \qquad \text{equ.2.a.39}$$

where the factor d takes values between $\frac{1}{2}$ and $\frac{1}{3}$ for plastic materials and between 2 and 3 for elastic ones.

The width B is given by WILLMANN as

$$B = b\left(1 + \frac{d}{2}\right) \qquad \text{equ.2.a.40}$$

The rock pressure acting upon the unsupported tunnel is the weight of the triangular zone defined by the three-hinged arch.

As a result of the installation of a support system there is a reduction of the height and width of the triangular zone and correspondingly of the intensity of rock pressure.

2.b. Stress and displacement calculation derived from the finite element method

The finite element method is essentially a process through which a continuum with infinite degrees of freedom can be approximated by an assemblage of subregions (or elements) each with a specified but finite number of unknowns (ZIENKIEWICZ, 1971).

In an elastic continuum the number of interconnection joints is infinite but the concept of the above method accepts a division of the continuous medium into elements interconnected only at a finite number of nodal points. Consequently the approximation employed in the finite element method is the substitution of the actual continuum by a modified structural system.

The term "finite element method" was first introduced by GLOUGH (1960) who used triangular and rectangular elements to solve plane strain, plane stress and axially symmetric problems.

J. ARGYRIS (1958, 1960, 1965) has done pioneering work in matrix analysis of three-dimensional isotropic and anisotropic, continua and discontinuous media.

O. ZIENKIEWICZ (1971) has studied extensively the application of the finite element method in many engineering problems involved with the calculation of stress, strain and strain energy in shells, bridges, dams, etc.

The finite element method has the ability to deal with complex geometries, boundary conditions and material properties and can be used as an excellent numerical tool

in the solution of a wide variety of problems dealing with soil and rock mechanics.

It is recognised that such a finite element method is a generalized RITZ method based on the principle of virtual work.

The type of element depends on the geometry of the boundaries, while the size, and consequently the number of elements, depends on the scale of stress gradients. Among the simple type available, the three noded triangular element is a popular choice for plane strain and plane stress problems.

The general procedure in this method contains the following steps:

i) structural idealization;

ii) evaluation of the element properties;

iii) structural analysis of the element assemblage.

There are three categories of models in the finite element technique: Displacement models, equilibrium models and mixed models.

The displacement model is based on parametric displacement fields and must satisfy the conditions

i) Equilibrium: At each nodal point the internal element forces must equilibrate the external forces;

ii) Compatibility: The deformation of adjacent elements must be compatible;

iii) Force -- deflection relationship: The relation between internal forces and displacements in each element depends upon its individual geometry and

material characteristics.

In this model the displacements of the nodal points are the basic unknown parameters. Also, a function is chosen to define uniquely the state of displacement within each element in terms of its nodal displacement. From this function a new function results which defines uniquely the state of strain within an element in terms of the nodal displacement. This state of strain together with any initial strains and the elastic properties of the material, defines the state of stress throughout the element.

The following brief analysis deals with the displacement model and can be readily applied in soil and rock mechanics problems.

The fundamental aspect of finite element numerical theory is that the finite element procedure represents a process in which the total energy of the system is minimised with respect to nodal displacements. This means that as the imposed displacement functions are an approximation of the true displacement functions, the potential energy is then either equal to or greater than that corresponding to the true equilibrium state.

The following convergence criteria are based upon the above requirement:

i) The deformation of each element is expected to be similar to that developed in the corresponding region of the continuum;

ii) The displacement function has to be of such a form that if nodal displacements are compatible with a constant strain condition, such constant strain

will in fact be obtained;

iii) The strains at an inerface between elements must be finite and the displacement functions are thus selected accordingly.

In the finite element method and in the case of elastic behaviour of an element the characteristic force-displacement relationship is

$$\{F\}^e = [K]\{\delta\}^e + \{F\}_p^e + \{F\}_{e0}^e \qquad \text{equ. 2.b.I}$$

where

$\{F\}^e$ represents the total nodal forces;

$[K]$ " the element stiffness matrix;

$\{\delta\}^e$ " the nodal displacements;

$\{F\}_p^e$ " the nodal forces required to balance any distributed loads acting on the element;

$\{F\}_{e0}^e$ represents the nodal forces required to balance any initial strains.

When, in the application of the finite element method, this stage has been reached, the solution procedure follows a standard structural routine.

The main efforts involved in the development of the above relationship, as well as in all the solution procedure, are embodied in the development of the stiffness matrix.

The solution procedure consists throughout the following operations.

i) Development of a stiffness matrix of an arbitrary element with respect to a convenient local coordinate system;

ii) Development of a transformation matrix (constraint matrix)for the transformation of the stiffness matrix from the local coordinate system to a generalized coordinate system (global coordinates);

iii) Generation of the final stiffness matrix for the entire assemblage,incorporating the boundary forces and deflections;

iv) Solution of a system of simultaneous equations,which we can substitute by a block tridiagonal matrix equation.

The stiffness coefficient is an elastic constant relating the force acting at point i on a body and the displacement caused by the force itself:

$$F_i = K_{ij}^{\lambda w} \delta_i \qquad \text{equ. 2.b.2}$$

where F_i is the force required at i in the λ direction to support a unit displacement at j in the w direction.

The stiffness matrix of an element is the whole of the stiffness coefficients of the element,each of them corresponding to a nodal force.

Briefly,the theoretical process of the finite element method in plane strain used in the calculation of stress and displacement around the Fleet Line Tunnel,London Transport, has the following characteristics:

In plane strain conditions and in rectangular coordinates the stress and strain tensors are

stress tensor

$$\begin{vmatrix} \sigma_x & \tau_{xz} & 0 \\ \tau_{zx} & \sigma_z & 0 \\ 0 & 0 & \sigma_y \end{vmatrix}$$

strain tensor

$$\begin{vmatrix} \varepsilon_x & \gamma_{xz} & 0 \\ \gamma_{zx} & \varepsilon_z & 0 \\ 0 & 0 & 0 \end{vmatrix}$$

Under the above conditions, and in linearly elasticity problems, the following stress-strain relationships are valid

$$\varepsilon_x = \frac{1}{E}\left[\sigma_x - \nu(\sigma_z + \sigma_y)\right]$$

$$\varepsilon_z = \frac{1}{E}\left[\sigma_z - \nu(\sigma_x + \sigma_y)\right] \qquad \text{equs. 2.b.3}$$

$$\varepsilon_y = \frac{1}{E}\left[\sigma_y - \nu(\sigma_z + \sigma_x)\right] = 0$$

$$\gamma_{xz} = \frac{\tau_{xz}}{G}$$

from $\varepsilon_y = 0$ and equs.2.b.3 result: $\sigma_y = \nu(\sigma_z + \sigma_x)$ equ.2.b.4

in matrix notation we have

$$\begin{Bmatrix} \varepsilon_x \\ \varepsilon_z \\ \gamma_{xz} \end{Bmatrix} = \frac{1+\nu}{E}\begin{bmatrix} 1-\nu & -\nu & 0 \\ -\nu & 1-\nu & 0 \\ 0 & 0 & \frac{E^2}{2(1+\nu^2)} \end{bmatrix}\begin{Bmatrix} \sigma_x \\ \sigma_z \\ \tau_{xz} \end{Bmatrix} \qquad \text{equs.2.b.5}$$

Now a triangular element ABC (Figure 2.b.I) is considered to be referred to its own coordinate system. In this element the internal displacements must vary linearly in two perpendicular directions. This means that any straight line in the undeformed element will remain straight during deformation.

Let us assume that the compatible displacements at any point (x, z) within the element are of the form:

$$\{f\} = [N]\{\delta\}^e \qquad \text{equ.2.b.6}$$

and

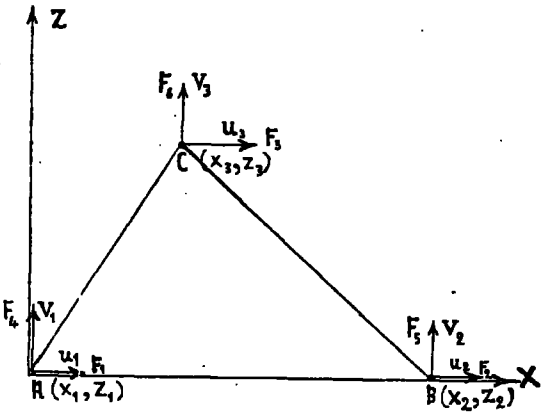

Fig. 2.b.I

$$\left.\begin{aligned} u &= a_1 + a_2 x + a_3 z \\ v &= a_4 + a_5 x + a_6 z \end{aligned}\right\}$$

where $[N]$ is a function of position, $a_1, a_2, \ldots, a_6$ are coefficients equal in number to the number of independent

nodal point displacement components, and $\{\delta\}^e$ is the nodal displacements of the element. Then the nodal displacements of the element are:

$$\left.\begin{aligned} u_1 &= a_1 \\ u_2 &= a_1 + a_2 x_2 \\ u_3 &= a_1 + a_2 x_3 + a_3 z_3 \\ v_1 &= a_4 \\ v_2 &= a_4 + a_5 x_2 \\ v_3 &= a_4 + a_5 x_3 + a_6 z_3 \end{aligned}\right\} \qquad \text{equs. 2.b.7}$$

In matrix notation equations 2.b.7 become

$$\begin{Bmatrix} u_1 \\ u_2 \\ u_3 \\ v_1 \\ v_2 \\ v_3 \end{Bmatrix} = \begin{bmatrix} 1 & & & & & \\ 1 & x_2 & & & & \\ 1 & x_3 & z_3 & & & \\ & & & 1 & & \\ & & & 1 & x_2 & \\ & & & 1 & x_3 & z_3 \end{bmatrix} \begin{Bmatrix} a_1 \\ a_2 \\ a_3 \\ a_4 \\ a_5 \\ a_6 \end{Bmatrix} \qquad \text{equs.2.b.8}$$

or $\{\delta\}^e = [A]\{a\}$. Solving with respect to $\{a\}$,

$$\{a\} = [A]^{-1}\{\delta\}^e \qquad \text{equ.2.b.9}$$

where $[A]^{-1}$ is the inverse of $[A]$. Consequently, if the nodal displacements are known, the $\{a\}$ can be determined.

By definition the strains are related to displacements as follows

$$\begin{Bmatrix} \varepsilon_x \\ \varepsilon_z \\ \gamma_{xz} \end{Bmatrix} = \begin{Bmatrix} \partial u/\partial x \\ \partial v/\partial z \\ \dfrac{\partial u}{\partial z} + \dfrac{\partial z}{\partial x} \end{Bmatrix} \qquad \text{equs. 2.b.10}$$

Differentiating equations 2.b.8 we get

$$\begin{Bmatrix} \varepsilon_x \\ \varepsilon_z \\ \gamma_{xz} \end{Bmatrix} = \begin{Bmatrix} a_2 \\ a_6 \\ a_3+a_5 \end{Bmatrix} = \begin{bmatrix} 0 & 1 & 0 & 0 & 0 & 0 \\ 0 & 0 & 0 & 0 & 0 & 1 \\ 0 & 0 & 1 & 0 & 1 & 0 \end{bmatrix} \begin{Bmatrix} a_1 \\ a_2 \\ a_3 \\ a_4 \\ a_5 \\ a_6 \end{Bmatrix} \qquad \text{equs.2.b.II}$$

or

$$\{\varepsilon\} = [B]\{\delta\}^e \qquad \text{equ. 2.b.I2}$$

Substituting $\{a\}$ from equations 2.b.9 , 2.b.II becomes

$$\begin{Bmatrix} \varepsilon_x \\ \varepsilon_z \\ \gamma_{xz} \end{Bmatrix} = \frac{1}{x_2 z_3} \begin{bmatrix} -z_3 & z_3 & 0 & 0 & 0 & 0 \\ 0 & 0 & 0 & x_3-x_2 & -x_3 & x_2 \\ x_3-x_2 & -x_3 & x_2 & -z_3 & z_3 & 0 \end{bmatrix} \begin{Bmatrix} u_1 \\ u_2 \\ u_3 \\ v_1 \\ v_2 \\ v_3 \end{Bmatrix} \qquad \text{equ. 2.b.I3}$$

From equations 2.b.5 we obtain

$$\begin{Bmatrix} \sigma_x \\ \sigma_z \\ \tau_{xz} \end{Bmatrix} = \frac{E(1-\nu)}{(1+\nu)(1-2\nu)} \begin{bmatrix} 1 & \frac{\nu}{1-\nu} & 0 \\ \frac{\nu}{1-\nu} & 1 & 0 \\ 0 & 0 & \frac{1-2\nu}{1(1-\nu)} \end{bmatrix} \begin{Bmatrix} \varepsilon_x \\ \varepsilon_z \\ \tau_{xz} \end{Bmatrix} \qquad \text{equs.2.b.I4}$$

or

$$\{\sigma\} = [D]\{\varepsilon\} \qquad \text{equ. 2.b.I5}$$

The matrix [D] is called elasticity matrix.

From equations 2.b.I4 and 2.b.I3 we obtain the stresses in the element

$$\begin{Bmatrix} \sigma_x \\ \sigma_z \\ \tau_{xz} \end{Bmatrix} = \frac{E(1-\nu)}{(1+\nu)(1-2\nu)x_2 z_3} \begin{bmatrix} -z_3 & z_3 & 0 & \frac{\nu\lambda_3}{1-\nu} & -\frac{\nu x_3}{1-\nu} & \frac{\nu x_2}{1-\nu} \\ -\frac{\nu z_3}{1-\nu} & \frac{\nu z_3}{1-\nu} & 0 & \frac{\nu\lambda_3}{1-\nu} & -\frac{\nu x_3}{1-\nu} & \frac{\nu x_2}{1-\nu} \\ \lambda_2\lambda_3 & -\lambda_2 x_3 & \lambda_2 x_2 & -\lambda_2 z_3 & \lambda_2 z_3 & 0 \end{bmatrix} \begin{Bmatrix} u_1 \\ u_2 \\ u_3 \\ v_1 \\ v_2 \\ v_3 \end{Bmatrix}$$

equs. 2.b.I6

where $\lambda_2 = \frac{1 - 2\nu}{2(1 - \nu)}$, $\lambda_3 = x_3 - x_2$

The next step is the evaluation of nodal forces using the principle of virtual work.

The nodal forces are equivalent statically to the boundary stresses and distributed loads on the element. The simplest procedure for making the nodal forces statically equivalent to the actual boundary stresses and distributed loads is to impose a virtual nodal displacement and to equate the external and internal work done by the various forces and stresses during that displacement.

If the nodal forces $\{F\}^e$, the virtual nodal displacements $d\{\delta\}^e$, and the distributed loads $\{p\}$ act on a unit volume of material within the element (a constant thickness of the element t is assumed), then the equations 2.b.6 and 2.b.I2 give us as result:

$$d\{f\} = [N]\, d\{\delta\}^e ,$$

$$d\{\varepsilon\} = [B]\, d\{\delta\}^e . \qquad \text{equs. 2.b.I7}$$

The external work done by the nodal forces is equal to the sum of the products of the individual force components and corresponding displacements:

$$W_{ex} = (d\{\delta\}^e)^T \{F\}^e \qquad \text{equ. 2.b.I8}$$

where $(d\{\delta\}^e)^T$ is the transpose of $d\{\delta\}^e$. The internal work per unit volume $W_{int.}$ done by the stresses (equations 2.b.I6) and distributed forces is

$$W_{int.} = d\{\varepsilon\}^T \{\sigma\} - d\{f\}^T \{p\}$$

or

$$W_{int.} = (d\{\delta\}^e)^T \left([B]^T \{\sigma\} - [N]^T \{p\} \right) \qquad \text{equ. 2.b.19}$$

By equating the external work with the internal work resulting from integration over the volume of the element, we obtain

$$(d\{\delta\}^e)^T\{F\}^e = (d\{\delta\}^e)^T\left(\int[B]^T\{\sigma\}d(vol) - \int[N]^T\{p\}d(vol)\right)$$

equ.2.b.20

By using equations 2.b.15 and 2.b.12 and substituting the $\{\sigma\}$ in equation 2.b.20 we obtain

$$\{F\}^e = \left(\int[B]^T[D][B]d(vol)\right)\{\delta\}^e - \int[N]^T\{p\}d(vol) \qquad \text{equ.2.b.21}$$

The equation 2.b.21 is the characteristic equation 2.b.1 and the stiffness matrix of the element will therefore be

$$[K]^e = \int[B]^T[D][B]\,d(vol) = \int[B]^T[D][B]\,t\,dxdz = [B]^T[D][B]\,t\Delta$$

equ.2.b.22

where Δ is the area of the triangle. From equation 2.b.21 the nodal forces due to distributed loads are

$$\{F\}^e_p = -\int[N]^T\{p\}\,d(vol) \qquad \text{equ.2.b.23}$$

where

$$[N]^T = \frac{1}{2\Delta}\begin{bmatrix} x_2z_3 - z_2x + (x_3 - x_2)z & 0 \\ z_3x - x_3z & 0 \\ x_2z & 0 \\ 0 & x_2z_3 - z_2x + (x_3 - x_2)z \\ 0 & z_3x - x_3z \\ 0 & x_2z \end{bmatrix} \qquad \text{equ.2.b.24}$$

The distributed loads $\{p\}$ can be analysed into the "body force" components X, Z

$$\{p\} = \begin{Bmatrix} X \\ Z \end{Bmatrix} \qquad \text{equ.2.b.25}$$

If the "body force" components X, Z are constant then using the equations 2.b.24 and 2.b.25, the equation 2.b.23 becomes

$$\{F\}^e_p = -\begin{Bmatrix} X \\ Z \end{Bmatrix}\begin{bmatrix} \frac{\Delta}{3} & 0 \end{bmatrix} \qquad \text{equ.2.b.26}$$

From equation 2.b.26 results that the body forces are equally distributed at the three nodes of the element.

Until now the stiffness matrix and the nodal forces were obtained as a function of a local coordinate system and according to a numbering convention. In assembling all the elements, it is convenient to refer all the elements to the same coordinate system (global) and also to change the local number which individually specifies the node and the direction of the associated nodal displacement. This is obtained by the use of a standard technique.

Generally there is no need to consider each element individually in order to calculate the stress and displacement at each point of a structure. The procedure used indicates the formation of the stiffness matrix and of the general equations. The same process is applied directly to the whole structure.

If $\{\delta\}$ represents the nodal displacements of the structure, then equation 2.b.6 becomes

$$\{f\} = [\bar{N}]\{\delta\} \qquad \text{equ. 2.b.27}$$

$\bar{N}_i = N_i^e$ when the point concerned is within a particular element e and i is a point associated with that element. The matrix $[\bar{B}]$ follows a similar definition and the virtual work principle is applied to the whole structure. If $d'\{\delta\}$ represents the virtual displacement of all nodes due to the external forces $\{R\}$, the external virtual work is

$$W'_{ext.} = d'(\delta)^T \{R\} \qquad \text{equ. 2.b.28}$$

The internal virtual work is

$$W_{int.} = \int_v d\{\varepsilon\}^T\{\sigma\}d(vol) - \int_v d\{f\}^T\{p\}d(vol) - \int_s d\{f\}^T\{g\}d(area) \qquad \text{equ. 2.b.29}$$

where $\{g\}$ is a distributed external loading per unit area on the boundaries and the integrals are taken over the whole region.

Equating internal and external virtual work we obtain

$$[K]\{\delta\}+\{F\}_p+\{F\} -\{R\} = 0 \qquad \text{equ. 2.b.30}$$

Then the stiffness matrix of the assemblage is

$$[K_{ij}] = \int[\bar{B}]_i[D][\bar{B}_j]d(vol) \qquad \text{equ. 2.b.31}$$

the integral being taken over the whole region. Consequently,

$$[K_{ij}] = \sum[K_{ij}]^e \qquad \text{equ. 2.b.32}$$

which means that the stiffness of the assemblage is the sum of the stiffnesses of the individual elements.

In considering the virtual work for the whole system (equation 2.b.29) and equating this to the sum of the element contributions it is implicitly assumed that no discontinuity between adjacent elements develops. This means that displacement continuity must exist to make the above equations valid. Equating external virtual work (equation 2.b.28) and internal virtual work (equation 2.b.29) we have

$$\int d\{\varepsilon\}^T\{\sigma\}d(vol) - [d\{\delta\}^T R + \int d\{f\}^T\{p\}d(vol) + \int d\{f\}^T\{g\}d(area)] = 0 \qquad \text{equ. 2.b.33}$$

In this equation, the first term represents the strain energy of the structure U while the second the potential energy of the extermal loads W. Consequently

$$d(U + W) = d(x_i) = 0 \qquad \text{equ. 2.b.34}$$

where the quantity x_1 represents the total potential energy. From equation 2.b.34 we have the result that for equilibrium to be ensured, the total potential energy must be constant and minimized for variation of admissible displacements.

2.C. Application of a modified KIRSCH solution and the finite element method for the case of the Fleet Line Tunnel, London Transport. Comparative representation of the results.

Application of a modified KIRSCH solution

Among the methods that have been examined of calculation of stress and displacement around a tunnel, a conventional one based on the KIRSCH's equations was selected for consideration and appraisal with respect to results based on the finite element method.

The tunnel upon which the above two methods were applied is situated in London in the stiff, fissured, overconsolidated blue - grey London Clay. The tunnel centre line direction is approximately East - West, while the depth, in the area under study, is about 29.57m. The diameter is 4.07m (Figure 2.c.I), but at the Green Park Station of the Fleet Line, the tunnel was opened to a diameter of 7.0m. Such a large opening provided an opportunity to investigate the clay surrounding of the tunnel.

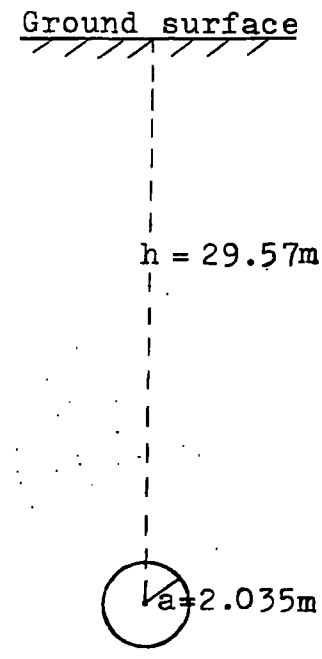

Figure 2.c.I

The shear strength characteristics of that clay, the discontinuity fabric and mainly the effect of the discontinuities on the stability of the tunnel are extensively discussed in the third and fourth chapter.

Geologically, the London Clay was deposited under marine conditions in the Eocene period. In Tertiary and Pleistocene, during uplift and erosion, I50m to 2I0m of overlying sediments were removed, which correspond to a preconsolidation load of at least 2.000 kN/m^2 (SKEMPTON and HENKEL I957; results for the area of central London). The removal of load by erosion caused a vertical expansion of the clay and, as a result, at any given depth the horizontal pressure is greater than the existing vertical pressure (Figure 2.c.2). The London Clay consists of a lower sandy clay, of an intermediate blue - grey clay and of an upper brown clay. The total present thickness of the London Clay is estimated to be between 90m and I20m and its structure takes the form of a very gentle syncline.

As already mentioned, the first method applied , with some modifications, in the calculation of stress and displacement in the above tunnel, has been developed by L. OBERT and W. DUVALL and was presented in pages 5,6,7,8,9. By this method, in the case of the Fleet Line Tunnel, it appears that we succeed in obtaining an appreciation of the new state of stress better than any other method referred to in Chapter 2.a. Some field data support the results obtained by the above method.

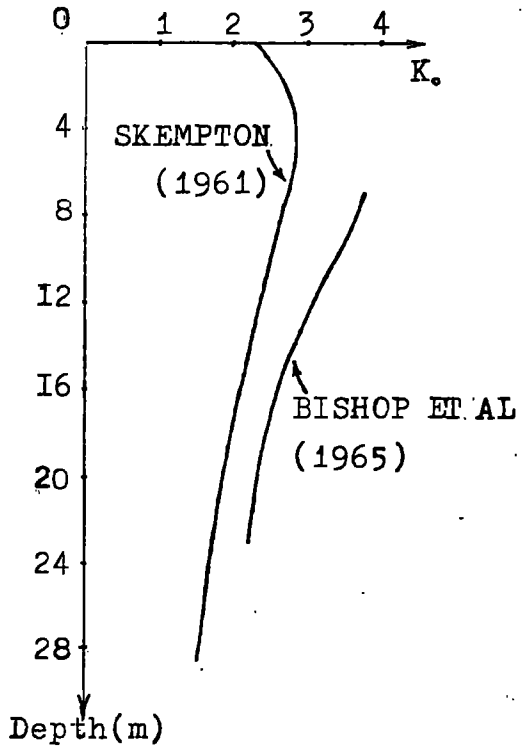

Figure 2.c.2

At first, the method considers an infinite plate of thickness t with a circular hole of radius a. A cross-section of a tunnel may be idealized to a semi-infinite plate in which plane strain conditions are assumed. The validity of the above method can be extended to the case of a semi-infinite plate if a specified relationship exists between the height of the tunnel (distance between cut surface and ground surface) and the radius of the tunnel.

J. SCHMIED(I926) suggested that the effect of the tunnel is of a localized character. He combined the radius (R_e) of the elastically-affected space by the presence of a tunnel with the modulus of elasticity (E) and Poisson's number of the mass ($m = \frac{1}{\nu}$)

$$R_e = a\pi\left(\frac{m^2(m-1)E}{\gamma(m+1)(m-2)h}\right)^{\frac{1}{2}} \qquad \text{equ.2.c.I}$$

R. MINDLIN (I940) basing his analysis upon Saint-VENANT's principle, again pointed out that the effect of the hole is of a very localized character. He showed that the disturbance essentially does not exceed an area of radius 8a.

S. TIMOSHENKO (I95I) also confirmed that if the distance of a hole from the straight bounderies of a semi-infinite elastic plate is not smaller than four-times the diameter of the hole itself the error, of the above solution does not exceed 6 per cent.

In the case of the Fleet Line tunnel, the axis depth is 29.57m (at Green Park); therefore $h > 8a$ and the above mentioned method can be used.

As already stated during the description of the method, the AIRY stress function used accepts zero body forces. In the case of an underground tunnel, the above assumption leads to basic errors in the calculation of stress and displacement. The errors increase when the lateral stress does not change uniformly in relation to the vertical stress, something that often occurs in the case of overconsolidated geological materials(Figure 2.c.2). For that reason , the stresses S_x, S_z were considered as acting not in infinity but upon the point under examination when calculating the values of stress and displacement. The above stresses were equated to the existing (prior to the opening of the tunnel) vertical and horizontal stresses. Following these adjustments, the equations 2.a.10, 2.a.II, 2.a.I2 became (Figure 2.c.3)

$$\sigma_r = \frac{1}{2}\sigma_v\left[(1+K_o)(1-\frac{a^2}{r^2}) + (K_o-1)(1+\frac{3a^4}{r^4}-\frac{4a^2}{r^2})\cos 2\theta\right] \quad \text{equ.2.c.2}$$

$$\sigma_\theta = \frac{1}{2}\sigma_v\left[(1+K_o)(1+\frac{a^2}{r^2}) - (K_o-1)(1+\frac{3a^4}{r^4})\cos 2\theta\right] \quad \text{equ.2.c.3}$$

$$\tau_{r\theta} = -\frac{1}{2}\sigma_v(K_o-1)(1-\frac{3a^4}{r^4}+\frac{2a^2}{r^2})\sin 2\theta \quad \text{equ.2.c.4}$$

$$\sigma_1 = \frac{1}{2}(\sigma_r+\sigma_\theta) + \frac{1}{2}\sqrt{(\sigma_r-\sigma_\theta)^2+4\tau_{r\theta}^2} \quad \text{equ.2.c.5}$$

$$\sigma_3 = \frac{1}{2}(\sigma_r+\sigma_\theta) - \frac{1}{2}\sqrt{(\sigma_r-\sigma_\theta)^2+4\tau_{r\theta}^2} \quad \text{equ.2.c.6}$$

$$\sigma_2 = \nu(\sigma_1+\sigma_3) \quad \text{equ.2.c.7}$$

$$\psi = \frac{1}{2}\tan^{-1}\frac{2\tau_{r\theta}}{\sigma_r-\sigma_\theta} \quad \text{equ.2.c.8}$$

where ψ is the angle between the principal stress σ_1 and the horizontal axis, and $\sigma_v = \gamma(h-r\sin\theta)$ (vertical stress ; h = the depth of tunnel axis).

The displacements under plane strain conditions are:

$$u = \frac{1-\nu^2}{2E}\sigma_v\left[(K_o+1)(r+\frac{a^2}{r}) + (K_o-1)(r-\frac{a^4}{r^3}+\frac{4a^2}{r})\cos 2\theta\right] -$$

$$- \frac{\nu+\nu^2}{2E}\sigma_v\left[(K_o+1)(r-\frac{a^2}{r}) - (K_o-1)(r-\frac{a^4}{r^3})\cos 2\theta\right].$$

equ.2.c.9

$$v = \frac{\nu^2-1}{2E}\sigma_v\left[(K_o-1)(r+\frac{2a^2}{r}+\frac{a^4}{r^3})\sin 2\theta\right] -$$

$$- \frac{\nu^2+\nu}{2E}\sigma_v\left[(K_o-1)(r-\frac{2a^2}{r}+\frac{a^4}{r^3})\sin 2\theta\right].$$

equ.2.c.10

It is generally accepted that heavily-overconsolidated clays behave essentially in a linearly elastic manner for the small changes of stress (the blue - grey London Clay is an orthotropic clay with a vertical axis of symmetry). The elastic moduli are dependent on the effective pressure and consequently they vary with the depth in a soil, increasing the soil's stiffness in relation to its depth. In this application the elastic modulii and the density maintain a constant average value in terms of depth. Also, the effect of discontinuities and any pore water pressure are ignored and an elastic situation is assumed throughout the tunnel.

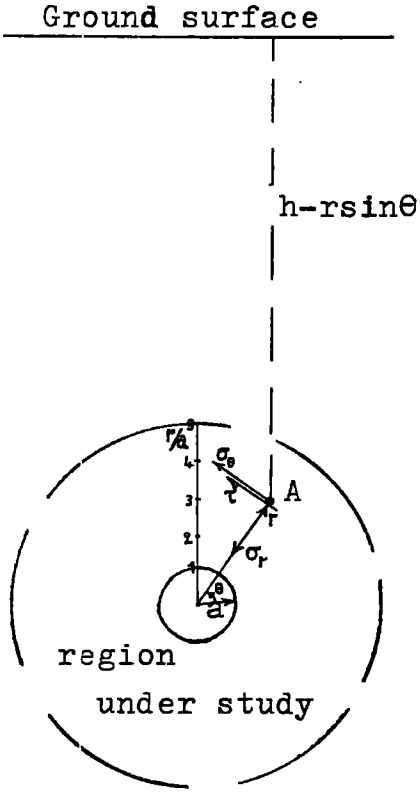

Figure 2.c.3

A computer programme P_1 was written to compute the radial, tangential and shear stresses, the principal stresses,

the angle of the principal stress σ_1 with the horizontal axis, the values of normalized to σ_1 radial, shear and tangential stress in the region up to 5.00 radii at every 0.20 radius and every 10.00 degrees from 90 to -90 degrees (Appendix 2.c.I).

The computed values of displacements, based upon the equations 2.c.9, 2.c.10, are not accepted (they do not change as a function of distance from the tunnel).

The values of radial, tangential and shear stress are normalized to the stress corresponding to the weight of overlying material prior the excavation, and they are plotted by computer (Figures 2.c.6 to 2.c.16).

On pages I52, I53 (Appendix 2.c.2), this computer programme P_2 is presented for calculating the stresses as in the case of the programme P_1, and for plotting the normalized stresses as well.

Application of finite element method

The finite element method in the form applied for the calculation of stress and displacement around the Fleet Line tunnel has already been discussed.

In this application, because of the symmetry which exists with respect to the vertical axis passing throught the centre of the tunnel, only the right half of the medium is considered.

The medium has been divided into two hundred and seventy nine triangular elements connected with each other at one hundred and sixtysix nodal points (Figure 2.c.5). As already mentioned, each element behaves as a planar, isotropic, homogeneous elastic plate. Also, the stresses are assumed to be uniformly distributed throughout the element. Since large stress gradients are expected to occur in the immediate vicinity of the tunnel, a large number of elements must be used especially for this area.

The following boundary conditions are determined (Figure 2.c.4) :

i) On AB, CD, EF only vertical displacements are allowed;

ii) On DE, only horizontal displacements are allowed;

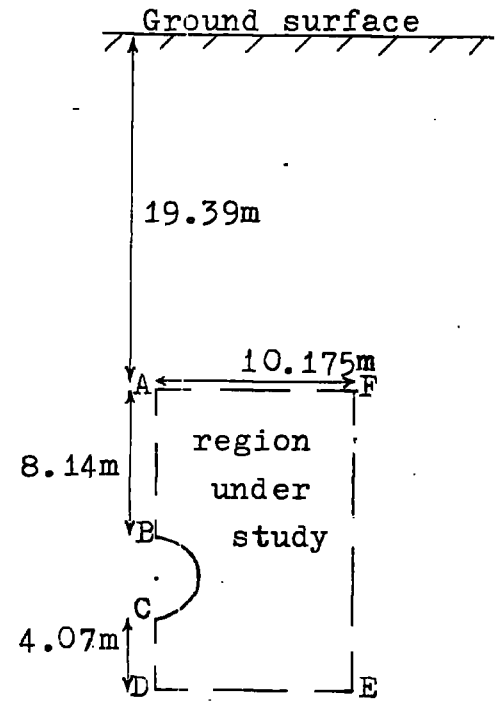

Figure 2.c.4

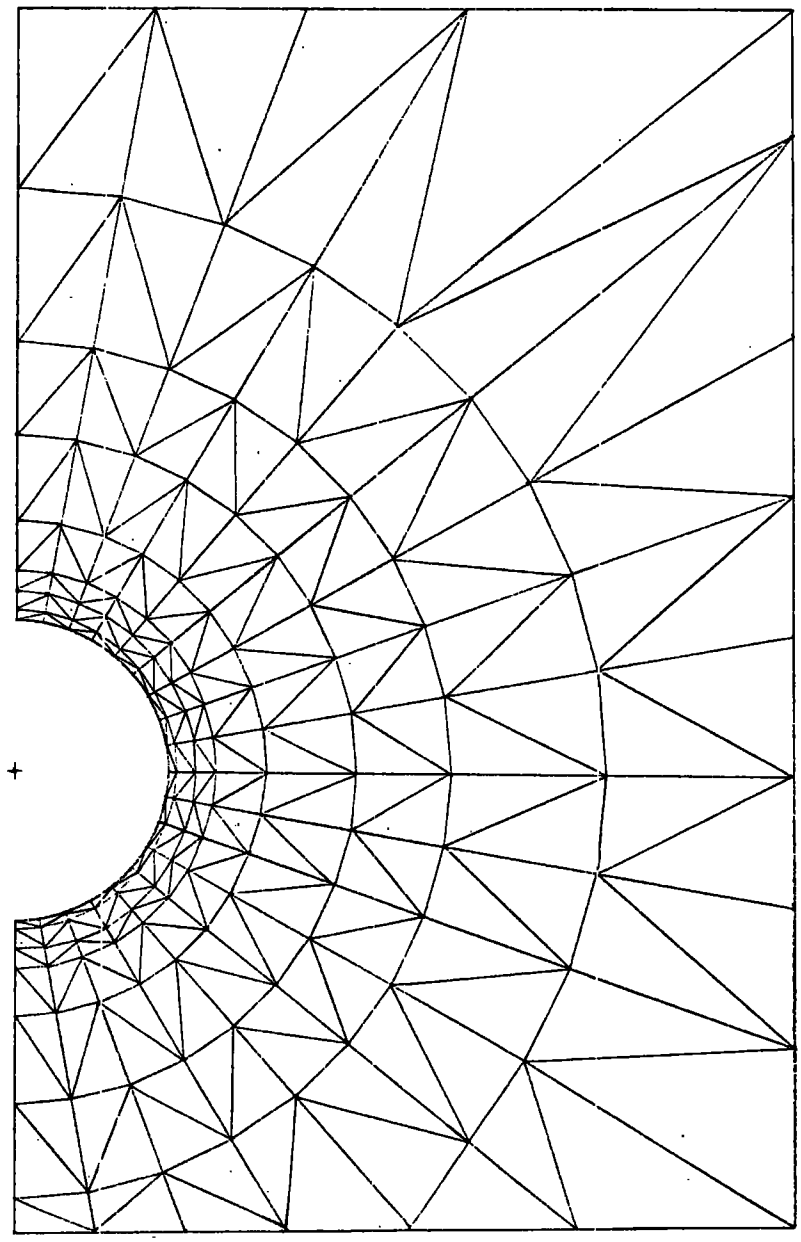

Fig. 2.c.5

Finite element model for the Fleet Line Tunnel

Mesh used in the calculation of stress and displacement

iii) On BC and the rest of the medium there are no displacement limitations.

The weight of each element is distributed equally to each of its three nodal points and consequently the gravity load at any nodal point is one-third of the weights of all elements connected at that point. At the two horizontal boundaries (AF, DE) stresses are applied corresponding to the weight of the overlying material. Also at the vertical right boundary (EF), the applied stresses are equivalent to the lateral pressures.

The Poisson' s ratio used is equal to 0.48.

The finite element programme was provided by the Mining Engineering Department of Newcastle Upon Tyne University and was run on the IBM 360/67 computer at Durham University. A part of the output of the programme is represented on the Appendix 2.t.3.

The stresses are computed in Cartesian coordinates. These have been transformed to polar coordinates and the values of stress are normalized to the stresses corresponding to the weight of overlying material prior to the excavation, and are plotted on pages 42 to 52.

In the following pages, the results of both the modified KIRSCH's solution and the finite element method are presented and can thus be compared.

Comparative representation of the stresses derived from the application of a modified KIRSCH' s solution and from the finite element method in the case of the Fleet Line Tunnel

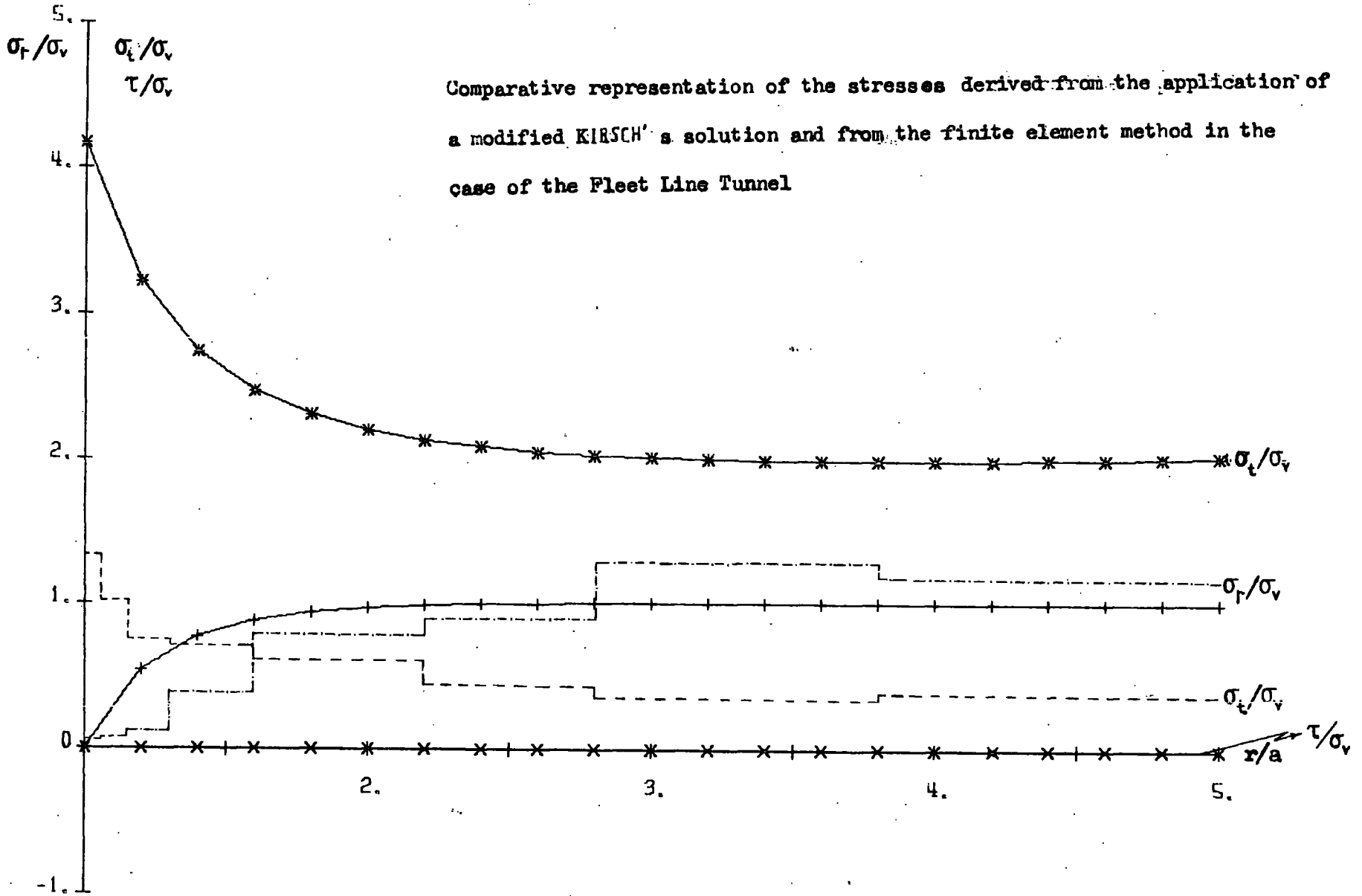

Fig. 2.c.6 Results for 90 degrees

———— results of a modified KIRSCH's solution

— · — · — results of the finite element method

Comparative representation of the stresses derived from the application of a modified KIRSCH' s solution and from the finite element method in the case of the Fleet Line Tunnel

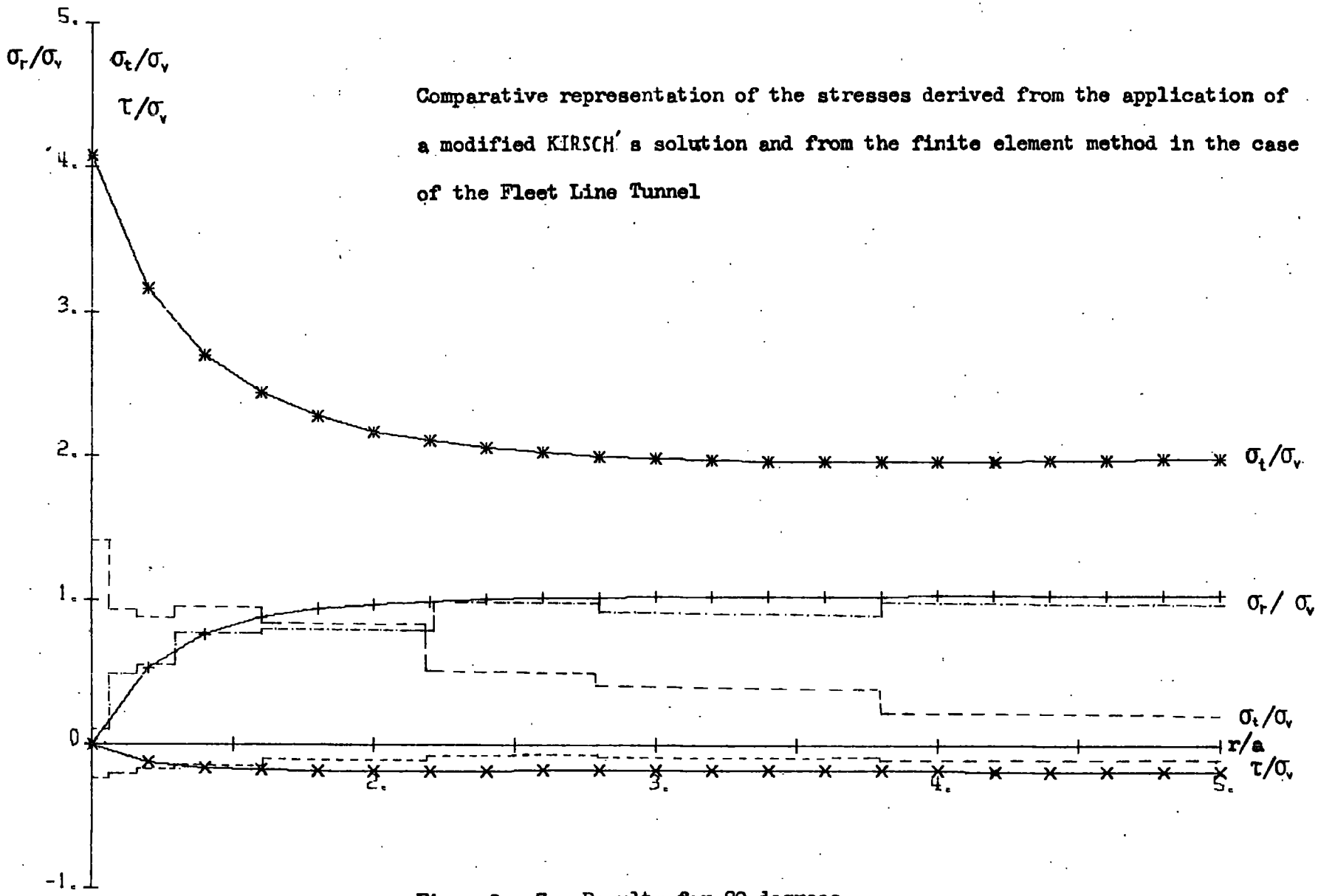

Fig. 2.c.7. Results for 80 degrees

——— results of a modified KIRSCH's solution

– – – – results of the finite element method

Comparative representation of the stresses derived from the application of a modified KIRSCH's solution and from the finite element method in the case of the Fleet Line Tunnel

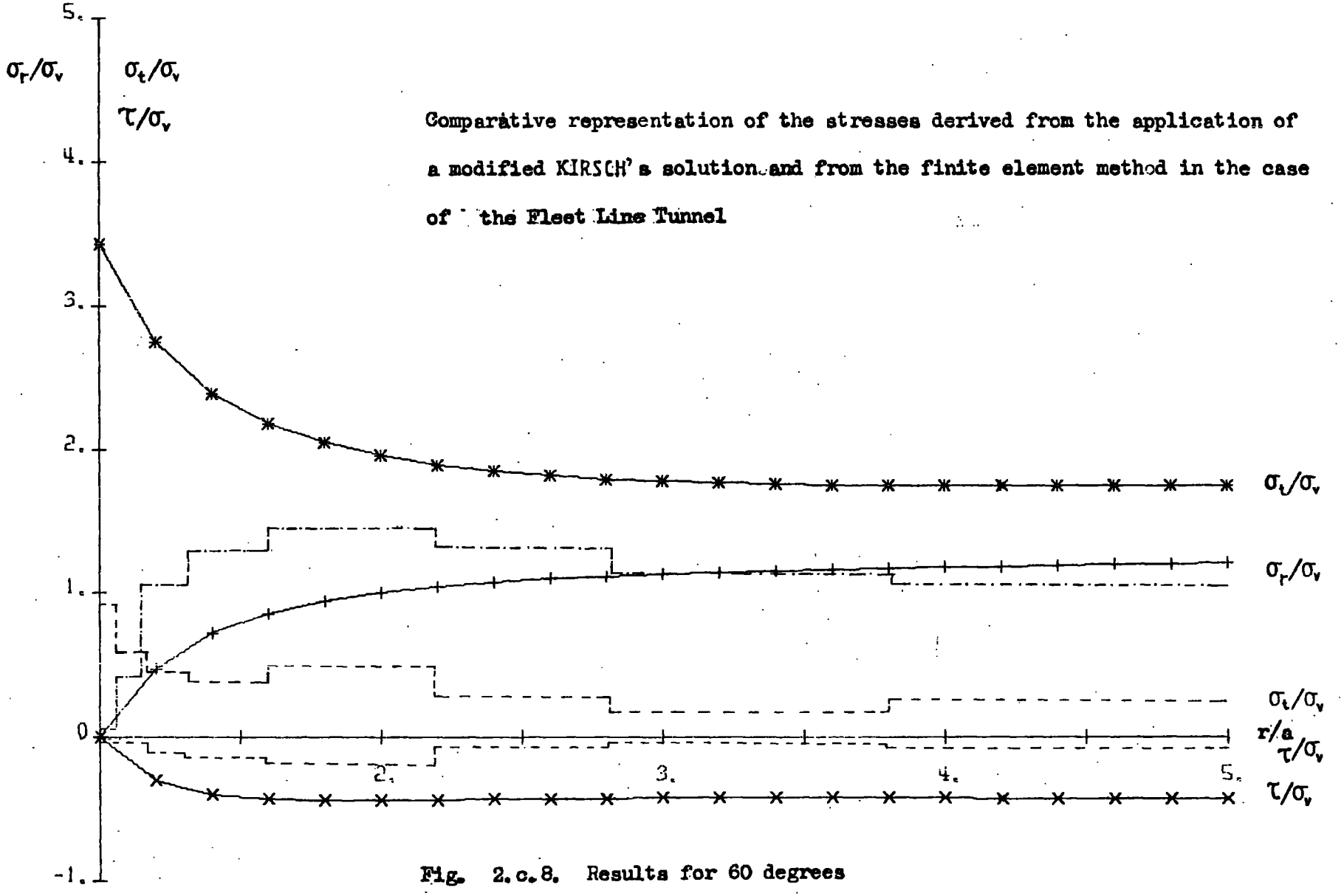

Fig. 2.c.8. Results for 60 degrees

——— results of a modified KIRSCH's solution

-.-.-.- results of the finite element method

Comparative representation of the stresses derived from the application of a modified KIRSCH's solution and from the finite element method in the case of the Fleet Line Tunnel

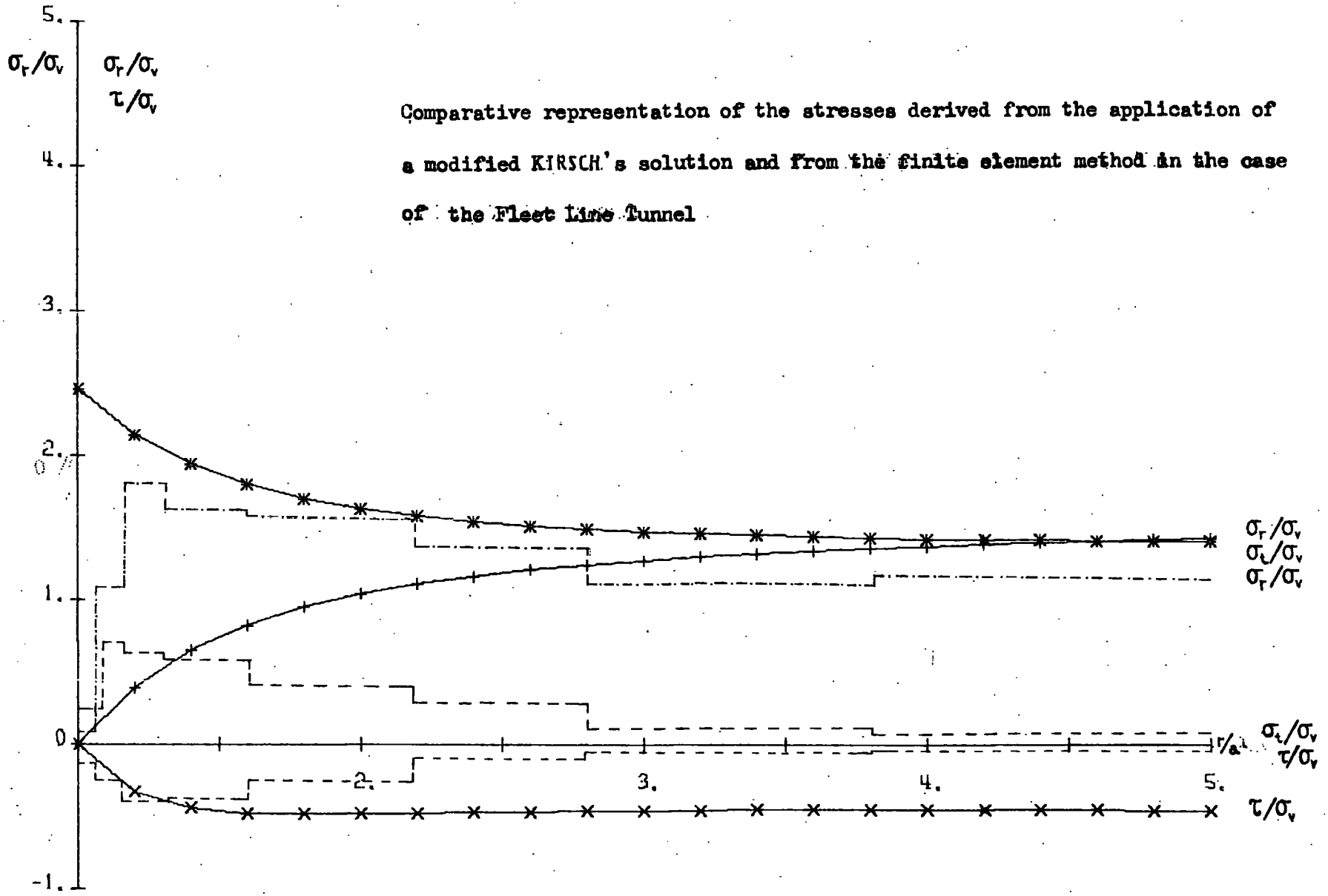

Fig. 2.c.9. Results for 40 degrees

——— results of a modified KIRSCH's solution

— · — · — results of the finite element method

Comparative representation of the stresses derived from the application of a modified KIRSCH' s solution and from the finite element method in the case of the Fleet Line Tunnel

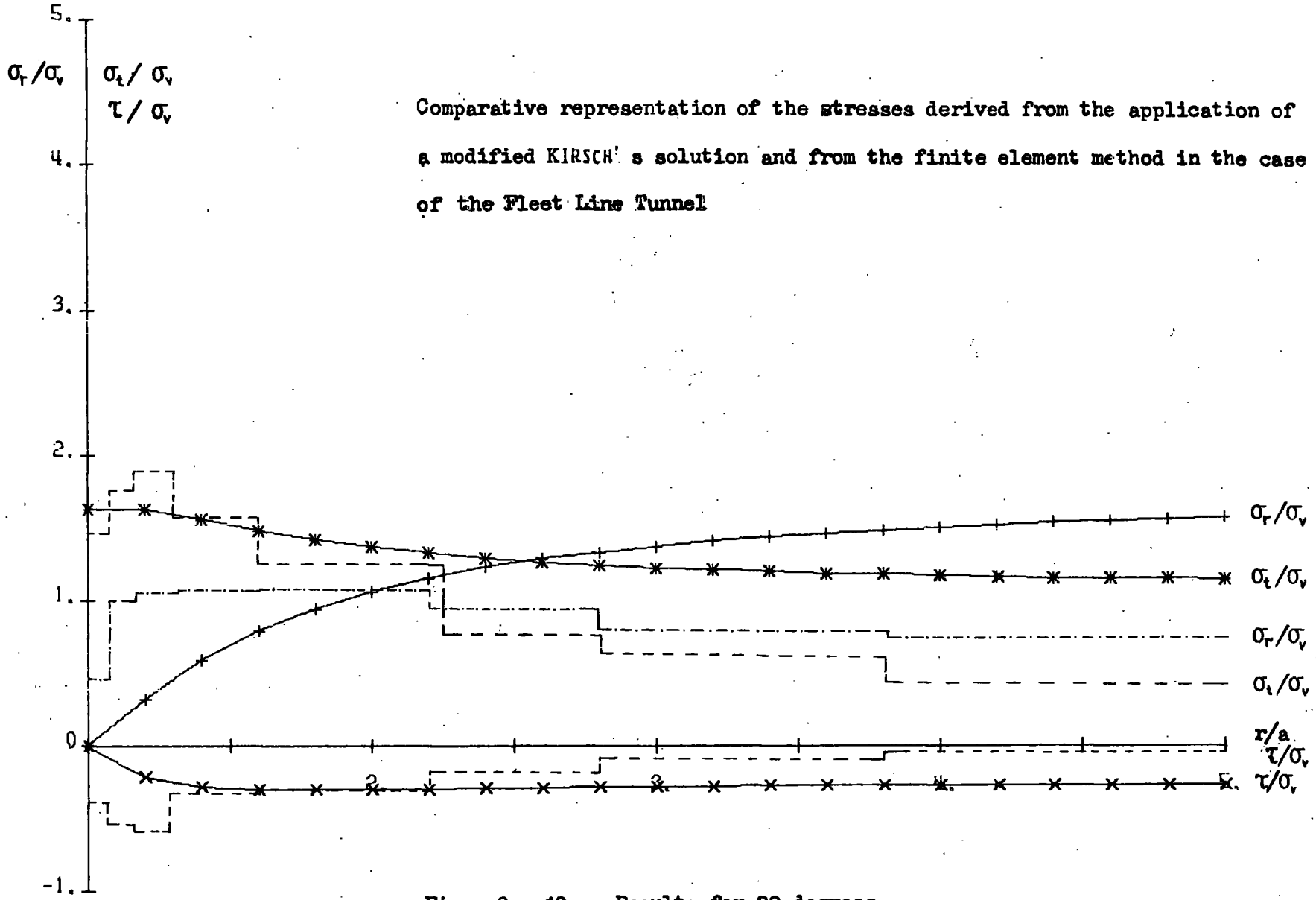

Fig. 2.c.10. Results for 20 degrees

——— results of a modified KIRSCH' s solution

-·-·-·- results of the finite element method

Comparative representation of the stresses derived from the application of a modified KIRSCH' s solution and from the finite element method in the case of the Fleet Line Tunnel

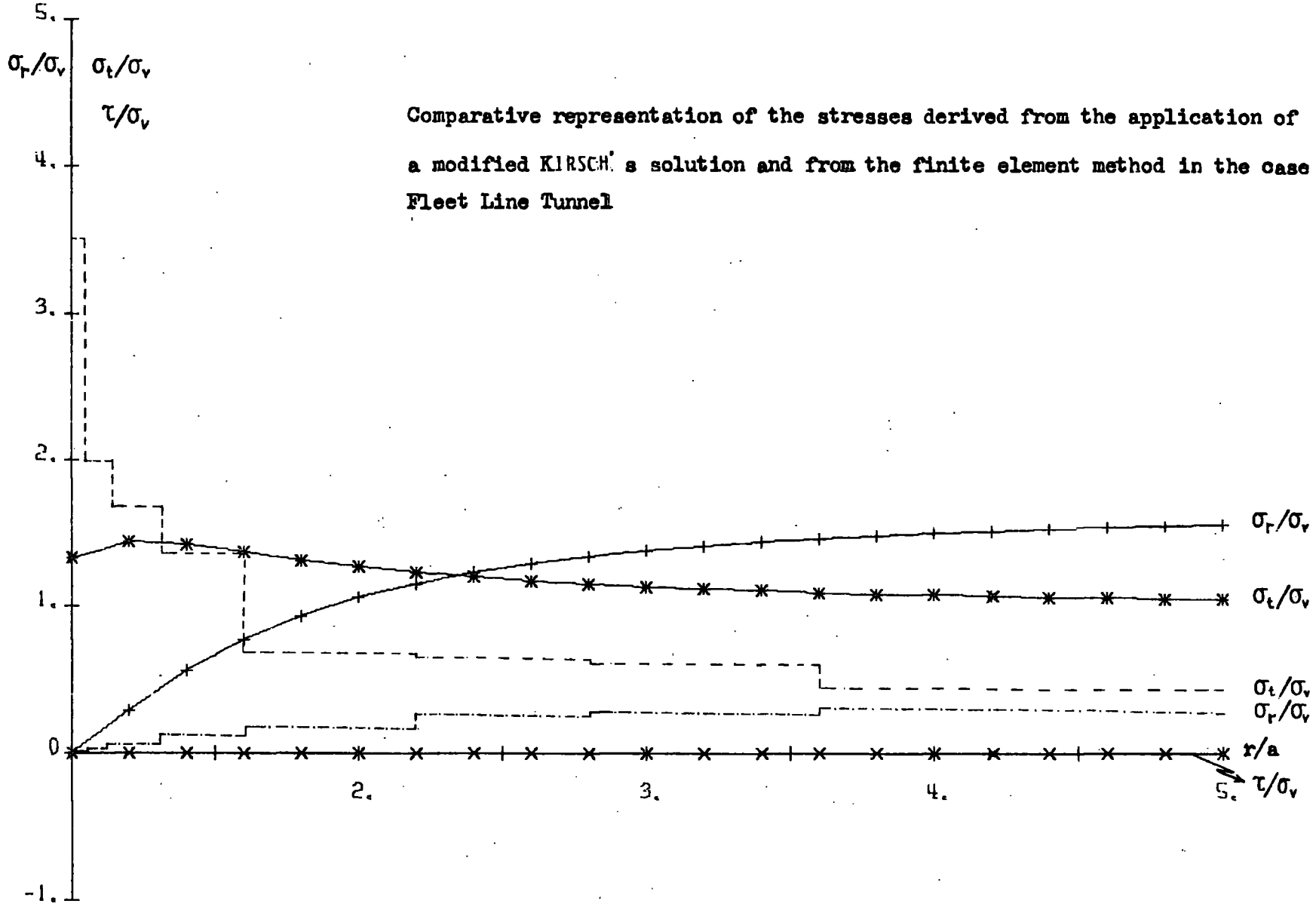

Fig. 2.c.11. Results for 0 degrees

——————— results of a modified KIRSCH's solution

— · — · — · — results of the finite element method

Comparative representation of the stresses derived from the application of a modified KIRSCH's solution and from the finite element method in the case of the Fleet Line Tunnel

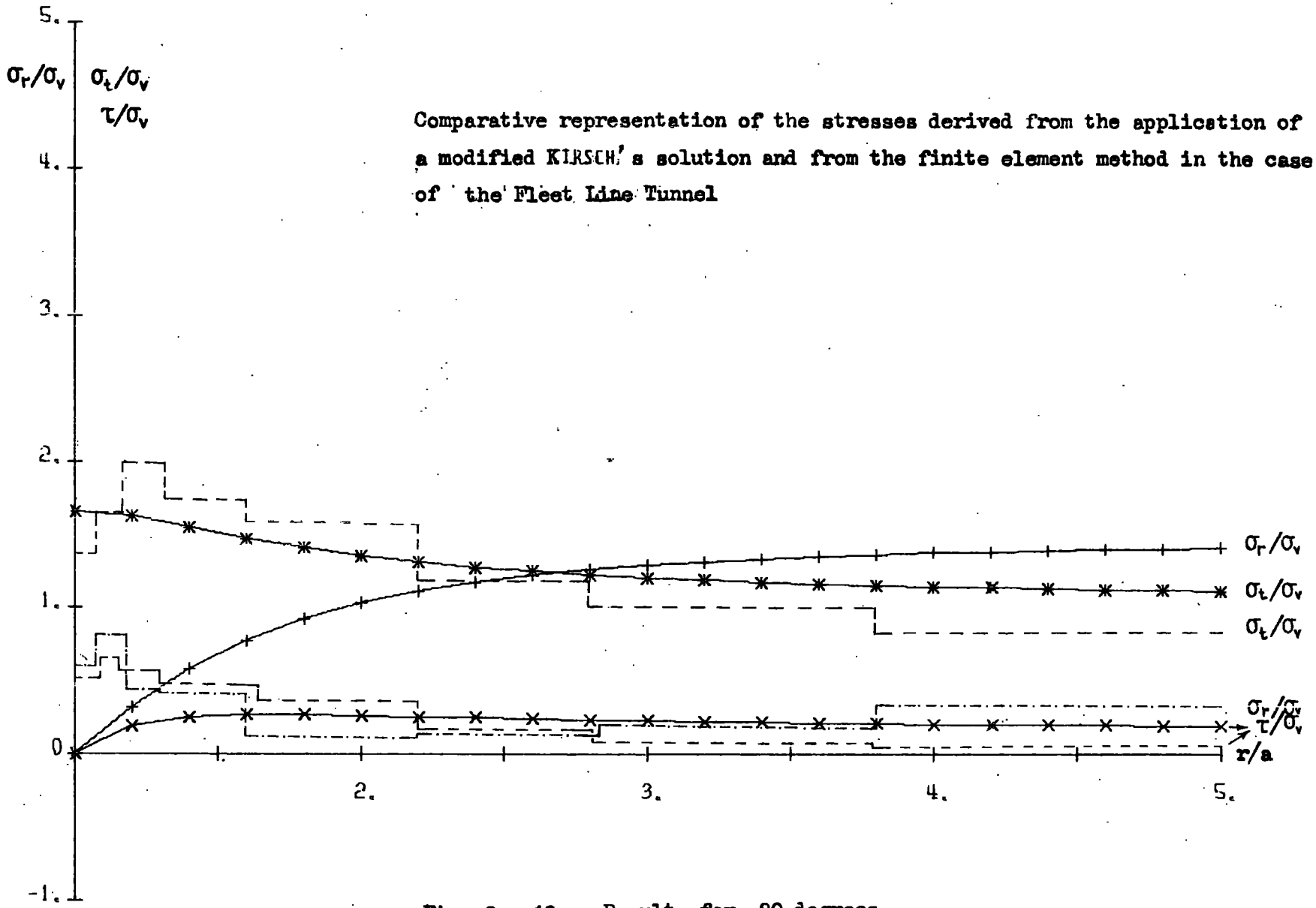

Fig. 2.c.12. Results for -20 degrees

——— results of a modified KIRSCH's solution

═·═·═ results of the finite element method

Comparative representation of the stresses derived from the application of a modified KIRSCH's solution and from the finite element method in the case of the Fleet Line Tunnel

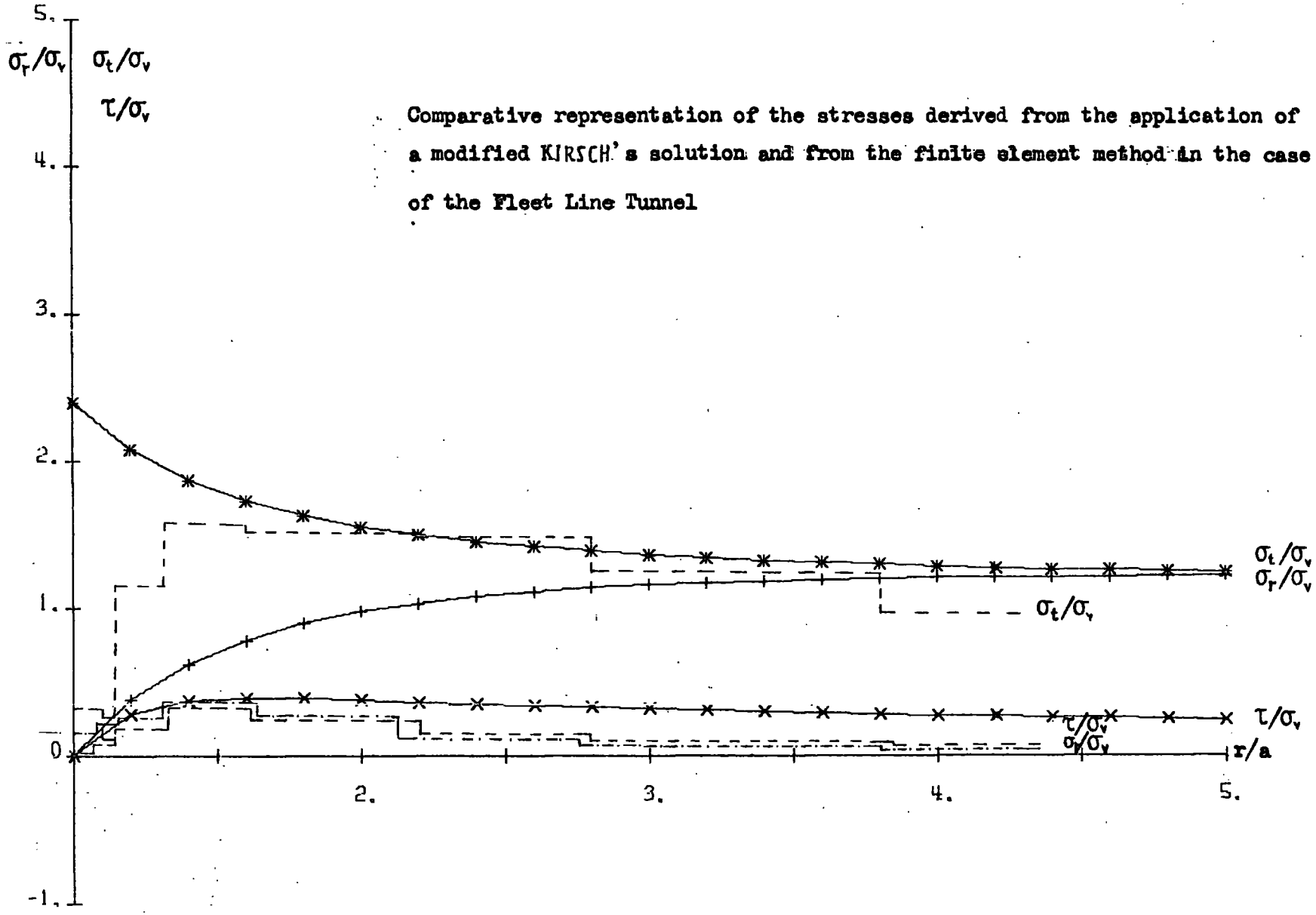

Fig. 2.c.13. Results for -40 degrees

——— results of a modified KIRSCH's solution

— · — · — results of the finite element method

Comparative representation of the stresses derived from the application of a modified KIRSCH' s solution and from the finite element method in the case of the Fleet Line Tunnel

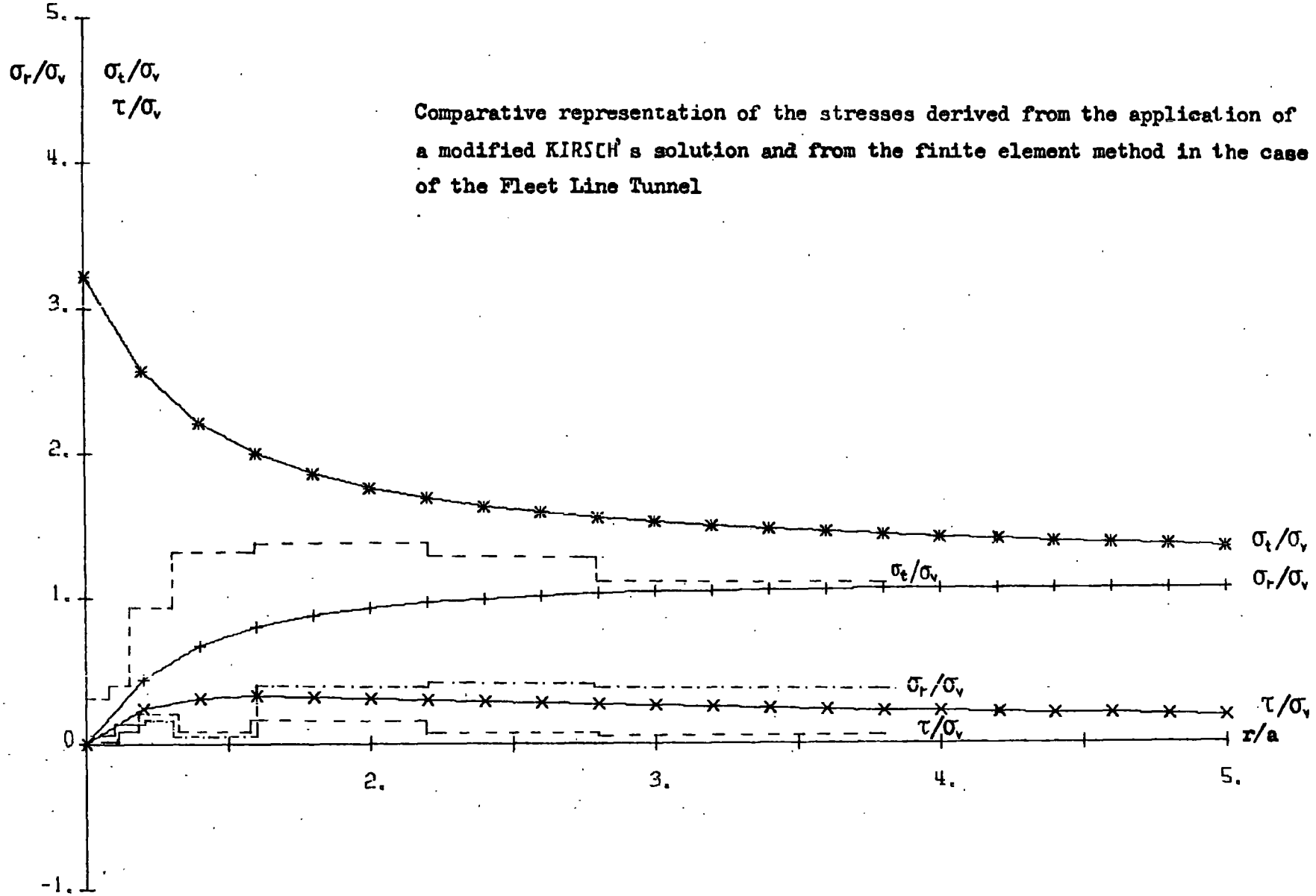

Fig. 2.c.14. Results for -60 degrees

——————— results of a modified KIRSCH' s solution

·—·—·—· results of the finite element method

Comparative representation of the stresses derived from the application of a modified KIRSCH' s solution and from the finite element method in the case of the Fleet Line Tunnel

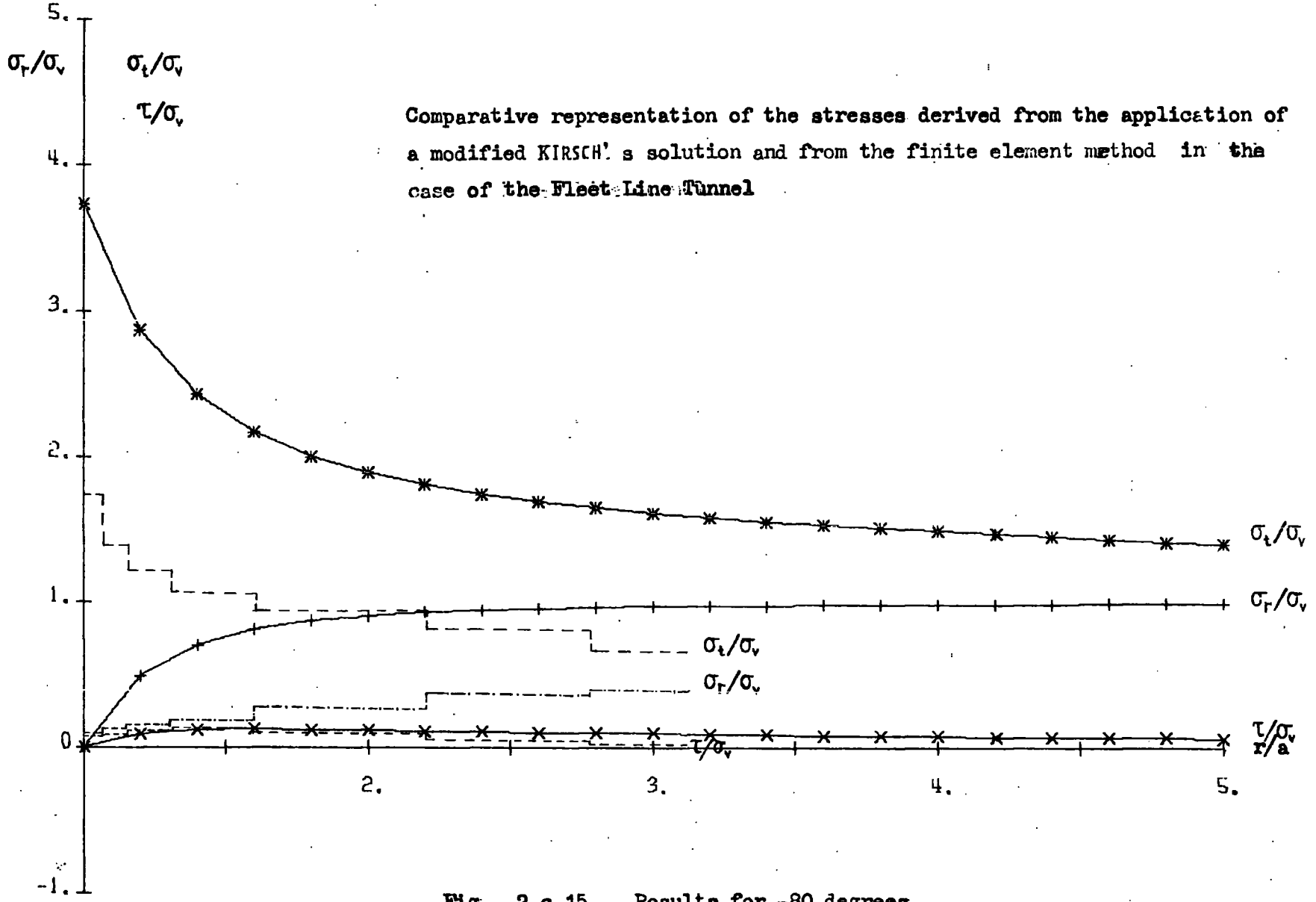

Fig. 2.c.15. Results for -80 degrees

——— results of a modified KIRSCH' s solution

— · — · — results of the finite element method

Comparative representation of the stresses derived from the application of a modified KIRSCH's solution and from the finite element method in the case of the Fleet Line Tunnel

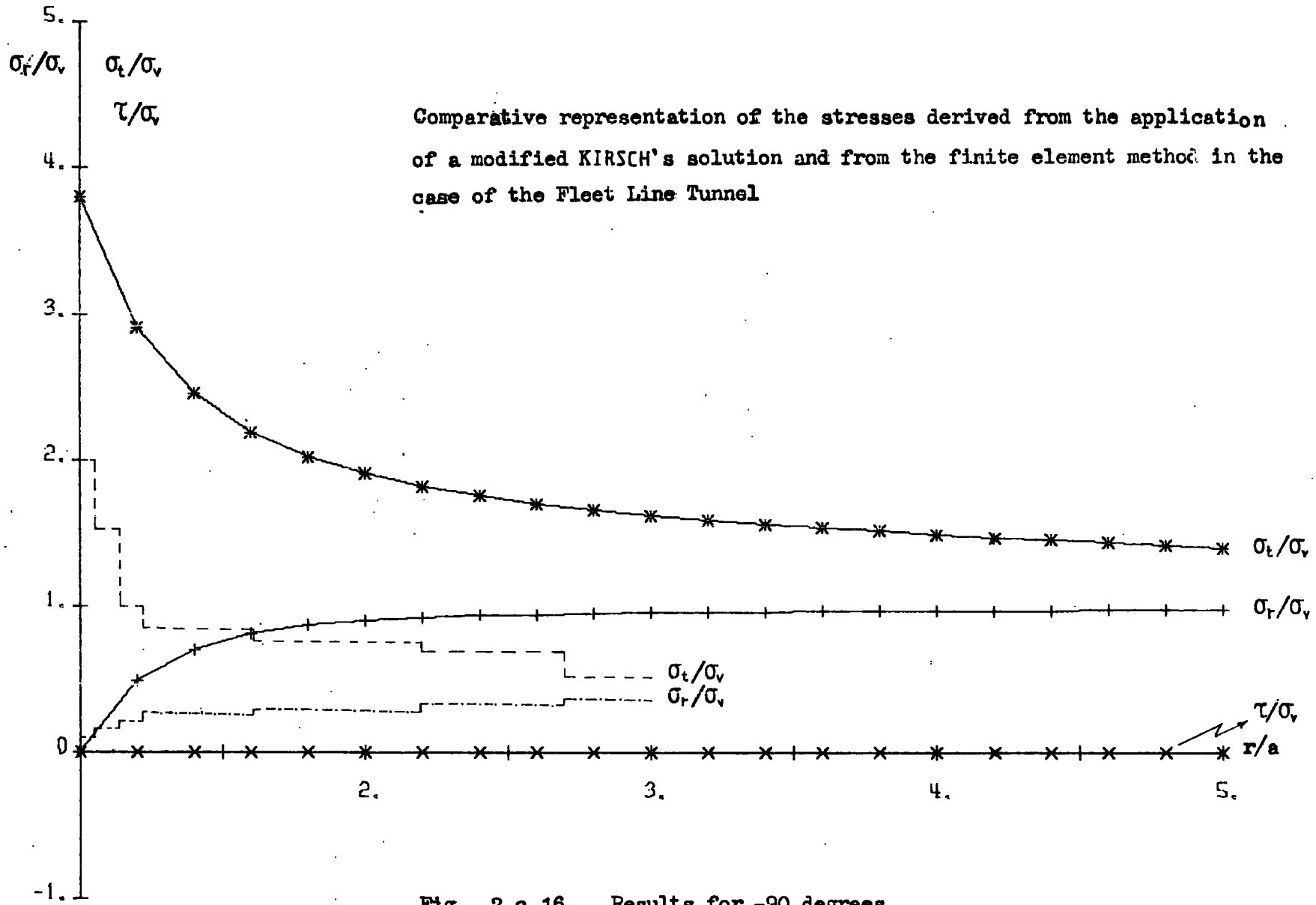

Fig. 2.c.16. Results for -90 degrees

——— results of a modified KIRSCH's solution

— · — · — results of the finite element method

Conclusions

According to the results presented in Figures 2.c.6 to 2.c.16 the following conclusions are made:

1) In both methods the stress disturbance caused by the excavation of the tunnel, is considerably reduced after a distance corresponding to 1.5 to 3 times the radius of the tunnel. The results of the finite element method indicate, as expected, a slightly larger area of stress disturbance.

2) Generally, the stresses derived from the application of the finite element method change, as a function of distance from the tunnel, in approximately the same way with those calculated from the modified KIRSCH's solution.

3) The values of radial stress, in a region lying above the tunnel, as derived from the finite element method, are in good agreement with the values derived from the modified KIRSCH's solution. In the remaining region the values of the results of the finite element method are much smaller than the corresponding values of the modified KIRSCH's solution. It should be noted that as it results from the assumptions of the use of triangular elements, the radial stress at the tunnel surface shows a finite value while the KIRSCH's solution shows zero values.

4) The values of tangential stress derived from the finite element method, are much smaller than the corresponding values of the modified KIRSCH's solution in the region lying above and below the tunnel. In the rest of the region the values of finite element method approach the corresponding values of the modified KIRSCH's solution.

5) The values of shear stress derived from the finite element method, depending on the values of radial and shear sresses, are smaller than the corresponding values of the modified KIRSCH's solution especially in the region located far from the tunnel surface.

Generally, as would be expected, the greatest differences occur near the surface of the tunnel where stress gradients are rapidly changing over short distances.

The differences in the stress values between the compared methods are mainly created on account of the not identical stress field conditions which were developed before the excavation took place.

In the modified KIRSCH's solution the initial stress field at each point consists of a vertical component $\sigma_v = h\gamma$ and a horizontal component $\sigma_h = K_o h\gamma$.
In the finite element method the initial stress field results in a vertical component $\sigma_v = h_1\gamma + \sigma_s$ (CASTIGLIANO A.) and in a horizontal $\sigma_h = \frac{\nu}{\nu-1}(h_1\gamma + \sigma_s) + \sigma_6$ (STINI J., 1950)

where h_1 is the depth of the point from the model boundary AF,

σ_s is a stress component with values depending on the vertical pressure acting upon the boundary AF and from the distance of the point from the boundary AF,

σ_6 is a stress component with values depending on the horizontal pressure acting upon the boundary EF and from the distance of the point from the boundary EF.

No data was available to input initial strains in the finite element programme and the limited time available did not permit extensive search of methods which could help to obtain a further equation of the initial stress fields in the two compared solutions.

It should be noted that initially another computing process was followed with different assumptions, and dealing with isoparametric rectangular elements, whose results were less satisfactory.

Figures 2.c.6 to 2.c.I6 indicate that an even greater number of elements should be used in the immediate vicinity of the tunnel and also that the boundaries should be at an even greater distance from the tunnel surface. The differences in the results of the compared methods may be partially due to the number of elements used and to the distance of the boundaries from the tunnel surface.

Although several differences were noticed in many results of the two methods, the fact that the results derived from the application of the finite element method change, as a function of distance from the tunnel, in approximately the same way with those calculated from the modified KIRSCH's solution, indicates that the results of the application of the finite element method may be successfully compared with those of an "applied" method (and therefore not on a theoretical basis) in the process of calculating the stress around a tunnel in a medium with a "complicated" initial stress field.

C H A P T E R 3rd

3. INFLUENCE OF DISCONTINUITIES ON THE SHEAR STRENGTH CHARACTERISTICS OF A CLAY MASS.

3.a. Laboratory testing on samples of London Clay. Comparison of shear strength along fissures with that of intact clay.

It is accepted that the stability of a discontinuous rock mass depends more directly on the shear strength characteristics of the discontinuities than on the strength of the intact elements.

The purpose of the laboratory tests is to obtain a simple estimation of the shear strength characteristics along the fissures in fissured samples of London Clay and then to compare the results with those from intact samples of London Clay.

Details of the tests

The samples were obtained from Regent's Park, in London, and with an orientation vertical with respect to the ground surface. The depths of the samples range from 19m to 25m below the ground level and the samples were tested for strength under normal and lateral pressures approximating those which were thought to have existed in the field.

The results of the index tests give us the following averages:

Wet bulk density 2.04 Mg/m^3

Nature moisture content 26.2%

Liquid limit 78%

Plastic limit 35%

Direct shear box tests. The shear strength along discontinuities and in the intact clay was determined by means of direct shear tests in a 6cm x 6cm shear box apparatus.

All the samples were consolidated prior to shear testing a period of twelve hours under the same normal stress as used for the shear failure stage.

The samples which contained a natural fissure were taken in such a manner that the test specimen could be set up with the fissure coinciding as nearly as possible with the designated shear plane in the shear box.

The displacement rates that were adopted were 0.005mm/min., which is sufficiently slow to permit drainage to take place (at least 95% pore pressure dissipation, as found from triaxial consolidation tests), and 0.375mm/min. which inhibits full drainage and which represents undrained conditions.

The residual strength was determined in the usual way by adopting the shear box reversal method (PETLEY,1966). When the first traverse was completed, the gears were reversed and by means of tie bars, the shear box was returned to its initial position. The procedure of shearing, as followed in the first shear, was then repeated until two consecutive travels showed a constant value of shear stress.

Triaxial tests. These tests were carried out in the triaxial compression apparatus with cylindrical specimens of 3.8cm diameter x 7.6cm high.

The samples which contained a fissure were taken in such a manner that the fissures were inclined at about 50°

to the horizontal and lying well clear of the end caps.

The strength of the intact clay was measured on specimens not containing an obvious macroscopic discontinuity.

Also, unconsolidated undrained tests with pore pressure measurements were carried out on intact samples of London Clay.

Radial filter drains were used and the specimens were placed in rubber membranes. All the samples were unconsolidated and they were compressed at a strain rate equal to I.5% per minute.A total correction of I5 kN/m^2 for filter drains and rubber membrane was applied to the compression strength of the sample because the membrane enclosing the sample imposes restraint on the sample(BISHOP and HENKEL,I962). The correction was applied to the axial stress and not to lateral pressure because the Poisson's ratio for rubber is almost 0.5 and consequently no hoop tension was introduced in the membrane.

In order to calculate the normal and shear stress upon the discontinuities a mathematical process was followed (Appendix 3.a.I).

Results of tests

These results should be interpreted with care. In spite of all the care taken it is not certain that all the discontinuities were set up with their entire length along the shear plane of the shear box or that the angle of these discontinuities to the horizontal was exactly as specified and close to 50° in the case of triaxial tests. Many of

the fissures may have been secondary and no time was available to determine whether the chosen fissures were wholly representative of the inherent fissures in general, especially in terms of the shape and the roughness which have an important influence on their shear strength. The comparative paucity of fissures in the available samples means that a large number of tests could not be conducted.

The residual shear strength, by definition, operates when there is no further decrease in shear strength with displacement ($\frac{d(\tau/\sigma_n)}{d(\text{displacement})} = 0$). When the above condition is satisfied, the curve in the standard plot τ/σ_n against displacement becomes horizontal. In practice, it is often difficult to visually judge from the above plot whether the soil has reached the residual state. The direct shear box test curves for stiff clays at normal stress greater than about 100kN/m^2 tend to show an increase of shear stress with displacement on the second and subsequent travels (Figures 3.a.4, 3.a.5, 3.a.10, 3.a.11).

Figures 3.a.4 to 3.a.13 show some representative stress-strain relationships for intact and fissured samples tested in the shear box and in Tables 3.a.1, 3.a.2 and Figures 3.a.1, 3.a.2 all the shear box results are summarised (the shear strength characteristics were calculated by the use of the method of least squares).

Figures 3.a.14 to 3.a.18 show, as well, some representative stress-strain relationships for intact and fissured samples tested in the triaxial aparatus and in Table 3.a.3 and in Figure 3.a.3 all the triaxial test results are summarized.

From the present results the following conclusions

may be derived:

I) In fissured samples, a significant reduction of the peak shear strength characteristics is taking place, in a direction co-planar with a discontinuity;

2) The residual values of shear strength along the fissures approach those of the intact clay but there is a finite cohesion across the fissure surface at the residual state in both types of tests (direct shear and triaxial) and both porewater conditions (drained-undrained);

3) In all the cases, a much smaller displacement was required in order to reach the residual strength from the peak strength along the fissures than was the case in intact clay. Usually, after less than 6mm displacement the shear strength fell to a value very near to residual and the surface became polished and striated.

4) The stress-strain curves for the fissured samples tested triaxially show a rapid increase of stress at small percentage strains, so indicating a brittle nature. But thereafter, the rate of increase of stress becomes low(in comparison with that of intact samples) showing more plastic behaviour, especially near failure.

Discussion of results

Examination of thin sections of London Clay under the polarized microscope (TCHALENKO,I967) indicated that no change in orientation of the clay particles took place as the surface of a typical fissure was approached. This fact, coupled with the apparent texture of the fissures which were studied, implies that no appreciable relative

movements (shear displacements) could have taken place along the fissures. This could explain the high values (in comparison with that of intact samples) of the cohesion across the surfaces of the fissures at the peak strength state in both types of tests and both porewater conditions (drained and undrained).

In all the tests with samples containing a fissure, after displacement of some millimetres (5-9mm) the fissure surface became polished and subplanar with striations or shallow grooves aligned in the direction of shearing. The polished nature of these surfaces indicates a considerable degree of particle orientation.

Clay particles within intact stiff clay may be only moderately orientated in the direction of displacement. Under a shearing stress, however, these clay particles shape up into a parallel face-to-face structure, orientated in the direction of the applied shearing force and, as a result of this, less resistance is offered to sliding. The degree of orientation would obviously depend on the amount of displacement, the nature of the pore fluid and absorbed water layer and the clay mineral type. This explains the reason why the value of the friction angle depends on the amount of movement that has taken place on the discontinuity.

SKEMPTON A.W.(I964) indicated that the effective residual value of the friction angle ϕ'_r is a function of particle size and that ϕ'_r decreases as the clay fraction (less than 0.002mm) increases.

During the tests, as the shear stress and normal stress increase, shearing begins to take place through

the asperities, dilation is inhibited and eventually the shear strength of the surface is controlled by shearing through the material high spots.

The disturbance in the orientation of particles on the shearing plane, after the first and subsequent reversals of the direct shear box, has an influence on the form of the plots of shear stress against displacement (Figure 3.a.4, 3.a.5, 3.a.IO, 3.a.II) and it is possible that subsequent travels of the box start at a higher shear stress than that obtained at the end of the previous travel.

The reduction of the peak shear strength parameters in a direction co-planar with a fissure may be partly due to a higher natural moisture content noticed near to the fissure area by other authors. Initial dilations of an overconsolidated clay undergoing shearing can lead to local pore pressure reductions and moisture movements into the shear plane from the body of the surrounding clay.

The existence of strong "diagenetic bonds"(BJERRUM, 1967) easily justifies the significant difference between the peak and the residual shear strength characteristics of the intact samples.

In Figure 3.a.I8 the shear stress increases rapidly in relation to the strain and reaches the highest value at about 7% strain. The pore water pressure also increases rapidly and approaches the highest values at about 3.5% strain. After this value the pore water decreases as the failure state is approached, and this is the characteristic behaviour of an overconsolidated clay.

TABLE 5.a.1

Results of undrained (at a rate of displ. of 0.375mm/min) consolidated shear box tests (LONDON CLAY)

	Peak values		Residual values	
	Normal Stress kN / m²	Shear Stress kN / m²	Normal Stress kN / m²	Shear Stress kN / m²
Intact samples	431	250	431	71
	641	302	641	105
	520	306	520	86
	570	285		
Fissured samples	400	205	400	92
	521	196	521	90
	435	209	435	103
	570.9	267	570.9	151
	641	251	641	130
	450	212	450	102

	Peak values		Residual values	
	$\hat{C}$ kN / m²	$\hat{\phi}$	C_r kN / m²	ϕ_r
Intact samples	167	12.5°	0	9.5°
Fissured samples	106	15°	16	11°

TABLE 3.a.2

Drained (at a rate of displ. of 0.005mm/min) consolidated shear box test results (LONDON CLAY)

	Peak values		Residual values	
	Normal Stress kN /m²	Shear Stress kN / m²	Normal Stress kN / m²	Shear Stress kN / m²
Intact samples	570.9	266	570.9	107
	641.5	271	641.5	153
	400	189	400	82
Fissured samples	435.1	164	435.1	114
	521.3	175	521.3	123
	641	230	641	162
	580	210	580	145

	Peak values		Residual values	
	$\hat{c}$ kN/ m²	$\hat{\phi}$	c_r kN / m²	ϕ_r
Intact samples	48.1	20°	0	11.5°
Fissured samples	11.5	18.5°	5	13.5°

TABLE 3. a. 5

Results of Undrained (at a rate of strain of 1.5% per minute) triaxial compression tests (LONDON CLAY)

	Peak values		Residual values	
	Normal Stress kN / m^2	Shear Stress kN / m^2	Normal Stress kN / m^2	Shear Stress kN / m^2
Intact samples	762	344		
	987	392		
	1125	404		
Fissured samples	551	260	520	238
	642	314	631	269
	725	290	712	270
	790	322	781	286
	875	315	850	275

	Peak values		Residual values	
	$\hat{C}$ kN / m^2	$\hat{\phi}$	C_r kN / m^2	ϕ_r
Intact samples	217	9.5		
	C_u = 325kN / m^2			
Fissured samples	193	8.5°	184	7°

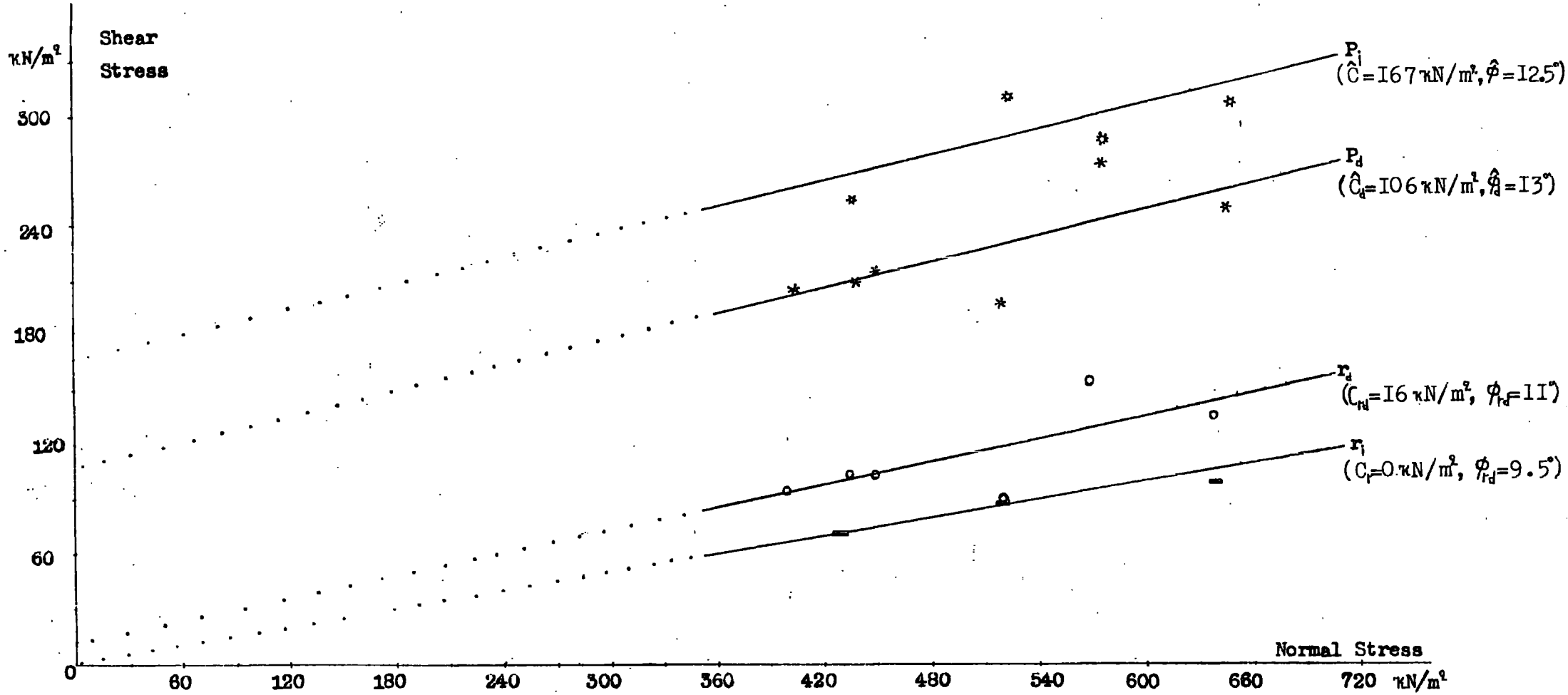

P_i : Peak value envelope for intact clay

P_d : Peak value envelope for fissured clay

r_i : Residual value envelope for intact clay

r_d : Residual value envelope for fissured clay

Fig. 3.a.1. Results of "Undrained" (at a rate of displacement of 0.375mm/min.) consolidated shear box tests (LONDON CLAY)
Comparison of shear strength along fissures with that of intact clay

Fig. 3.a.2. Drained (at a rate of displ. of 0.005mm/min.) consolidated shear box test results (LONDON CLAY)

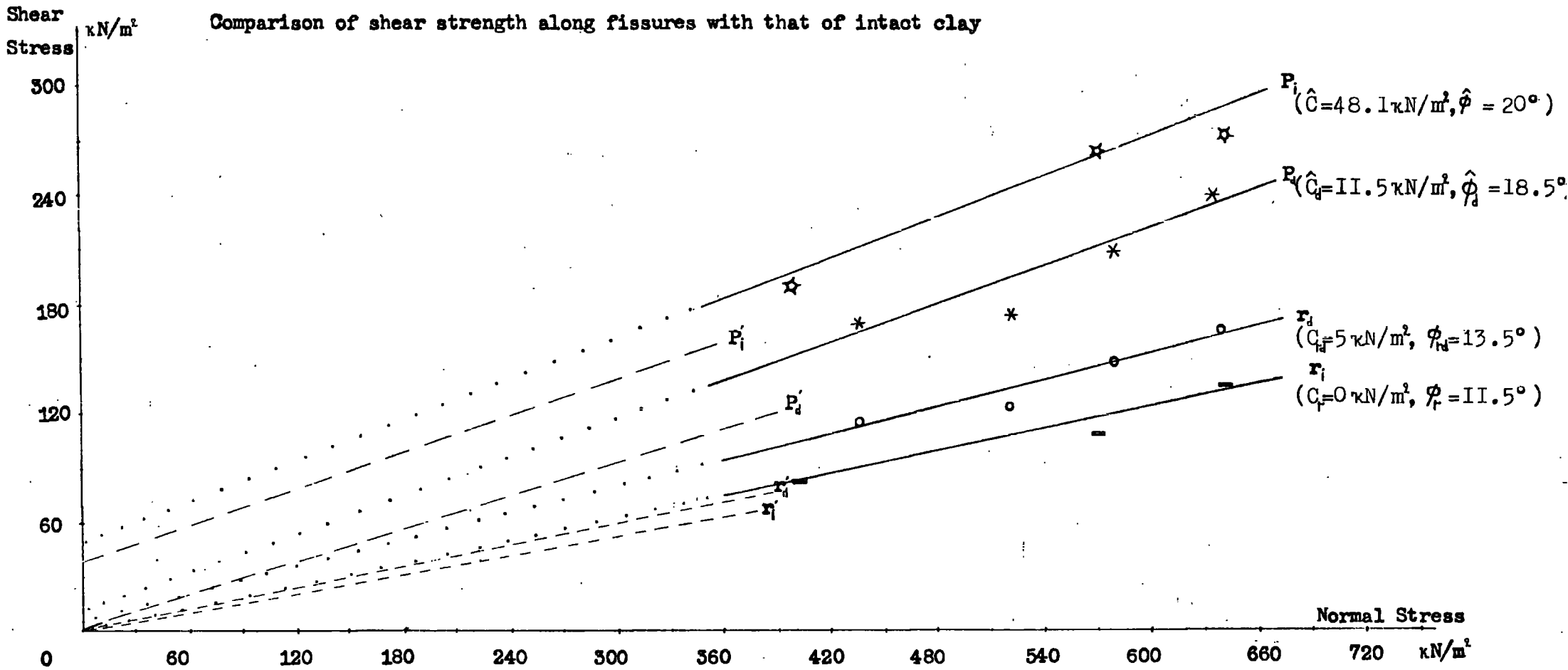

P_i : Peak value envelope for intact clay

P_d : Peak value envelope for fissured clay

r_i : Residual value envelope for intact clay

r_d : Residual value envelope for fissured clay

— — Test results, obtained by K. AGARWAL(1967)on intact samples and along slip surfaces of London Clay at Wraysbury, for lower values of Normal stress (the rate of displ. is 0.00135 mm/min.).

Fig. 3.a.3. Results of Undrained (at a rate of strain of 1.5% per min.) triaxial compression tests (LONDON CLAY)

Comparison of shear strength along fissures with that of intact clay

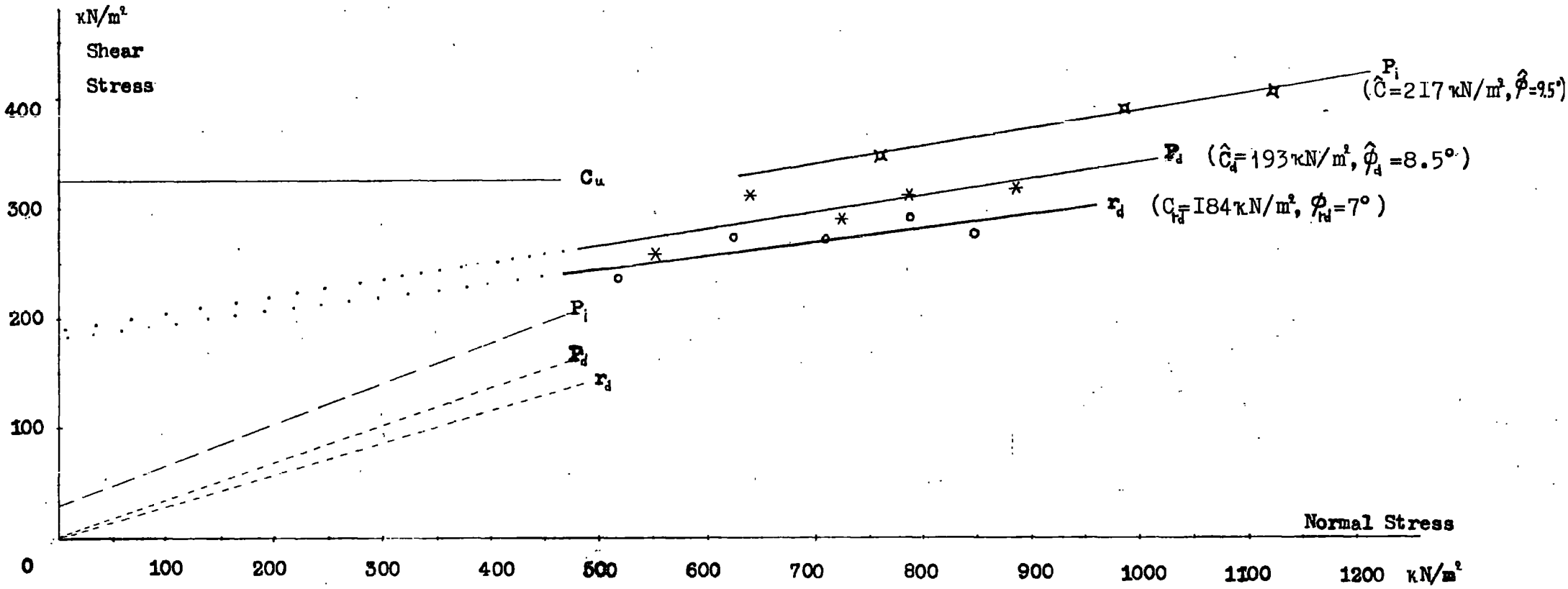

P_i : Peak value envelope for intact clay — C_u: Uniaxial compressive strength

P_d : Peak value envelope for fissured clay — r_d : Residual value envelope for fissured clay

— — — Test results, obtained by A.SKEMPTON and D.PETLEY(1967)on intact samples and on joints of London Clay at Wraysbury, for lower values of normal stress(Drained tests with rate of strain of 0.00367%per mi

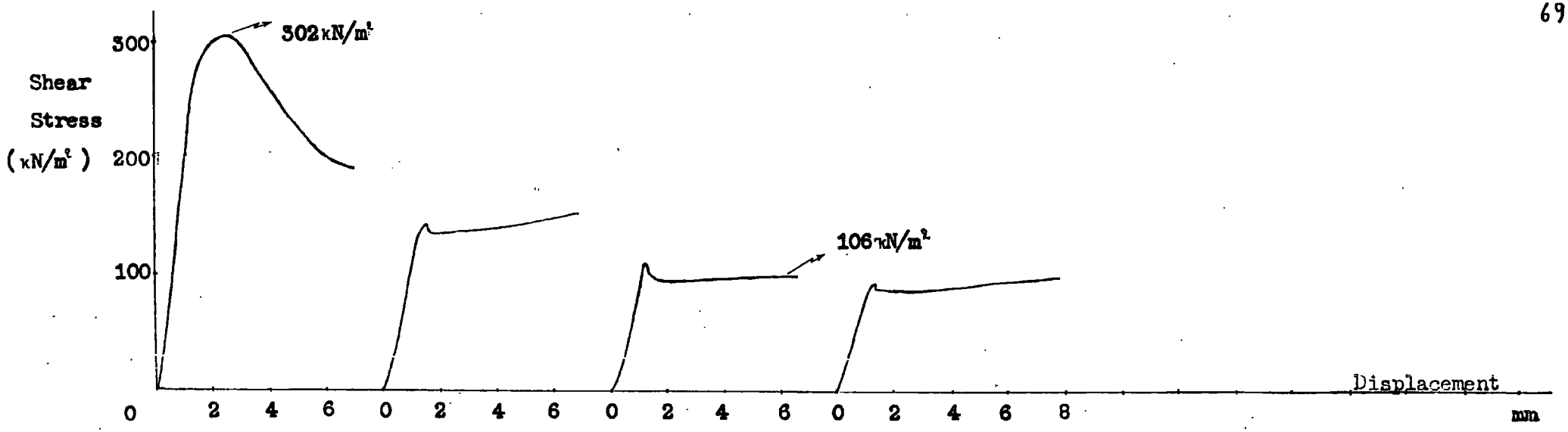

Fig. 3.a.4. Intact sample , σ_n=641kN/m²

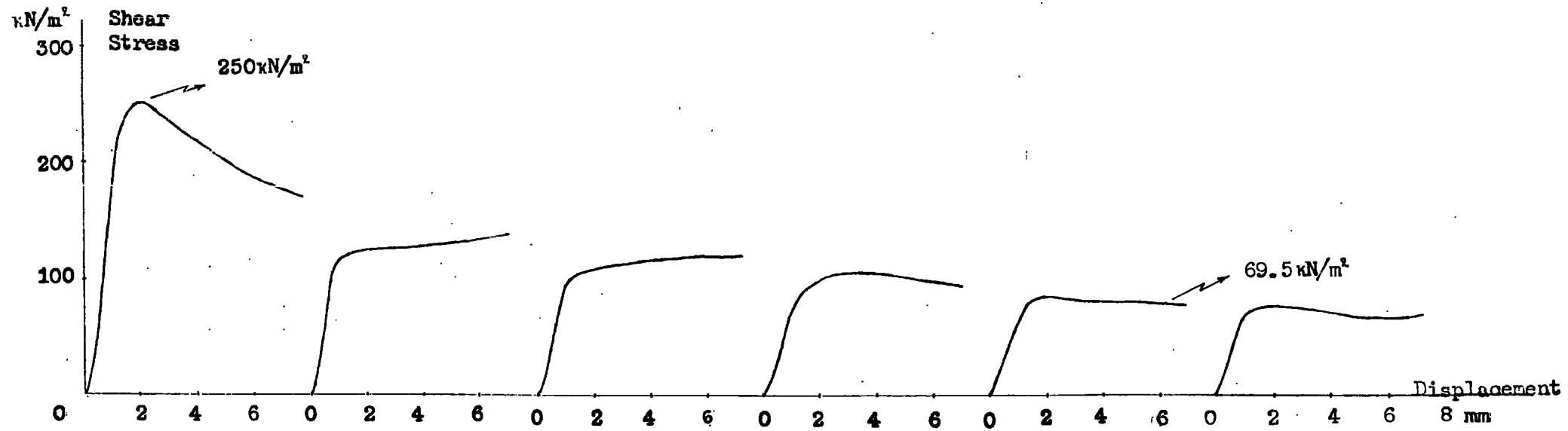

Fig. 3.a.5. Intact sample , σ_n= 431kN/m²

CONSOLIDATED UNDRAINED SHEAR BOX TESTS

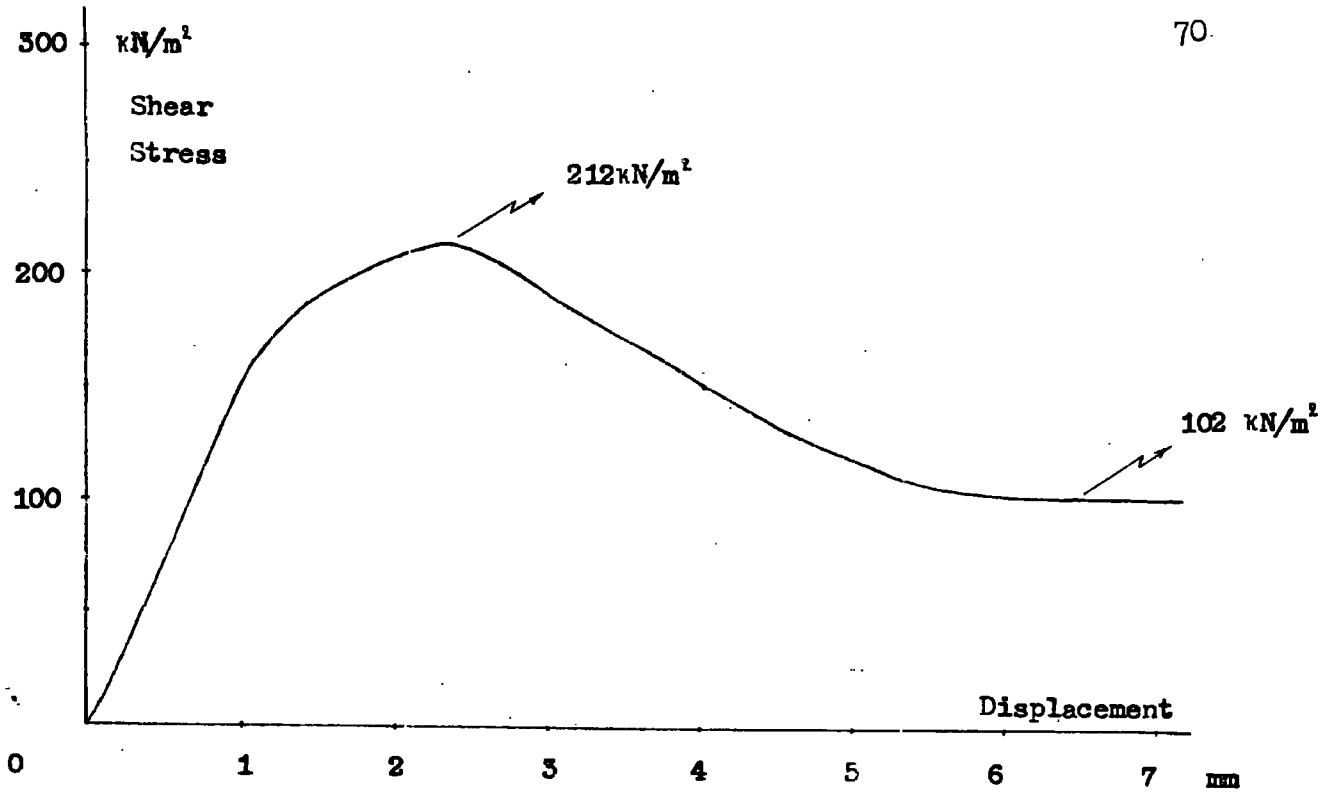

Fig. 3.a.6. Fissured sample, Subplanar discontinuty, σ_n= 450 kN/m²

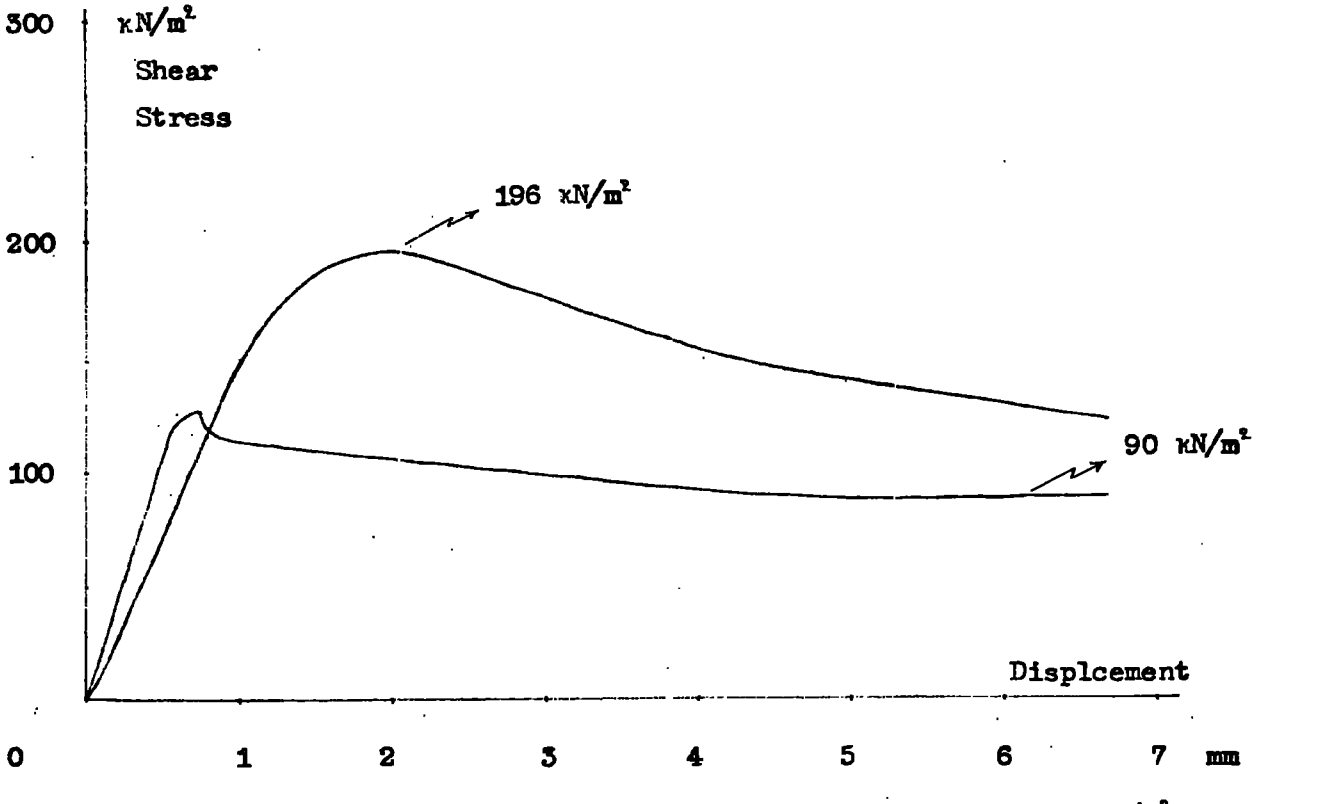

Fig. 3.a.7. Fissured sample, planar discontinuity, σ_n=521 kN/m²

CONSOLIDATED UNDRAINED SHEAR BOX TESTS

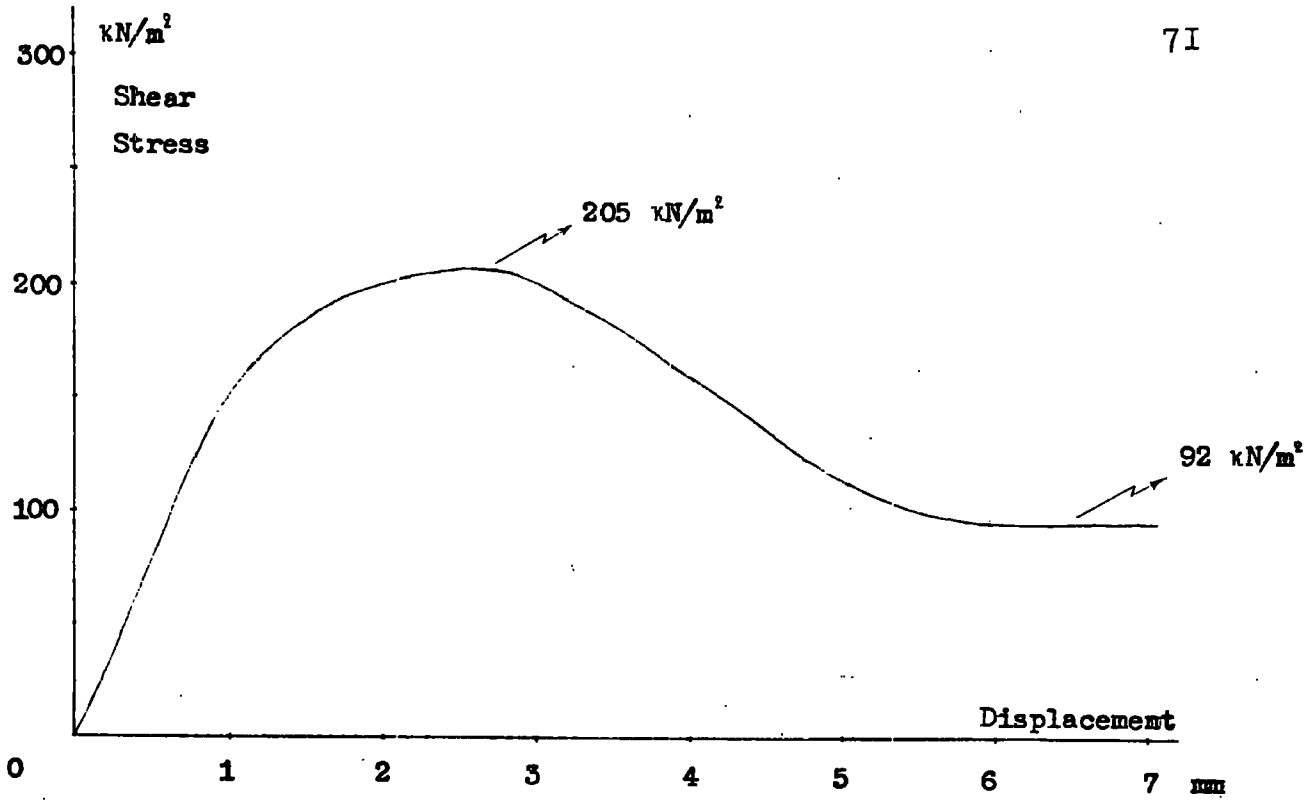

Fig. 3.a.8. Fissured sample, Planar discontinuity, σ_n= 400 kN/m²

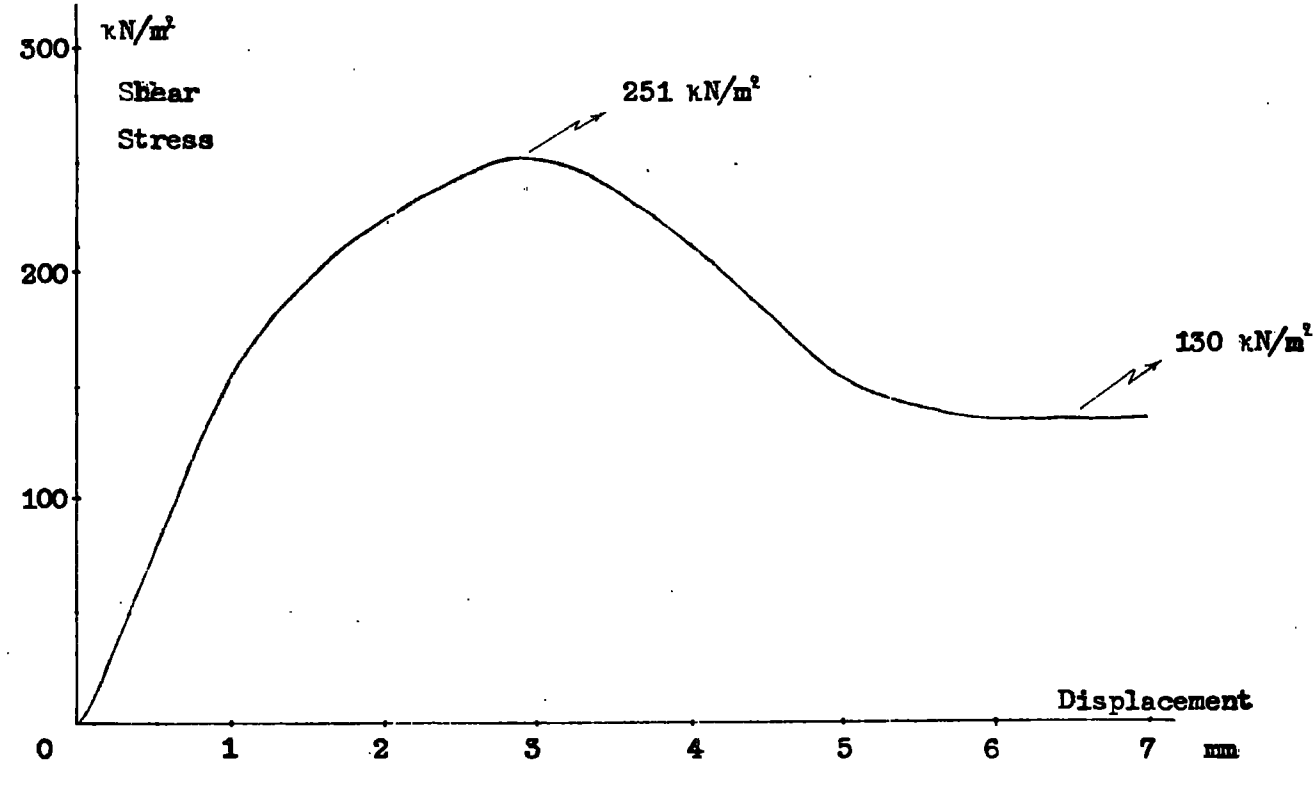

Fig. 3.a.9. Fissured sample, Subplanar discontinuity, σ_n= 641 kN/m².

CONSOLIDATED UNDRAINED SHEAR BOX TESTS

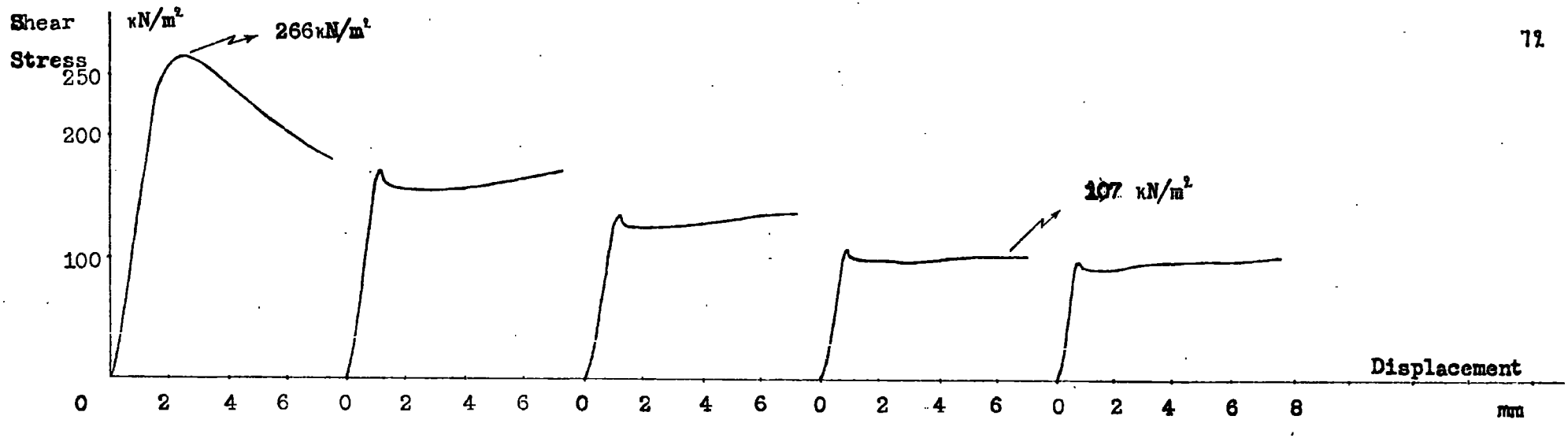

Fig. 3.a.10. Intact sample , σ_n= 570.9 kN/m²

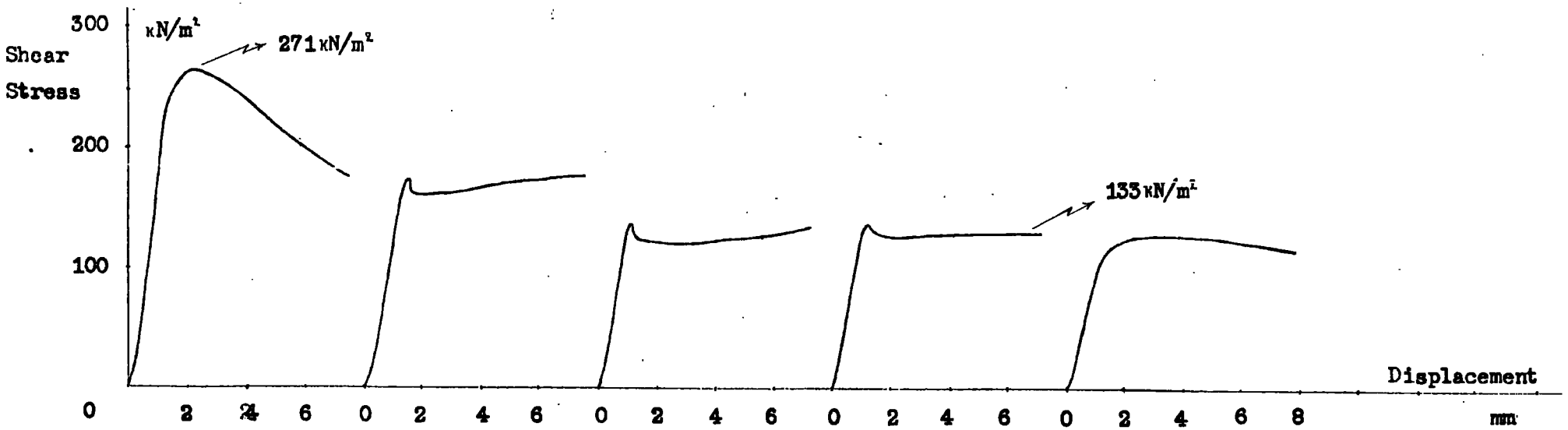

Fig. 3.a.11. Intact sample , σ_n= 641.5 kN/m²

CONSOLIDATED DRAINED SHEAR BOX TESTS

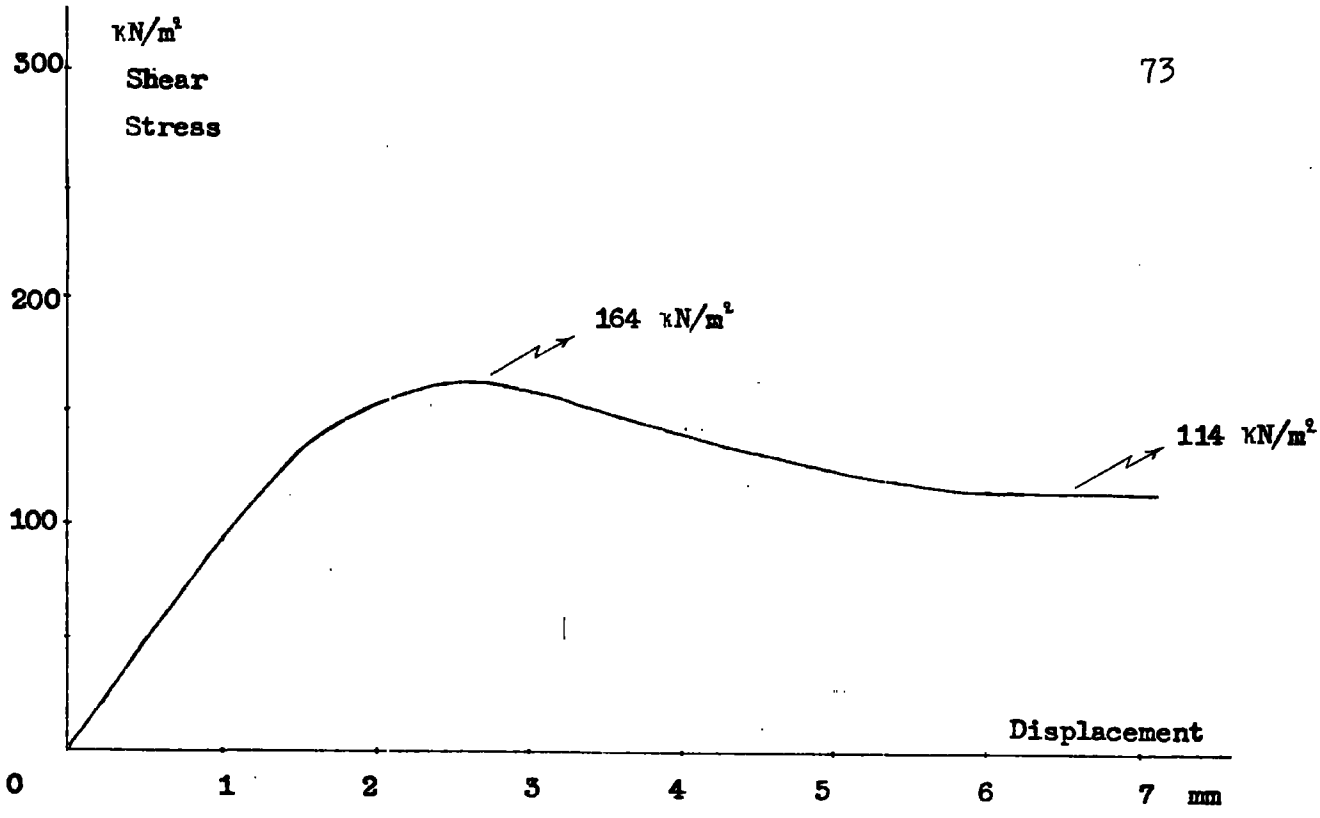

Fig. 3.a.12. Fissured sample, Planar discontinuity, σ_n=435.1 kN/m²

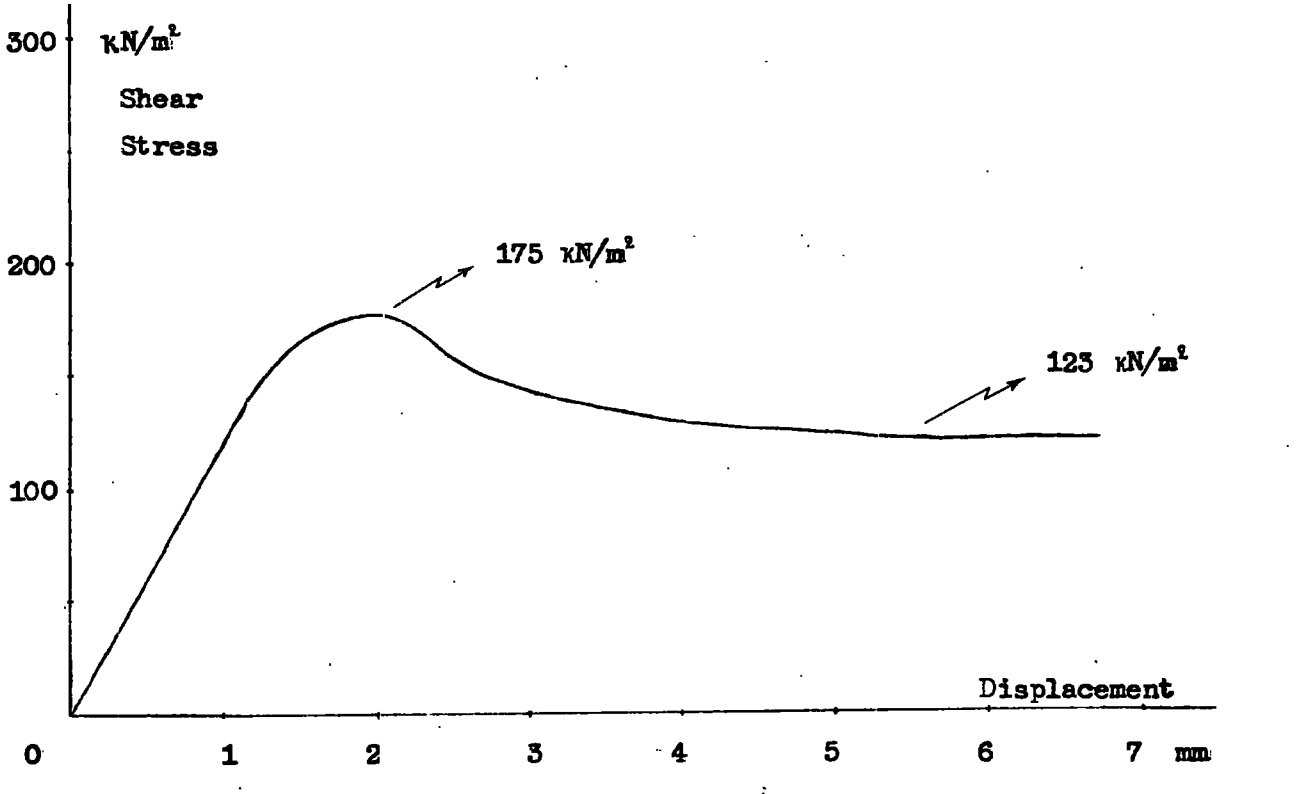

Fig. 3.a.13. Fissured sample, Subplanar discontinuity, σ_n=521.3 kN/m²

CONSOLIDATED DRAINED SHEAR BOX TESTS

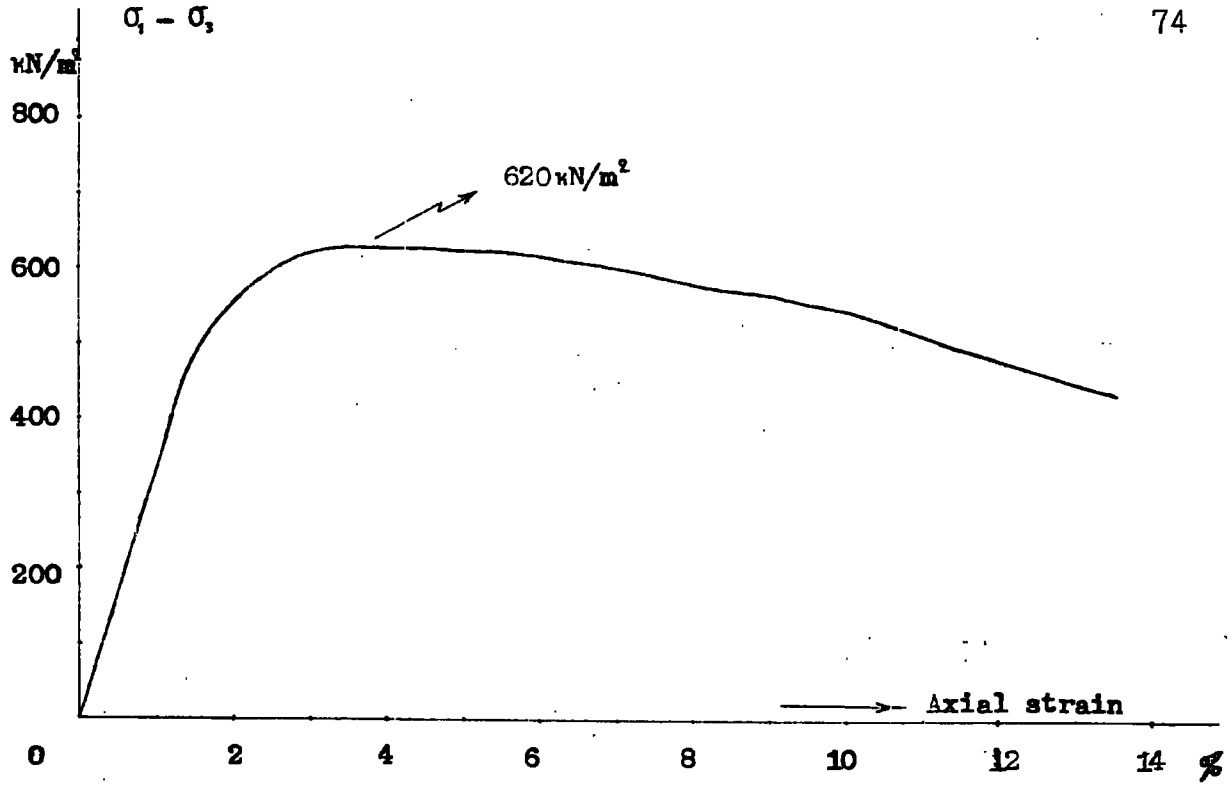

Fig. 3. a. 14. Intact sample , σ_n = 600 kN/m²

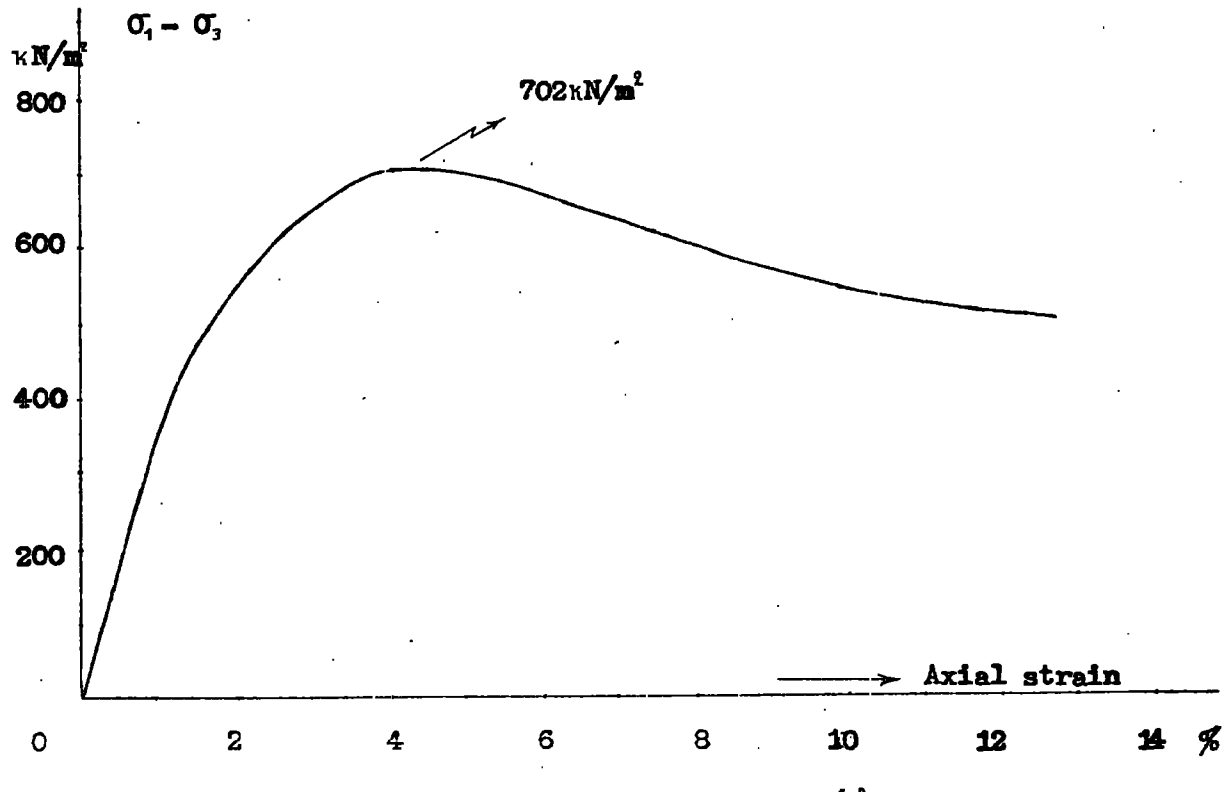

Fig. 3. a. 15. Intact sample , σ_n = 700 kN/m²

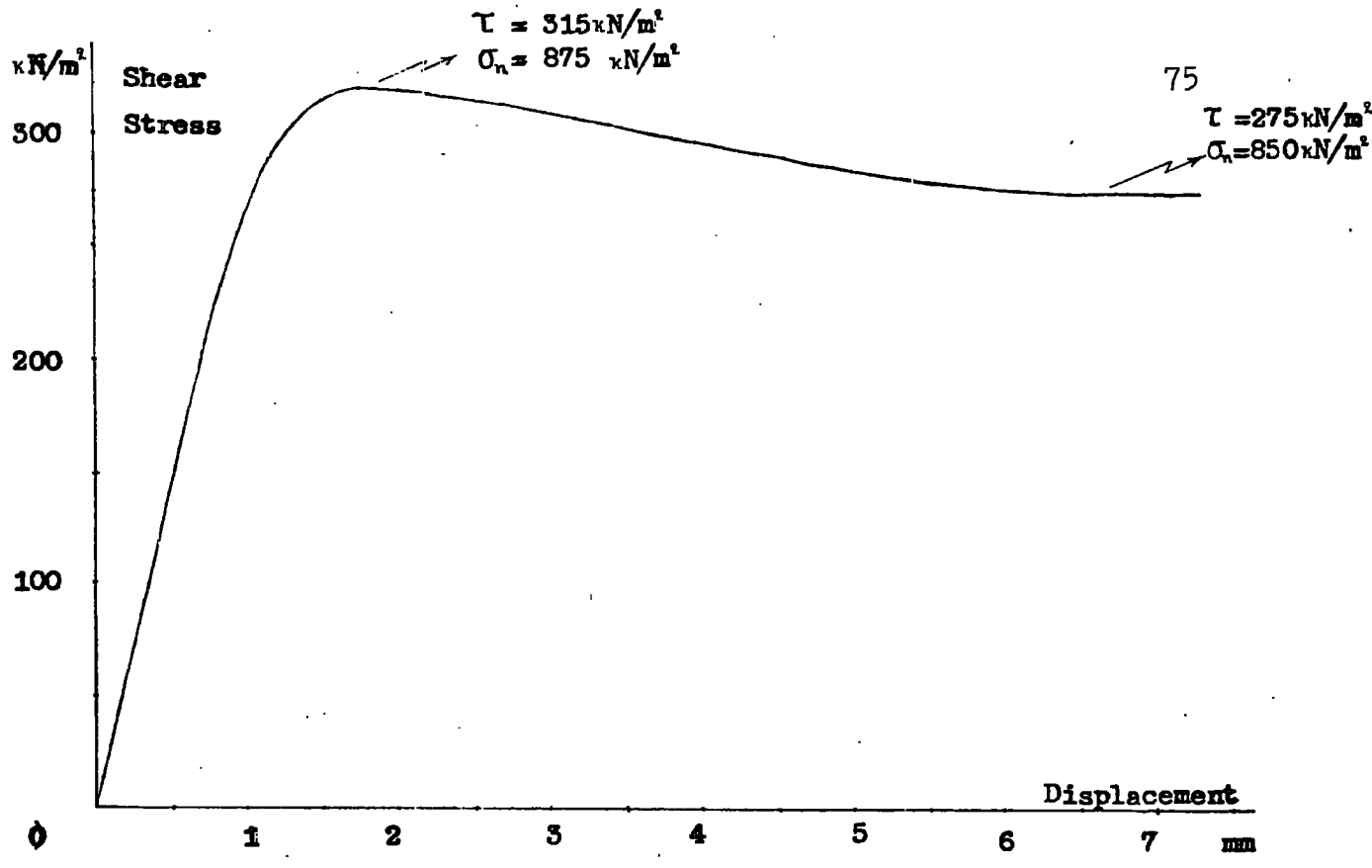

Fig. 3. a. 16. Fissured sample , Subplanar discontimuity

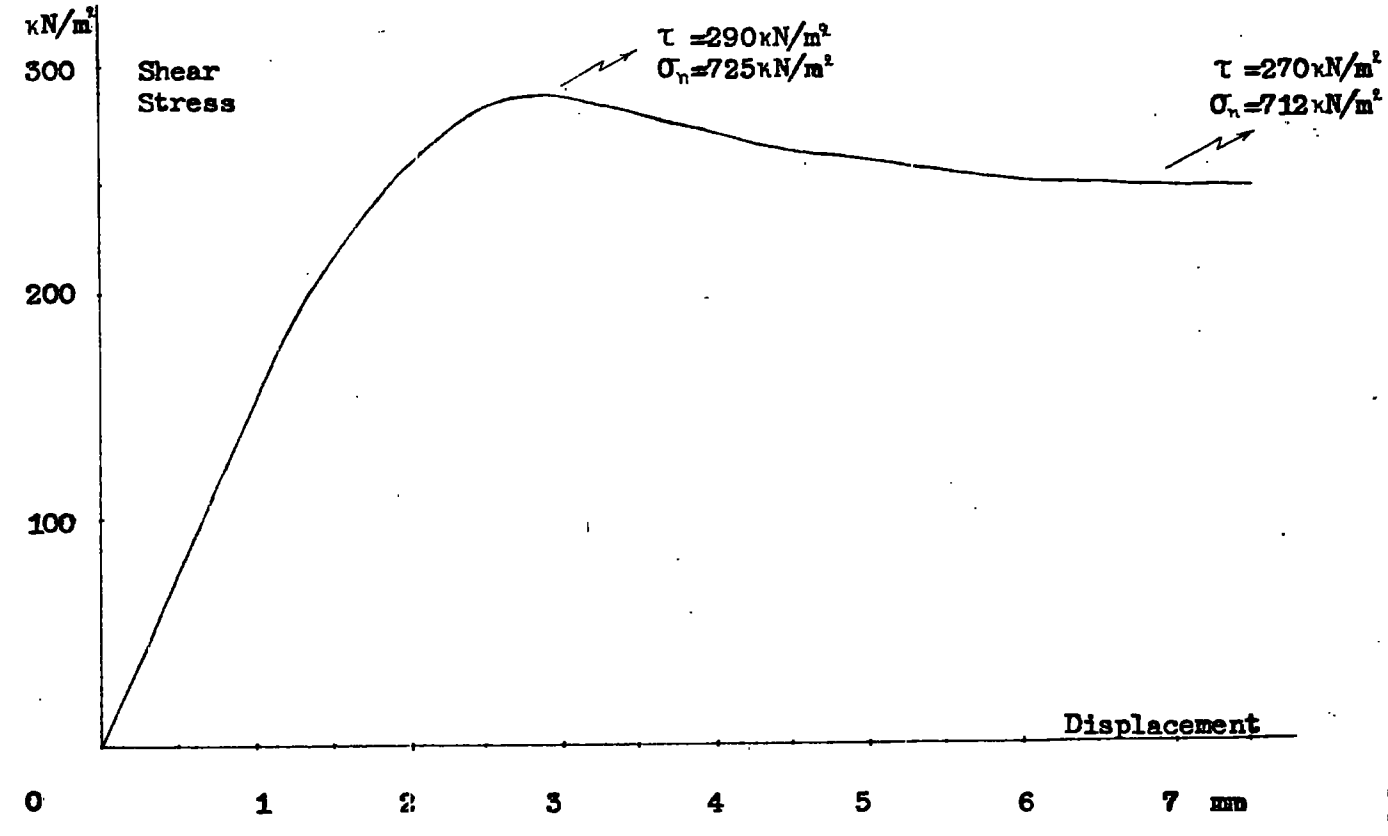

Fig. 3. a. 17. Fissured sample , Subplanar discontinuty

Fig. 3. a. 18. UNDRAINED TRIAXIAL COMPRESSION TEST WITH PORE WATER PRESSURE MEASUREMENTS

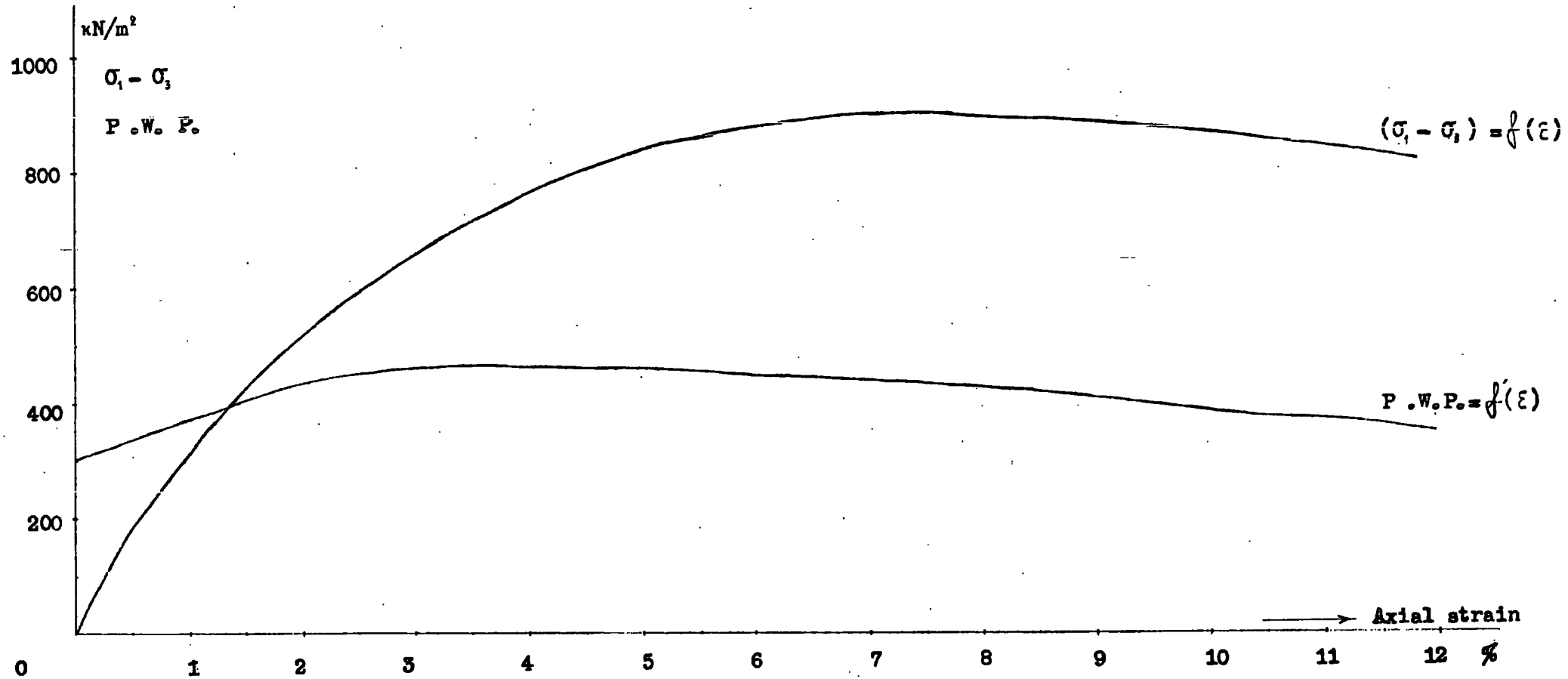

σ_3 = 600 kN/m²

Back pressure = 300 kN/m²

$$A = \frac{\Delta u}{\Delta \sigma_1} = 0.175$$

C H A P T E R 4th

4. THE SHEAR STRAIN ENERGY CRITERION AND ITS APPLICATION TO LONDON CLAY DISCONTINUITIES IN THE CASE OF THE FLEET LINE TYNNEL, LONDON TRANSPORT

4.a. Theoretical approach

The effect of the stress system on brittle fracture has been actively studied in recent years.

If σ_1, σ_2, σ_3 are the principal stresses acting upon a solid element, then in principal space the points (σ_1, σ_2, σ_3), which represent different states of stress just necessary to produce failure might form a surface:

$$\sigma_1 = f\ (\sigma_2, \sigma_3) \qquad \text{equ. 4.a.1}$$

The original and foundamental problem is the study of the shape of this surface.

In rocks en masse the existence of large-scale structural discontinuities has a large influence on the shape of that surface, resulting in an analysis of increased complexity.

In the simple case of brittle or semi-brittle materials (rocks, stiff fissured clays) the complete strain-stress curve may be used to distinguish three regions of the material behaviour when the state of stress is increasing.

Figure 4.a.1. shows the relationship between the principal stress σ_1 and the corresponding strain ε_1. In that figure the first region is an elastic region where the strain increases almost linearly with the stress. In the second region, the

slope of the strain-stress curve decreases with stress but remains positive. In both these cases the complete strain-stress curves imply stability and the material behaviour is regarded as a fundamental property of that material. In the third region, the slope of the strain-stress curve becomes negative and the region is potentially unstable. If the "failed" material yields there is a decrease in the applied stress and if these reductions are more pronounced than the slope of the strain-stress curve, the material is in stable equilibrium with the stress. This situation usually exists in the materials in the vicinity of the surface of most underground excavations. If the stress decreases less rapidly than the slope of the strain-stress curve, violent failure will take place. In this case the problem is to determine the point at which potentially "unstable" failure starts.

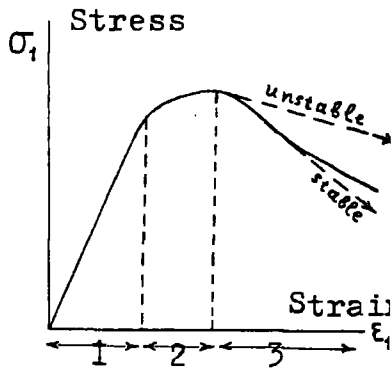

Fig. 4.a.1

The first fracture theories were based on empirical data. They either assumed that fracture will occur if a specific tensile stress is exceeded or they related the fracture process to the increase of the minor principal stress.

A. GRIFFITH (1924) developed a fracture theory for brittle materials, based upon the assumption that fracture begins at small inherent discontinuities, such as cracks. According to OROWAN's (1949) interpretation of GRIFFITH's theory, these cracks produce a tensile stress concentration at which the stress might reach the theoretical tensile strength

of the material, even though the applied stress is at a far lower level.

The first simplification is that the GRIFFITH solution is the two-dimensional solution of a three-dimension problem. Also, the cracks are assumed to be very flat elliptical openings (which remain open and unchanged until fracture occurs), subject to a tensile stress field and having a random orientation distribution.

Figure 4.a.2. shows the stresses acting upon a crack which is inclined at an angle Θ to the direction of the major principal stress σ_1. The tangential stress σ_t around the boundary of the crack (the tensile stress which is assumed to cause fracture near the tip of the crack) was determined by C.INGLIS(1913).He found the stress in terms of the elliptical coordinates ξ and n. The coordinate ξ characterizes the sharpness of the elliptical crack and the coordinate n designates a point on the surface of the crack. These are transformed to the cartesian system (x,z) as follows

$$x = c \sinh\xi \sin n , \qquad z = c \cosh\xi \cos n \qquad \text{equ.4.a.2}$$

For a flat crack ξ_o (the value of ξ on the crack boundary) and n are small and the tangential stress near the crack tip is:

$$\sigma_t = \frac{2(\xi_o \sigma_z - n\tau_{xz})}{\xi_o^2 + n^2} \qquad \text{equ. 4.a.3}$$

Differentiating 4.a.3. with respect to n, equating $\frac{\partial \sigma_t}{\partial n}$ to zero and substituting these values of n into 4.a.3. we obtain the maximum and minimum tangential stress:

$$\sigma_t \xi_o = \sigma_z \pm (\tau_{xz}^2 + \sigma_z^2)^{\frac{1}{2}} \qquad \text{equ. 4.a.4}$$

In this equation, the negative sign gives σ_t negative and this is the maximum tensile stress which causes fracture. This equation in terms of the principal stresses becomes:

$$\sigma_t = \frac{[(\sigma_1 + \sigma_3) - (\sigma_1 - \sigma_3)\cos 2\theta] \pm [(\sigma_1^2 + \sigma_3^2) - 2(\sigma_1^2 - \sigma_3^2)\cos 2\theta]^{\frac{1}{2}}}{2\xi_0}$$

equ. 4.a.5

By differentiating 4.a.5 with respect to θ and letting $\frac{\partial \sigma_t}{\partial \theta} = 0$, the critical crack orientation is found :

$$\cos 2\theta_{crit} = -\frac{\sigma_1 - \sigma_3}{2(\sigma_1 + \sigma_3)} \qquad \text{equ. 4.a.6}$$

This equation is meaningful when

$|\cos 2\theta| < 1$ which requires $\sigma_1 + 3\sigma_3 > 0$

If $\frac{\sigma_3}{\sigma_1} = K_o$ then from equation 4.a.6 becomes $K_o \geqslant -0.33$

If $K_o = -0.33$ equation 4.a.6 becomes

$$\sigma_t = \frac{2\sigma_3}{\xi_0} \qquad \text{equ. 4.a.7}$$

This means that the fracture depends upon the magnitude of σ_3 only.

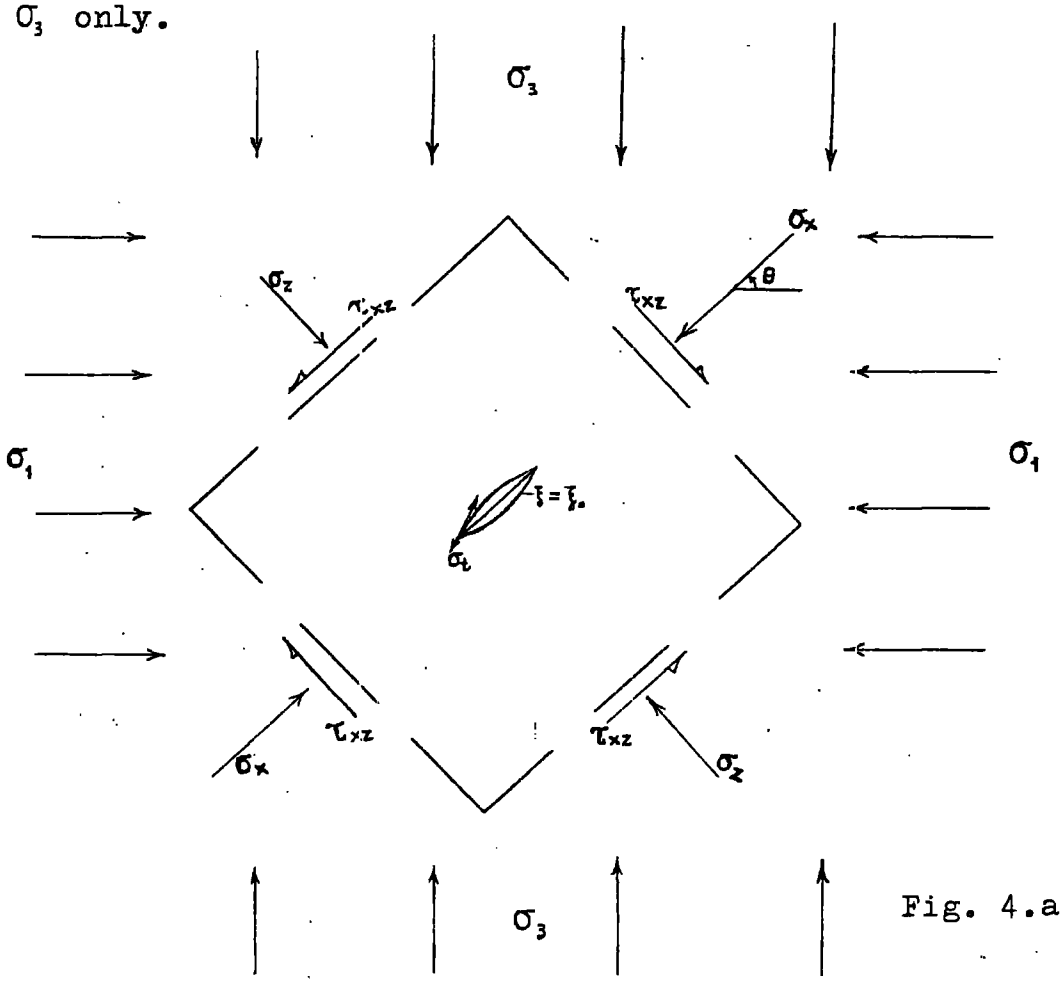

Fig. 4.a.2

Now it is assumed that fracture takes place when:

$$\sigma_3 = -T_o \qquad \text{equ.4.a.8}$$

where T_o is the uniaxial tensile strength of the material. Consequently, the maximum tangential stress σ_t at fracture takes a value characteristic of the material.

If $K_o > -0.33$ $(\sigma_1 + 3\sigma_3 > 0)$ then substituting equation 4.a.6. into equation 4.a.5. and equating $\sigma_t = \frac{2T_o}{\xi}$ we obtain:

$$(\sigma_1 - \sigma_3)^2 - 8T_o(\sigma_1 + \sigma_3) = 0 \qquad \text{equ. 4.a.9}$$

which constitutes with equation 4.a.8. the GRIFFITH criterion for fracture.

The above criteria are applicable only if the σ_z is tensile.

F. McCLINTOCK and J. WALSH(I962) modified the GRIFFITH fracture theory by assuming that the crack under normal compressive stress can close after which it will begin to carry shear stress due to friction along its faces.These normal and shear stresses will increase the strength of the rock by reducing the stress concentration at the end of the crack.

Also, the fluid pressure (pore pressure) in a partially closed crack will affect the stresses at the tip of the crack.

For the following analysis the case of an initially closed crack is of greatest importance. In that case,when the stress σ_z becomes compressive, a normal stress $\sigma_n = \sigma_z$ will act upon the surface of the crack. Consequently, a frictional shear resistance τ will occur

$$\tau = \mu \sigma_n \qquad \text{equ. 4.a.I0}$$

where μ is the coefficient of friction.

The shear stress τ_{xz} can only induce tensile stress at the crack tip when $\tau_{xz} > \mu\sigma_n$ Therefore, the effective shear stress inducing tensile stress on the crack is

$$\tau_{xz} - \mu\sigma_n = \tau' \qquad \text{equ. 4.a.11}$$

The tangential stress σ_t on the boundary of a closed crack due to the above shear stress is given by a similar form to equation 4.a.3 :

$$\sigma_t = \frac{2n(\tau_{xz} - \mu\sigma_n)}{\xi^2 + n^2} \qquad \text{equ. 4.a.I2}$$

With the same process as we used in calculating equation 4.a.4. we obtain the maximum and minimum stress on the boundary of the crack:

$$\sigma_t = \pm \frac{\tau_{xz} - \mu\sigma_n}{\xi_o} \qquad \text{equ. 4.a.I3}$$

In this equation, the negative value is taken because the tensile stress is producing an elongation of the crack. In terms of the major principal stress and the ratio K_o, this equation becomes:

$$\sigma_t = \frac{-\{(1 - K_o)\sin 2\theta - \mu[(1 + K_o) - (1 - K_o)\cos 2\theta]\}}{2\xi_o}\sigma_1 \qquad \text{equ. 4.a.I4}$$

with the same process that was used in calculating equation 4.a.6. we found:

$$\tan 2\theta_{crit} = \frac{1}{\mu} \qquad \text{equ. 4.a.I5}$$

If again we equate the maximum tangential stress (equ. 4.a.I4) to $\frac{-2T_o}{\xi_o}$ we then obtain the fracture criterion for closed cracks:

$$\sigma_1 = \frac{-4T_o}{(1 - K_o)(1 + \mu^2)^{\frac{1}{2}} - \mu(1 + K_o)} \qquad \text{equ. 4.a.I6 .}$$

R.SACK(I946) extended GRIFFITH' s theory to the 3-dimentional showing that the most dangerous cracks lie in the plane of the intermediate principal stress.The GRIFFITH,COULOMB and MOHR criteria suggested that the strength of the rock is independent of the value of the intermediate principal stress.

K.MOGI and B.MANZANTI(I967) pointed out that the intermediate principal stress has a definite effect on the strength of the rock.

C.FAIRHURST and N.COOK(I966),in disagreement with the modified GRIFFITH theories,suggested that under normal compressive stress crack propagation takes place in a direction parallel to the direction of the greatest compressive stress.In that case progressively greater stress increments are necessary to produce continuous lengthening of the crack.Consequently (except the case of propagation in torsion), in order for fracture to occur,an increasing level of stress is required.

G.WIEBOLS and N.COOK(I968) developed a criterion based upon the assumption that failure occurs when the shear strain energy due to the closed cracks approaches a limiting value characteristic of the material. They considered an intact rock specimen with a large number of closed plane cracks uniformly distributed and randomly oriented.They calculated the quantity $|\tau|-\mu\sigma_n$ (equation 4.a.I0, 4.a.11) for each crack in the case of uniaxial, biaxial and polyaxial stresses ,and for all the cracks for which $|\tau|-\mu\sigma_n>0$ they obtained the shear strain energy (per

unit volume) which is stored around the cracks as a result of the sliding produced by the above stress state. When this shear strain energy reaches a constant value, failure will occur under any system of compressive stresses.

B. BRADY (1969) suggested that fracture occurs when a maximum value of volumetric strain is attained within the rock. This requires a large number of microcracks able to form a macroscopic fracture surface. The same crack distribution function was assumed as was assumed in the WEIBOLS and COOK criterion.

P. ATTEWELL and M. SANDFORD (1971, 1974) using an texture goniometer, found that the assumed random orientation of the cracks for the calculation of the shear strain energy is a rather special case. They indicated that each crystal face defines a small planar discontinuity (closed crack) along which localized shear movement can take place. The crack density distribution function was approximated by a series of associated LEGENDRE polynomials and, by the use of a digital computer, the limiting strain energy was calculated in the case of polyaxial compression. They concluded that the GRIFFITH theory suffices to describe the intrinsic strength anisotropy of the materials.

P. ATTEWELL and J. WOODMAN (1971), investigating the stability of a discontinuous rock under polyaxial stress, applied the criterion of shear strain energy to the large-scale structural discontinuities (fissures, joints, bedding planes). By the use of equal area projections they delimited potentially unstable zones in terms of the

COULOMB-NAVIER-MOHR criterion of failure. A computer programme was developed for the projection of the large-scale discontinuities and the calculation of shear strain energy. It was pointed out that the intermediate principal stress and the orientation density distribution of the large scale discontinuities exert a big effect on the stability of a discontinuous rock.

The following analysis deals with the application of the above criterion in the case of the Fleet Line tunnel.

4.b.General analysis on the application of the criterion.

As has already been stated, the Fleet Line tunnel is excavated in the stiff fissured, overconsolidated blue London Clay(Chapters 2.c, 3.a.)

S.PRIEST(I973) measured the orientation, size,shape and texture of numerous discontinuities in the clay surrounding a running tunnel during the excavation of one the Fleet Line station tunnels at Green Park. The tunnel surroundings were divided into one hundred and forty four curvilinear cells(Figure 4.b.I).One thousand five hundred and ninety eight discontinuities were measured around the tunnel, and the total number in each cell noted.The fissures were mainly planar(less than 20% were conchoidal), more rough than smooth in the texture and rarely more than I5cm in size.The number of the fissures per unit volume increases and the corresponding size decreases as the depth decreases.

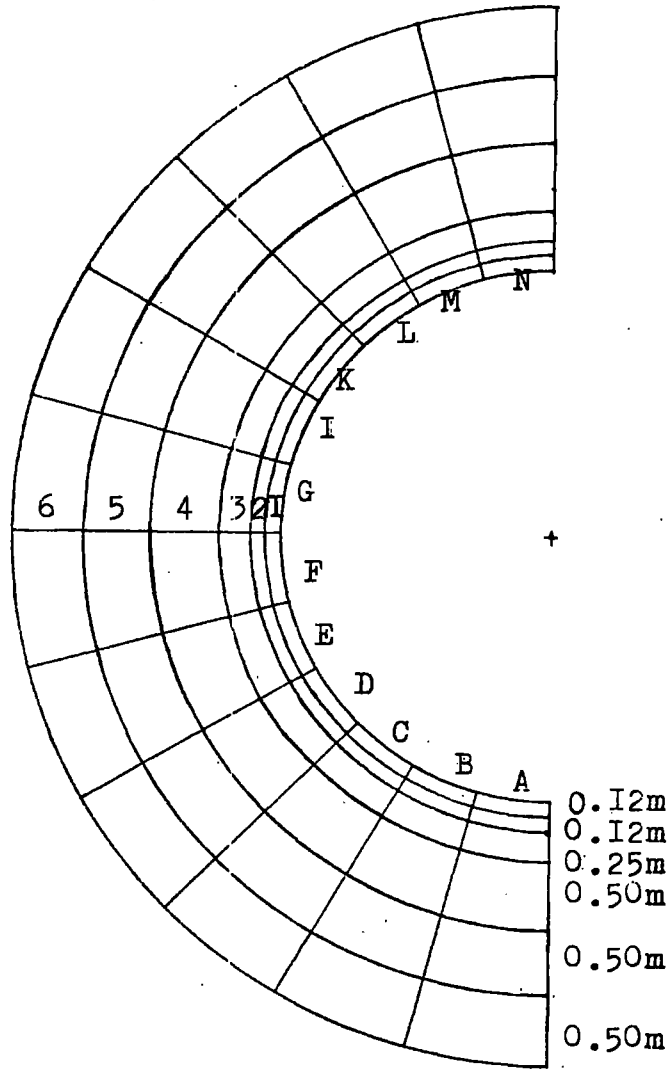

Fig. 4.b.I

N.PRICE(I966) suggested that shear discontinuities have a tendency to be planar, smooth and unaffected by local lithological changes,

while tensile ones tend to be more irregular and to follow minor lithological variations.

L.COOLING and A.SKEMPTON(I940)suggested that the fissures in the London Clay below a surface, remain closed, but when the clay is subjected to stress release(for example excavation), the removal of lateral restraint has the effect of opening many of the fissures and providing paths to moving groundwater.

Figure 4.b.2. shows a contour diagram of the poles to the discontinuities.Originally a point diagram was plotted using a SCHMIDT equal area net and projecting the upper hemisphere.Then a peripheral counter with a circle of one percent area was used and a contour diagram was plotted. This may be compared with a contour diagram plotted by the computer.From Figure 4.b.2. two major groups of fissures can be distinguished

i) A group of near horizontal, gently dipping fissures

ii) A group of steeply dipping fissures

The fabric of the fissures was plotted thousand times by the computer (Type IBM system 360/67) using a technique described by P.ATTEWELL and J.WOODMAN(I97I).Briefly, the theoretical process is as follows.

The probability distribution P(W,Y) of a subset of the fabric is a sum of generalized DIRAC delta functions (W is the latitude and Y is the azimuth of the discontinuity normals).The DIRAC delta function $\delta(x)$ has the following property

$$\int_{-\infty}^{\infty} \delta(x)\, dx = 1 \qquad \text{equ. 4.b.I}$$

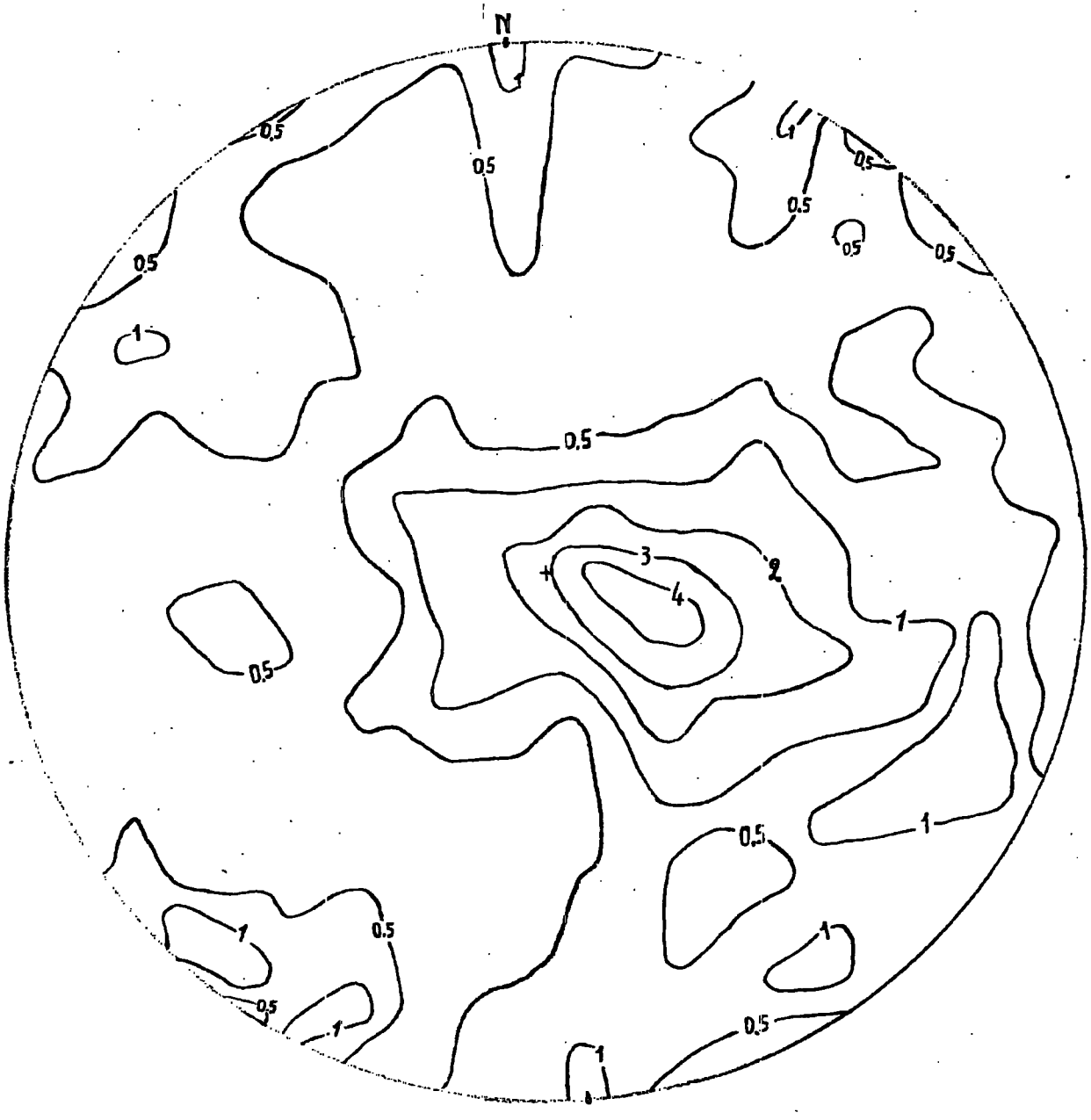

Figure 4 . b. 2. Contour diagram of the poles to the discontinuities of London Clay at Green Park Station.

For a two dimensional problem and especially for the case in which one element A(making an angle Θ_i with the OB) lies on the periphery(Fig.4.b.2),the probability of finding it at an angle Θ is

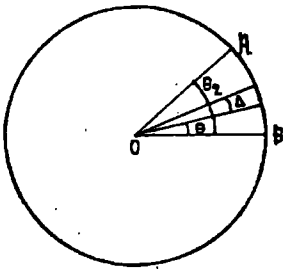

Fig. 4.b.3

$$P(\Theta) = \delta(\Theta - \Theta_i) \qquad \text{equ. 4.b.2}$$

or increasing the angle Θ at Δ degrees the probability will be

$$P(\Theta,\Theta+\Delta) = \int_{\Theta}^{\Theta+\Delta} P(\Theta)\, d\Theta = \int_{\Theta}^{\Theta+\Delta} (\Theta-\Theta_i)d\Theta = \begin{cases} I & \Theta_i \in (\Theta,\Theta+\Delta) \\ 0 & \Theta_i \notin (\Theta,\Theta+\Delta) \end{cases}$$

equ. 4.b.3

In the case of the sphere of projection, the probability of finding one pole $E_i(W_i,Y_i)$of the discontinuity normal at $E(W,Y)$ is

$$P(W_i, Y_i) = \delta(W - W_i)\delta(Y - Y_i) \frac{1}{\sin W_i} \qquad \text{equ. 4.b.4}$$

or increasing the angles W,Y at Δ degrees we obtain

$$P(Y,Y+\Delta Y\ ;\ W,\ W+\Delta W) = \int_{W}^{W+\Delta W} dW \int_{Y}^{Y+\Delta Y} dY\ \sin Y\ P(W,Y) =$$

$$= \begin{cases} 1 & \text{if } \begin{cases} W_i \in (W,W+\Delta W) \\ Y_i \in (Y,Y+\Delta Y) \end{cases} \\ 0 & \text{otherwise} \end{cases} \qquad \text{equ. 4.b.5}$$

The probability distribution of N poles is

$$P(W,Y) = \frac{1}{N}\sum_{i=1}^{N}\delta(W - W_i)\ \delta(Y - Y_i)\ \frac{1}{\sin W_i} \qquad \text{equ. 4.b.6}$$

and over the sphere $= \int_{\text{sphere}} P(W,Y)\ \sin W\ dW\ dY = 1$

equ. 4.b.7

In order to smooth out the delta function in some way, a small circular area a_o is allocated at each pole and a new function S(W,Y) is defined,which is strongly peaked at $W = W_i$, $Y = Y_i$ and is non-zero at $W \neq W_i, Y \neq Y_i$. It has the following properties:

$\int_G S\,dG_1 = qa_o$ if G_1 wholly includes a_o

$=qaf$ if G_1 partly includes a_o $(0 < f < I)$ equ. 4.b.8

$= 0$ if G_1 excludes a_o

then $P(W,Y) = \sum_{i=1}^{N} S(W,Y\ ;\ W_i\ ,\ Y_i)$ equ. 4.b.9

and consequently

$$\int_{sphere} P(W,Y)\ \sin W\ dW\ dY =$$

$$= \sum_{i=1}^{N} \int S(W,Y\ ;\ W_i\ ,\ Y_i)\ \sin W\ dW\ dY \cong qa_oN \qquad \text{equ. 4.b.IO}$$

Defining q and a_o (a_o usually represents one percent area), finding P(W,Y) for each location on the upper hemisphere of the sphere and using matrix calculus, an equal area projection is obtained showing the probability density of the fissures (example projection and projections 1 to 96).

4.c. Delimitation of potentially unstable orientation zones.

The clay around the tunnel was divided into three hundred and sixty elements (Fig. 4.c.I).A unit thickness of the elements and, initially, a uniform distribution of discontinuities in each element is assumed.The equal area projections of these discontinuities are plotted for all the elements around the tunnel.

The state of stress upon each element is calculated by the equations 2.c.5.,2.c.6. ,2.c.7.On the projections 1 to 96 the directions of the principal stresses $\sigma_1, \sigma_2, \sigma_3$ of each element are denoted by the symbols P,Q,R respectively, while the symbols X(north), Y(west) and Z (vertical) denote the global axes.

A preliminary assesment of the potentially unstable zones is obtained applying the COULOMB-NAVIER-MOHR criterion for failure for each discontinuity.

The normal and the shear stress upon each discontinuity was calculated by the equations

$$\sigma_n = l^2 \sigma_1 + m^2 \sigma_2 + n^2 \sigma_3 \qquad \text{equ. 4.c.1}$$

$$\tau^2 = l^2 \sigma_1^2 + m^2 \sigma_2^2 + n^2 \sigma_3^2 - \sigma_n^2 \qquad \text{equ. 4.c.2}$$

where l,m,n are the direction cosines of the normals to the discontinuities.

According to the above criterion shear movement occurs along a discontinuity when the shear stress exceeds a limiting value given by the equation

$$|\tau_{crit}| = c_d + \sigma_n \tan\phi_d \qquad \text{equ. 4.c.3}$$

where c_d, ϕ_d are the shear strength parameters of the

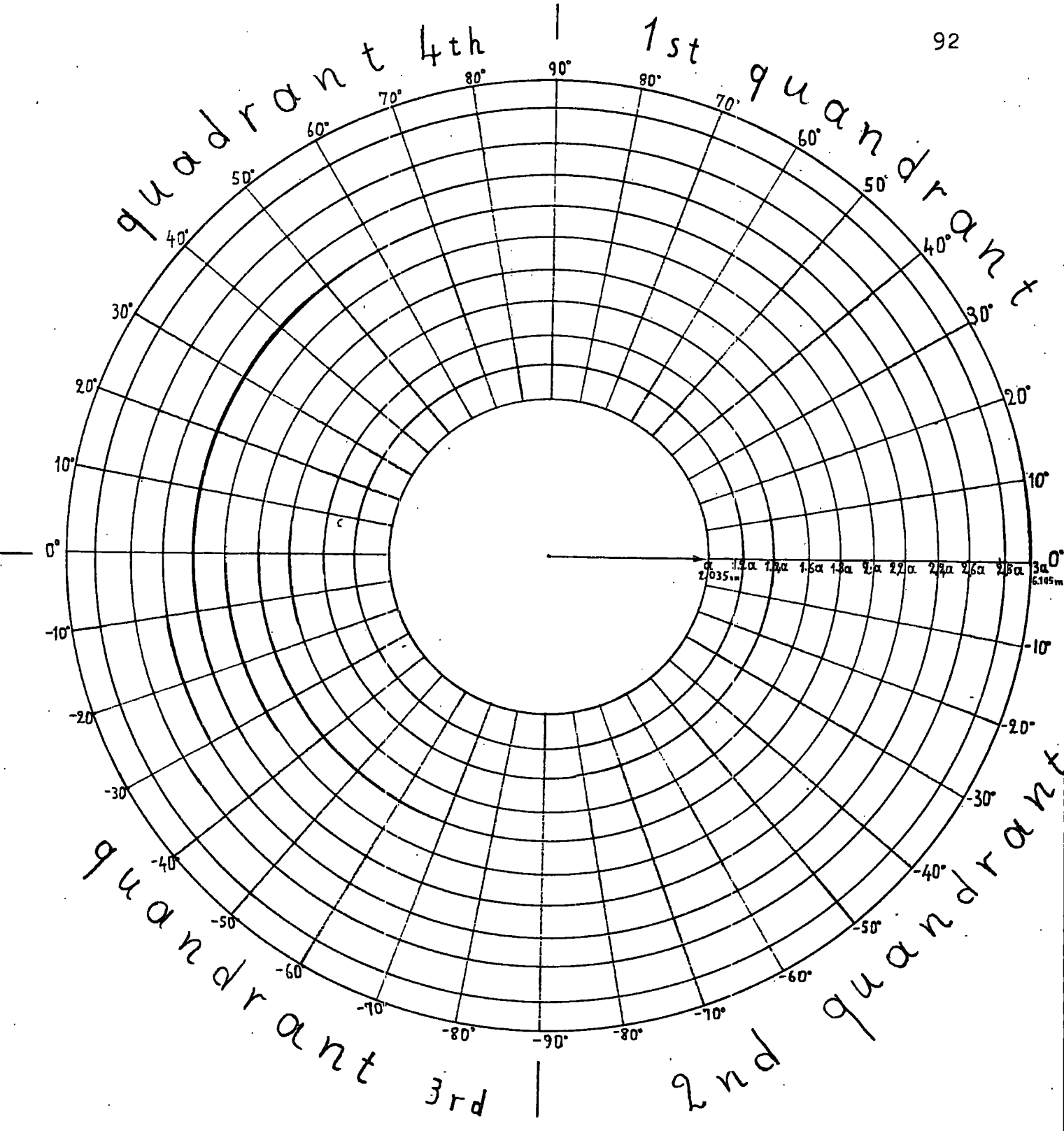

Figure 4.c.1. Division of the clay around the tunnel into elements.

discontinuity which approach the corresponding parameters of the intact material (Chapter 3).For every assumed discontinuity for which the inequality $|\tau| > \sigma_n \tan\varphi_d + c_d$ (equations 4.a.IO,4.a.II) equ. 4.c.4 was valid, a symbol + was printed by the computer at the corresponding location of the projection. If the normal stress upon a discontinuity becomes tensile and the inequality 4.c.4. is valid the computer programme will calculate this additional shear strain energy.

On the example projection(p.IO7)and on the projection 1 to 96 the potentially unstable spaces are defined by the symbols + .The ratio τ/σ_n is greater towards the centre of an unstable area and is reduced towards the projection line of critical equilibrium.It is always accepted that a small space around each principal direction is stable(the shear stress normal to that direction is equal to zero and therefore discontinuity poles coaxial with a principal stress direction are always stable).The empty(white) space on the projections means that no data were input at the corresponding direction.

So far, assuming uniform distribution of the discontinuities in each element and on the basis of the COULOMB-NAVIER-MOHR criterion we have defined potentially unstable orientation zones in each element in terms of the particular triad of principal stresses.In fact the above unstable zones are quite independent of the actual presence of any discontinuity.

The concept of an unstable zone in principal stress

place incorporates the idea of potential discontinuity shear movement of varying amplitudes over a range of orientations.The (modified) shear strain energy criterion uses the above idea, taking into account the strength anisotropy arising from a non-random discontinuity orientation.

4.d. The shear strain energy approach to failure interpretation.

As has been obvious (pages 82),the crack is extended if the equation 4.a.16 is valid and a source supplying energy is available. Consequently the GRIFFITH theory and its modifications, explain the initiation of the failure process while the COULOMB-NAVIER-MOHR criterion expresses the ultimate failure plane direction and the limiting values of τ, σ_n upon it.

It is known that a difference exists between the strain energy of the body containing a crack under specified external forces and the strain energy of the same body without a crack under the same external forces. According to G.WIEMBOLS and G.COOK.(I968)this difference is defined as "effective shear strain energy" and this is the

strain energy stored around the cracks as a result of the sliding produced by the "effective shear stress"

$$\tau_o' = |\tau| - (\sigma_n - u)\tan\varphi \qquad \text{equ. 4.d.I}$$

where u is the pore water pressure.

If the shear strain energy criterion is applied to small structural discontinuities (fissures), then the corresponding shear strain energy for one discontinuity for which

$$\tau_o = |\tau| - (\zeta_d + \sigma_n \tan\varphi_d) > 0 \quad \text{(equ. 4.a.ii)} \qquad \text{equ. 4.d.2}$$

(the pore water pressure is assumed to be equal to zero) is given in the form:

$$W_d = s l^3 \tau_o^2 \qquad \text{equ. 4.d.3}$$

where s is a function of the material, the shape of the discontinuity and its position and orientation relative to other discontinuities, and l is a dimension of the discontinuity.

From equation 4.d.3 follows that, for a solid with a unit volume, the shear strain energy depends on the magnitude of the shear stress (which acts on each discontinuity and consequently on the magnitudes of the principal stresses, the orientation of the discontinuities relative to the direction of these stresses), on the number of such discontinuities, and on their size and shape.

It should also be noted that R.SACK(I946)has found a similar equation for the strain energy due to cracks (penny-shaped cracks of diameter 2a)equal to

$$W_d = \frac{8(I - \nu^2)}{3E} a^3 \sigma_n^2 \qquad \text{equ. 4.d.4}$$

In this application, although the non-random orientation distribution indicates discontinuities different in size and shape, a constant length, and also a planar shape for discontinuities are assumed.

Now the basic assumption is that failure will take place when the total shear strain energy, generated by sliding between the opposite surface of N closed discontinuities, exceeds a limiting value.

If a number of discontinuity poles falls in the potentially unstable area (as was discussed in the last chapter), the total shear strain energy can be calculated. Consequently, if the discontinuity fabric of each element of a rock mass is known, superimposing it on the projection sphere of each element (Figure 4.c.I) we can calculate, for each element, the shear strain energy in terms of the fabric and the principal stress field.

For N discontinuities the total shear strain energy will be

$$W_d = Nsl^3 \int_{\tau_o>0} P\tau_o^2 dG_1 \qquad \text{equ. 4.d.5}$$

where G_1, as before, denotes the range of integration on the sphere of projection.

Using the equation 4.b.9 and 4.d.5 we obtain the equation

$$W_d = Nsl^3 q \sum_{i=1}^{N} \int_{a_i} \tau_o^2 dG_1 \qquad \text{equ. 4.d.6}$$

(the integral covers the area a_i representing the i^{th} point).

For comparative purposes, the shear strain energy W_{dI} with respect to an equivalent isotropic discontinuity

distribution (a probability density of unity) was computed. In this case, the potentially unstable spaces on the projection contain a uniform density distribution of discontinuities. The W_{dI} is calculated by the equation

$$W_{dI} = sl^3 N \int_{\tau_o > 0} \tau_o^2 dG_1 \qquad \text{equ. 4.d.7}$$

From equation 4.d.7 it can be deduced that the shear strain energy is independent of the discontinuity fabric and this provides a base for comparison of the stability of a series of different discontinuity fabrics with equivalent stress and strength conditions.

Accordingly the ratio W_{dI} / W_d ,can be regarded as a "safety index". In that case,limiting equilibrium will not exist when $\frac{W_{dI}}{W_d} = 1$ (as usual) because potential shear failure can take place when $W_d > 0$.

4.e. Computation.

In order to establish the delimitation of the potentially unstable orientation zones and the evaluation of shear strain energy in the case of the non-random discontinuity fabric of London Clay, and in the case of the equivalent isotropic fabric, a computing process was followed, according to P.ATTEWELL and J.WOODMAN.

At first, for each element, a triad of principal stresses appropriate to the coordinate location in the clay surrounding the tunnel was applied to the total discontinuity fabric (Figure 4.b.2) and the consequential shear strain energy computed (projections I to 76). In every projection case, the discontinuity fabric remains invariable while the principal stress magnitudes and directions change as a function of position. The fabric is always orientated with North at the top (N) and West at the left (Y).

In order to make a particular study of the stability of the tunnel in the immediate vicinity of the excavation, the clay around the tunnel was again divided into one hundred and eight smaller elements (Figure 4.e.I). Again, for each element, a triad of principal stresses appropriate to the coordinate location in the clay surrounding the tunnel was applied to the discontinuity

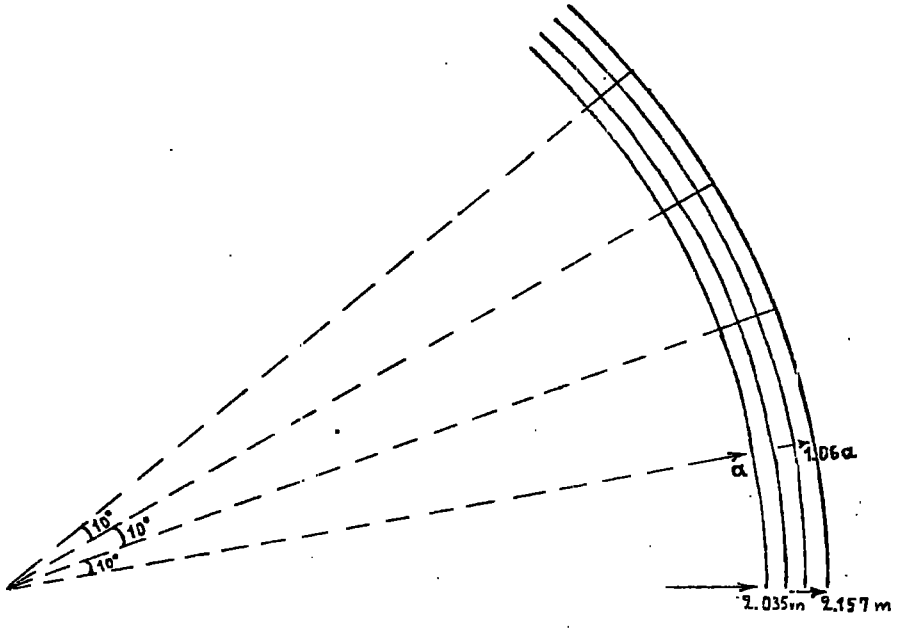

Fig. 4.e.I

fabric consisting of the discontinuities measured at the zone I (Figure 4.b.I). The potentially unstable spaces were delimited and the "skin" shear strain energy was calculated both for the actual non-random discontinuity distribution and for the equivalent isotropic distribution (projections 77 to 96).

Special care was taken to ensure that the shear strength characteristics, used in the calculation of shear strain energy, represented a wide range of shear strength parameters for the clay as created by the effect of the discontinuities and the pore water conditions. (Table 4.e.I). The whole process was repeated seven times, using each time different shear strength characteristics (c, ϕ), corresponding to drained and undrained conditions on intact samples and on fissures surfaces, on samples with orientation vertical, inclined at 45° and horizontal with respect to ground surface.

TABLE 4.e.I The shear strength parameters of London Clay used in the application of the criterion

SKEMPTON	BISHOP	MARSLAND	AGARWAL	MYRIANTHIS	MICHELIS
Drained triaxial tests along fissures	Drained shear box tests	Drained triaxial tests on samples inclined at 45°	Undrained triaxial tests on samples inclined at 45°	Undrained triaxial tests on fissured samples	Drained shear box tests along fissures
$\hat{\phi}_d = 18.5°$	$\phi_r = 9.4°$	$\hat{\phi} = 29°$	$\hat{\phi} = 18.9°$	$\hat{\phi} = 0.43°$ (vertic. samples) $\hat{\phi} = 0.43°$ (horiz. samples)	$\phi_{rd} = 13.5°$
$\hat{C}_d = 7 kN/m^2$	$C_r = 0 kN/m^2$	$\hat{C} = 0 kN/m^2$	$\hat{C} = 33.12 kN/m^2$	$\hat{C} = 235 kN/m^2$ (vertical samp.) $\hat{C} = 400 kN/m^2$ (horizon. sampl.)	$C_{rd} = 5 kN/m^2$

In the case of the calculation of the shear strain energy in the vicinity of the excavation ("skin" shear strain energy) the process was repeated twice,applying first of all the peak shear strength characteristics for fissure surfaces in drained pore water conditions as derived by A.SKEMPTON(I967) and secondly the corresponding characteristics as are shown in the table 3.a.2 of Chapter 3.

In the pages I03 to I2I,only four elements from every 10 degrees between 90° and -90° are presented(the total number of the projections exceeds two thousand).The shear strength parameters that has been used are: $\varphi_{rd} = 13.5°$ and $C_{rd}=5\kappa N/m^2$ as obtained by laboratoty testing.The shear strain energy was calculated in arbitrary units because the factors s,1 (equation4.d.3)are difficult to determine with accuracy. The principal stresses $\sigma_1, \sigma_2, \sigma_3$ were normalized with respect to σ_1.

Figures 4.e.2to 4.e.I6and 4.e.I7to 4.e.20show contour diagrams of the shear strain energy for all the elements around the tunnel.In the middle of each element (Figure4.c.I) the corresponding shear strain energy was recorded and the contours were drawm by hand.

Figure 4.e.2therefore represents the distribution of the shear strain energy around the tunnel for non-random discontinuity distribution.The shear strength parameters used were $\varphi_{rd}= 13.5°$, $C_{rd}= 5\kappa N/m^2$.

Figure 4.e.3 represents the distribution of shear strain energy for the equivalent isotropic distribution.The shear strength characteristics used were again $\varphi_{rd}=13.5°$, $C_{rd}=5\kappa N/m^2$.

Figure 4.e.4 represents the distribution of the "safety index" W_{el}/W_d of the above shear strain energies.

GREEN PARK FLEET LINE LONDON CLAY DISCONTINUITY STABILITY +50 DEG. 1ST QU
ISPHERE UPPER PROJECTION 16.00CM CIRCLE
598 W: 0.063
) PER CENT AREA WINDOW USED

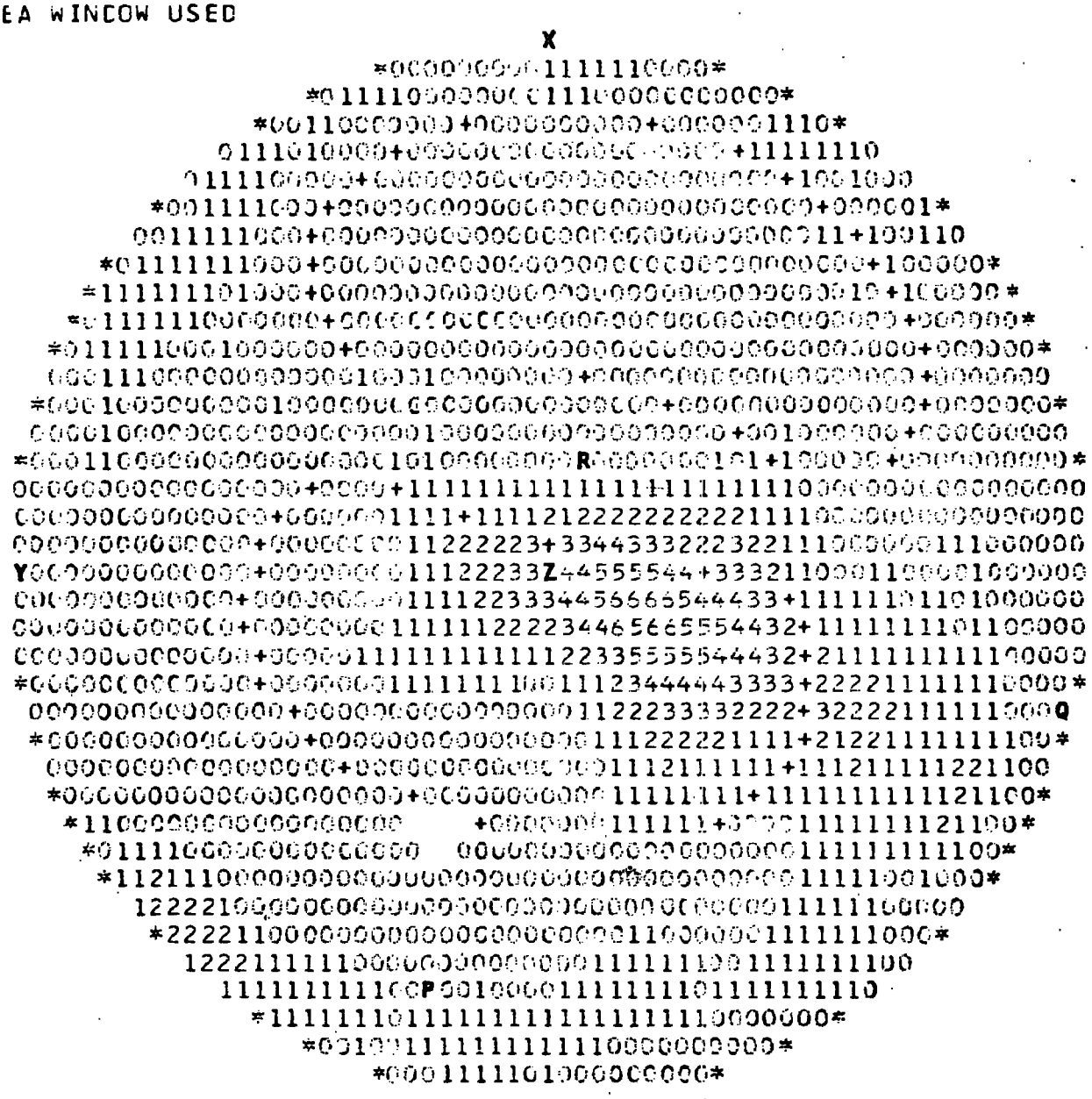

: 1.0000 (-0.921271 0.246854 0.300539)
: 0.6820 (-0.258819 -0.965926 0.000000)
: 0.3641 (0.290298 -0.077785 0.953770)
FRICTION: 0.3346 COHESION: 0.0065
ENERGY W_d: 2.1398 W_{dI}: 1.9867 W_d/W_{dI}: 1.0770 W_{dI}/W_d: 0.9285

EXAMPLE OF AN EQUAL AREA PROJECTION for an element inclined at 50 deg., 1st quad. and terminating at a distance r = 1.8 a. ($\hat{C}_d$ = 7 kN/m², $\hat{\varphi}_d$ = 18.5°).

It shows :
1) The probability density of the poles to the discontinuities measured in London Clay at Green Park Station (Pi diagram).
2) The directions of the principal axes P, Q, R .
3) The potentially unstable spaces delimited by the symbols +
4) The values of the normalized principal stresses and the values of direction cosines (in brackets).
5) The values of W_d, W_{dI}, W_d/W_{dI}, W_{dI}/W_d.

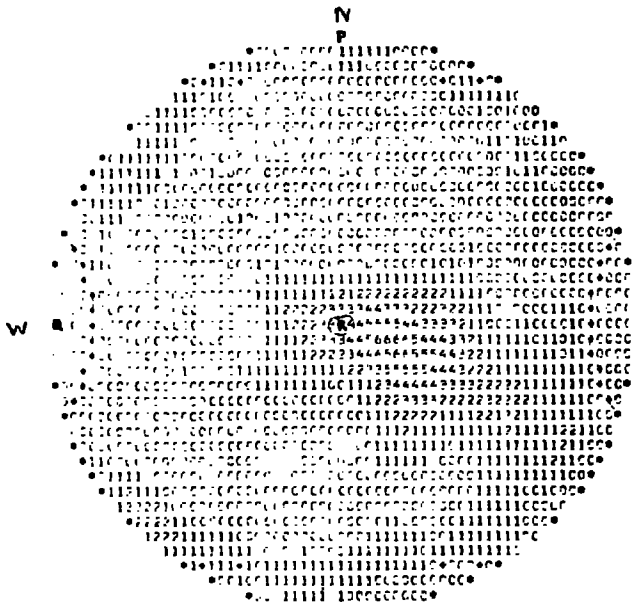

Projection 1 , r = a

W_d = 71.03 W_{dI} = 84.19

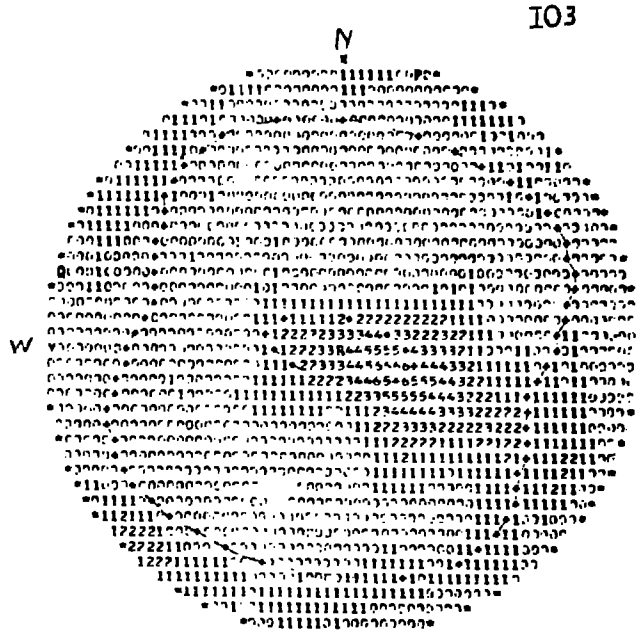

Projection 2 , r = 1.6 a

W_d =5.39 W_{dI} = 8.66

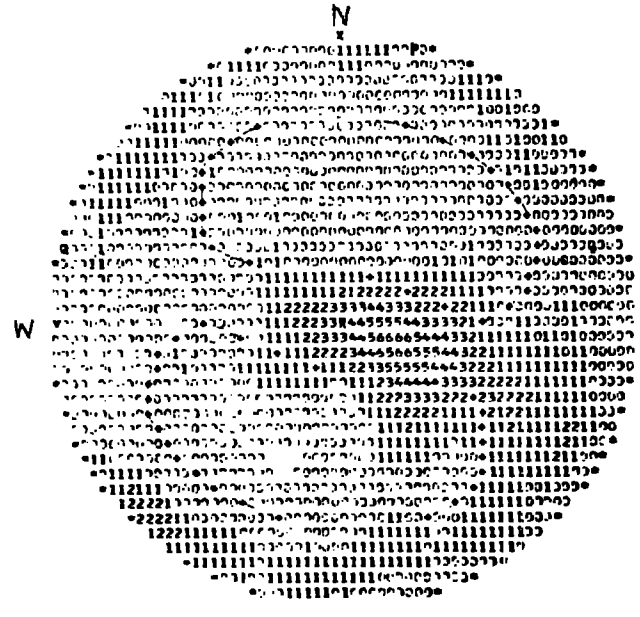

Projection 3 , r = 2.2 a

W_d =0.92 W_{dI} = 1.82

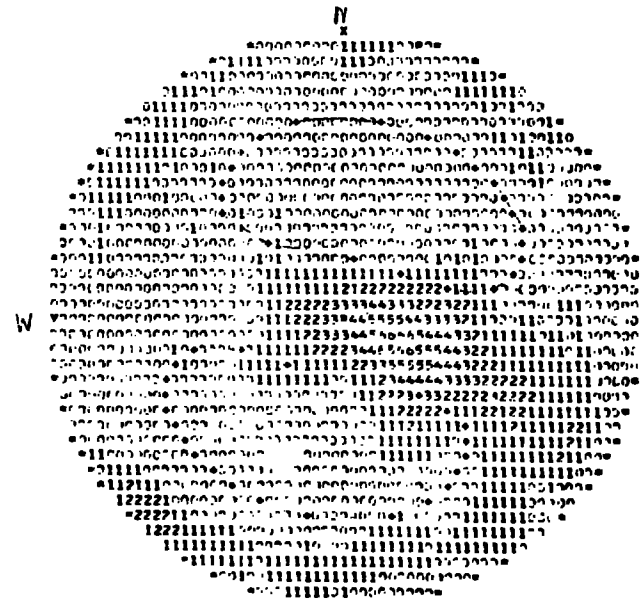

Projection 4 , r = 3 a

W_d = 0.35 W_{dI} = 0.77

Equal area projections of the London Clay discontinuity fabric at Green Park Station

Elements inclined at 90°, 1st Quadrant (C_{rd} = 5κN/m² ϕ_{rd} = 13.5°)

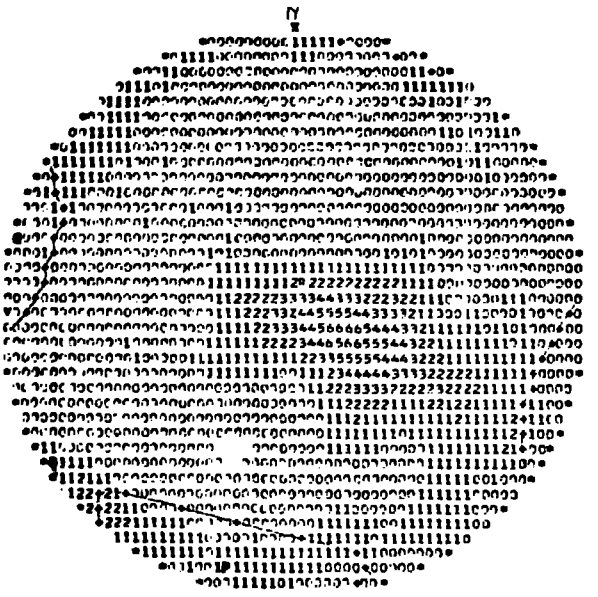

Projection 5 , r = a

W_d = 75.68 W_{dI} = 84.19

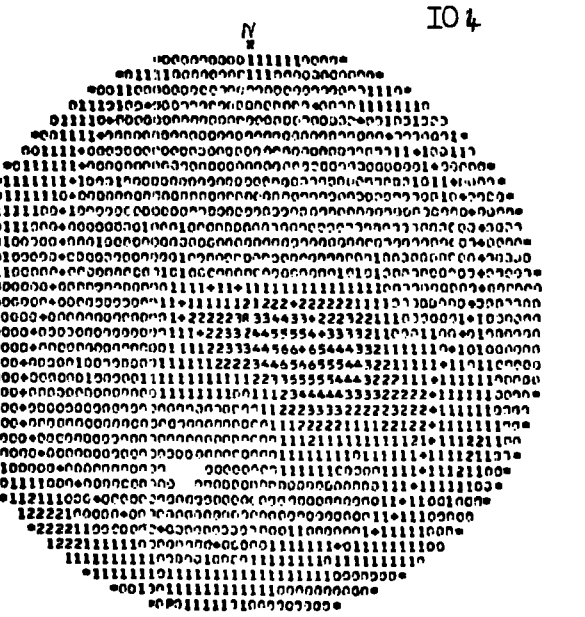

Projection 6 , r = 1.6a

W_d = 6.15 W_{dI} = 9.21

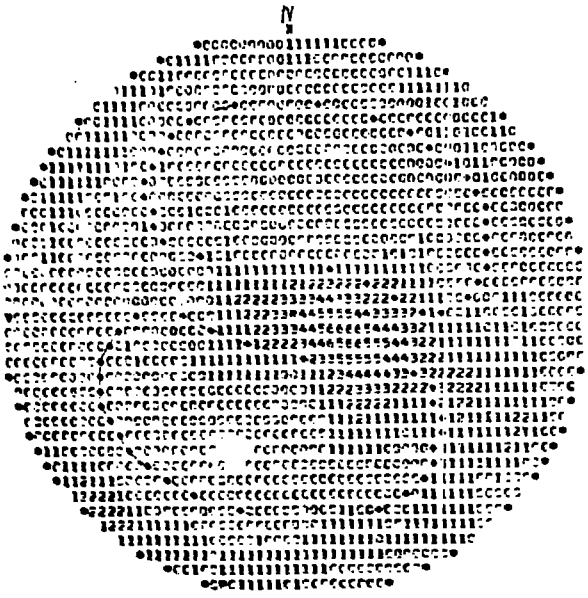

Projection 7 , r =2.2 a

W_d = 1.19 W_{dI} = 2.13

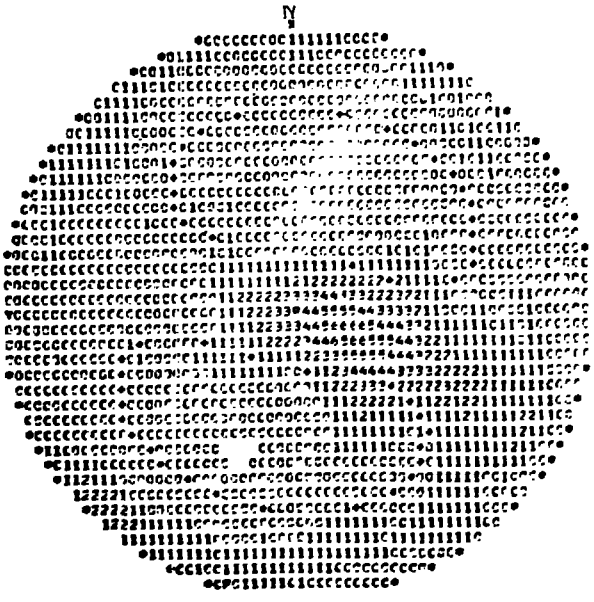

Projection 8 , r = 3 a

W_d = 0.43 W_{dI} = 0.92

Equal area projections of the London Clay discontinuity fabric at Green Park Station.

Elements inclined at 80°, 1st Quadrant (C_{rd}=5 kN/m², ϕ_{rd}= 13.5°)

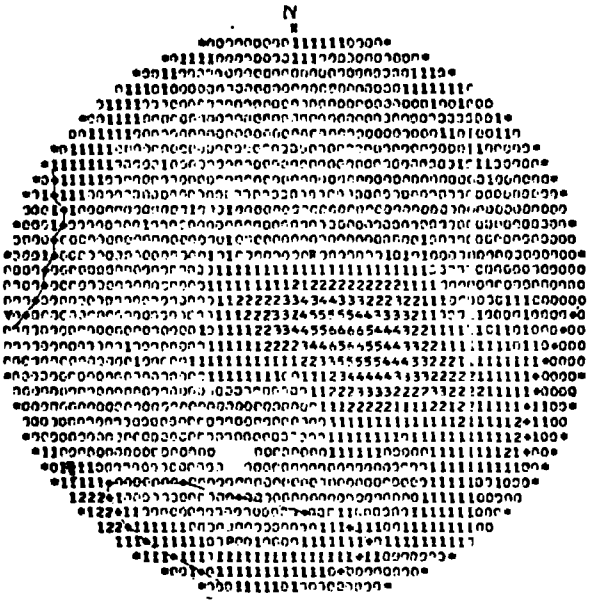

Projection 9 , r= a

W_d = 93.26 W_{dI}= 84.01

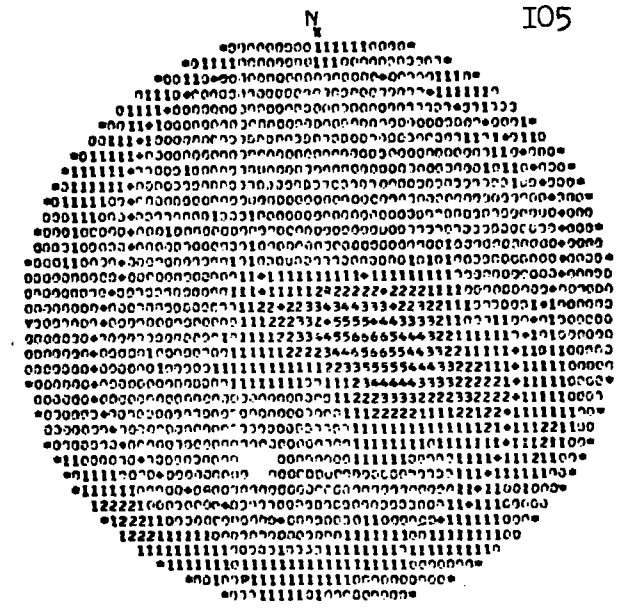

Projection 10 , r = 1.6 a

W_d =8.14 W_{dI}= 10.65

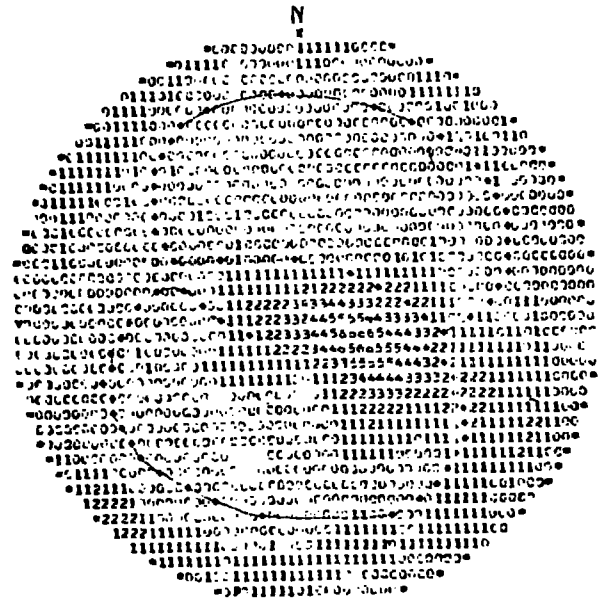

Projection 11 , r=2.2 a

W_d= 1.69 W_{dI}= 2.94

Projection 12 , r = 3a

W_d = 0.65 W_{dI}= 1.32

Equal area projections of the London Clay discontinuity fabric at Green Park Station.

Elements inclined at 70° , 1st Quadrant (C_R= 5 kN/m², ϕ_R= 13.5°)

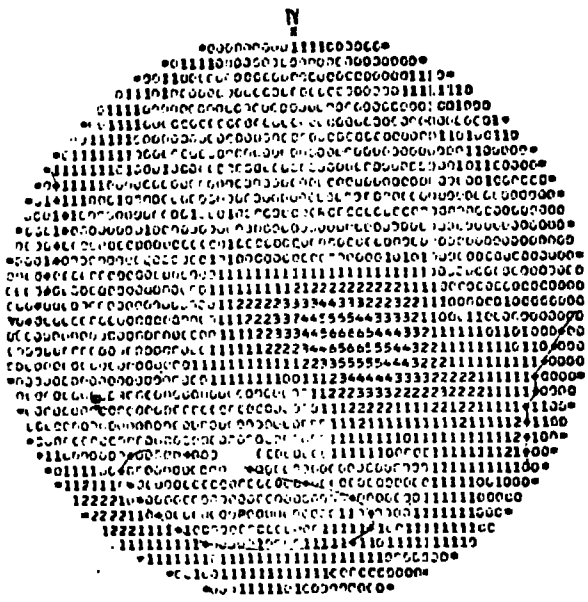

Projection 13 , r = a

W_d = 108.06 W_{dI} = 85.80

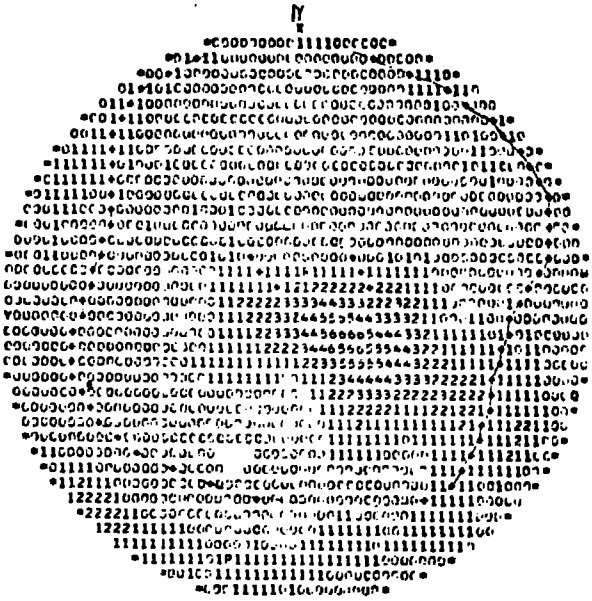

Projection 14 , r = 1.6 a

W_d = 11.48 W_{dI} = 12.32

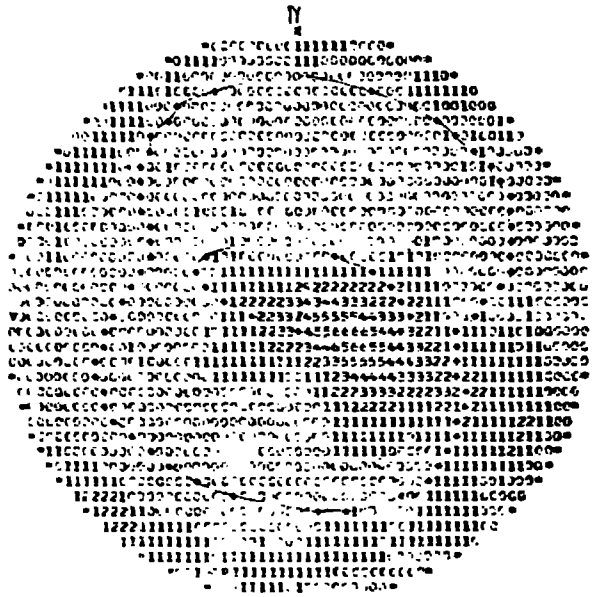

Projection 15 , r = 2.2 a

W_d = 2.54 W_{dI} = 3.80

Projection 16 , r = 3 a

W_d = 0.89 W_{dI} = 1.66

Equal area projections of the London Clay discontinuity fabric at Green Park Station.

Elements inclined at 60°, 1st Quadrant (C_{rd} = 5 kN/m², ϕ_{rd} = 13.5°)

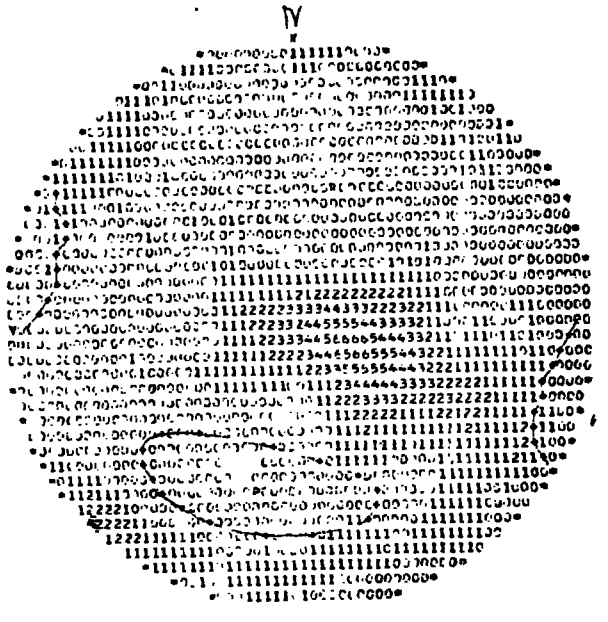

Projection 17 , r = a

W_d = 113.05 W_{dI} = 85.45

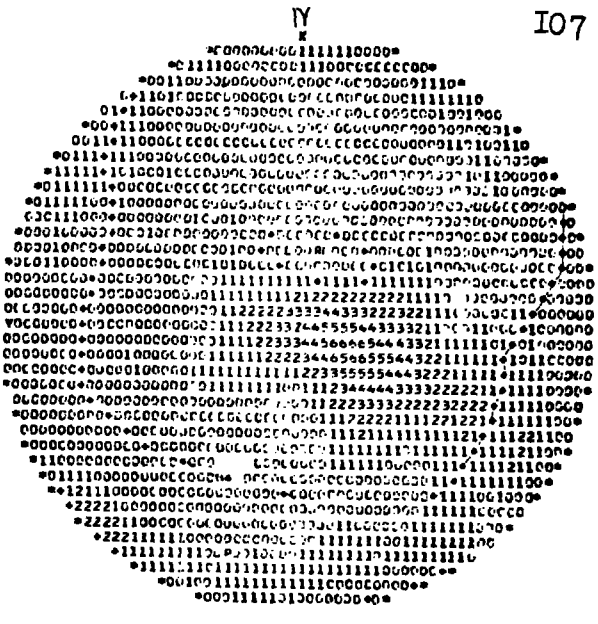

Projection 18 , r = 1.6 a

W_d = 15.28 W_{dI} = 13.05

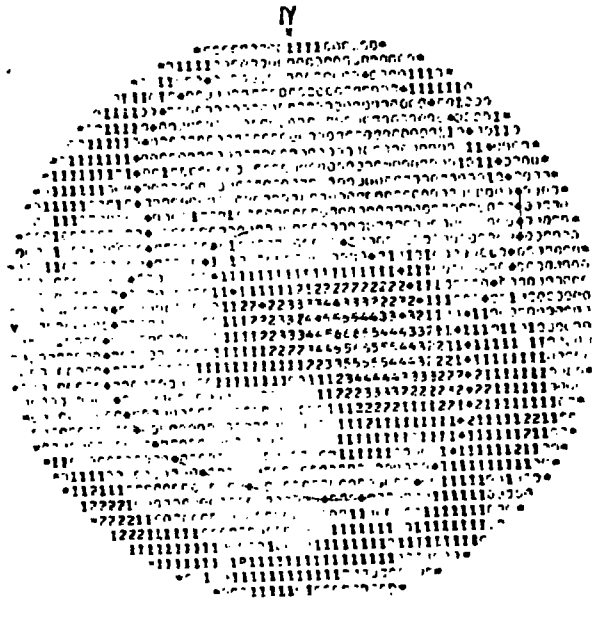

Projection 19, r = 2.2 a

W_d = 3.15 W_{dI} = 3.82

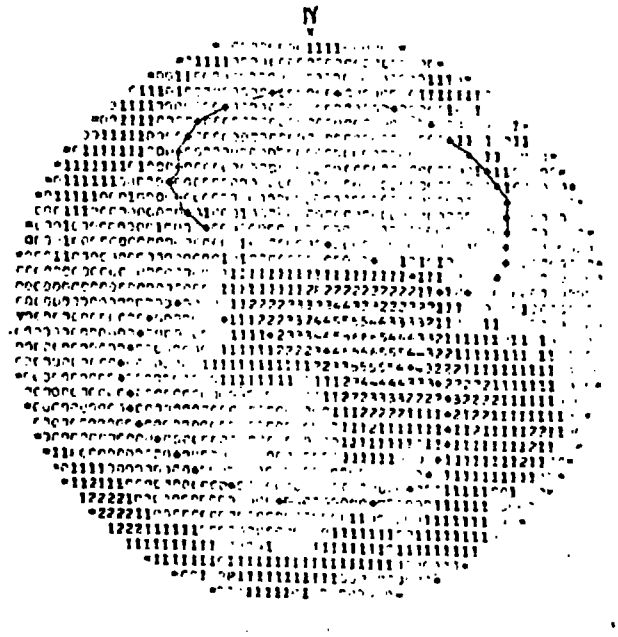

Projection 20 , r = 3 a

W_d = 0.89 W_{dI} = 1.50

Equal area projections of the London Clay discontinuity fabric at Green Park Station.

Elements inclined at 50°, 1st Quadrant (C_{rd} = 5 kN/m², ϕ_{rd} = 13.5°)

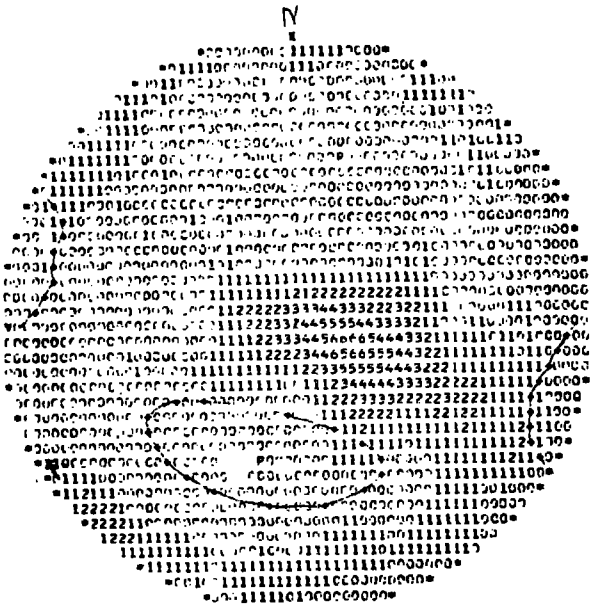

Projection 21 , r = a

W_d = 104.30 W_{dI} = 83.26

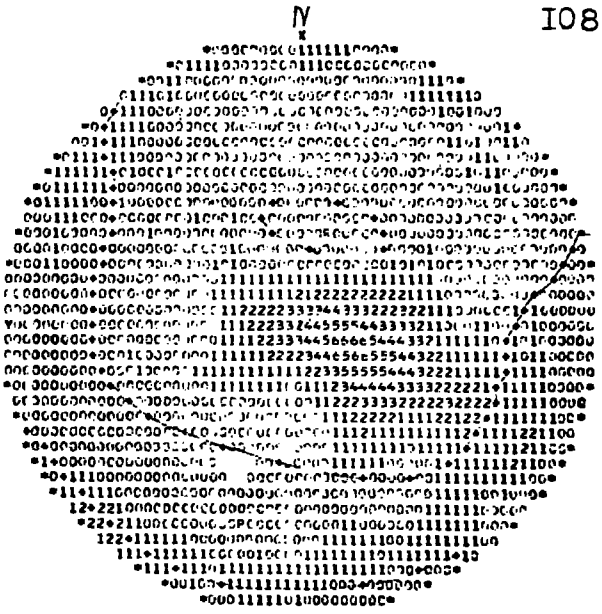

Projection 22 , r = 1.6 a

W_d = 16.16 W_{dI} = 11.60

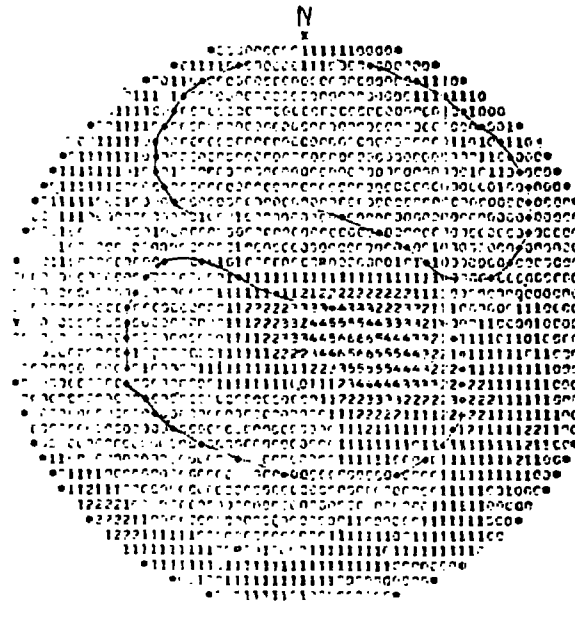

Projection 23 r = 2.01a

W_d = 2.70 W_{dI} = 2.50

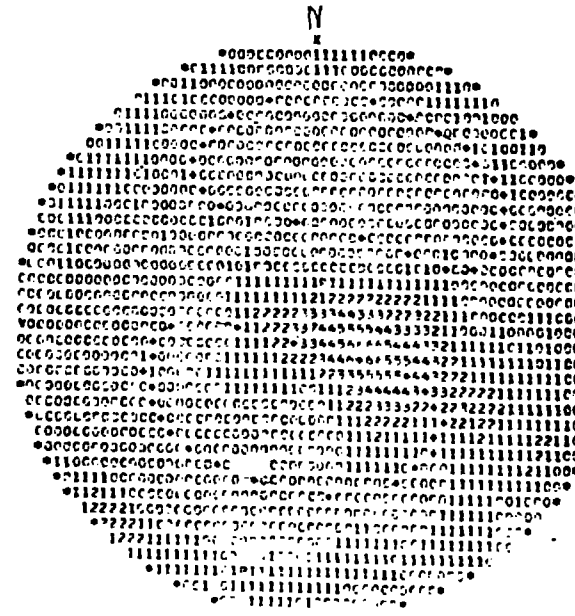

Projection 24 , r = 3 a

W_d = 0.49 W_{dI} = 0.74

Equal area projections of the London Clay discontinuity fabric at Green Park Station

Elements inclined at 40°, 1st Quadrant (C_{fd} = 5 kN/m², ϕ_{fd} = 13.5°)

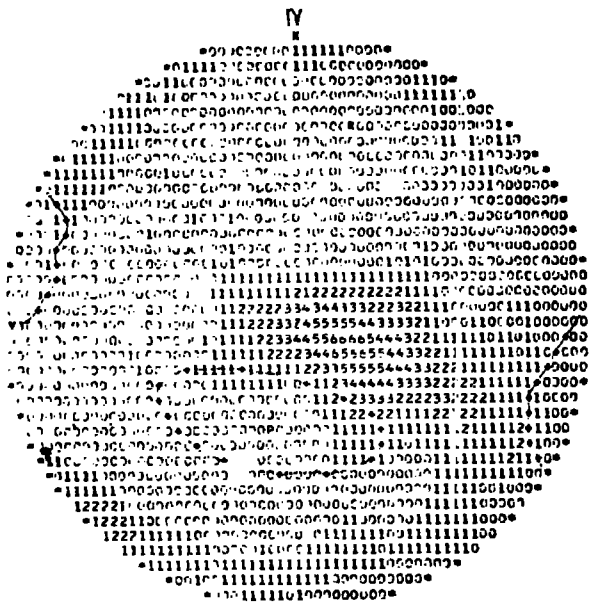

Projection 25 , r = a

W_d = 86.45 W_{dI} = 83.23

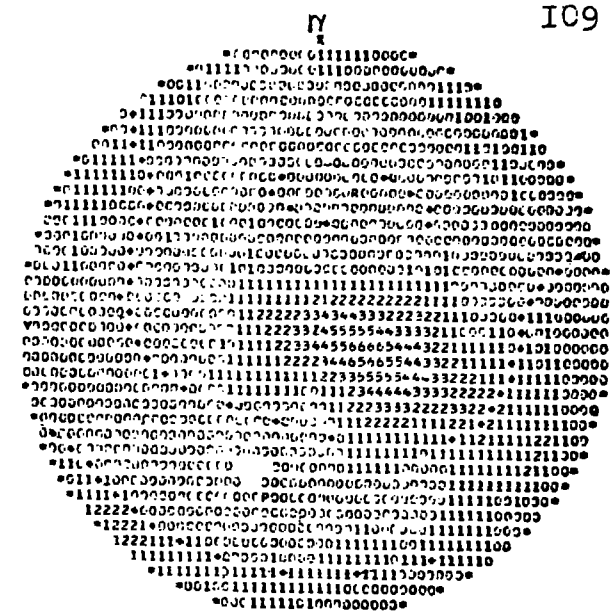

Projection 26 , r = 1.6 a

W_d = 12.13 W_{dI} = 7.65

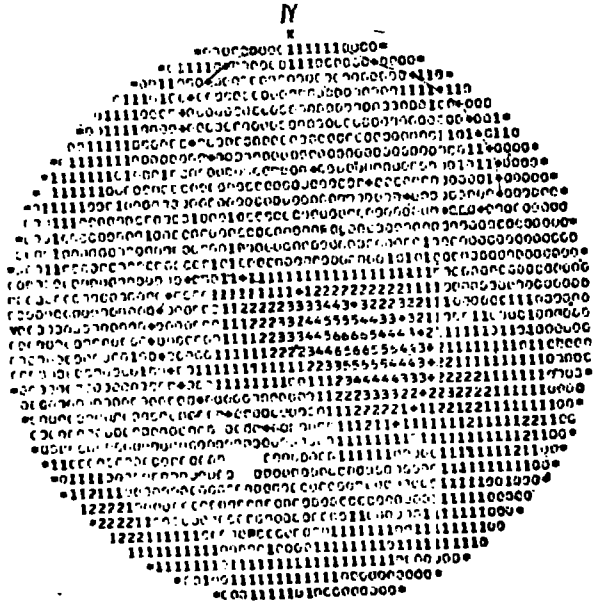

Projection 27 , r = 2.2 a

W_d = 0.89 W_{dI} = 0.59

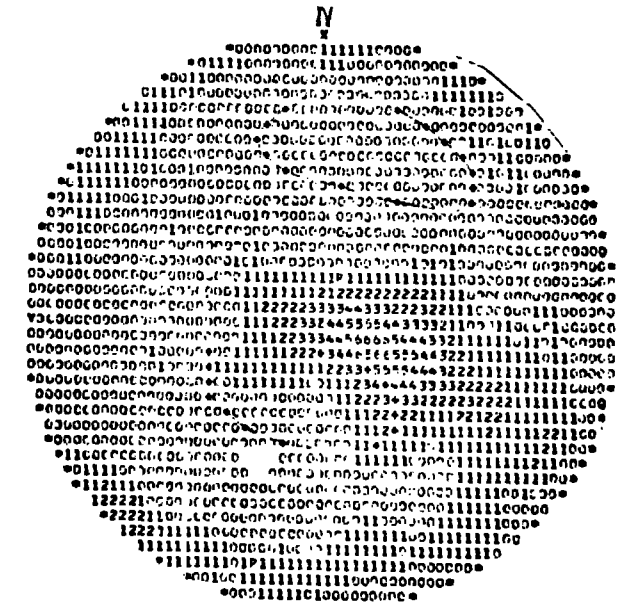

Projection 28 , r = 3 a

W_d = 0.048 W_{dI} = 0.06

Equal area projections of the London Clay discontinuity fabric at Green Park Station

Elements inclined at 30°, 1st Quadrant (C_d = 5 kN/m², ϕ_{rd} = 13.5°)

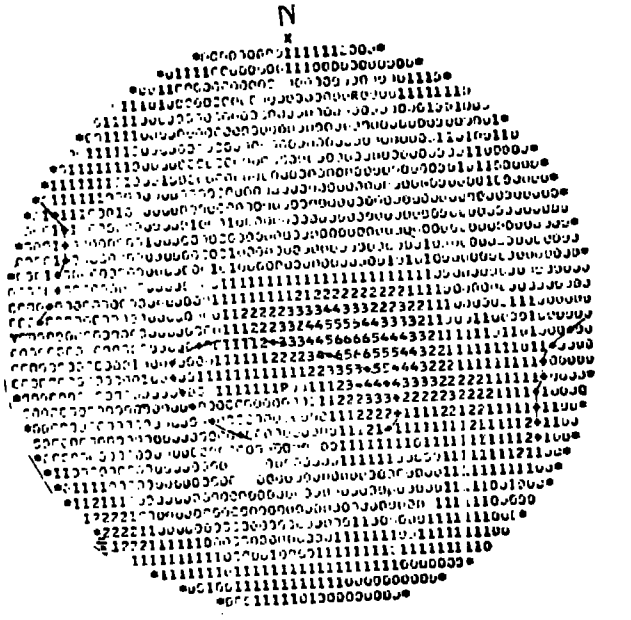

Projection 29 , r = a

W_d = 68.78 W_{dI} = 83.67

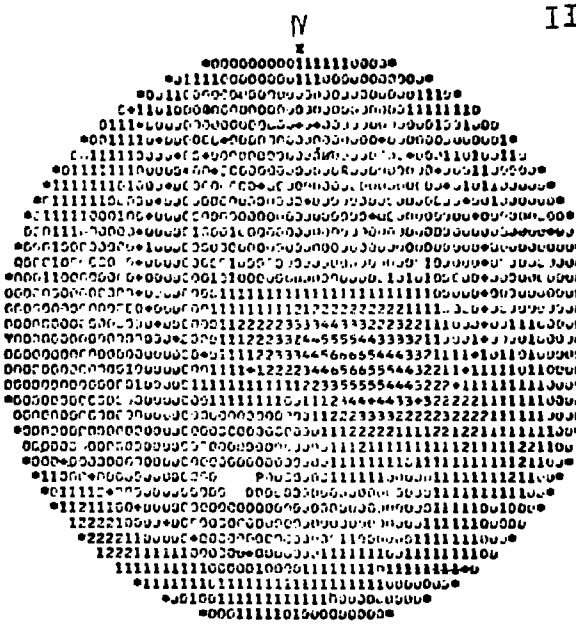

Projection 30 , r=1.6 a

W_d = 4.16 W_{dI} = 3.04

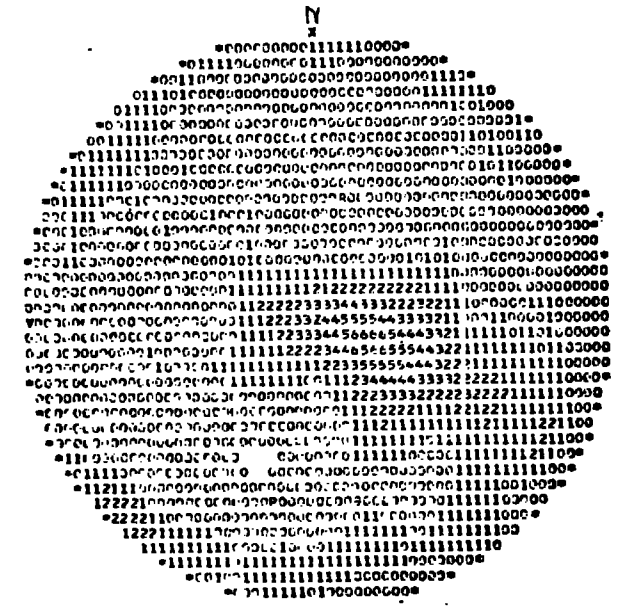

Projection 31 , r = 2.2 a

W_d = 0.0 W_{dI} = 0.6

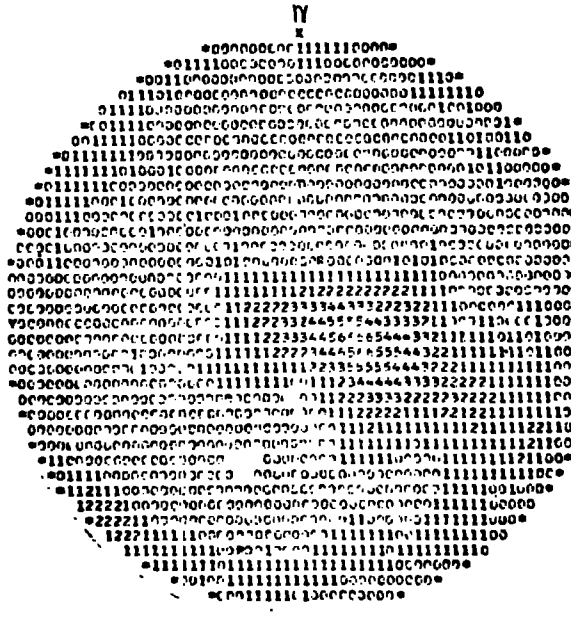

Projection 32 , r = 3 a

W_d = 0.0 W_{dI} = 0.0

Equal area projections of the London Clay discontinuity fabric at Green Park Station.

Elements inclined at 20°, 1st Quadrant (C_{rd}=5kN/m², ϕ_{rd}= 13.5°)

Projection 33 , r = a

W_d = 57.08 W_{dI} = 83.93

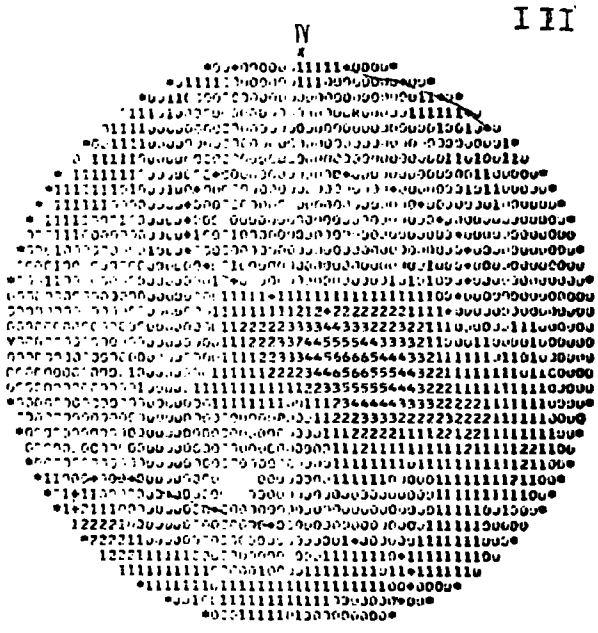

Projection 34 , r= 1.6 a

W_d = 0.43 W_{dI} = 0.57

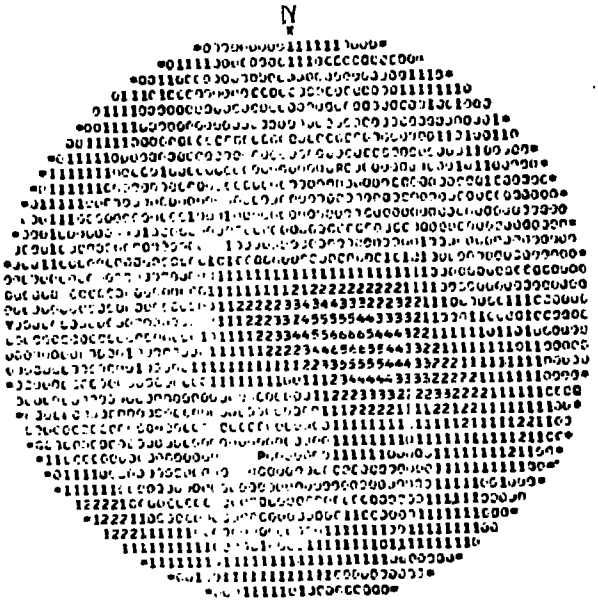

Projection 35 , r= 2.2 a

W_d = 0.0 W_{dI}=0.0

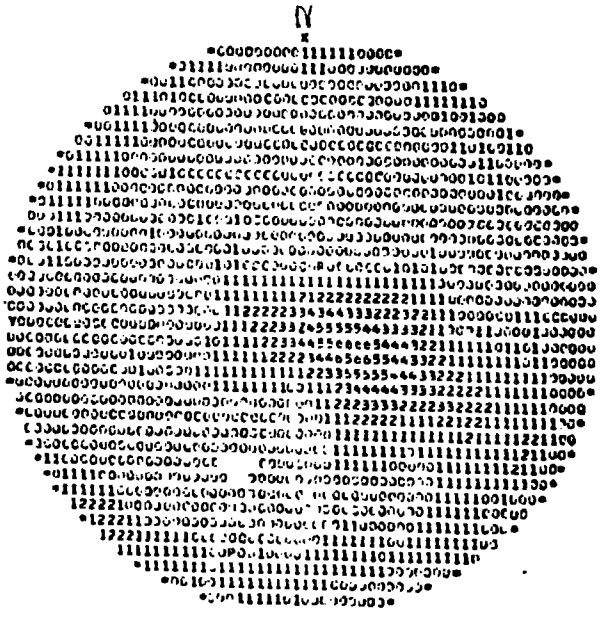

Projection 36 , r = 3 a

W_d = 0.0 W_{dI}= 0 .0

Equal area projections of the London Clay discontinuity fabric at Green Park Station

Elements inclined at 10° , 1st Quadrant (C_{rd}= 5 kN/m², ϕ_{rd}= 13.5)

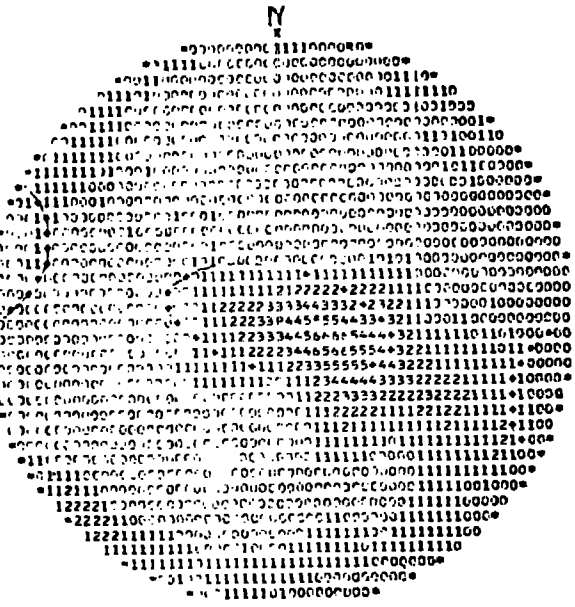

Projection 37 , r = a

W_d = 52.58 W_{dI} = 84.08

Projection 38 , r = 1.6 a

W_d = 0.060 W_{dI} = 0.15

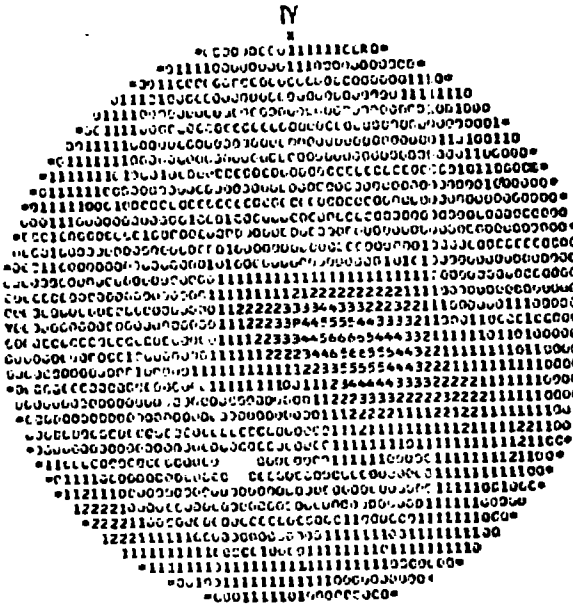

Projection 39 , r = 2.2 a

W_d = 0.0 W_{dI} = 0.0

Projection 40 , r = 3 a

W_d = 0.0 W_{dI} = 0.0

Equal area projections of the London Clay discontinuity fabric at Green Park Station

Elements inclined at : 0°, 2nd Quadrant (C_{rd} = 5 kN/m^2 , ϕ_{rd} = 13.5°)

Projection 41 r = a

W_d= 57.75 W_{dI}= 83.93

Projection 42 r = 1.6 a

W_d= 0.44 W_{dI}= 0.64

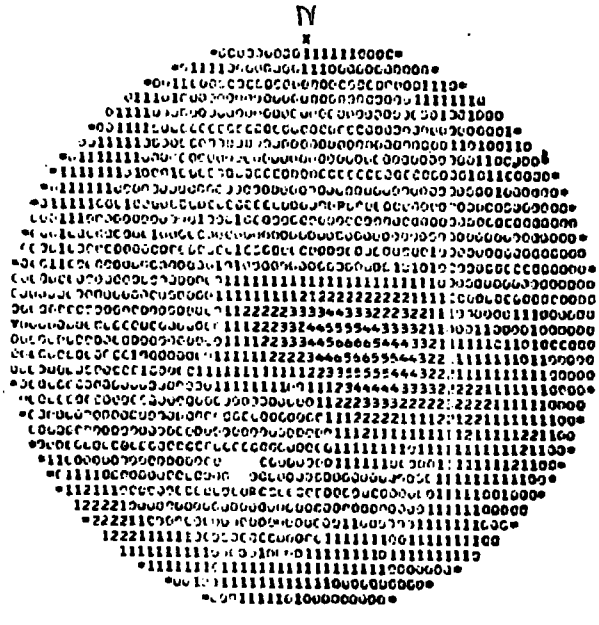

Projection 43 , r = 2.2 a

W_d=0.0 W_{dI}= 0.0

Projection 44 , r = 3.6

W_d= 0.0 W_{dI}= 0.0

Equal area projections of the London Clay discontinuity fabric at Green Park Station.

Elements inclined at -10°, 2nd Quadrant (C_{rd}=5 kN/m², ϕ_{rd}= 13.5°)

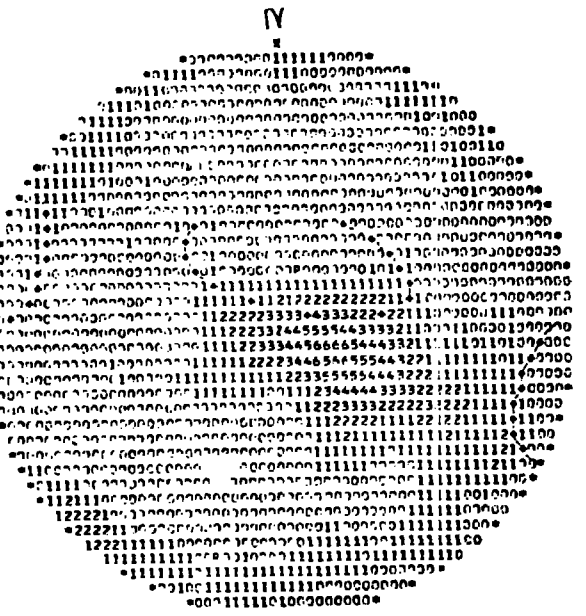

Projection 45 , r = a

W_d = 72.45 W_{dI} = 83.61

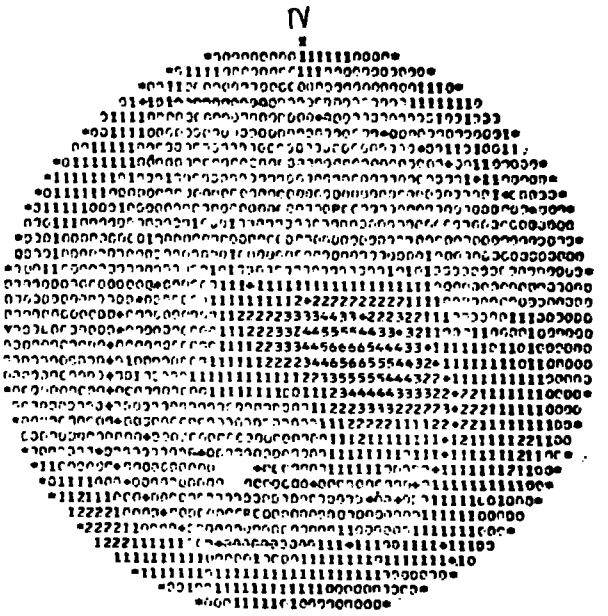

Projection 46 , r = 1.6 a

W_d = 3.77 W_{dI} = 2.59

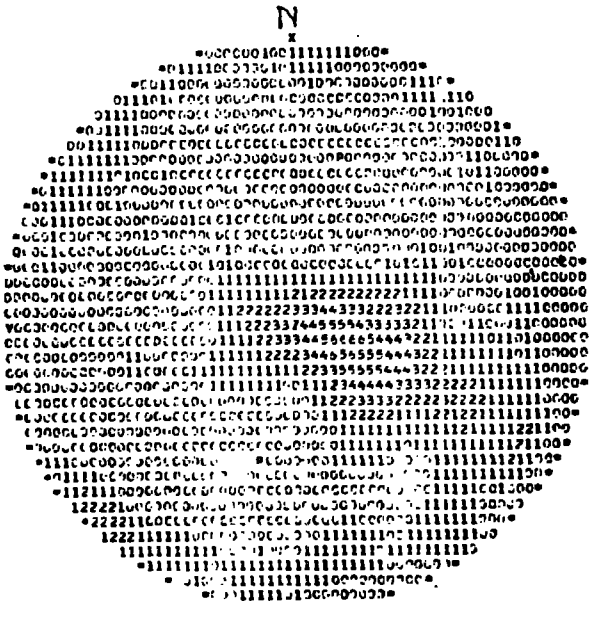

Projection 47 , r = 2.2 a

W_d = 0.0 W_{dI} = 0.0

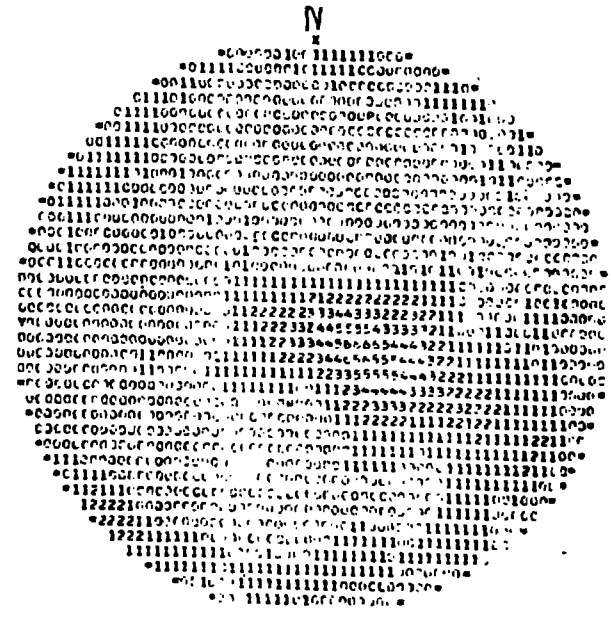

Projection 48 , r = 3 a

W_d = 0.0 W_{dI} = 0 .0

Equal area projections of the London Clay discontinuity fabric at Green Park Station.

Elements inclined at -20° , 2nd Quadrant (C_{rd} = 5 kN/m² , ϕ_{rd} = 13.5°)

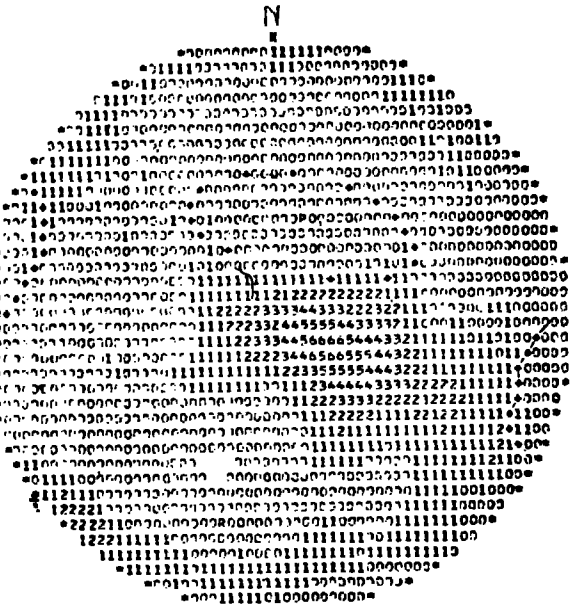

Projection 49 , r = a

W_d = 94.49 W_{dI}= 83.32

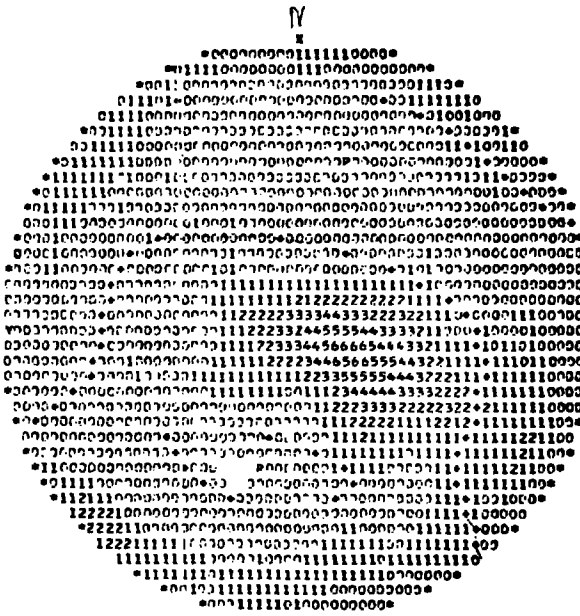

Projection 50 , r = 1.6 a

W_d = 10.05 W_{dI}= 5.66

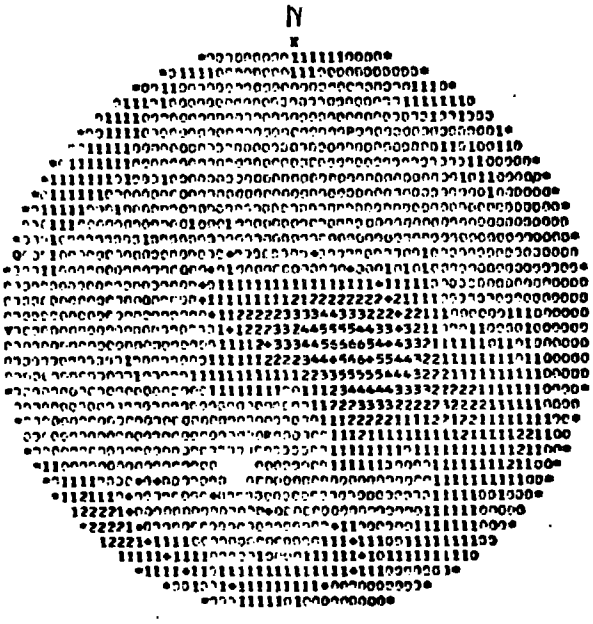

Projection 51 , r =2.2 a

W_d = 0.11 W_{dI}= 0.06

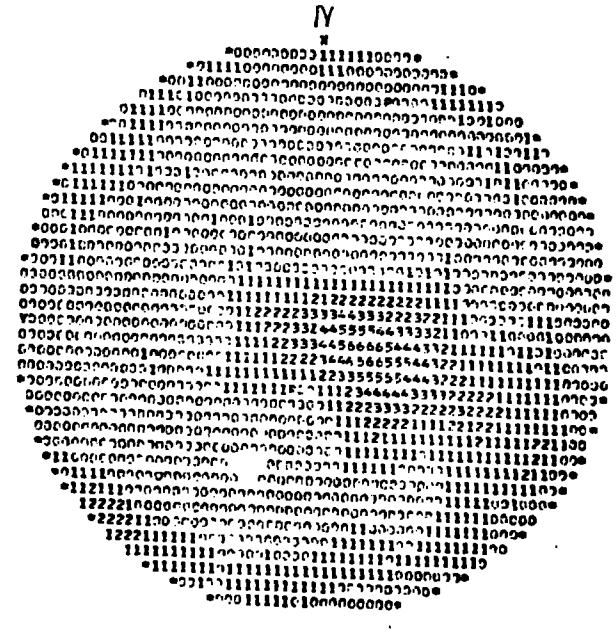

Projection 52 , r = 3 a

W_d = 0.0 W_{dI}= 0.0

Equal area projections of the London Clay discontinuity fabric at Green Park Station.

Elements inclined at -30° , 2nd Quadrant (C_{rd}= 5 kN/m², ϕ_{rd}= 13.5°)

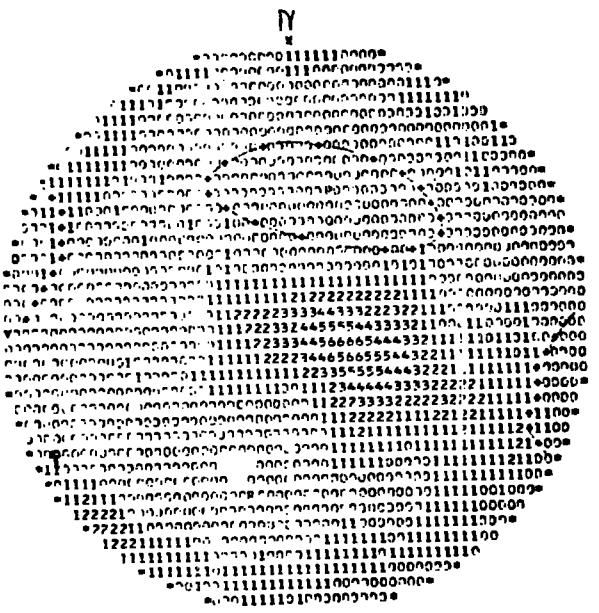

Projection 53 , r = a

W_d=113.91 W_{dI}= 83.25

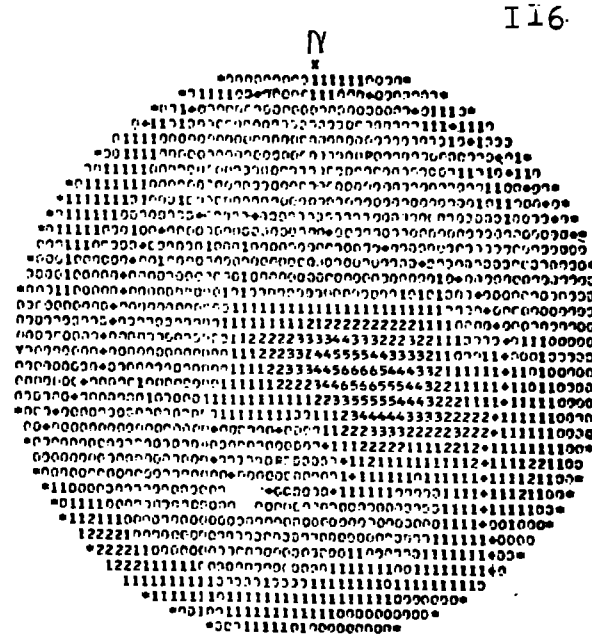

Projection 54 , r = 1.6 a

W_d= 12.89 W_{dI}= 8.27

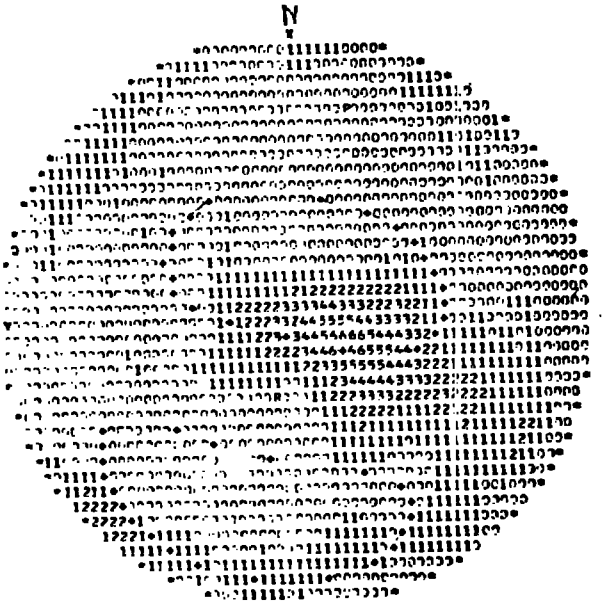

Projection 55 , r = 2.2 a

W_d= 0.63 W_{dI}= 0.59

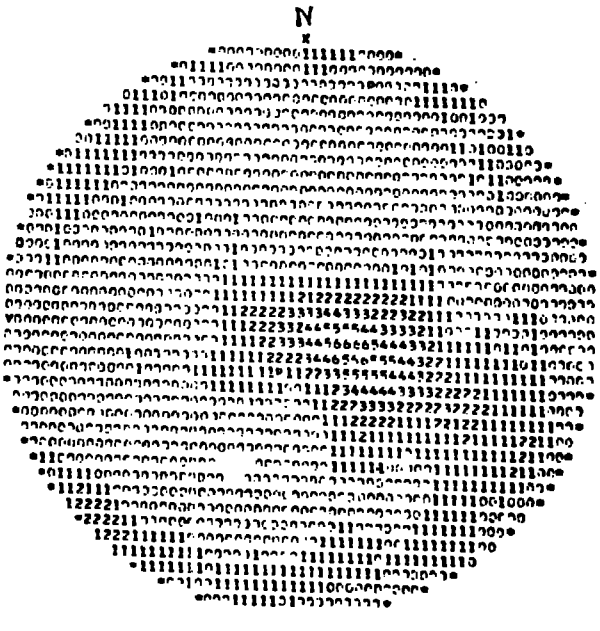

Projection 56 , r =3 a

W_d= 0.0 W_{dI}= 0.0

Equal area projections of the London Clay discontinuity fabric at Green Park Station.

Elements inclined at -40°, 2nd Quadrant (C_{rd}= 5kN/m², ϕ_{rd}= 13.5°)

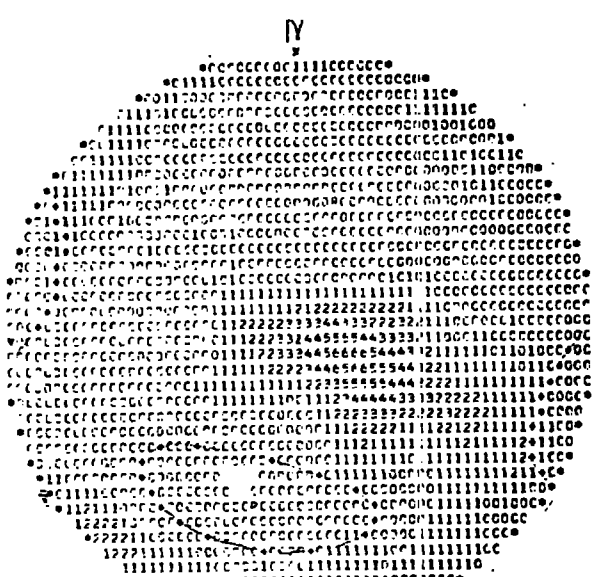

Projection 57 , r = a

W_d = 112.39 W_{dI}=83.45

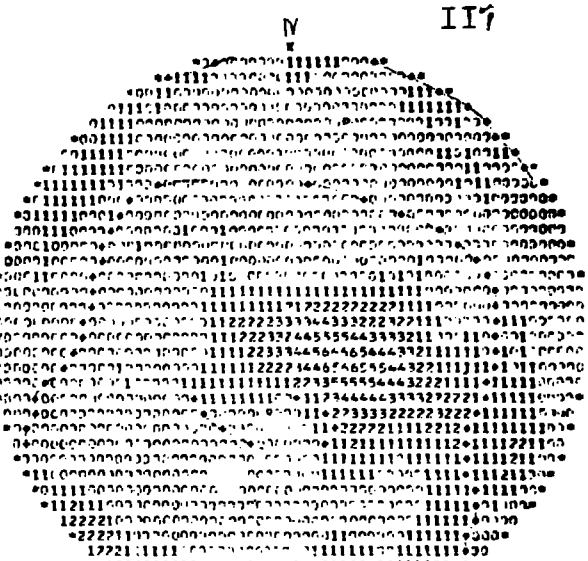

Projection 58 , r = 1.6 a

W_d =11.34 W_{dI}=9.43

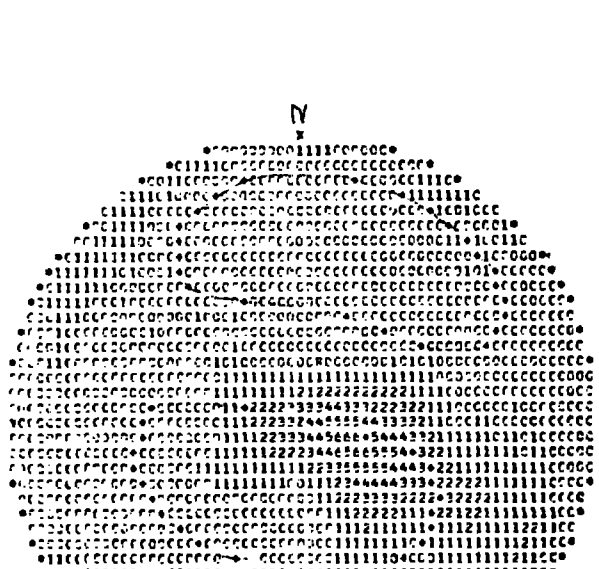

Projection 59 , r = 2.2 a

W_d = 0.87 W_{dI}= 0.97

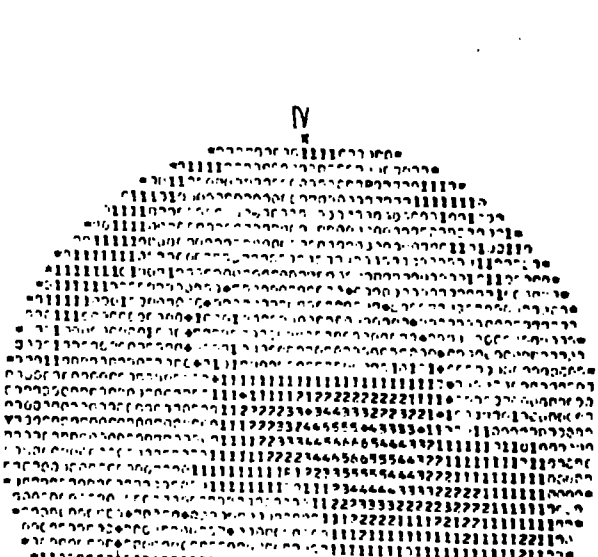

Projection 60 , r = 3 a

W_d= 0.20 W_{dI}= 0.35

Equal area projections of the London Clay discontinuity fabric at Green Park Station.

Elements inclined at -50°, 2nd Quadrant (C_{rd}= 5kN/m², ϕ_{rd}= 13.5)

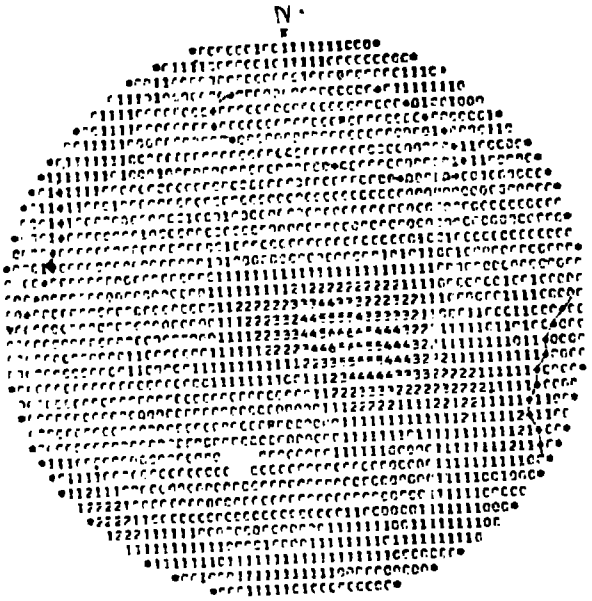

Projection 61, r = a

W_d = 110.39 W_{dI} = 83.79

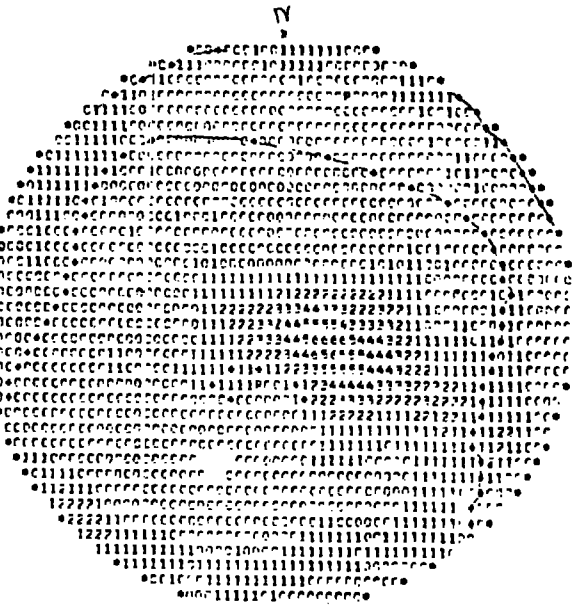

Projection 62 , r = 1.6 a

W_d = 19.61 W_{dI} = 18.66

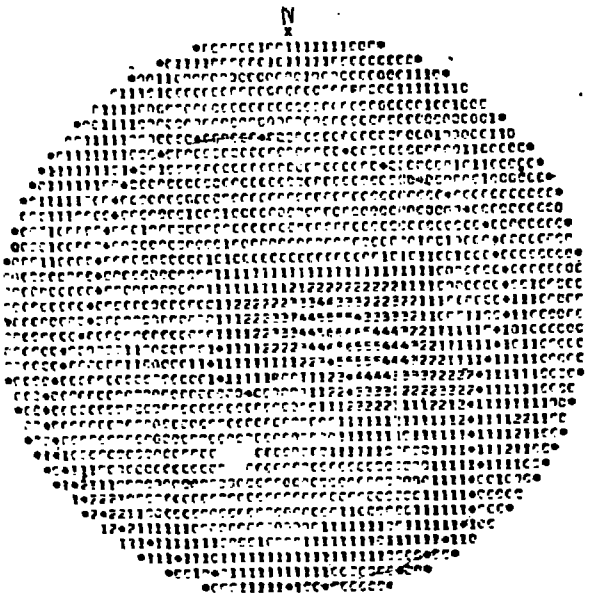

Projection 63 , r = 2.2 a

W_d = 8.26 W_{dI} = 9.20

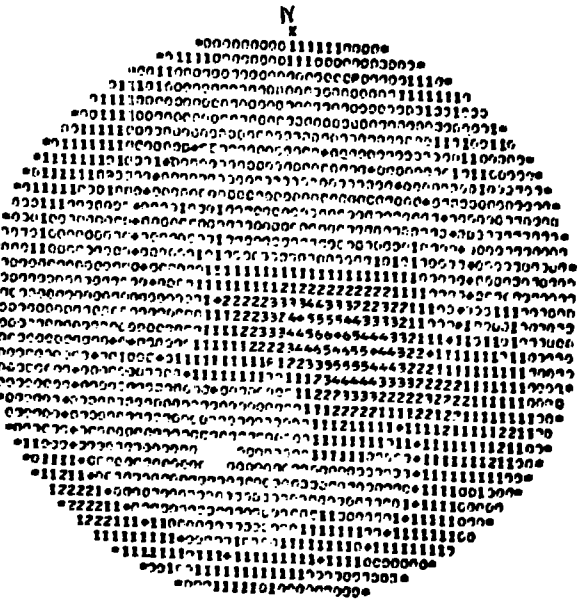

Projection 64, R = 3 a

W_d = 1.37 W_{dI} = 2.13

Equal area projections of the London Clay discontinuity fabric at Green Park Station.

Elements inclined at -60°, 2nd Quadrant (C_{rd}=5kN/m², ϕ_{rd}= 13.5°)

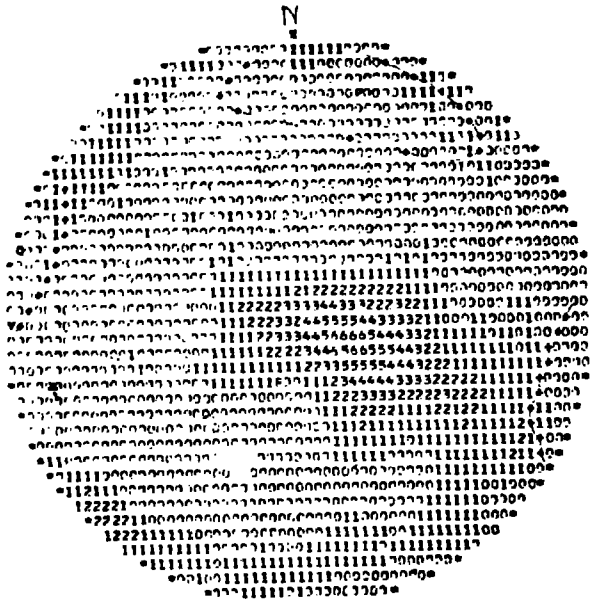

Projection 65, r = a

W_d= 90.73 W_{dI}= 84.10

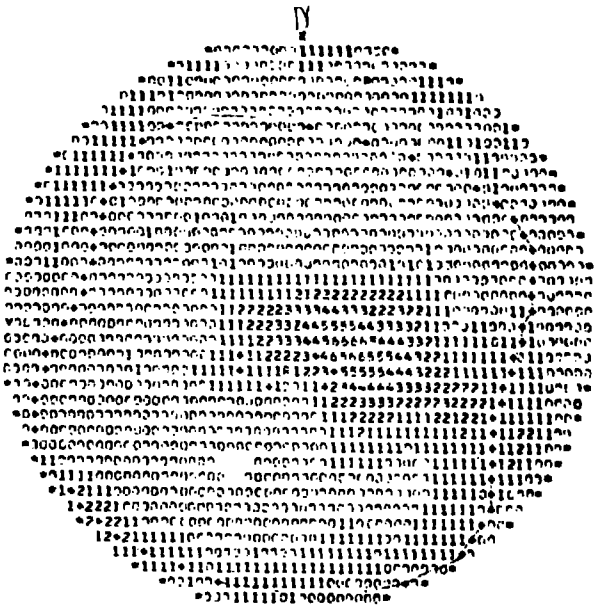

Projection 66 , r = 1.4 a

W_d= 14.76 W_{dI}= 17.70

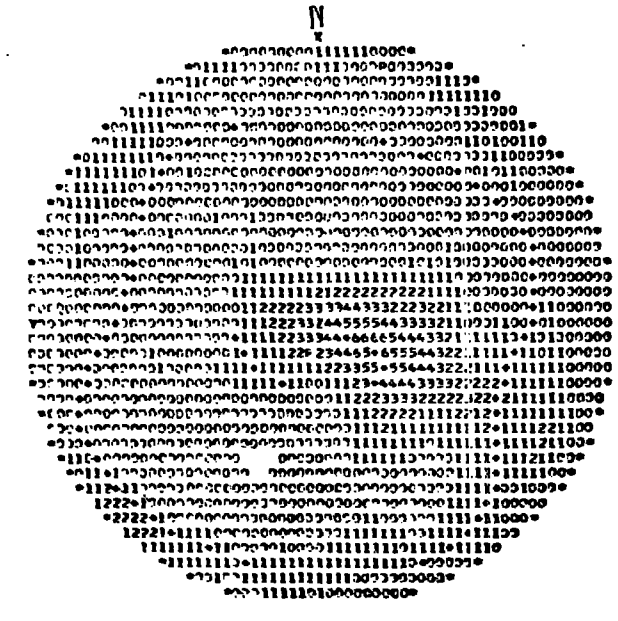

Projection 67 , r = 1.6 a

W_d= 5.87 W_{dI}= 8.36

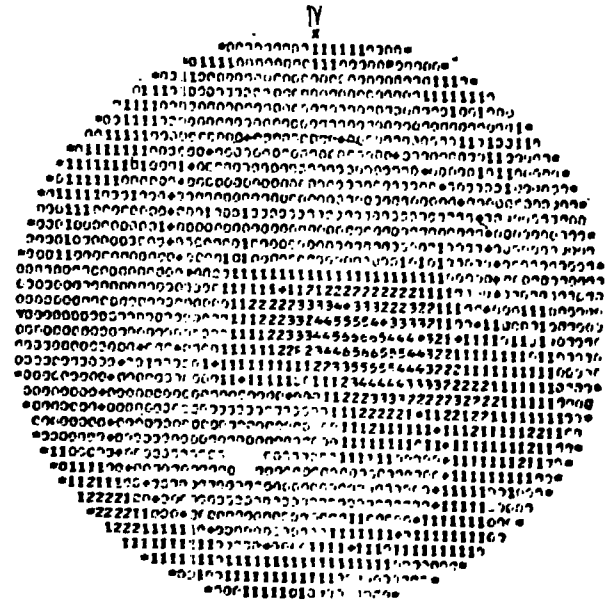

Projection 68, r = 2 a

W_d= 0.89 W_{dI}= 1.70

Equal area projections of the London Clay discontinuity fabric at Green Park Station.

Elements inclined at -70 degrees , 2nd Quadrant (C_{rd}= 5kN/m^2 , ϕ_{rd}= 13.5°)

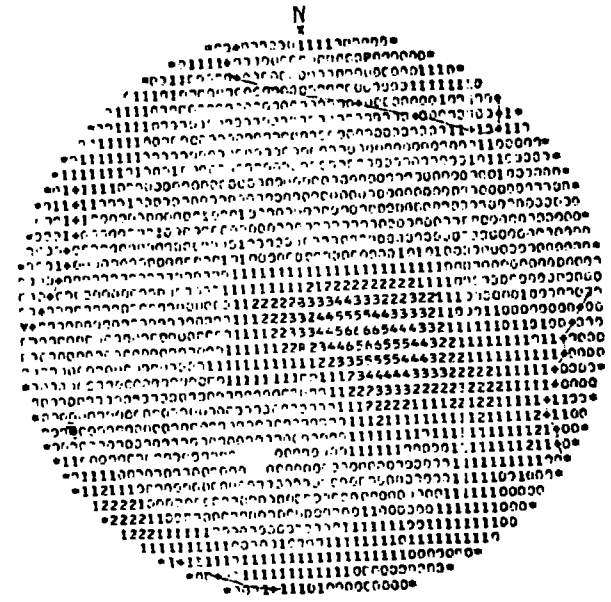

Projection 69 , r = a

W_d = 71.53 W_{dI} = 84.19

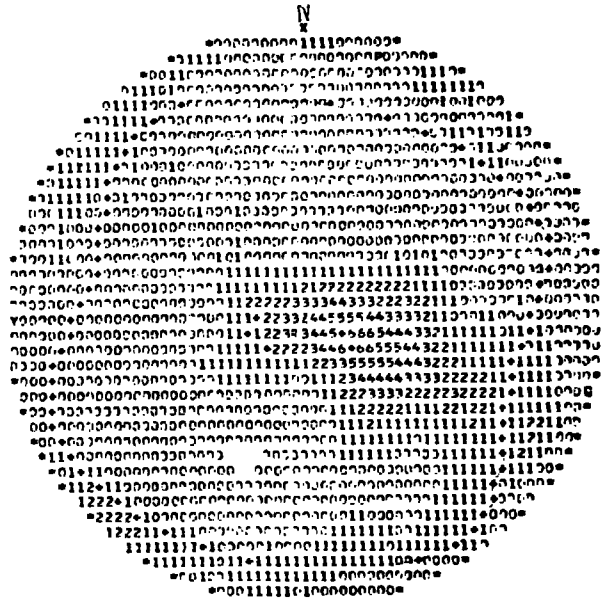

Projection 70 , r = 1.4 a

W_d = 11.64 W_{dI} = 16.88

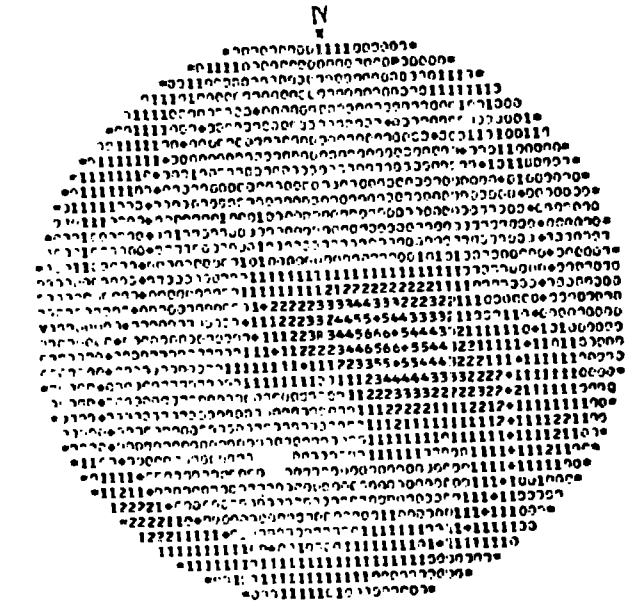

Projection 71 , r = 1.6 a

W_d = 4.62 W_{dI} = 7.59

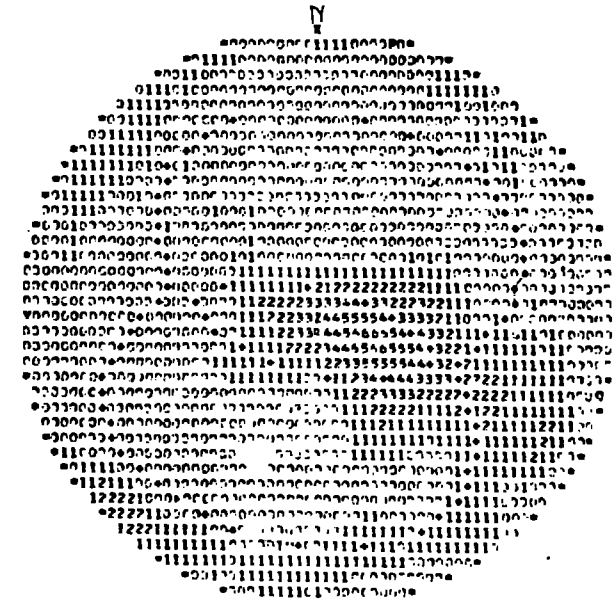

Projection 72, r = 1.8 a

W_d = 1.79 W_{dI} = 3.33

Equal area projections of the London Clay discontinuity fabric at Green Park Station.

Elements inclined at -80 degrees , 2nd Quadrant (C_{rd} = 5κN/m², ϕ_{rd} = 13.5°)

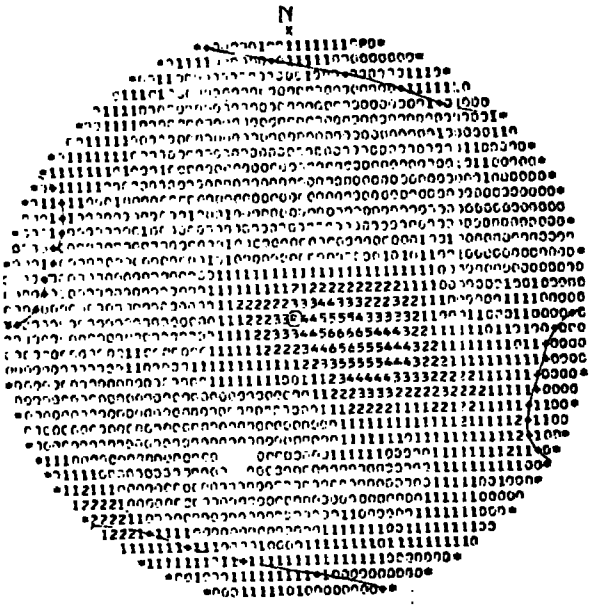

Projectio 73 , r = a

W_d = 66.12 W_{dI} = 84.19

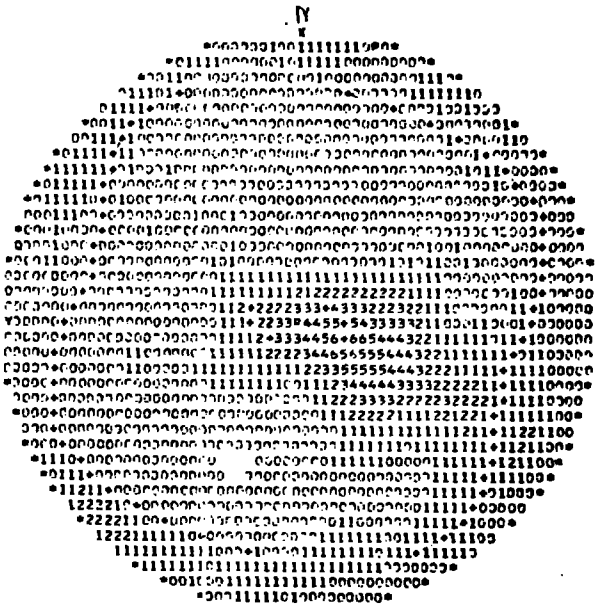

Projection 74, r = 1.4 a

W_d = 11.20 W_{dI} = 16.57

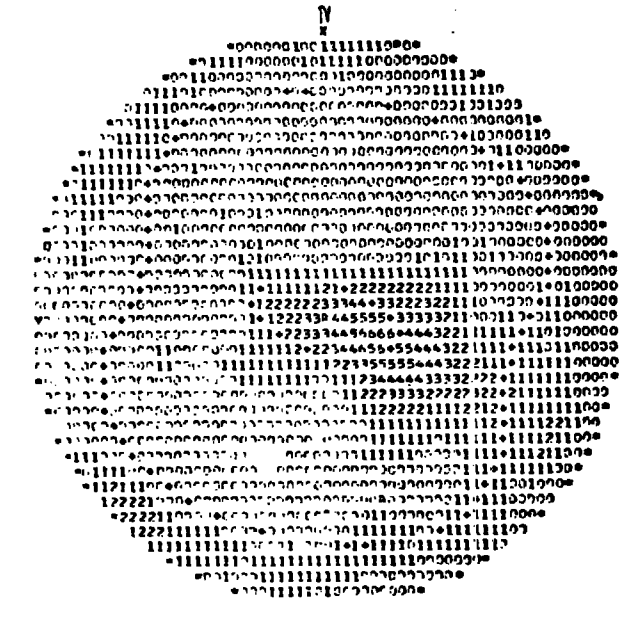

Projection 75 r = 1.6 a

W_d = 4.43 W_{dI} = 7.29

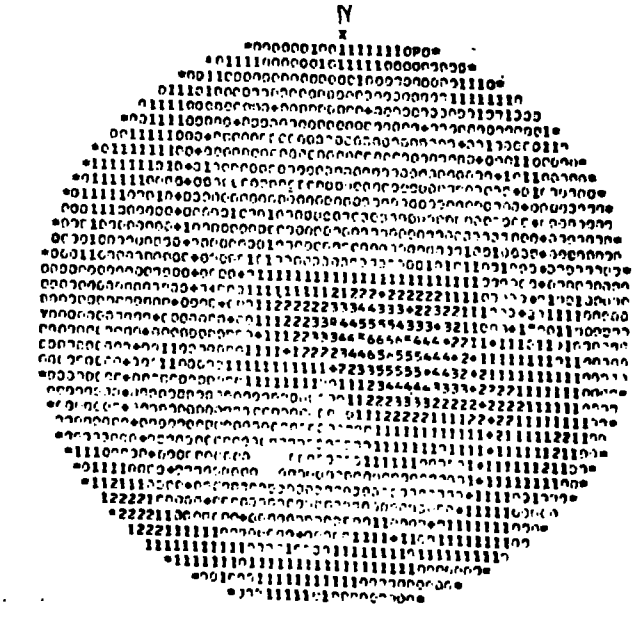

Projection 76 , r = 1.8 a

W_d = 1.69 a W_{dI} = 3.13 a

Equal area projections of the London Clay discontinuity fabric at Green Park Station.

Elements inclined at -90 degrees , 3rd Quadrant (C_{rd} = 5κN/m², ϕ_{rd} = 13.5°)

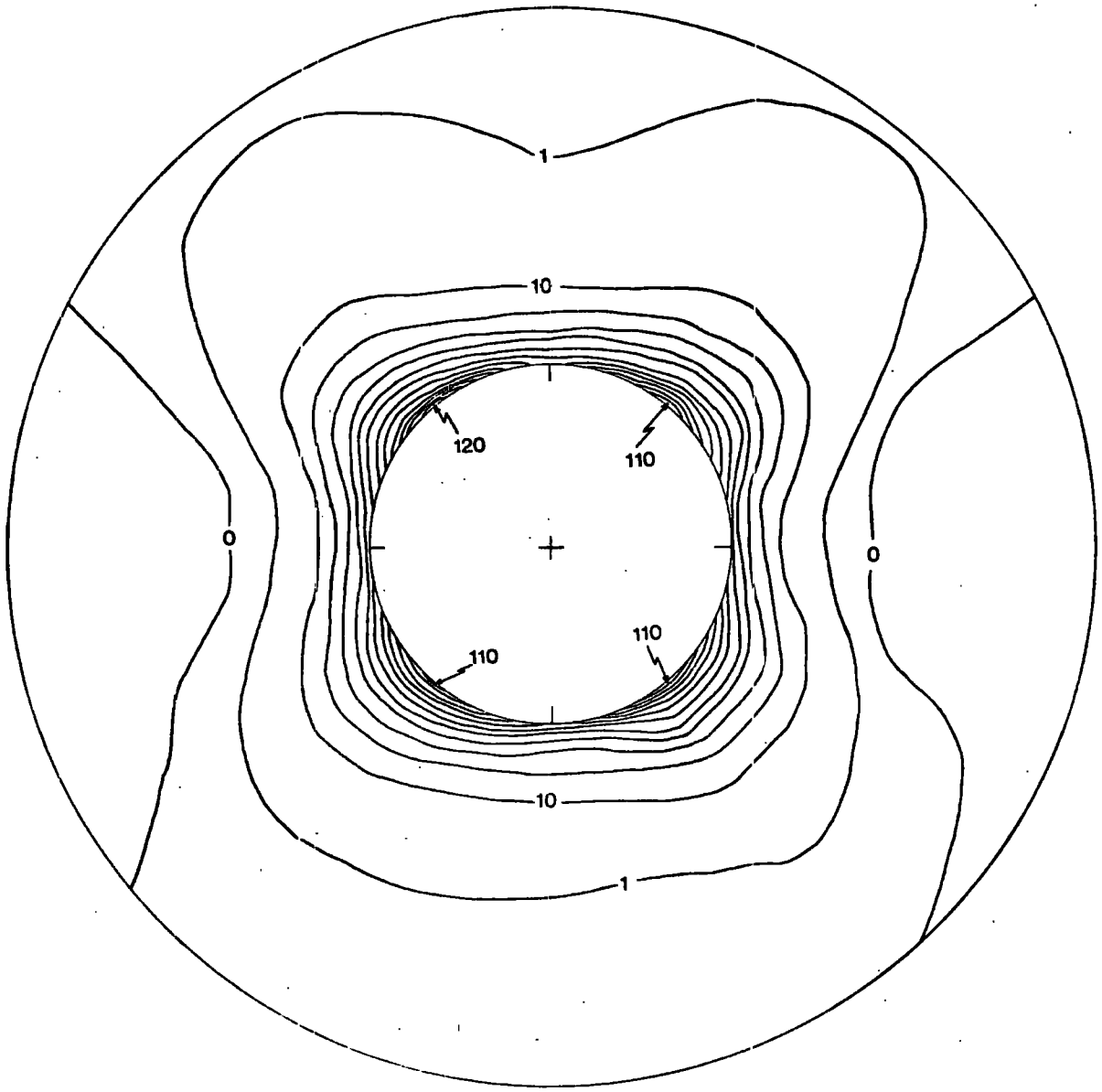

Fig. 4. e. 2. Distribution of shear strain energy (W_d) around the tunnel, generated by the non-random discontinuity fabric of London Clay at Green Park Station.

The shear strength characteristics used are C_{fd}= 5kN/m², ϕ_{fd} = 13.5°.

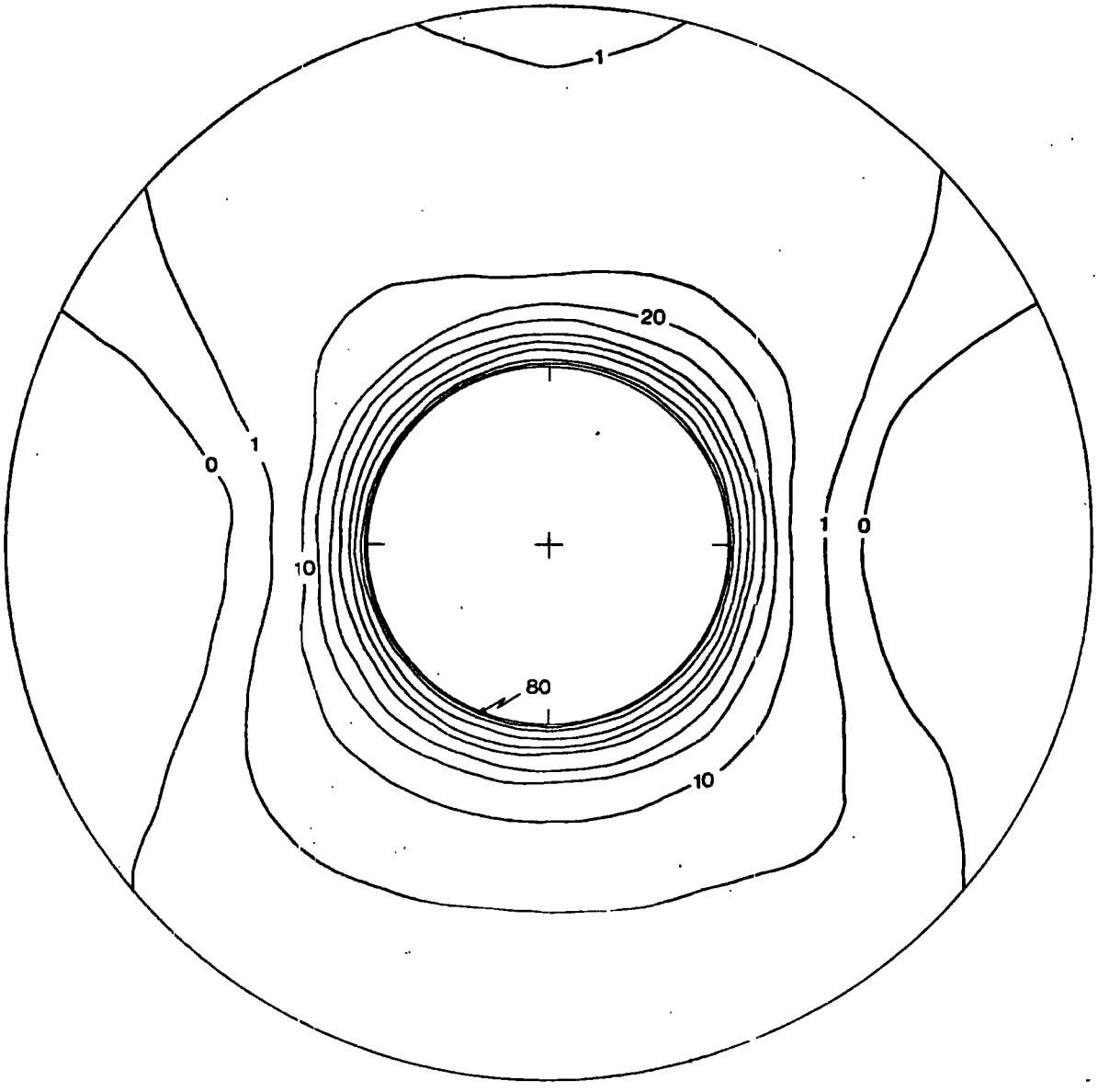

Fig. 4. e. 3. Distribution of shear strain energy (W_{dI}) around the Fleet Line Tunnel generated by a random discontinuity fabric equivalent to London Clay discontinuity fabric at Green Park Station. The shear strength characterisics used are C_{rd}= 5kN/m^2, ϕ'_{rd}= 13.5°.

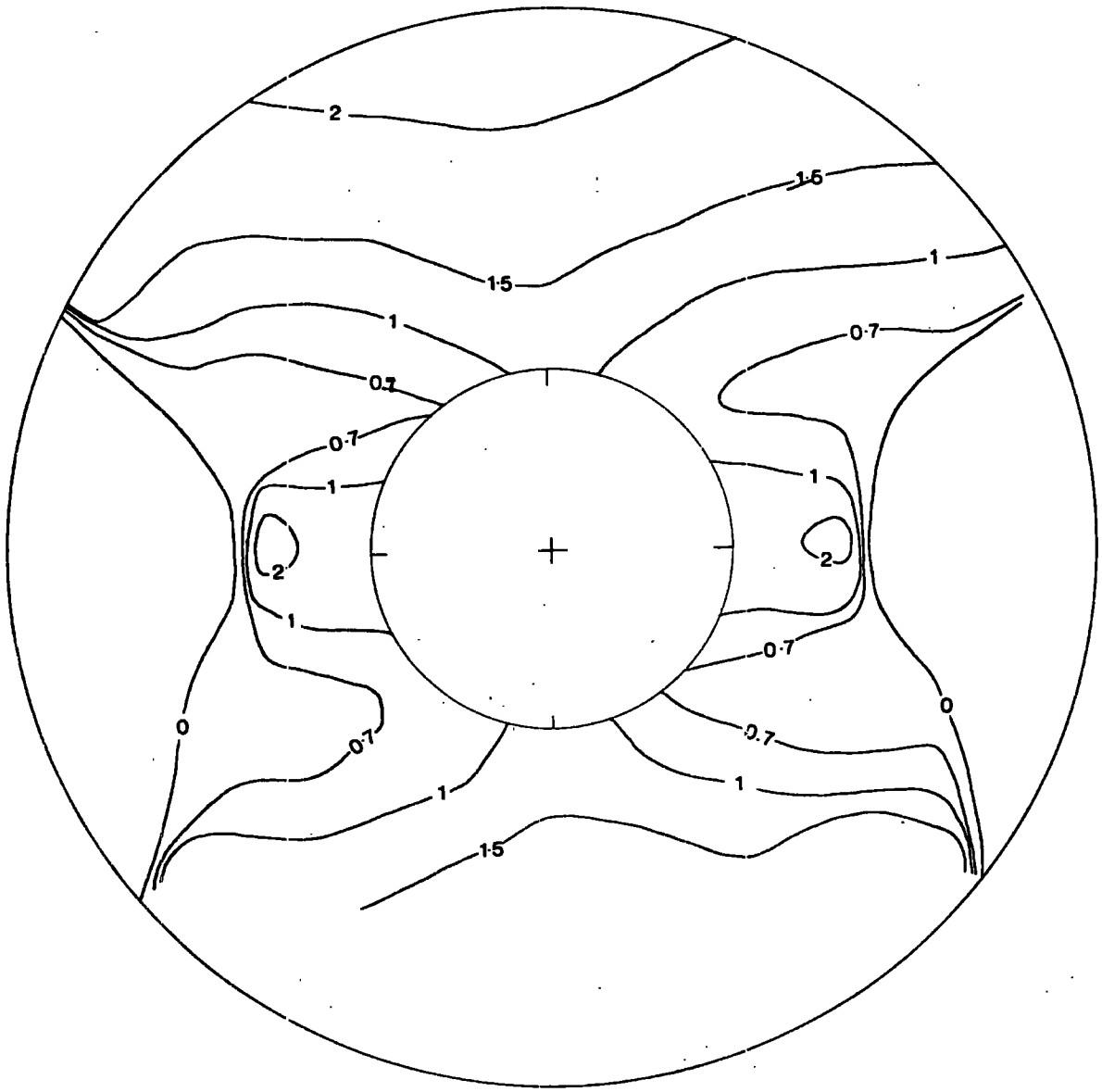

Fig. 4. e. 4. Distribution of the "safety index" (W_{cr}/W_d) around the tunnel.
The shear strength characteristics used are C_{fd}= 5kN/m², ϕ_{fd}= 13.5°.

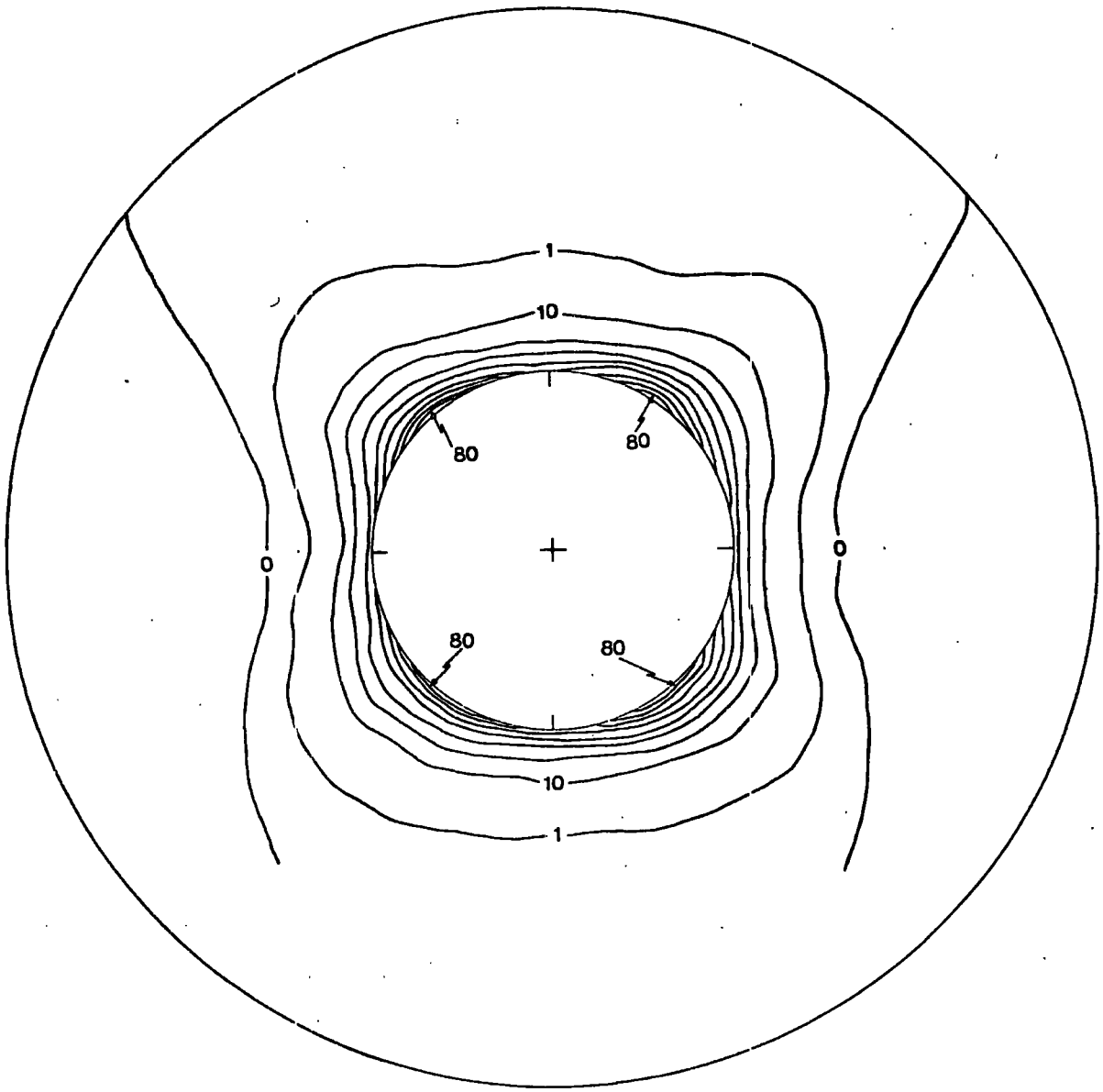

Fig. 4.e.5. Distribution of shear strain energy (W_d) around the tunnel, generated by the non-random discontinuity fabric of London Clay at Green Park Station.
The shear strength characteristics used are $\hat{C}_d = 7\kappa N/m^2$, $\hat{\phi}_d = 18.5°$

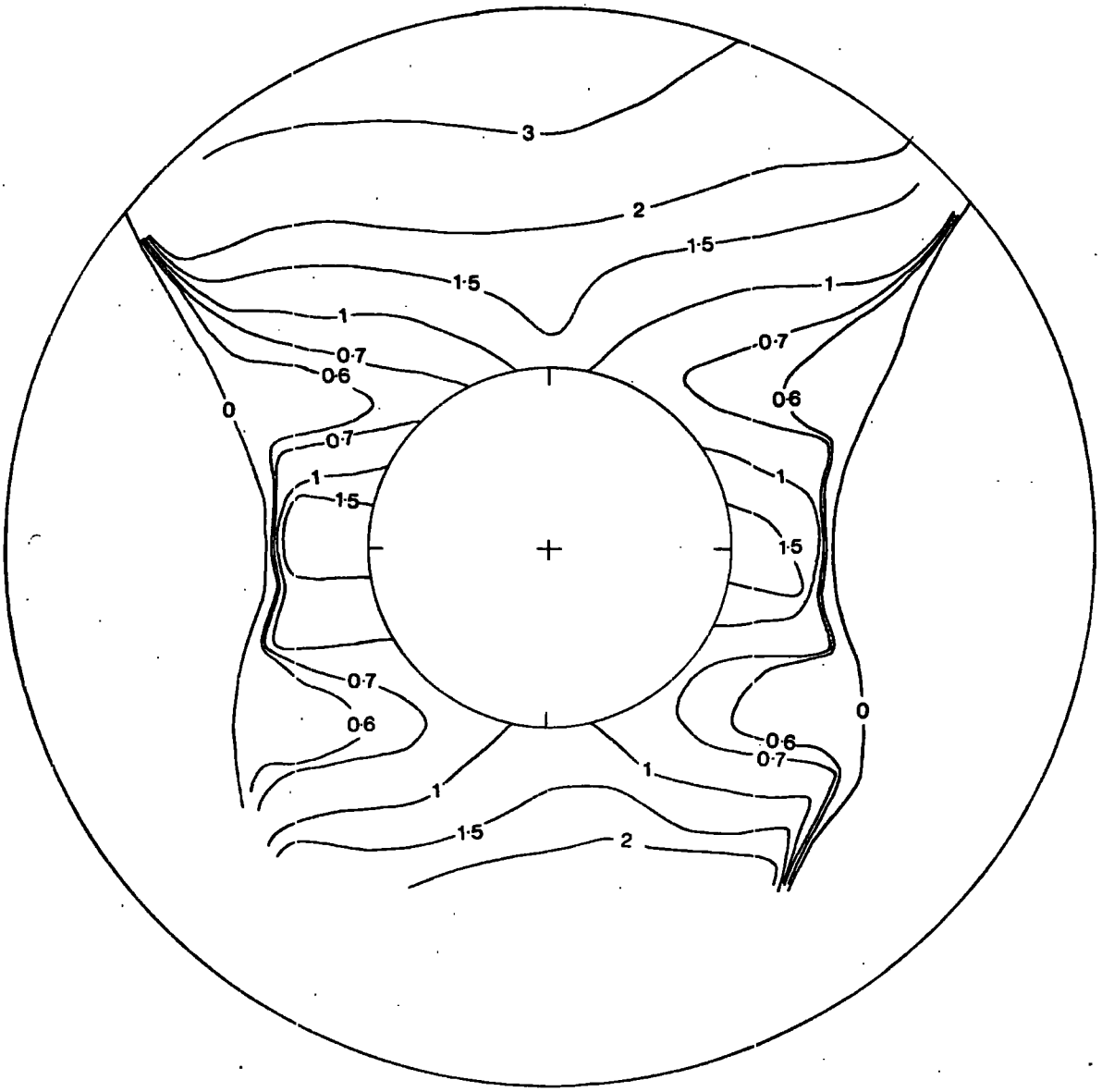

Fig. 4.e.6. Distribution of the "safety index" (W_{dl}/W_d) around the Fleet Line Tunnel

The shear strength characteristics used are $\hat{C}_d = 7\,kN/m^2$, $\hat{\phi}_d = 18.5°$.

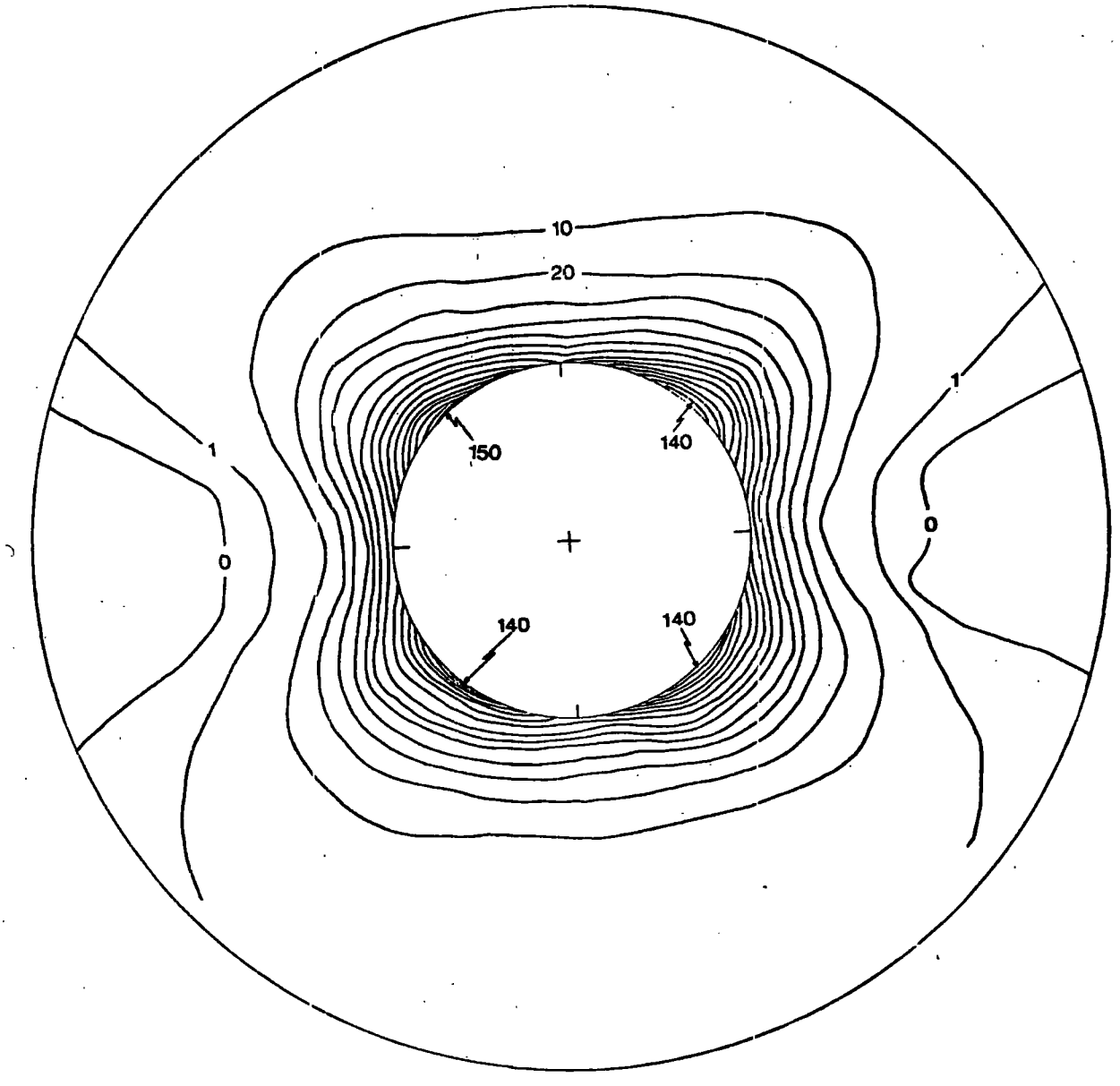

Fig. 4.e.7. Distribution of shear strain energy (W_d) around the Fleet Line Tunnel, generated by the non-random discontinuity fabric of London Clay at Green Park Station.
The shear strength characteristics used are $C_r = 0 kN/m^2$, $\phi_r = 9.4°$.

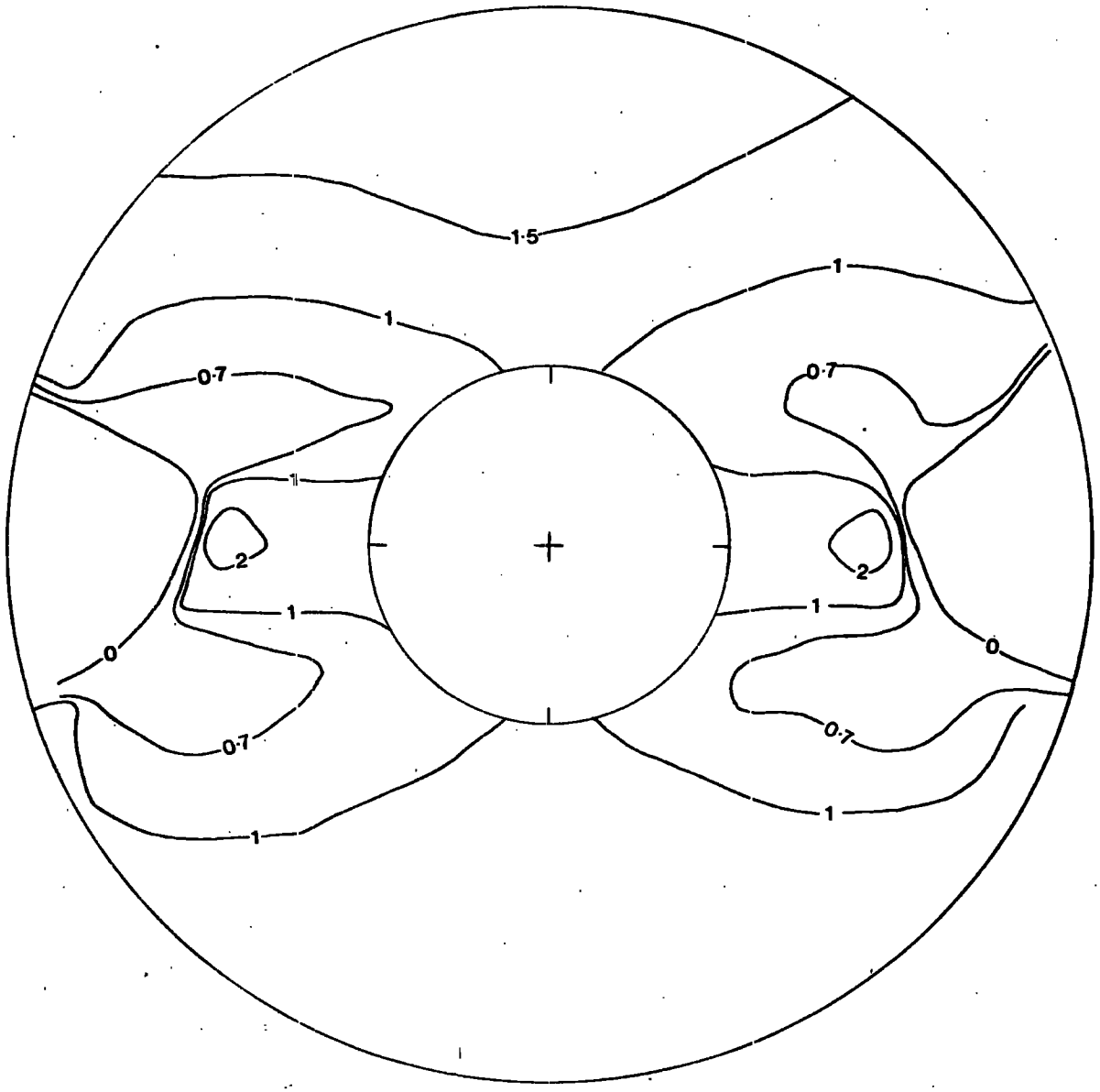

Fig. 4.e.8. Distribution of the "safety index" (W_{st}/W_d) around the Fleet Line Tunnel.

The shear strength characteristics used are $C_r = 0 kN/m^2$, $\phi_r = 9.4°$.

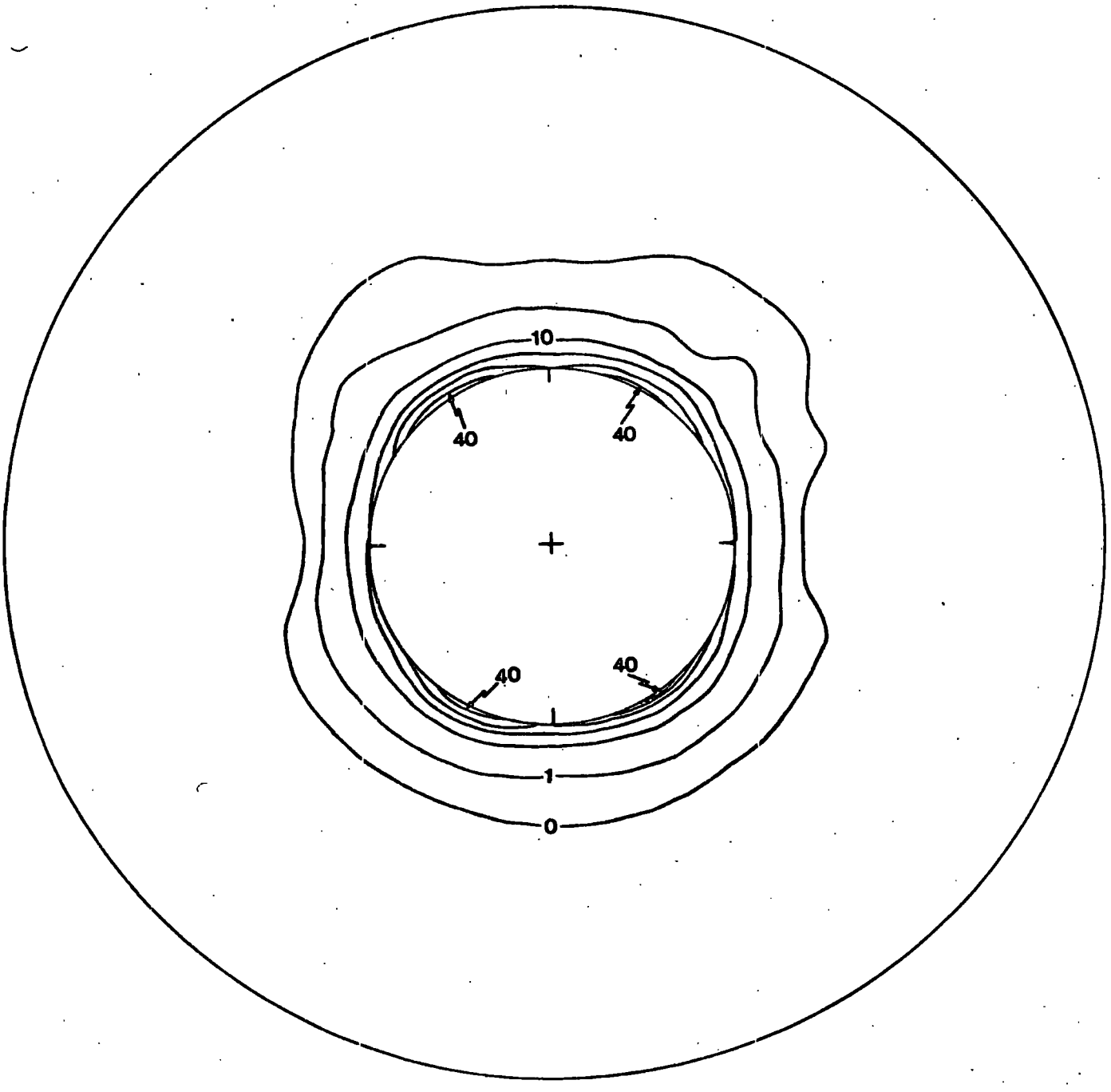

Fig. 4.e.9. Distribution of shear strain energy (W_d) around the Fleet Line Tunnel , generated by the non-random discontinuity fabric of London Clay at Green Park Station.
The shear strength characteristics used are $\hat{C} = 0$ kN/m², $\hat{\phi} = 29°$.

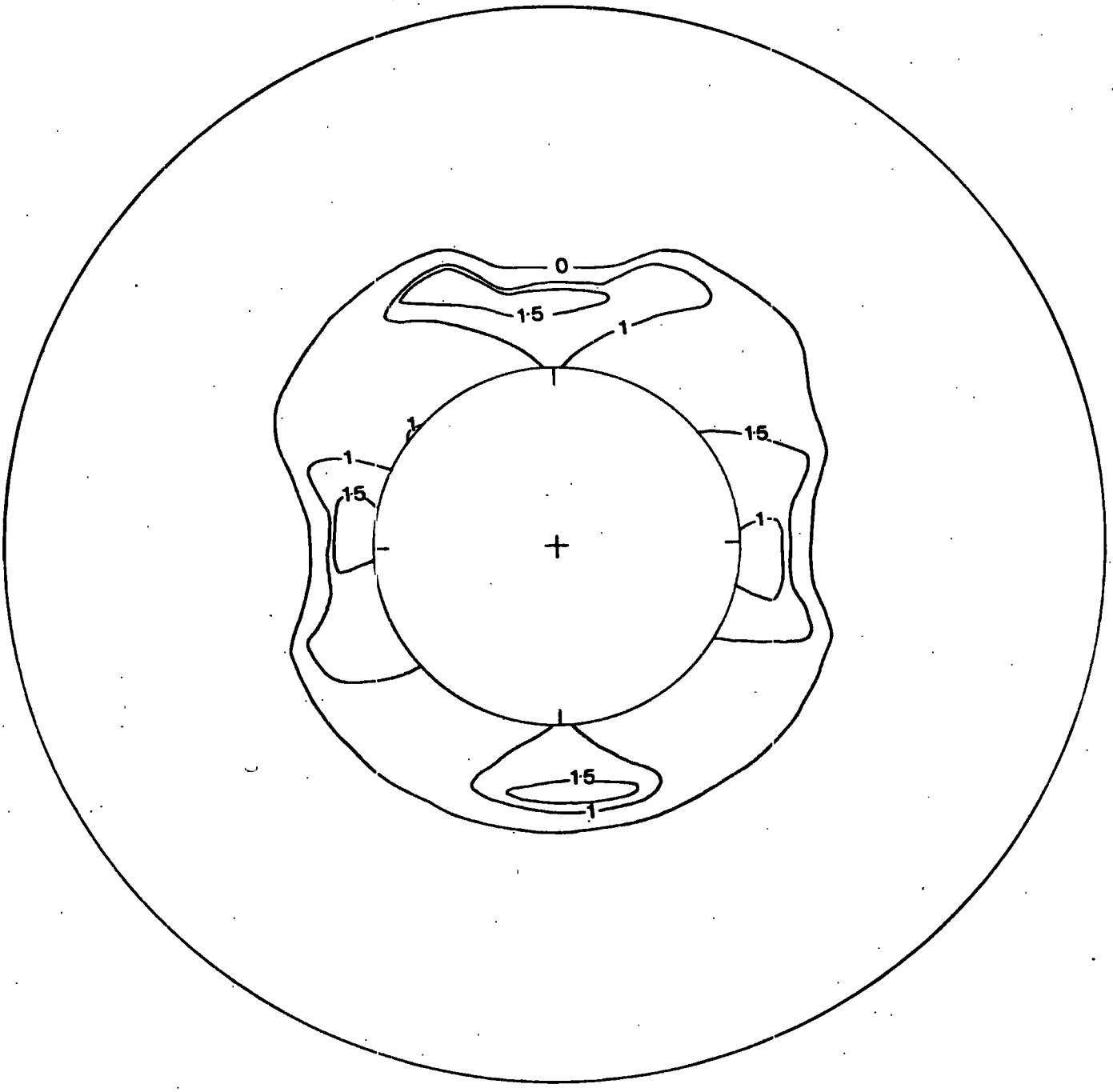

Fig. 4.e.10. Distribution of the "safety index" (W_{dU}/W_d) around the Fleet Line Tunnel.
The shear strength characteristics used are $\hat{C}$ = 0 kN/m², $\hat{\phi}$ = 29°.

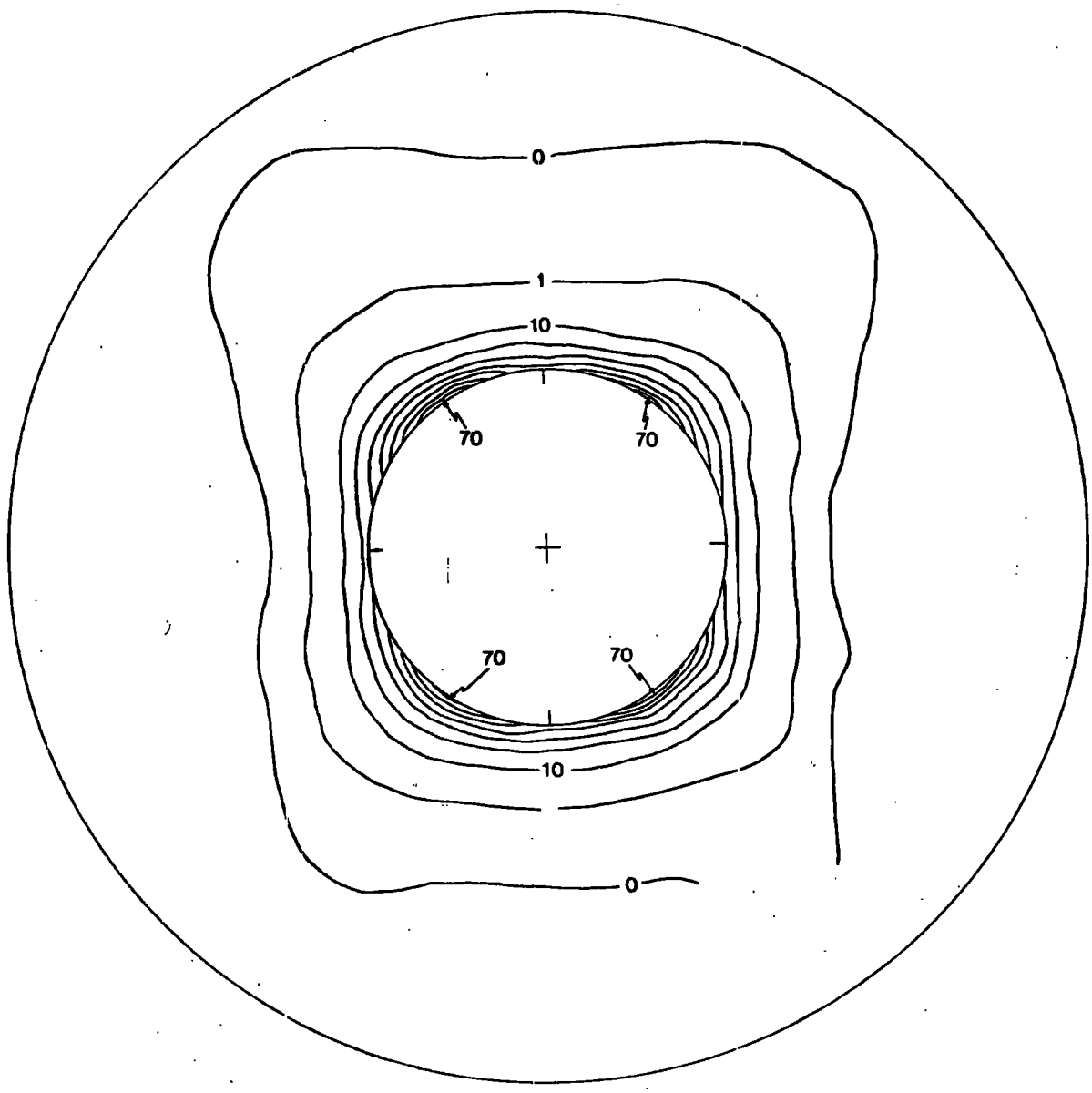

Fig. 4.e.11. Distribution of shear strain energy (W_d) around the Fleet Line Tunnel., generated by the non-random discontinuity fabric of London Clay at Green Park Station.
The shear strength characteristics used are $\hat{C}$ = 33.12kN/m², $\hat{\phi}$ = 18.9°.

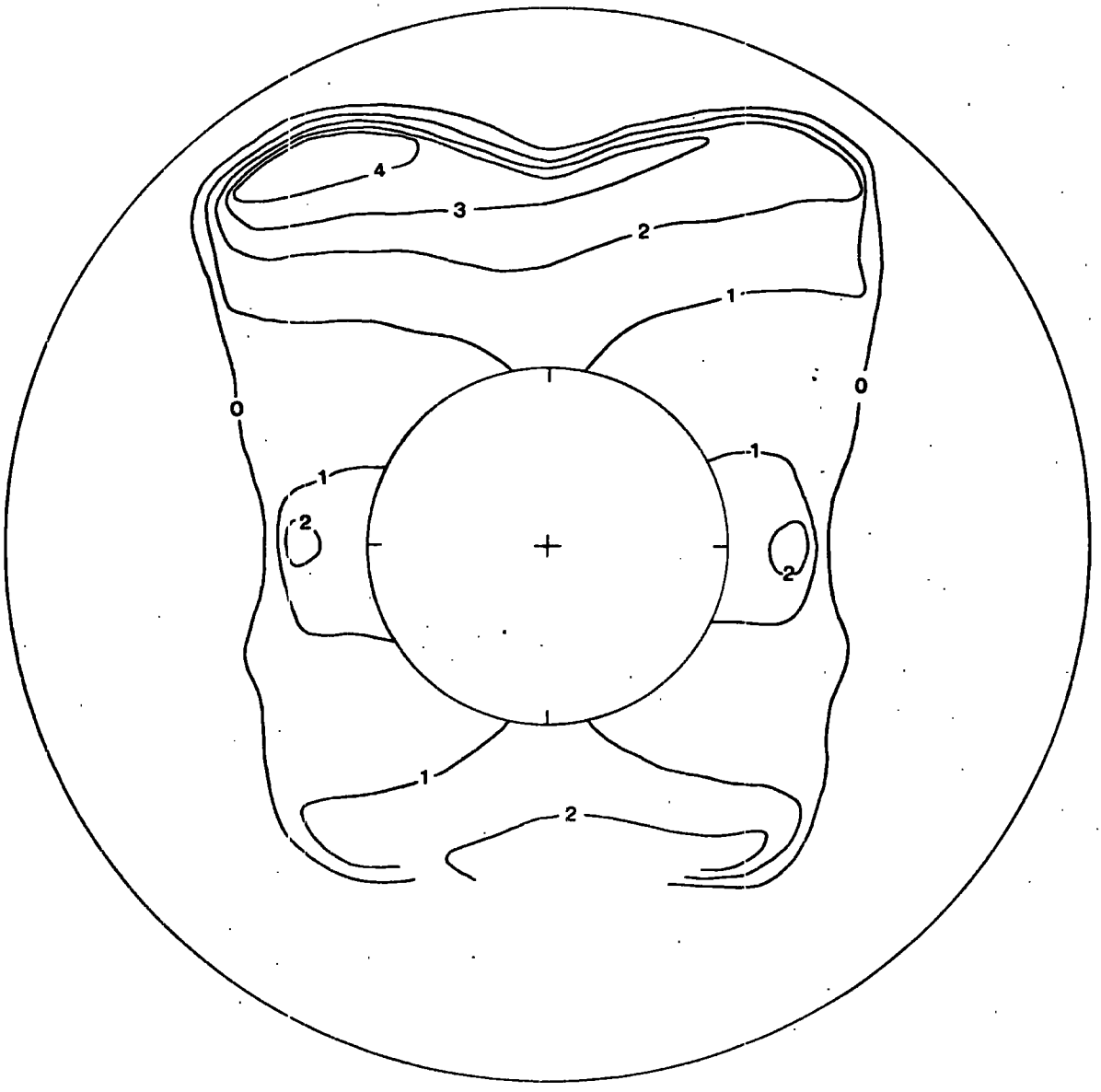

Fig. 4.e.12. Distribution of the "safety index"(W_{dI}/W_d) around the Fleet Line Tunnel.
The shear strength characteristics used are $\hat{C}$ = 33.12 kN/m², $\hat{\phi}$ = 18.9°.

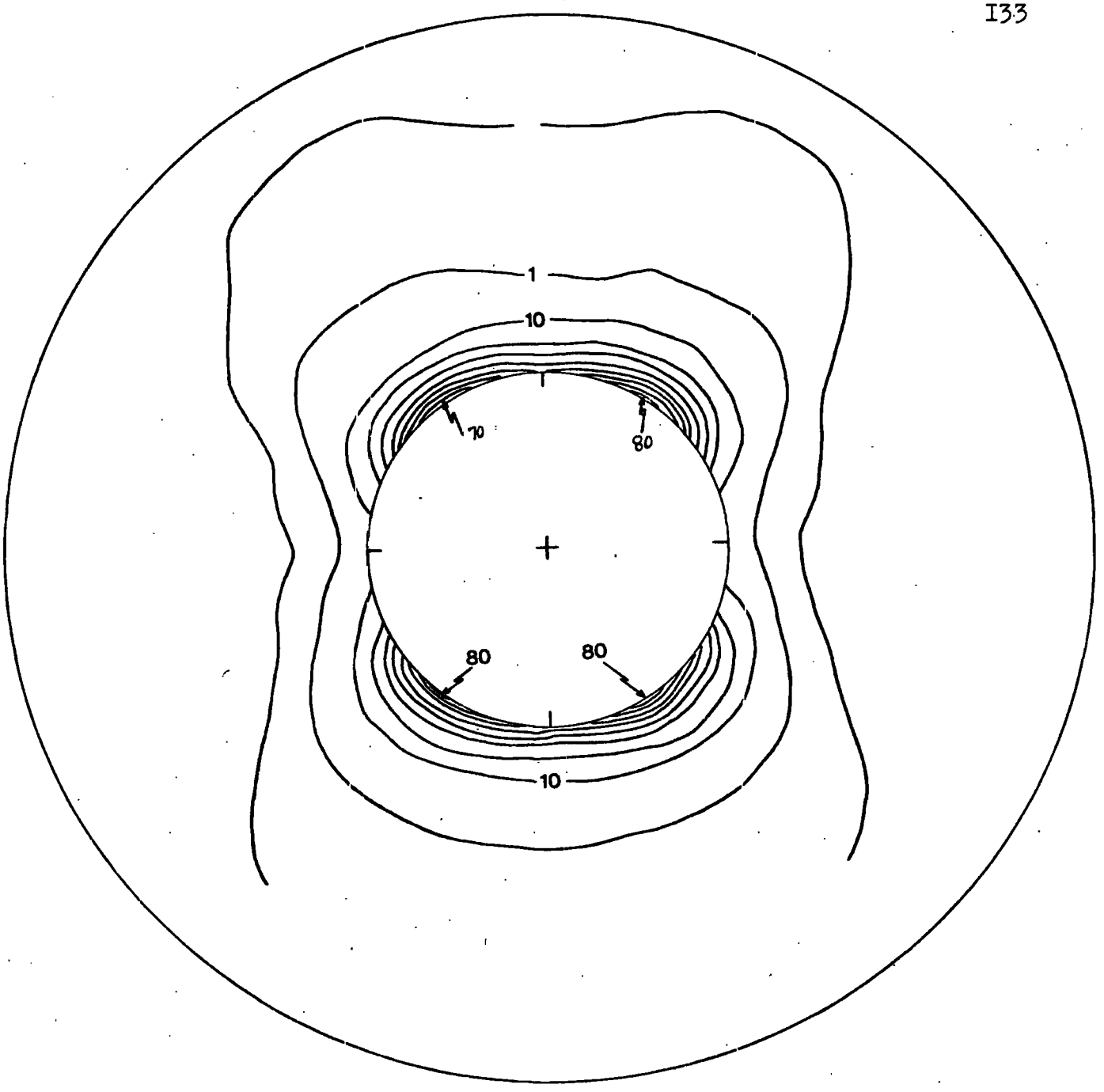

Fig. 4.e.13. Distribution of shear strain energy (W_d) around the Fleet Line Tunnel , generated by the non-random discontinuity fabric of London Clay at Green Park Station.
The shear strength characteristics used are $\hat{C}$ = 235 $\kappa N/m^2$, $\hat{\phi}$ =0.45°.

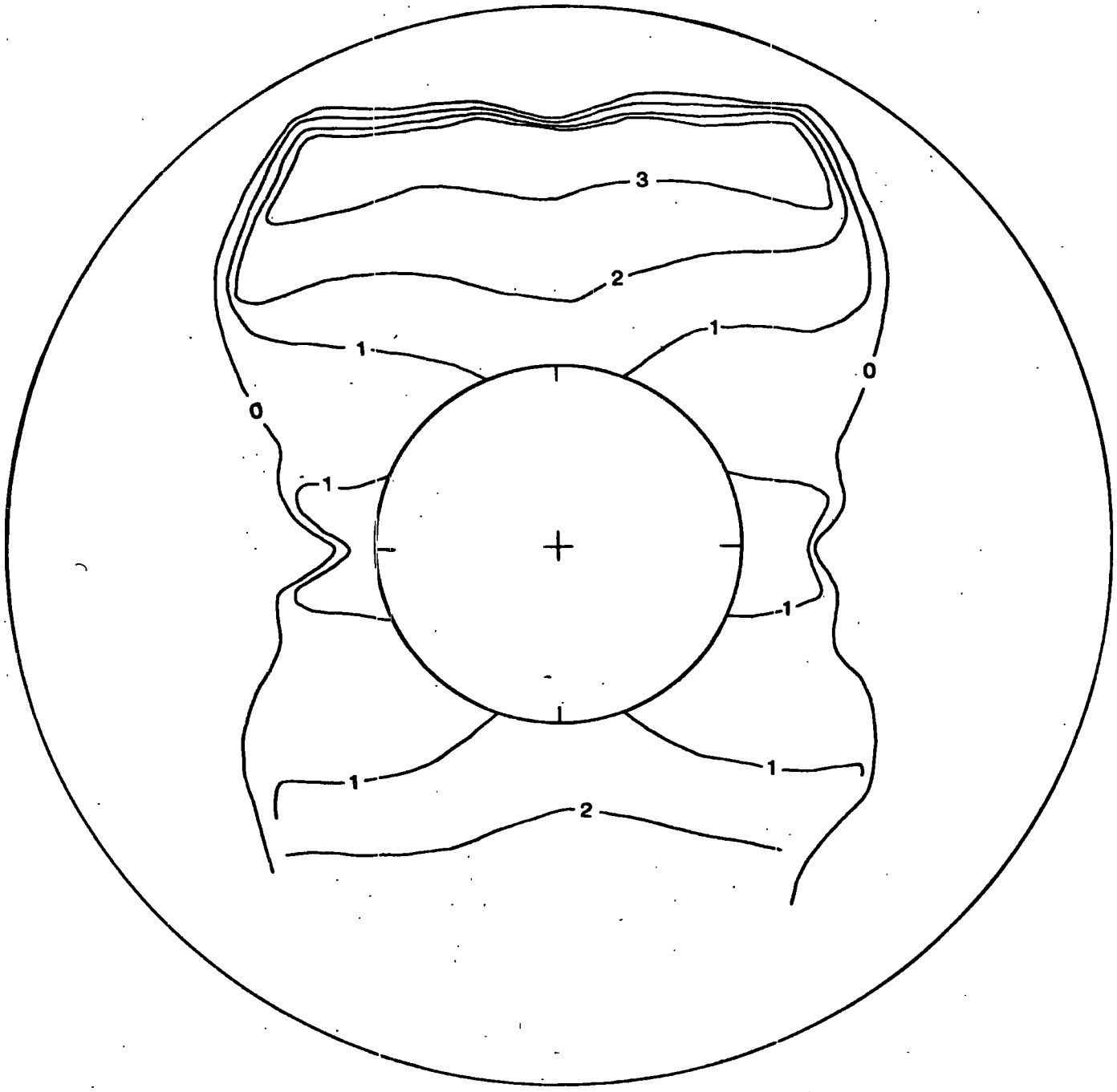

Fig. 4.e.14. Distribution of the "safety index" (W_{dl}/W_d) around the Fleet Line Tunnel.
The shear strength characteristics used are $\hat{C}$= 235 kN/m^2, $\hat{\phi}$ = 0.43°.

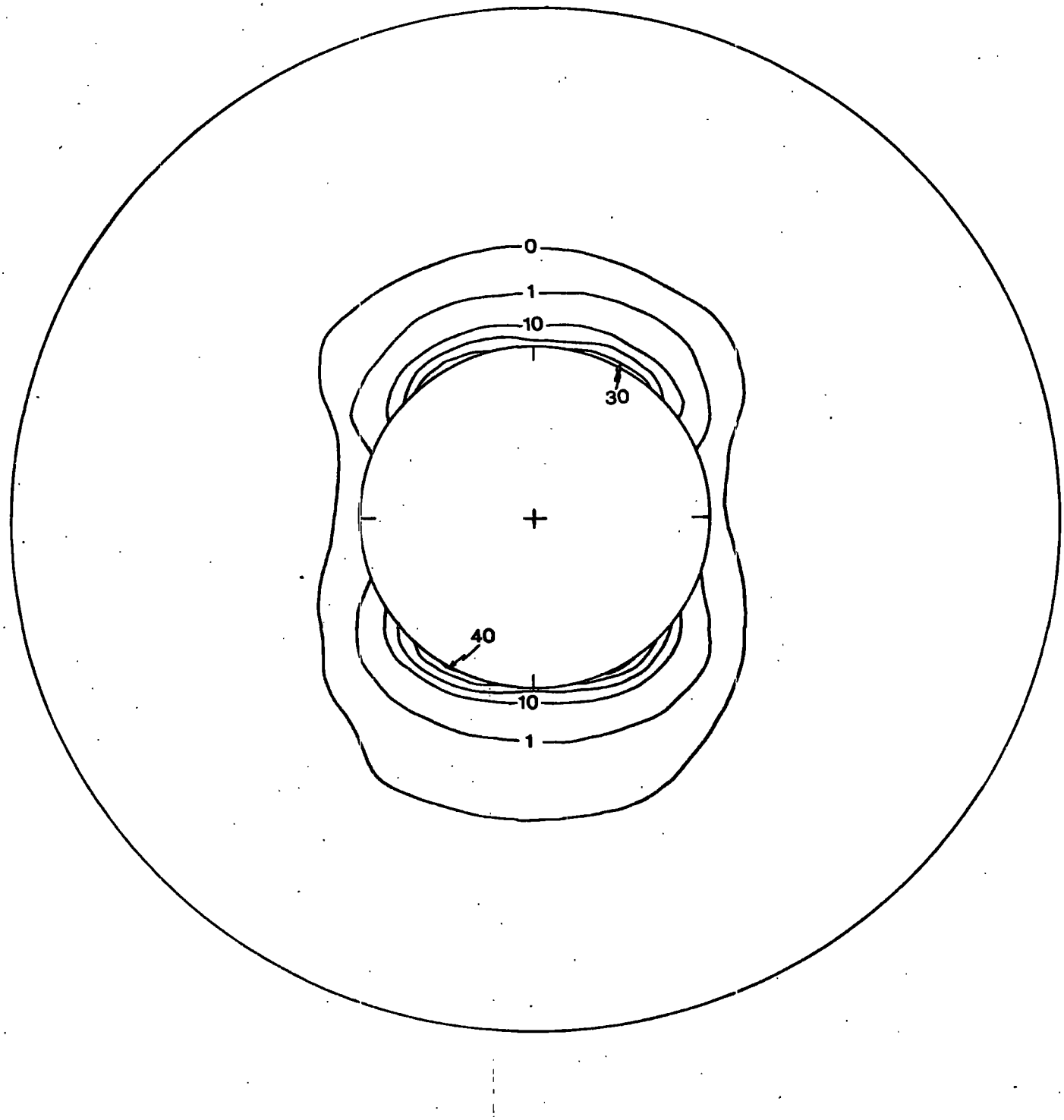

Fig. 4.e. 15. Distibution of shear strain energy (W_d) around the Fleet Line Tunnel , generated by the non-random discontinuity fabric of London Clay at Green Park Station.
The shear strength charactiristics used are $\hat{C}$= 400 KN/m², $\hat{\phi}$ = 0.43°.

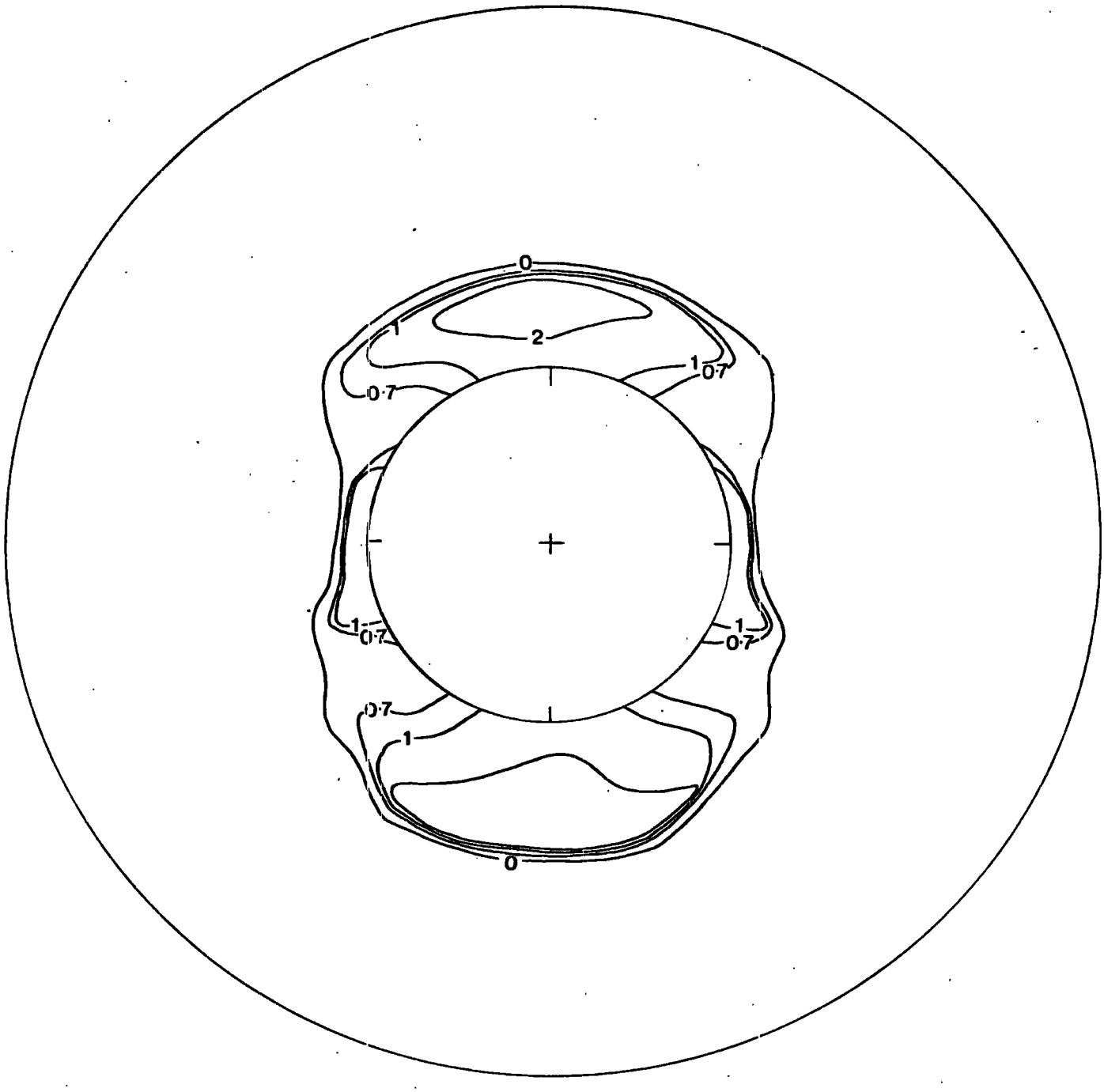

Fig. 4.e.16. Distribution of the safety index (W_{dI}/W_d) around the Fleet Line Tunnel.
The shear strength characteristics used are $\hat{C}$ = 400 kN/m², $\hat{\phi}$ = 0.43°.

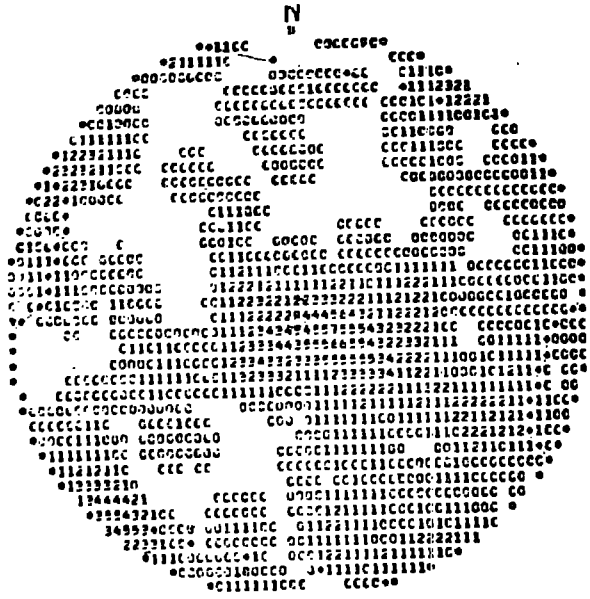

Projection 77 , r = a

W_d = 61.22 W_{dI} = 84.19

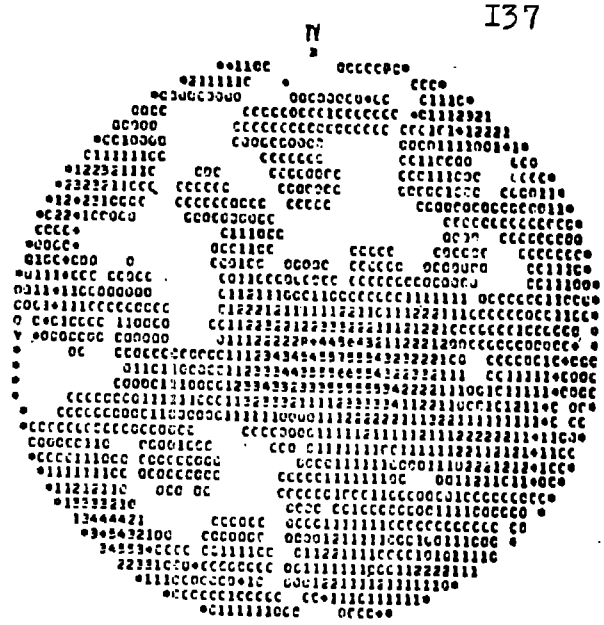

Projection 78 , r = 1.02 a

W_d = 56.27 W_{dI} = 77.77

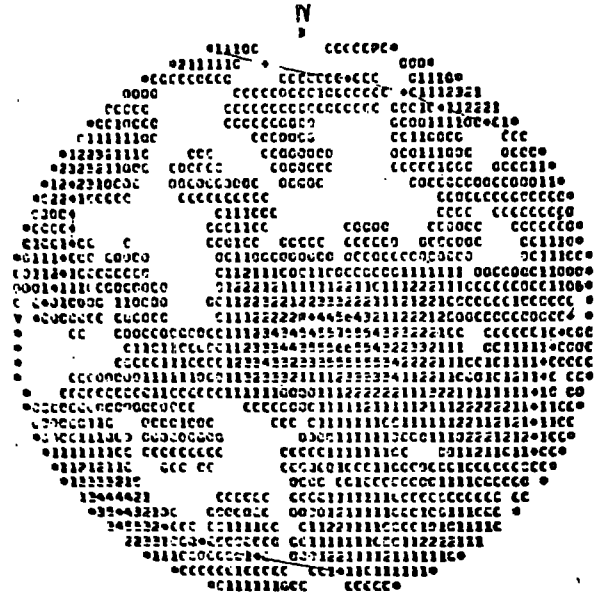

Projection 79 , r = 1.04 a

W_d = 51.58 W_{dI} = 71.77

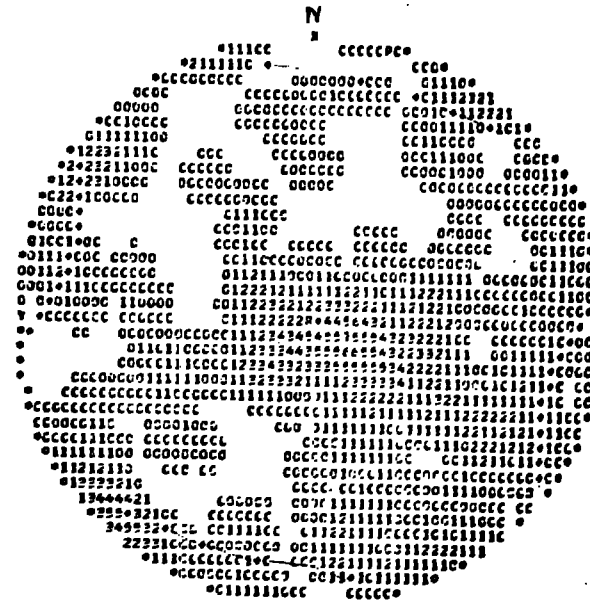

Projection 80, r = 1.06 a

W_d = 47.33 W_{dI} = 66.27

Equal area projections of a section of the London Clay discontinuity fabric at Green Park Station.

The elments are inclined at 90 degrees, 1st Quadrant (C_{rd}= 5 kN/m^2, ϕ_{rd}=13.5°).

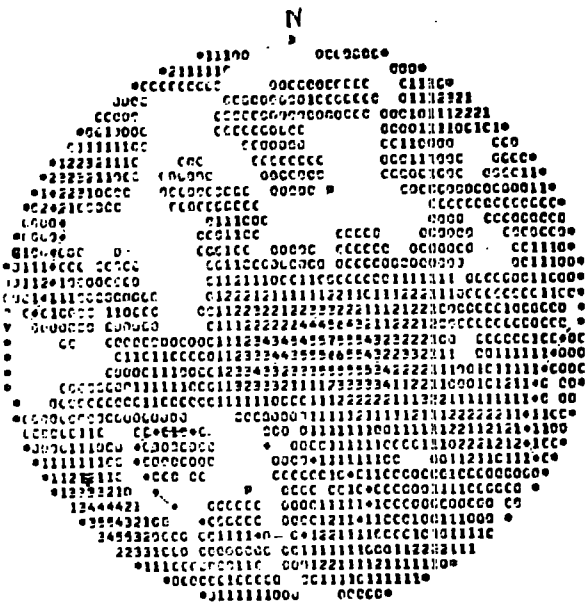

Projection 81, r = a

W_d = 107.58 W_{dl} = 83.45

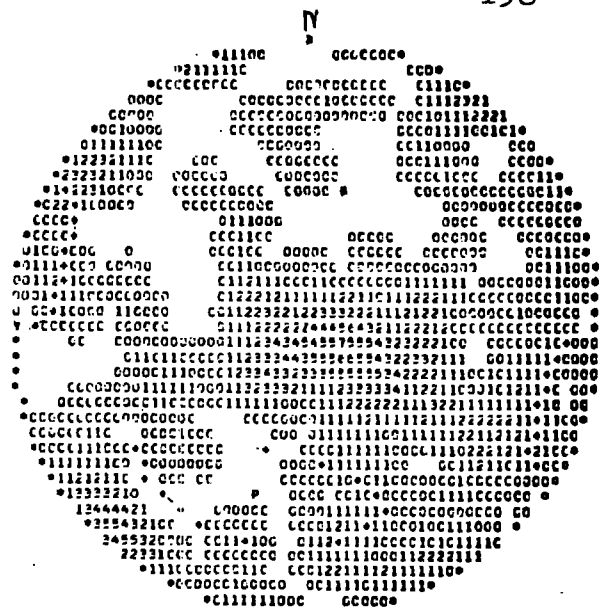

Projection 82, r = 1.02 a

W_d = 100.09 W_{dl} = 77.13

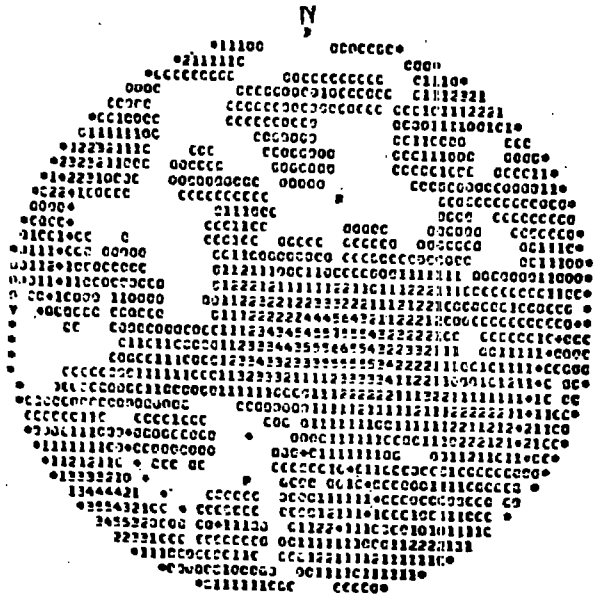

Projection 83, r = 1.04 a

W_d = 93.17 W_{dl} = 71.42

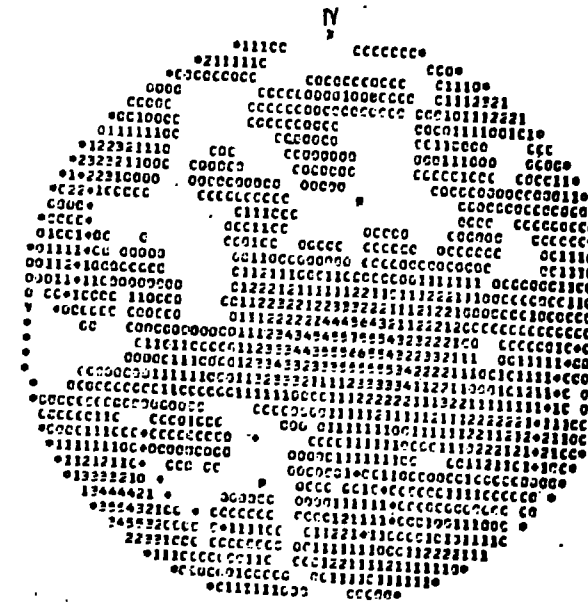

Projection 84, r = 1.06 a

W_d = 86.73 W_{dl} = 66.21

Equal area projections of a section of the London Clay discontinuity fabric at Green Park Station.

The elements are inclined at 50° degrees , 1st Quadrant (C_{fd} = 5 kN/m², ϕ_{fd} = 13.5°

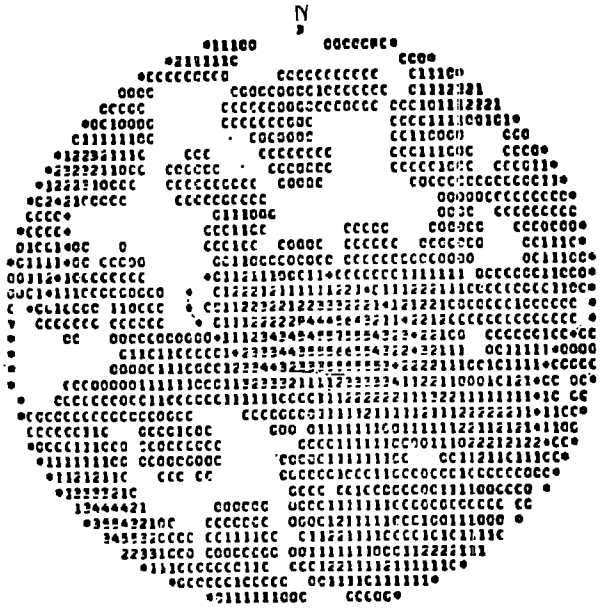

Projection 85, r = a

W_d = 53.21 W_{dI} = 84.08

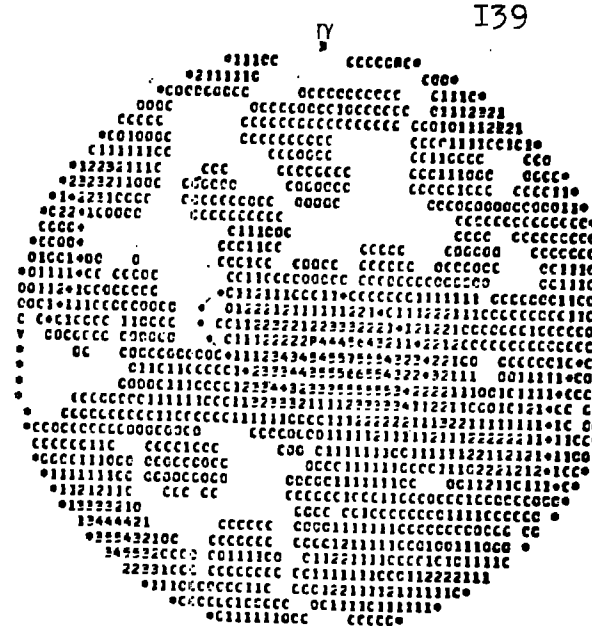

Projection 86, r = 1.02 a

W_d = 48.81 W_{dI} = 77.53

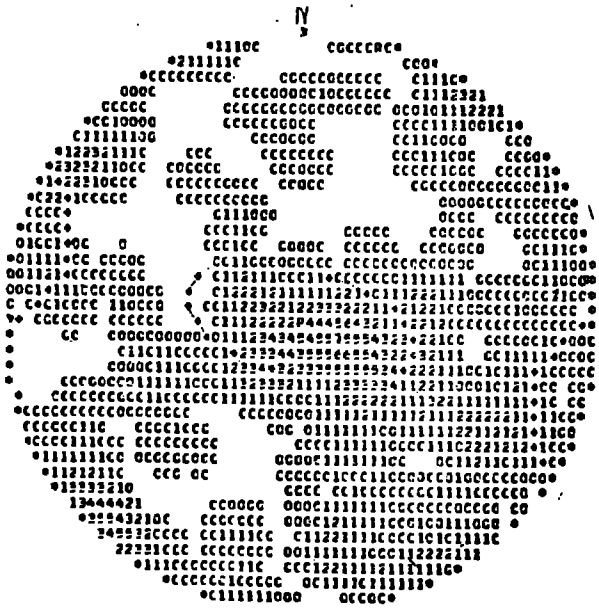

Projection 87, r = 1.04 a

W_d = 44.61 W_{dI} = 71.28

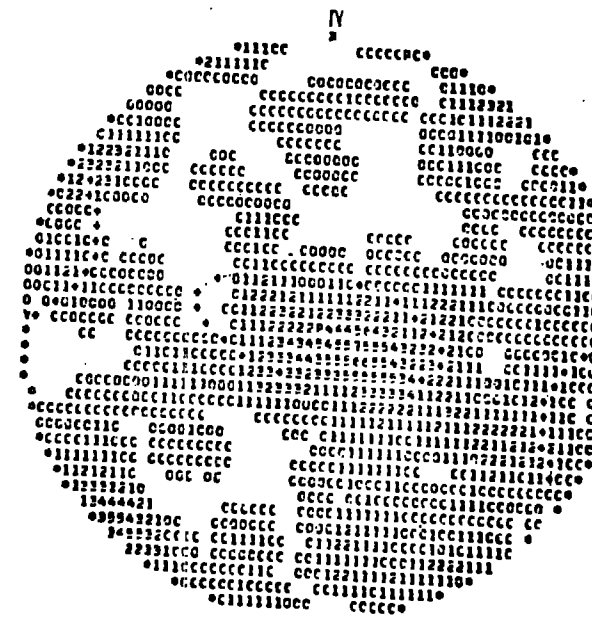

Projection 88, r = 1.06 a

W_d = 40.04 W_{dI} = 65.01

Equal area projections of a section of the London Clay discontinuity fabric at Green Park Station.

The elements are inclined at 0.0 degrees , 2nd Quadrant (C_{rd}= 5kN/m^2; ϕ_{rd}= 13.5°).

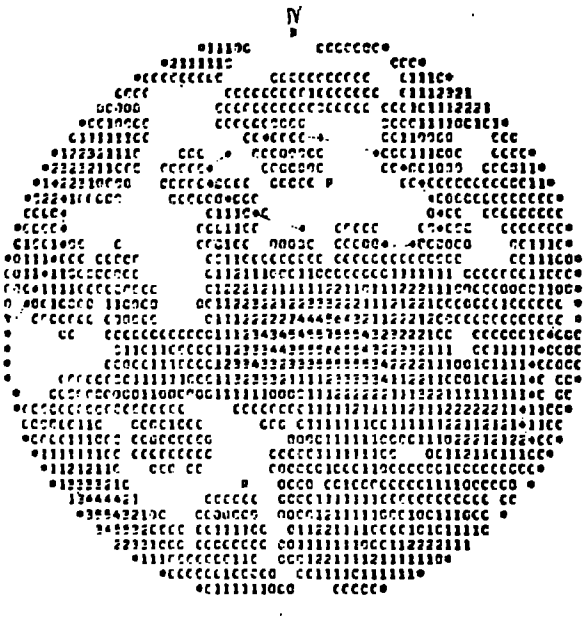

Projection 89, r = a

W_d = 119.98 W_{dI} = 83.25

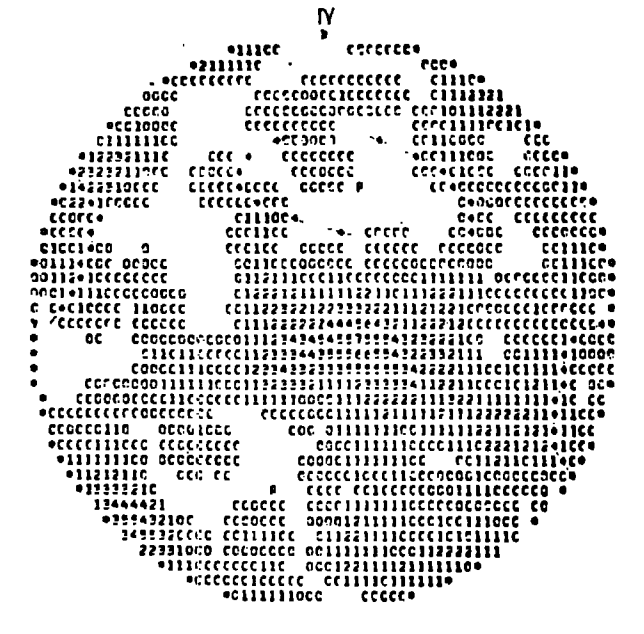

Projection 90, r= 1.02a

W_d = 112.40 W_{dI} = 76.93

Projection 91, r = 1.04 a

W_d = 105.19 W_{dI} = 71.12

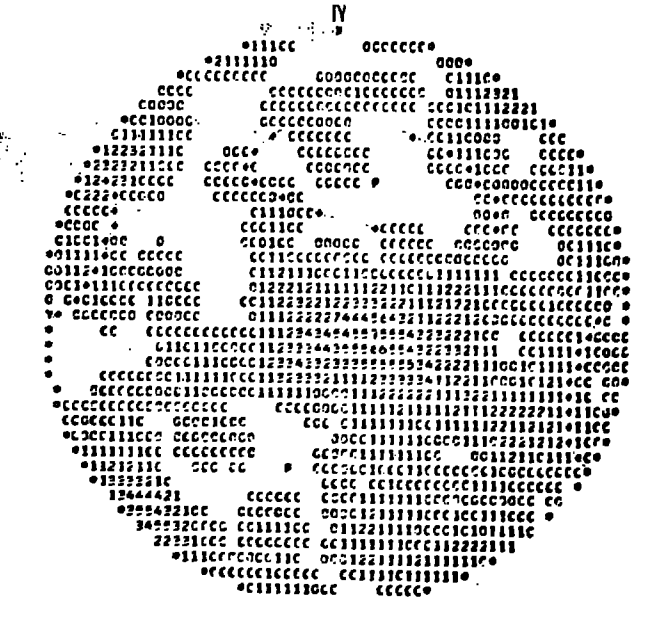

Projection 92 r = 1.06 a

W_d = 98.42 W_{dI} = 65.82

Equal area projections of a section of the London Clay discontinuity fabric at Green Park Station.

The elements are inclined at -40 degrees , 2nd quadrant, (C_{rd}= 5 kN/m^2, ϕ_{rd}= 13.5°).

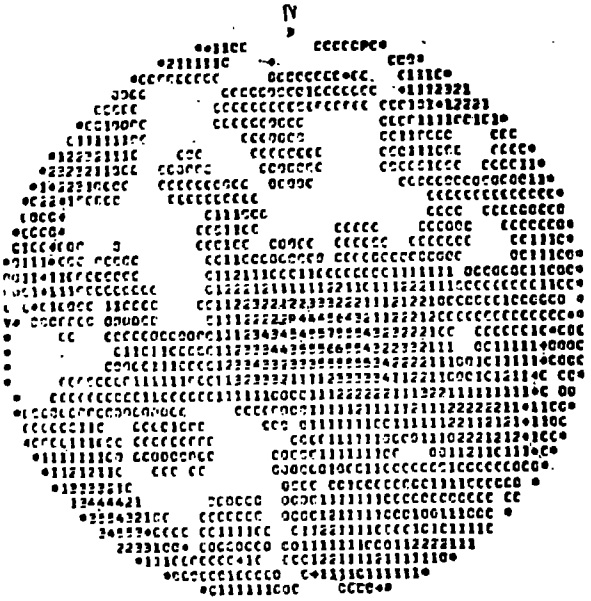

Projection 93, r = a

W_d = 61.22 W_{dI} = 84.19

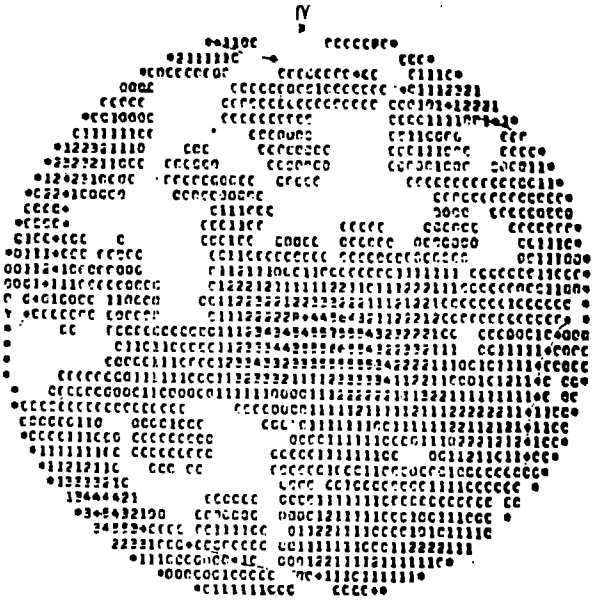

Projection 94, r = 1.02 a

W_d = 56.20 W_{dI} = 77.75

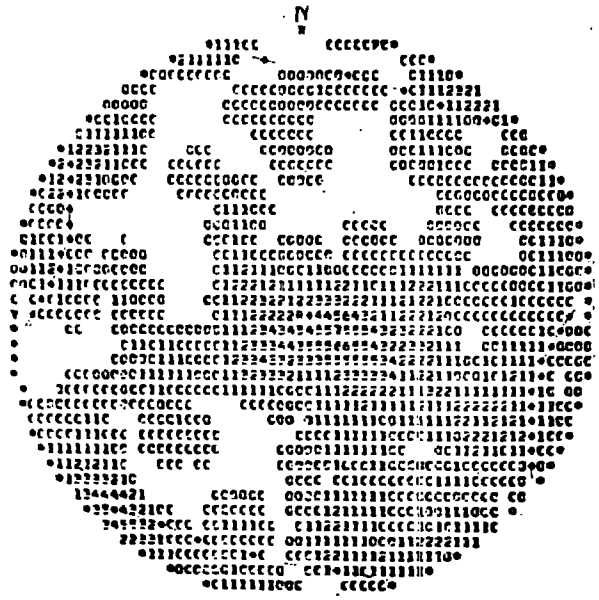

Projection 95, r = 1.04 a

W_d = 51.58 W_{dI} = 71.77

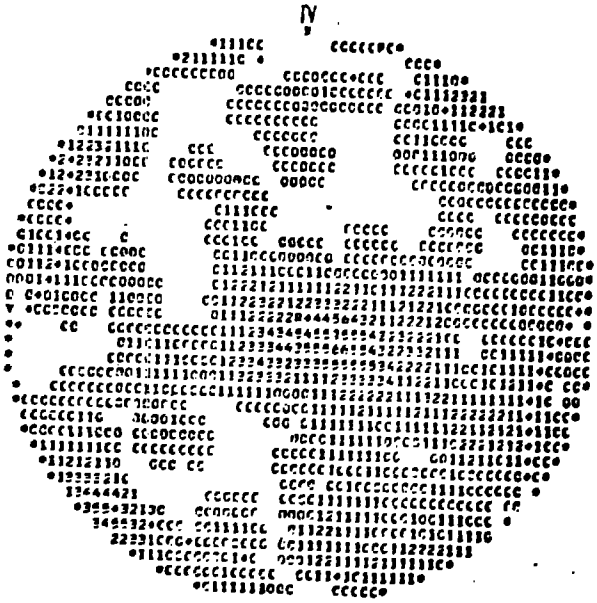

Projection 96, r = 1.06 a

W_d = 47.29 W_{dI} = 66.21

Equal area projections of a section of the London Clay discontinuity fabric at Green Park Station.

The elements are inclined at -90 degrees, 3rd Quadrant, (C_{Fd} = 5kN/m², $\%_{Fd}$ = 13.5).

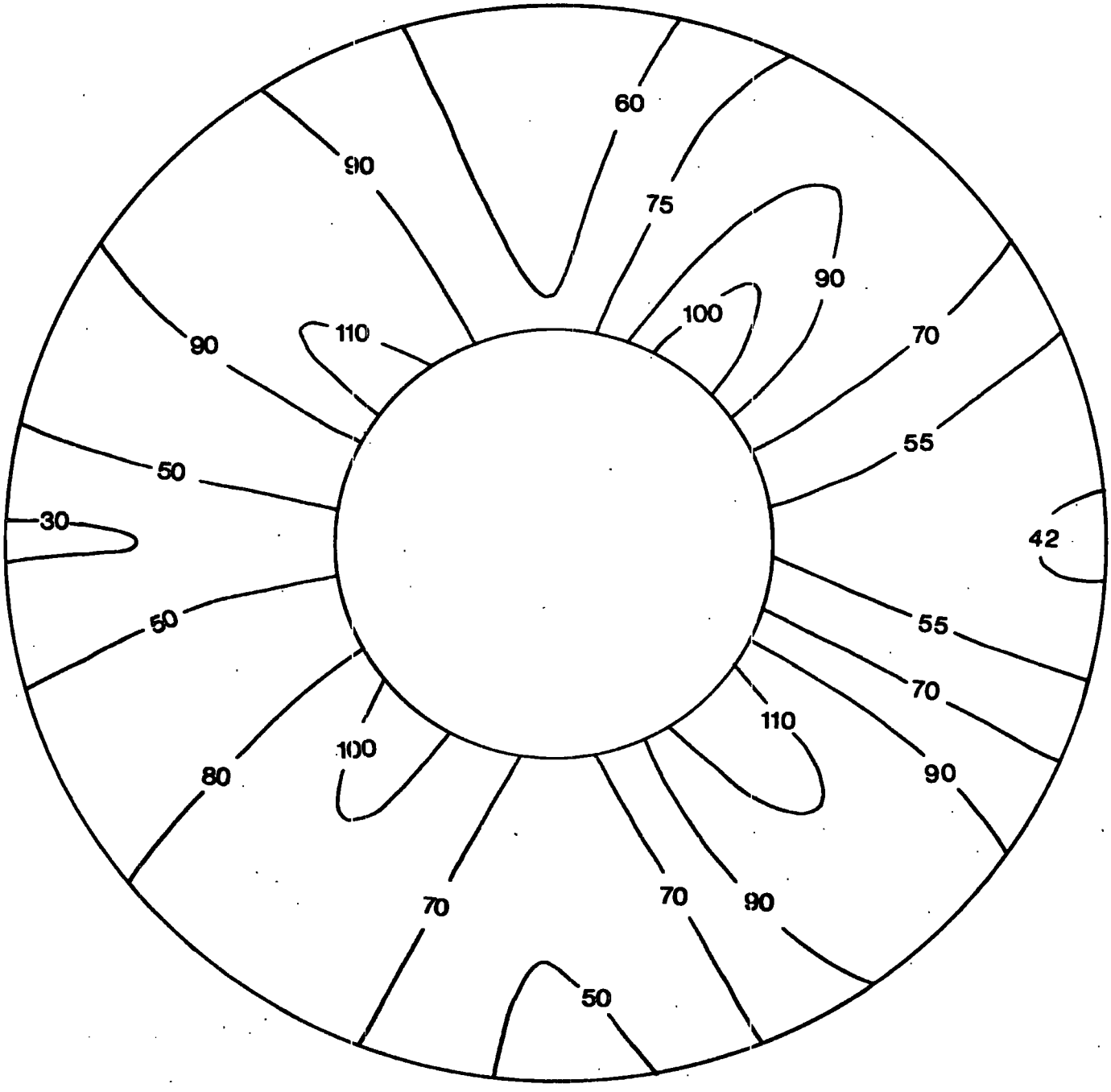

Fig. 4.e.17. Distribution of shear strain energy (W_d) around the tunnel, generated by a section of the non-random discontinuity fabric of London Clay at Green Park Station, which section represents the discontinuities existing in the immediate vicinity of the tunnel. The shear strength characteristics used are C_{rd}= 5kN/m^2 ϕ_{rd}= 13.5°. (Diameters of inner and outer circles are drawn to different scales, Fig. 4.e.I).

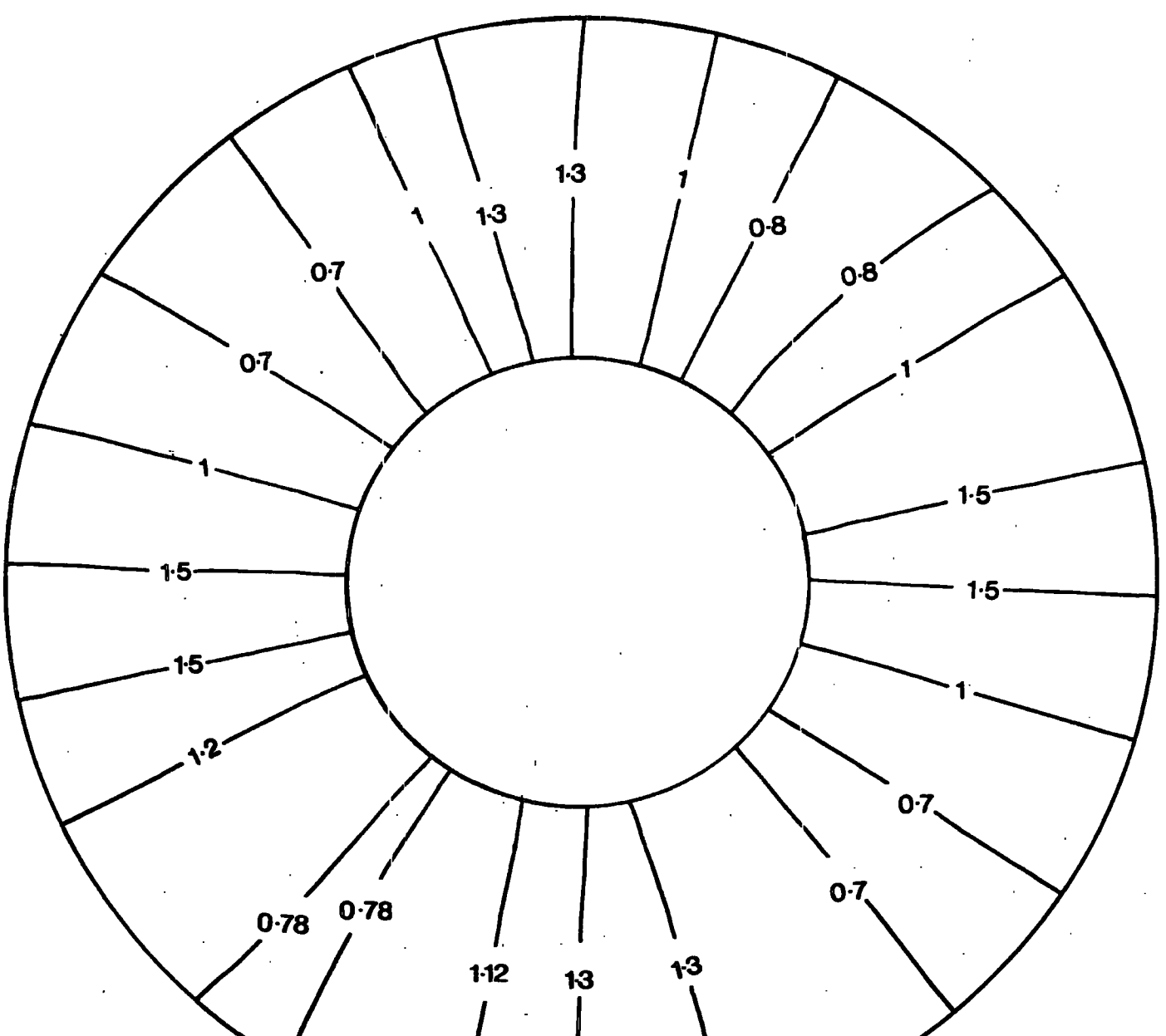

Fig. 4.e.18. Distribution of the "safety index" (W_{dI}/W_d) around the Fleet Line Tunnel.
The shear strength charactiristics used are C_{rd}= 5kN/m², ϕ_{rd}= 13.5°.
(Diameters of inner and outer circles are drawn to different scales , Fig. 4.e.I).

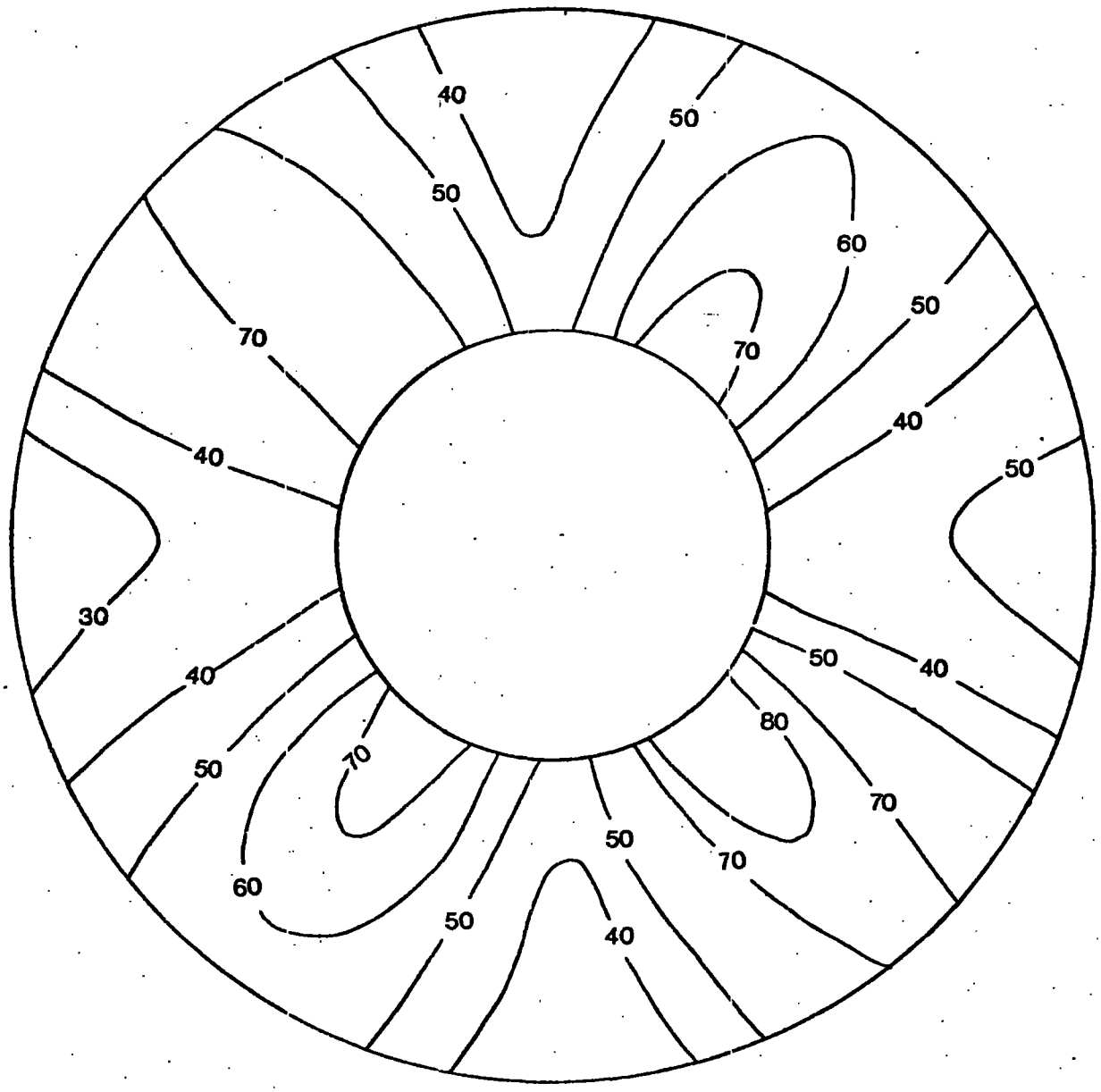

Fig. 4.e. 19. Distribution of shear strain energy (W_d) around the tunnel generted by a section of the non-random discontinuity fabric of London Clay at Green Park Station , which section represents the discontinuities existing in the immediate vicinity of the tunnel. The shear strength characteristics used are $\hat{C}_d = 7 kN/m^2$, $\hat{\phi}_d = 18.5°$. (Diameters of inner and outer circles are drawn to different scales, Fig. 4.e.I).

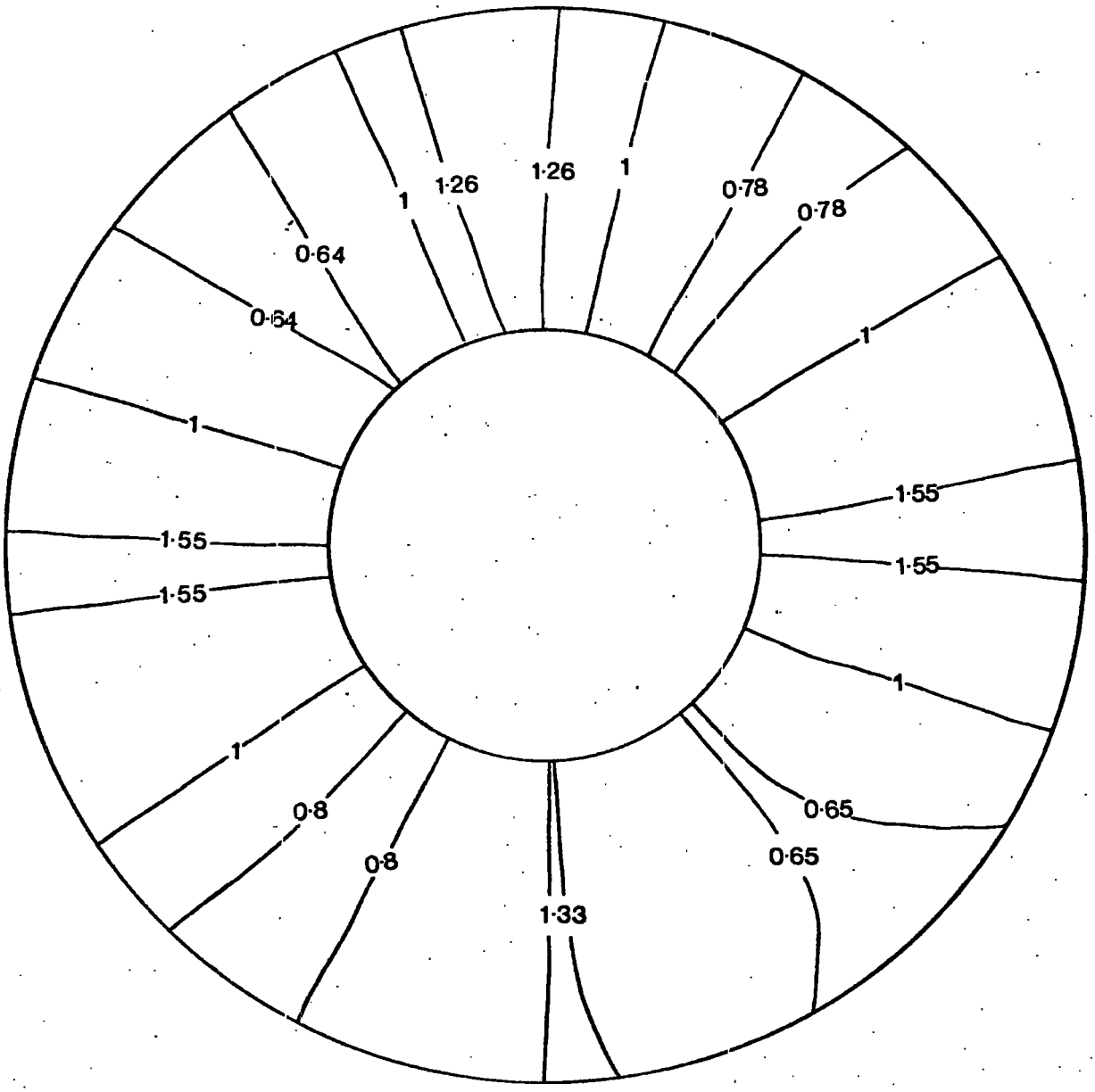

Fig. 4.e.20. Distribution of the safety index (W_{dI}/W_d) around the Fleet Line Tunnel.
The shear strength characteristics used are $\hat{C}_d = 7\ kN/m^2$, $\hat{\varphi}_d = 18.5°$.
(Diameters of inner and outer circles are drawn to different scales, Fig. 4.e.I).

4.f. Results

From all the Figures which represent the distribution of the shear strain energy generated by the discontinuity fabric of London Clay as tunnelled at Green Park Station (a non-random discontinuity fabric), it can be seen that a distinct concentration of shear strain energy takes place at directions ranging between 48° to 60° in each quadrant and at a distance equal to the radius of the tunnel (that is on the periphery of the tunnel).

In the case where the shear strength characteristics represent drained conditions, the direction of the concentration lies at an orientation of $(45° + \frac{\phi}{2})$ degrees to the horizontal in each quadrant.

This does not indicate that the presence of the discontinuity fabric has no effect on the direction of the concentration of W_d (and consequently on the potential failure). It simply means that, the character of the fabric is a not-unduly sensitive factor in the generation of the shear strain energy value, especially when it is assumed that the same discontinuity fabric exists in each element.

The zone around the tunnel with $W_d > 0$ tends to extend vertically, especially for lower values of W_d. This follows

from the original state of stress in the surrounding clay.

The slope of the relationship between W_d and r (distance from the centre of the tunnel) is very steep following the disturbance (generated by the excavation) of the in situ principal stresses.

For elements in the immediate vicinity of the tunnel surface (r=a, $\frac{\sigma_1}{\sigma_1}=1$, $\frac{\sigma_3}{\sigma_1}=0$, $\frac{\sigma_2}{\sigma_1}=\frac{\nu(\sigma_1+\sigma_3)}{\sigma_1}=\nu$) with an anisotropic discontinuity distribution, the differences in the values of shear strain energy W_d are generated by the different numbers of poles falling in approximately the same potentially unstable orientation zones (Projections I, 5, 9,... 77, 81, 85, 89 and 93; values of W_d). In the case of an equivalent isotropic distribution the same number of poles fall in the same potentially unstable orientation zones and consequently the generated shear strain energy W_{dI} is the same for all the elements in the immediate vicinity of the tunnel (Projections I, 5, 9, ... 77, 81, 85, 89 and 93; values of W_{dI}. Figure 4.e.3; radial symmetry for the highest values of W_{dI}).

The axial symmetry of the Figures, which represent the distribution of the shear strain energy, results from the special technique which was followed for the superimposition of the discontinuity fabric on each element.

The anisotropic fabric specifies the values of W_d in the potentially unstable space which have been delimited in terms of the principal stresses and shear strength characteristics.

On Figure 4.e.4, which shows the distribution of the "safety index", more and less stable areas are defined.

Obviously, the topography of the Figure results from the corresponding shape of the Figure 4.e.2. The line joining points having a value of zero (corresponding to zero W_d) expresses, in this case, the bounderies of the studied area. It is noticeable that the crown and the sides of the tunnel are more stable with respect to shear than are the areas disposed at 45° or hereabout to the horizontal.

The differences in Figures 4.e.4, 4.e.6, 4.e.8, 4.e.IO, 4.e.I2, 4.e.I4, 4.e.I6 and 4.e.I8, 4.e.20, arising from the different values of the shear strength characteristics, emphasize the effect of these characteristics on the stability of the tunnel.

4.g. Discussion

It was assumed that the state of stress around the tunnel does not exceed the limiting stress condition for elastic behaviour of the surrounding clay. However the calculated values of stresses, at the immediate vicinity of the tunnel, indicate that the clay may have been brought into the plastic state. Futhermore, the existing discontinuities may have influenced the re-distribution of the stresses during the excavation. Consequently, the above mentioned assumption concerning the elastic behaviour of the surrounding clay in the process of calculating the values of stress may

have been a cause of inaccuracy in the obtained results.

As already mentioned (in 4.d.), in every projection case the discontinuity fabric remains invariable as a function of position. This fact reduced the influence of the discontinuity fabric on the differentiation of values of the shear strain energy among the elements. More accurate results could have been obtained if the discontinuity fabric was a function of position. In such a case, however, the work load would have been immense and really unacceptable.

The effect of the presence of water on discontinuity shear stability has not been of particular concern in this application. Two effects can be observed:

i) If the pore water pressure is zero the presence of the water on the stability surface decreases the shear strength. It has been pointed out that an important difference exists between the shear strength parameters of a dry discontinuity and those of a wet discontinuity and, further, that the peak-to-residual reduction in the friction angle is more significant in the case of a wet discontinuity. Defining the residual shear strength parameters of the discontinuities during shear box tests, the above reduction has been estimated.

ii) If the pore water pressure is greater than zero the effective shear stress may be calculated (equation 4.d.I). The effect of pore water pressure on the distribution of stress around a small discontinuity (a crack) and consequently its influence on crack propagation, has been investigated by F. McCLINTOCK and J. WALSH (p. 8I). Generally, it is suggested that the failure mechanism

of higly fissured clays, in a large cross-section unlined excavation, appears to take place under drained rather than undrained conditions. If drainage does occur, then the effect of pore water pressure on the reduction of the normal stress is rather small.

Under the above assumptions, the use of shear strength parameters representative mainly of drained conditions can reasonably be justified. Its absolute validity is however, a function of clay exposure time and hence, ultimately, the rate at which the tunnel advances.

Generally, this application shows that the criterion may be used in the case of problems dealing with tunnel stability.

It may provide an estimate of the instability of each position around a tunnel in terms of the principal stresses σ_1, σ_2, σ_3, the shear strength characteristics of the material and the discontinuity fabric of the particular location.

A P P E N D I X

APPENDIX 2.c.I. Computer programme P_1

```
      DOUBLE PRECISION K,SIGR,SIGT,TAU,THETA,X,DEGREE,V,H,R,G,A,N,E,
     1                 SIG1,SIG2,SIG3,SIGV,SIGRV,SIGTV,TAUV
      V = 0.48D0
      E = 100000.0D0
      H = 29.57D0
      G = 20.09D0
      A = 2.035D0
    5 R = 2.035D0
      N = 1.0D0
      READ (5,100) DEGREE
  100 FORMAT (F5.1)
      IF (DEGREE.GE.999.0D0) STOP
      WRITE(6,120) DEGREE
  120 FORMAT('1',32X,'R E S U L T S   F O R  ',F6.1,'  D E G R E E S'
      WRITE(6,150)
  150 FORMAT(///,4X,'R',5X,'SIGR',6X,'SIGT',8X,'TAU',5X,'THETA',5X,
     1       'SIG1',6X,'SIG2',6X,'SIG3',6X,
     1       'SIGRV',5X,'SIGTV',6X,'TAUV',/)
      X = DEGREE/(180.0D0/3.14159265358979320D0)
      DO 10 I=1,21
      K = 2.55D0 - (H - R*DSIN(X)) * 0.03D0
      SIGV = G * (H -R*DSIN(X))
      SIGR = 0.5D0 * G * (H-R*DSIN(X)) * ((1.0D0+K)*(1.0D0-A**2/R**2)
     1      +(K - 1.0D0) * (1.0D0+3.0D0*A**4/R**4 - 4.0D0*A**2/R**2)
     1      * DCOS(2.0D0*X))
      SIGT = 0.5D0 * SIGV * ((1.0D0+K)*(1.0D0+A**2/R**2)
     1      -(K - 1.0D0)*(1.0D0+3.0D0*A**4/R**4) * DCOS(2.0D0*X))
      TAU  = -0.5D0 * G * (H-R*DSIN(X)) * (K -1.0D0)
     1      *(1.0D0- 3.0D0*A**4/R**4 + 2.0D0*A**2/R**2) * DSIN(2.0D0*X)
      THETA= 0.5D0 * DATAN(2.0D0*TAU/(SIGR-SIGT))
     1      *(180.0D0/3.14159265358979320D0)
      IF (DEGREE.GE.0.0D0) GOTO 170
      THETA = THETA + (90.0D0-DABS(DEGREE))
      GOTO 180
  170 THETA = THETA - (90.0D0-DEGREE)
  180 CONTINUE
      SIG1 = 0.5D0*(SIGR+SIGT)+0.5D0*DSQRT((SIGR-SIGT)**2+4.0D0*TAU**2)
      SIG3 = 0.5D0*(SIGR+SIGT)-0.5D0*DSQRT((SIGR-SIGT)**2+4.0D0*TAU**2)
      SIG2 = V * (SIG1+SIG3)
      SIGRV = SIGR/SIGV
      SIGTV = SIGT/SIGV
      TAUV = TAU/SIGV
      WRITE(6,200) N,SIGR,SIGT,TAU,THETA,SIG1,SIG2,SIG3,
     1             SIGRV,SIGTV,TAUV
  200 FORMAT(1H0,F4.1,'A',7(F10.3),3(F10.3))
      N = N + 0.2D0
      R = N * A
   10 CONTINUE
      GOTO 5
      END
```

Computer programme symbols

$V = \nu$, $H = h$, $G = \gamma$, $A = a$, $R = r$

SIGV $= \sigma_v$, SIGR $= \sigma_r$, SIGT $= \sigma_t$, TAU $= \tau_{r\theta}$, THETA $= \psi$,

SIG1 $= \sigma_1$, SIG2 $= \sigma_2$, SIG3 $= \sigma_3$, SIGTV $= \sigma_t / \sigma_v$, SIGRV $= \sigma_r / \sigma_v$

TAUV $= \tau_{r\theta} / \sigma_v$

APPENDIX 2.c.2.

Computer programme P_2

```
      DOUBLE PRECISION K,SIGR,SIGT,TAU,THETA,X,DEGREE,V,H,P,G,A,N,E,
     1                 SIG1,SIG2,SIG3,SIGV,SIGRV,SIGTV,TAUV
      DOUBLE PRECISION PLTVAL
      DIMENSION PX(100), PA(100),PB(100),PC(100),PD(100),PE(100)
      V = 0.48D0
      E = 100000.0D0
      H = 29.57D0
      G = 20.09D0
      A = 2.035D0
    5 R = 2.035D0
      N = 1.0D0
      READ (5,100) DEGREE
  100 FORMAT (05.0)
      IF (DEGREE.GE.998.0D0) STOP
      WRITE(6,120) DEGREE
  120 FORMAT('1',32X,'R E S U L T S    F O R  ',F6.1,'   D E G R E E S)
      WRITE(6,150)
  150 FORMAT(///,4X,'R',5X,'SIGR',6X,'SIGT',8X,'TAU',5X,'THETA',5X,
     1       'SIG1',6X,'SIG2',6X,'SIG3',6X,
     1       'SIGRV',5X,'SIGTV',6X,'TAUV',/)
      X = DEGREE/(180.0D0/3.14159265358979320D0)
      DO 10 I=1,21
      K = 2.55D0 - (H - R*DSIN(X)) * 0.03D0
      SIGV = G * (H -R*DSIN(X))
      SIGR = 0.5D0 * G * (H-R*DSIN(X)) * ((1.0D0+K)*(1.0D0-A**2/R**2)
     1      +(K - 1.0D0) * (1.0D0+3.0D0*A**4/R**4 - 4.0D0*A**2/R**2)
     1      * DCOS(2.0D0*X))
      SIGT = 0.5D0 * SIGV * ((1.0D0+K)*(1.0D0+A**2/R**2)
     1      -(K - 1.0D0)*(1.0D0+3.0D0*A**4/R**4) * DCOS(2.0D0*X))
      TAU  = -0.5D0 * G * (H-R*DSIN(X)) * (K -1.0D0)
     1      *(1.0D0- 3.0D0*A**4/R**4 + 2.0D0*A**2/R**2) * DSIN(2.0D0*X)
      THETA= 0.5D0 * DATAN(2.0D0*TAU/(SIGR-SIGT))
     1      *(180.0D0/3.14159265358979320)
      IF (DEGREE.GE.0.0D0) GOTO 170
      THETA = THETA + (90.0D0-DABS(DEGREE))
      GOTO 180
  170 THETA = THETA - (90.0D0-DEGREE)
  180 CONTINUE
      SIG1 = 0.5D0*(SIGR+SIGT)+0.5D0*DSQRT((SIGR-SIGT)**2+4.0D0*TAU**2)
      SIG3 = 0.5D0*(SIGR+SIGT)-0.5D0*DSQRT((SIGR-SIGT)**2+4.0D0*TAU**2)
      SIG2 = V * (SIG1+SIG3)
      SIGRV = SIGR/SIGV
      SIGTV = SIGT/SIGV
      TAUV = TAU/SIGV
      PX(I)=N
      PA(I)=U1
      PB(I)=U2
      PC(I)=SIGRV
      PD(I)=SIGTV
      PE(I)=TAUV
      WRITE(6,200) N,SIGR,SIGT,TAU,THETA,SIG1,SIG2,SIG3,
     1             SIGRV,SIGTV,TAUV
  200 FORMAT(1HO,F4.1,'A',7(F10.3),2(F10.5),3(F10.3))
      N = N + 0.2D0
      R = N * A
```

```
   10  CONTINUE
C------PLOT 1
      CALL PLTOFS( 1.0, 0.5, -1.0, 1.0, 2.0, 2.0 )
C-----DRAW Y AND X AXIS
      CALL PAXIS( 2.0, 2.0, 0, 0, -6.0, 90.0, -1.0, 0.5, 1.0 )
      YY=8.0
      PLTVAL=5.0
      DO 111 I = 1, 7
      CALL PNUMBR( 1.5, YY, 0.1, PLTVAL, 0.0, 5HF3.0* )
      PLTVAL=PLTVAL-1.0
      YY=YY-1.0
  111 CONTINUE
      CALL PAXIS(2.0, 3.0, 0, 0, -8.0, 0.0, 1.0, 2.0, 1.0 )
      PLTVAL=2.0
      YY=4.0
      DO 112 I=1, 4
      CALL PNUMBR( YY-0.3, 2.7, 0.1, PLTVAL, 0.0, 5HF3.0* )
      YY=YY+2.0
      PLTVAL=PLTVAL+1.0
  112 CONTINUE
C-----DRAW SIGV, SIGTV AND TAUV
      CALL PLINE( PX, PC, 21, 1, 1, 3, 1.0 )
      CALL PLINE( PX, PD, 21, 1, 1, 11, 1.0 )
      CALL PLINE( PX, PF, 21, 1, 1, 4, 1.0 )
C-----DRAW TITLE
      CALL PNUMBR( 3., 10.0, 0.2, DEGREE, 0.0,
     X29H'RESULTS FOR DEGREES =',F6.1* )
C-----END CURRENT PLOT
      CALL PLTEND
      GOTO 5
      END
FILE
```

LOAD CASE NO. 1

NODE	X-FORCE	Y FORCE	NODE	X-FORCE	Y-FORCE	NODE	X-FORCE	Y-FORCE
1	0.0	0.717E 03	2	0.0	0.717E 03	4	0.0	0.717E 03
8	0.0	0.717E 03	14	0.0	0.717E 03	22	0.0	0.717E 03
32	.995E 03	0.717E 03	42	.957E 03	0.0	55	.935E 03	0.0
68	.917E 03	0.0	81	.905E 03	0.0	93	.880E 03	0.0
105	.851E 03	0.0	116	.784E 03	-.390E 03	127	0.0	-.390E 03
137	0.0	-.390E 03	147	0.0	-.390E 03	156	0.0	-.390E 03
166	0.0	-.390E 03						

••• OUTPUT OF STRESSES AND DISPLACEMENTS •••

NODE	X CO-ORD	Y CO-ORD	LD. NO.	DISPLACEMENTS X	Y	RESULTANT	SIGMA-X	SIGMA-Y
1	0.0	0.0		*	*	:		
			1	0.0	0.0	0.0	-374.9192	-20?.4282
2	1.0760	0.0			*	:		
			1	0.0016	0.0	0.0016	-441.4270	-38?.4333
3	0.0	0.4070		*		:		
			1	0.0	0.0005	0.0005	-488.4375	-32?.6367
4	2.2220	0.0			*	:		
			1	-0.0007	0.0	0.0007	-344.4072	-48?.1421
5	1.9490	0.7510				:		
			1	-0.0018	-0.0010	0.0021	-367.1973	-44?.5044
6	0.9890	0.4940				:		
			1	-0.0015	0.0003	0.0015	-496.8162	-39?.2180
7	0.0	1.6280		*		:		
			1	0.0	0.0019	0.0019	-396.3281	-18?.7686
8	3.5290	0.0			*	:		
			1	0.0004	0.0	0.0004	-557.5701	-72?.1682
9	2.8490	1.1700				:		
			1	-0.0014	-0.0022	0.0026	-581.7371	-72?.6724
10	1.5310	1.8980				:		
			1	-0.0021	-0.0011	0.0024	-401.9558	-39?.6042
11	0.7770	1.6960				:		
			1	-0.0014	0.0017	0.0022	-509.9673	-31?.5256
12	0.0	2.8490		*		:		
			1	0.0	0.0039	0.0039	-520.3015	-34.0219
13	3.6630	1.7400				:		
			1	-0.0012	-0.0026	0.0029	-407.3950	-563.3477
14	5.1230	0.0			*	:		
			1	0.0016	0.0	0.0016	-463.8916	-558.6912
15	2.2380	2.2280				:		
			1	0.0026	-0.0026	0.0037	-650.4197	-742.3987
16	2.8780	2.6750				:		
			1	-0.0026	-0.0043	0.0051	-374.5171	-559.1045
17	1.1140	3.0450				:		
			1	-0.0037	0.0002	0.0037	-416.6326	-182.5137
18	0.5650	2.8980				:		
			1	-0.0024	0.0056	0.0061	-669.7534	-233.8778
19	0.0	3.6400		*		:		
			1	0.0	0.0071	0.0071	-626.2009	63.6042
20	5.9240	1.1350				:		
			1	0.0006	-0.0005	0.0008	-499.6355	-565.9565
21	4.3640	2.4420				:		
			1	-0.0008	-0.0034	0.0035	-531.0405	-670.6704
22	9.4900	0.0			*	:		
			1	0.0002	0.0	0.0002	-592.0063	-599.9534
23	1.6280	3.2850				:		
			1	-0.0056	-0.0007	0.0056	-680.4104	-607.2815
24	2.0930	3.6110				:		
			1	-0.0056	-0.0051	0.0075	-279.9719	-455.8816
25	3.4300	3.2170				:		
			1	0.0030	-0.0054	0.0061	-618.4753	-838.0117
26	0.9050	3.6190				:		
			1	-0.0040	0.0030	0.0050	-511.0603	-5.7887
27	0.4590	3.5000				:		
			1	-0.0025	0.0084	0.0087	-654.6514	-58.0201

329	28	0.0	3.7440	*		:		
330			1	0.0	0.0076	0.0076	-697.8076	95.6648
331	29	4.9350	3.2560			:		
332			1	-0.0020	-0.0031	0.0037	-363.4321	-473.7163
333	30	6.6970	2.2390			:		
334			1	-0.0001	-0.0009	0.0009	-435.0374	-493.9709
335	31	3.8770	3.8670			:		
336			1	-0.0041	-0.0059	0.0072	-302.6533	-495.3176
337	32	10.1750	0.0	*	*	:		
338			1	0.0	0.0	0.0	-495.4099	-515.1655
339	33	1.3220	3.8140			:		
340			1	-0.0072	0.0025	0.0077	-715.0117	-413.2795

341	34	1.7000	4.0780			:		
342			1	-0.0077	-0.0034	0.0084	-223.0782	-262.6145
343	35	2.4940	4.0120			:		
344			1	-0.0074	-0.0063	0.0097	-541.3184	-897.1460
345	36	2.8200	4.4770			:		
346			1	-0.0077	-0.0088	0.0117	-168.6976	-581.6914
347	37	0.8070	3.8870			:		
348			1	-0.0044	0.0050	0.0066	-576.5884	50.1636
349	38	0.4100	3.7800			:		
350			1	-0.0026	0.0099	0.0102	-743.6907	-32.9926
351	39	0.0	3.9480	*		:		
352			1	0.0	0.0089	0.0089	-943.7871	56.5616
353	40	5.3540	4.1560			:		
354			1	-0.0033	-0.0036	0.0049	-355.2935	-550.9907
355	41	7.2670	3.4610			:		
356			1	-0.0014	-0.0017	0.0022	-389.7263	-509.3501
357	42	10.1750	2.4020	*		:		
358			1	0.0	-0.0012	0.0012	-388.9346	-453.0906
359	43	4.2070	4.5740			:		
360			1	-0.0059	-0.0066	0.0089	-342.2915	-675.9570
361	44	1.1800	4.0610			:		
362			1	-0.0082	0.0047	0.0094	-581.3110	-209.2651
363	45	1.5340	4.2850			:		
364			1	-0.0092	0.0015	0.0093	-127.6499	-78.4973
365	46	2.0260	4.4050			:		
366			1	-0.0116	-0.0050	0.0126	-538.7017	-956.8936
367	47	2.2910	4.7830			:		
368			1	0.0114	-0.0100	0.0151	-41.5908	-711.4697
369	48	3.0600	4.9920			:		
370			1	-0.0111	-0.0099	0.0149	-281.5103	-923.3936
371	49	0.7380	4.0780			:		
372			1	0.0053	0.0064	0.0083	-513.9434	0.3082
373	50	0.3750	3.9810			:		
374			1	-0.0031	0.0112	0.0117	-979.9465	-9.5480
375	51	0.0	4.0700	*		:		
376			1	0.0	0.0098	0.0098	1270.7588	-55.1857
377	52	4.4090	5.3280			:		
378			1	0.0063	-0.0083	0.0104	-84.5929	-421.2463
379	53	5.6110	5.1160			:		
380			1	-0.0036	-0.0050	0.0062	-153.4674	-389.2532
381	54	7.6160	4.7620			:		
382			1	-0.0007	-0.0036	0.0036	-237.5267	-394.0386
383	55	10.1750	4.3110	*		:		
384			1	0.0	-0.0023	0.0023	-231.4653	-289.2761
385	56	3.2060	5.5400			:		
386			1	-0.0102	-0.0128	0.0164	-9.6083	-639.3247
387	57	1.0780	4.2370			:		
388			1	-0.0096	0.0062	0.0114	-227.0140	-35.2470
389	58	1.3860	4.4530			:		
390			1	-0.0109	0.0005	0.0109	51.4676	84.8469

391-	59	1.8090	4.5870					
392				1	-0.0140	-0.0034	0.0144	-297.6772	-643.8845
393	60	2.0450	4.9250					
394				1	0.0138	0.0094	0.0167	11.0795	-693.6428
395	61	2.4850	5.2000					
396				1	0.0155	-0.0118	0.0195	-136.0206	-1081.4844
397	62	2.4280	5.6770					
398				1	0.0148	-0.0162	0.0220	63.6117	-884.6460
399	63	0.6960	4.1930					
400				1	0.0074	0.0079	0.0102	-353.0730	92.0274
401	64	0.3530	4.1010					
402				1	-0.0043	0.0123	0.0130	1114.0833	9.9177
403	65	4.7770	6.1050					
404				1	-0.0087	0.0093	0.0128	92.8892	-469.8882
405	66	5.6980	6.1050					
406				1	-0.0065	-0.0069	0.0095	-183.4070	-456.4370
407	67	7.7330	6.1050					
408				1	-0.0031	-0.0057	0.0065	-237.3578	-440.3528
409	68	10.1750	6.1050		*			
410				1	0.0	-0.0033	0.0033	-205.5857	-313.4319
411	69	3.2560	6.1050					
412				1	0.0152	-0.0153	0.0216	-113.3292	-79.9746
413	70	1.0180	4.3430					
414				1	-0.0109	0.0068	0.0128	-145.1380	-78.0768
415	71	1.3080	4.5460					
416				1	-0.0121	0.0016	0.0122	1.7999	5.7474
417-	72	1.6520	4.7190					
418				1	-0.0155	-0.0014	0.0155	38.1674	-115.2627
419	73	1.8650	5.0270					
420				1	-0.0154	-0.0075	0.0171	-51.9637	-403.7927
421	74	2.2190	5.2990					
422				1	-0.0181	-0.0120	0.0217	-135.5299	-1261.2170
423	75	2.3250	5.6950					
424				1	-0.0156	0.0167	0.0229	88.5745	1091.4277
425	76	2.6450	6.1050					
426				1	-0.0189	-0.0181	0.0262	-62.8685	-993.8176
427	77	3.2060	6.6700					
428				1	-0.0080	-0.0181	0.0198	19.2407	-580.2004
429	78	4.4090	6.8820					
430				1	-0.0051	-0.0125	0.0135	-73.2255	-337.3364
431	79	5.6110	7.0940					
432				1	-0.0029	-0.0090	0.0094	-130.1663	-338.8264
433	80	7.6160	7.4480					
434				1	-0.0001	-0.0079	0.0079	-203.3771	-337.5820
435	81	10.1750	7.8990		*			
436				1	0.0	-0.0039	0.0039	-193.9334	-217.2839
437	82	2.6050	6.5640					
438				1	-0.0116	-0.0213	0.0243	85.5331	-85.2551
439-	83	1.5590	4.7970					
440				1	-0.0161	-0.0002	0.0161	-83.5427	-167.9614
441	84	1.7620	5.0880					
442				1	0.0160	0.0051	0.0168	105.4302	-168.4156
443	85	2.0270	5.3670					
444				1	-0.0203	-0.0109	0.0230	-113.7348	-1137.4773
445	86	2.1240	5.7300					
446				1	-0.0177	-0.0171	0.0246	-11.1392	-1404.8315
447	87	2.3610	6.1050					
448				1	-0.0212	-0.0200	0.0291	6.0727	1214.3994
449	88	2.3250	6.5150					
450				1	-0.0140	-0.0237	0.0275	116.2069	-1096.1826
451	89	3.0600	7.2180					
452				1	-0.0096	-0.0223	0.0243	-306.2170	-849.5911
453	90	4.2070	7.6360					
454				1	-0.0050	-0.0151	0.0160	-404.0945	-627.9595
455	91	5.3540	8.0540					
456				1	-0.0027	-0.0112	0.0115	-349.8342	-482.3384
457	92	7.2670	8.7490					

58				1	-0.0002	-0.0097	0.0097	-361.3774	-454.3640
59	93	10.1750	9.8080	*			:		
60				1	0.0	-0.0044	0.0044	-333.3201	-351.0691
61	94	2.4850	7.0100				:		
62				1	-0.0139	-0.0266	0.0300	-226.3839	-1048.4836
63	95	1.9120	5.4090				:		
64				1	-0.0213	-0.0088	0.0231	25.6023	-886.1221
65	96	2.0040	5.7520				:		
66				1	-0.0189	-0.0148	0.0240	26.4243	-1641.5615
67	97	2.1570	6.1050				:		
68				1	-0.0233	-0.0212	0.0315	-179.3380	2034.5200
69	98	2.1240	6.4800				:		
70				1	-0.0161	-0.0257	0.0303	7.6215	-1414.3452
71	99	2.2190	6.9110				:		
72				1	-0.0164	-0.0297	0.0340	-189.8256	-1235.8418
73	100	2.2910	7.4270				:		
74				1	-0.0080	-0.0299	0.0309	28.1902	-543.4602
75	101	2.8200	7.7330				:		
76				1	-0.0045	0.0249	0.0253	-47.6638	-393.3486
77	102	3.8770	8.3430				:		
78				1	-0.0013	0.0173	0.0173	-141.2715	251.5837
79	103	4.9350	8.9540				:		
80				1	-0.0004	0.0125	0.0125	-140.5776	-178.6981
81	104	6.6970	9.9710				:		
82				1	0.0008	0.0111	0.0112	-244.5219	-273.5459
83	105	10.1750	13.7210	*			:		
84				1	0.0	0.0046	0.0046	-212.9244	-197.7215
85	106	2.0440	7.2850				:		
86				1	-0.0102	-0.0340	0.0355	28.6717	-611.5930
87	107	2.0350	6.1050				:		
88				1	-0.0256	-0.0219	0.0337	-0.0246	2685.4141
89	108	2.0040	6.4580				:		
90				1	-0.0174	0.0294	0.0342	1.2054	-1648.6379
91	109	2.0270	6.8430				:		
92				1	-0.0187	0.0332	0.0382	-157.6559	1129.6204
93	110	1.8680	7.1830				:		
94				1	-0.0120	-0.0381	0.0400	75.6136	-388.7998
95	111	2.0260	7.8050				:		
96				1	-0.0092	-0.0387	0.0398	-563.0806	-948.1238
97	112	2.4940	8.1980				:		
98				1	-0.0054	-0.0316	0.0320	-466.0493	-825.3462
99	113	3.4300	8.9930				:		
100				1	-0.0016	-0.0227	0.0227	-615.7449	-814.7170
101	114	4.3640	9.7680				:		
102				1	0.0004	-0.0155	0.0155	-280.6528	-381.6721
103	115	5.9240	11.9790				:		
104				1	0.0013	-0.0129	0.0130	-165.7349	-206.7128
105	116	10.1750	16.2800	*			:		
106				1	0.0	-0.0046	0.0046	-351.0010	-330.1213
107	117	1.8090	7.6230				:		
108				1	-0.0112	-0.0437	0.0451	-383.6785	-664.5369
109	118	1.9120	6.8010				:		
110				1	-0.0199	-0.0368	0.0418	6.7348	-864.7002
111	119	1.7620	7.1220				:		
112				1	-0.0128	-0.0419	0.0438	115.7618	-173.6808
113	120	1.6520	7.4910				:		
114				1	-0.0127	-0.0476	0.0493	33.1549	-123.9921
115	121	1.4520	7.8350				:		
116				1	-0.0069	0.0507	0.0512	39.2141	30.0597
117	122	1.7000	8.1320				:		
118				1	-0.0050	0.0441	0.0444	-145.1282	-169.7189
119	123	2.0930	8.5990				:		
120				1	0.0034	0.0368	0.0370	-112.9341	-257.4719

521	124	2.8780	9.5350					
522			1	-0.0004	-0.0284	0.0284	-210.3479	-289.7734
523	125	3.6630	10.4700					
524			1	-0.0014	-0.0207	0.0207	-122.6600	-169.3602
525	126	4.9700	12.0290					
526			1	0.0016	-0.0153	0.0154	101.1954	145.5203
527	127	8.5400	16.2800					
528			1	0.0008	-0.0076	0.0077	-222.6319	-113.6971
529	128	1.3860	7.7570					
530			1	-0.0075	-0.0526	0.0531	59.6383	115.8196
531	129	1.5580	7.4130					
532			1	-0.0134	-0.0502	0.0519	-119.0410	-197.4641
533	130	1.3080	7.6630					
534			1	-0.0086	-0.0549	0.0555	-9.6517	28.0370
535	131	1.1800	8.1490					
536			1	-0.0062	-0.0608	0.0611	-515.4656	-247.0057
537	132	1.3220	8.3960					
538			1	-0.0052	-0.0565	0.0567	-594.7227	-367.2053
539	133	1.6280	8.9250					
540			1	0.0040	-0.0485	0.0487	-580.6021	-535.2739
541	134	2.2380	9.9820					
542			1	-0.0008	-0.0381	0.0381	-582.7056	-619.5725
543	135	2.7870	11.0750					
544			1	-0.0013	-0.0306	0.0306	-564.5247	-547.8755
545	136	3.8660	12.8050					
546			1	0.0027	-0.0217	0.0219	-316.3176	-368.7114
547	137	5.8750	16.2800					
548			1	0.0051	-0.0087	0.0100	-290.3425	-240.5893
549	138	1.0780	7.9730					
550			1	0.0072	-0.0641	0.0645	-190.9245	-13.5751
551	139	1.0170	7.8670					
552			1	-0.0082	-0.0659	0.0664	-167.3391	-82.5952
553	140	0.7380	8.1320					
554			1	-0.0032	-0.0704	0.0704	-419.9153	60.2420
555	141	0.8070	8.3230					
556			1	-0.0025	-0.0675	0.0676	-444.4775	105.8488
557	142	0.9050	8.5910					
558			1	-0.0021	-0.0637	0.0638	-346.9312	90.7495
559	143	1.1140	9.1650					
560			1	-0.0018	0.0569	0.0569	-280.2800	-51.7939
561	144	1.5310	10.3120					
562			1	0.0004	-0.0483	0.0483	-261.0969	-176.5152
563	145	1.9490	11.4590					
564			1	0.0000	-0.0398	0.0398	-249.9174	-162.6769
565	146	2.6450	13.3720					
566			1	0.0029	-0.0325	0.0326	-144.7419	-176.0162
567	147	3.7030	16.2800					
568			1	0.0043	-0.0258	0.0262	-140.5833	-217.8639
569	148	0.6960	8.0170					
570			1	-0.0048	-0.0719	0.0721	-306.0764	116.1982
571	149	0.3750	8.2290					
572			1	-0.0018	-0.0847	0.0847	-681.4287	-146.5580
573	150	0.4100	8.4300					
574			1	0.0014	-0.0827	0.0827	-497.1040	-95.2970
575	151	0.4590	8.7100					
576			1	-0.0012	-0.0801	0.0802	-471.9648	-172.2837
577	152	0.5650	9.3120					
578			1	-0.0009	-0.0752	0.0752	-538.9761	-346.1631
579	153	0.7770	10.5140					
580			1	0.0007	-0.0666	0.0666	-331.0803	-354.5984

```
154     0.9890     11.7160                                     :
                         1    0.0010    -0.0607    0.0607   -375.1692   -429.1638
155     1.3430     13.7210                                     :
                         1    0.0035    -0.0511    0.0512   -270.5254   -422.0552
156     1.7940     16.2800                                     :
                         1    0.0031    -0.0422    0.0423   -127.2871   -293.6084
157     0.3530      8.1090                                     :
                         1   -0.0026    -0.0862    0.0862   -711.4092     12.7617
158     0.0         8.1400    *                                :
                         1    0.0       -0.0980    0.0980   -763.3250    -60.5513
159     0.0         8.2620    *                                :
                         1    0.0       -0.0974    0.0974   -576.2297    -27.6359
160     0.0         8.4660    *                                :
                         1    0.0       -0.0968    0.0968   -421.6418    -2[illegible].4052
161     0.0         8.7500    *                                :
                         1    0.0       -0.0961    0.0961   -362.4248    -62.1645
162     0.0         9.3610    *                                :
                         1    0.0       -0.0952    0.0952   -312.2612    -17[illegible].2579
163     0.0        10.5820    *                                :
                         1    0.0       -0.0965    0.0965   -227.4295     38[illegible].1816
164     0.0        11.8030    *                                :
                         1    0.0       -0.0980    0.0980   -210.8896   -421.3367
165     0.0        13.8380    *                                :
                         1    0.0       -0.1038    0.1038   -182.4247   -538.1033
166     0.0        16.2800    *                                :
                         1    0.0       -0.1090    0.1090   -189.6343   -451.1089
ITERATIONS    CARDS    MAX STR.     MAX DSP.   MAX X-COORD
         0    1001    2685.4136     0.1090      10.1750
*  INDICATES PRESCRIBED DISPLACEMENT
END OF FILE


£L  G(LAST)
END OF FILE


£L  F(LAST)
   1.332             W £
END OF FILE


£SIG
```

APPENDIX 3.a.I

In the triaxial tests the normal and shear stress upon the fissures was calculated as follows.

It is assumed that the discontinuity is planar and inclined to the horizontal plane at an angle of $\theta°$. In the specimen, the discontinuity will be included in an ellipse (Fifure 3) having the equation

$$\frac{x^2}{b^2} + \frac{y^2}{b^2-c^2} = 1 \qquad \text{or} \qquad y = A\sqrt{b^2-x^2}$$

where

$b = DC = \frac{AB}{2} = \frac{a}{\cos\theta}$ (Figures I and 3)

a = radius of the specimen

$c = OC = a\tan\theta$ (Figure 3)

$A = \sqrt{\frac{b^2-c^2}{b^2}} = \cos\theta$

then the surface $S_{(DOB)}$ (Figure 3) is

$$S_{(DOB)} = \int_{x=0}^{x=b} A\sqrt{b^2 - x^2}\,dx =$$

$$= \frac{A}{2}\left[x\sqrt{b^2-x^2} + b^2 \sin^{-1}\frac{x}{|b|}\right]$$

and consequently

$$S_{ellipsis} = 4\frac{A}{2}\left[x\sqrt{b^2-x^2} + b^2 \sin^{-1}\frac{x}{|b|}\right]$$

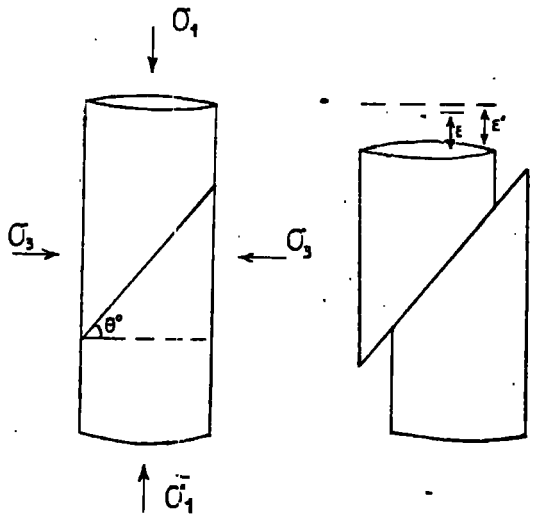

Figure I

Figure 2

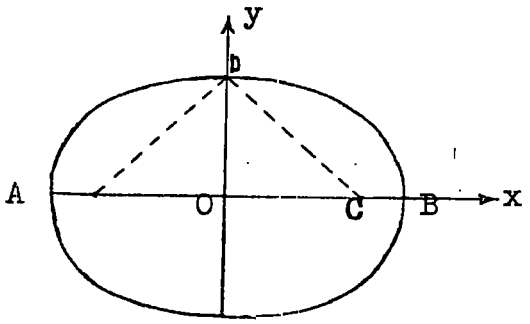

Figure 3

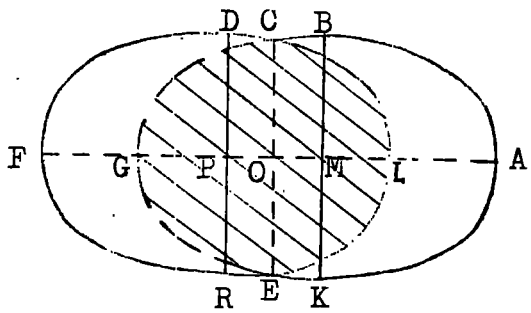

Figure 4

It is assumed that the specimen starts to slide on the discontinuity just after the yield point. Then the sliding is connected by the axial strain (after the yield) with the equation $AL = \frac{\xi}{\sin\theta}$ (Figure 4).

Now the new stressed surface $S_{(CGEL)}$ consists from $S_{(CGE)}$ and $S_{(ELC)}$ It is easy to prove that

$OM = OP = \frac{AL}{2}$ if

$AL \leqslant AM$. In that case

$$S_{(COL)} = \int_{x=OP}^{x=b} A\sqrt{b^2 - x^2}\,dx$$

and consequently

$$S_{(CGEL)} = 4\int_{x=OP}^{x=b} A\sqrt{b^2 - x^2}\,dx$$

Then knowing the stressed surface the stresses σ_1 and σ_3 are analysed and the normal and shear stress are obtained

$$\sigma_n = \sigma_1 \cos\theta + \sigma_3 \sin\theta$$

$$\tau = \sigma_1 \sin\theta - \sigma_3 \cos\theta \ .$$

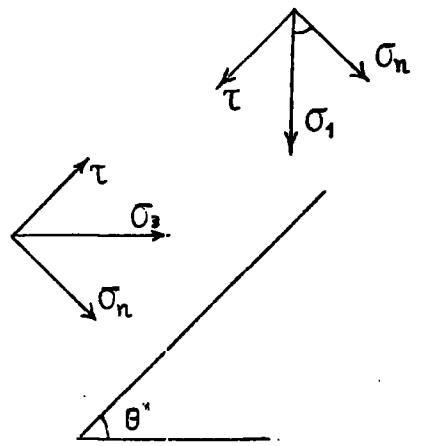

Figure 5

ACNOWLEDGEMENTS

This study was undertaken by the author in the Engineering Geology Laboratories of Durham University in fulfilment of requirements for the degree of Master of Science by research.

The author would like to express his gratitude to Dr. P. B. ATTEWELL for his supervision during the study.

Gratitude is also extended to my colleagues Messrs. A. COBB and T. SMITH for their help in the laboratory tests, and to Dr. E. PASSARIS and Mr. R. LIM for their assistance in the computer programming aspects.

REFERENCES

AGARWAL K.B. (1967) The influence of size and orientation of sample on the undrained strength of London clay,
Ph.D.Thesis, Univ. of London.

AKROYD T.N. (1969) Laboratory testing in Soil Engineering, G. FOULIS, London.

ARGYRIS J.H. (1958) On the analysis of complex elastic structures, Appl.Mech.Rev., vol. II,pp.331-349.

ARGYRIS J.H. (1960) Second A.S.C.E. conference on electronic computation,
Pittsburg Pa.,Sept. 1960 (Special Publication).

ARGYRIS J.H. (1965) Matrix analysis of three-dimensional elastic media, small and large displacements,
Journal of A.I.A.A.,Vol.3, pp.45-51.

ATTEWELL P.B. and BODEN J.B. (1971) Development of stability ratios for tunnels driven in clay,
Tunnels and Tunnelling,Vol.3, No.3, pp.195-198.

ATTEWELL P.B. and WOODMAN J.P. (1971) Stability of disconti - nuous rock masses under polyaxial stress system.
13th Symposium on Rock Mechanics,
Univ.of Illinois, August 1971, pp.665-683.

ATTEWELL P.B, and SANFORD M.R. (1974) Intrinsic Shear Strength of a Brittle, Anisotropic rock,
Int. J.Rock Mech. Min. Sci. and Geomech. Abstr., Vol. 11, pp.423-451.

BALLA A. (1963) Rock pressure determined from shearing re- sistance,
Proc. Int. Conf.Soil M. and Found.Eng.,
Budapest 1963, pp.461-471.

BARLA G. (1970) The distribution of stress around a single underground opening in a layered medium under gravity loading,
Int. J.R.Mech.Min.Sci., Vol.9, pp.127-154.

BISHOP A., HENKEL P. (1962) The measurement of soil properties in the triaxial test,
2nd ed. London, Arnold, 1962.

BISHOP A.W., WEBB D.L, and LEWIN P.I. (1965) Undisturbed samples of London clay from the Ashford Common shaft: strength-effective stress relationship,
Geotechnique, Vol.15, pp 1-16.

BJERRUM L. (1967) Progressive failure in slopes of over-consolidated plastic clay and clay shales,
J.Soil Mech.Fdns Div. A.S.C.E., v.93, SM5, Part 1.

BLAKE W. (1966) Application of the finite element method of analysis in solving boundary value problems in rock mechanics,
Intern. J.Rock Mech. Min.Sci., vol.3, pp.169-180.

BRADY B.T.A. (1969) A statical theory of brittle fracture for rock materials:
i) Brittle failure under homogenous axisymmetric states of stress,
Int. J.Rock Mech.Min. Sci.,v.6, pp.21-42;
ii) Brittle failure under homogenous triaxial states of stress,
Int. J.Rock Mech. Min.Sci., v.6, pp.285-300.

BRAY J.W. (1966) A study of jointed and fractured Rock.
Part I: Fracture Patterns and their failure characteristics,

Rock Mech. and Eng. Geology, Vol.2, pp.117-136;
Part 2: Theory of Limiting Equilibrium,
Rock Mech. and Eng. Geology, Vol. 4, 1967,
pp. 197-216.

CALABRESI G. and MANFREDINI G. (1973) Shear strength characteristics of the jointed clay of S. Barbara, Geotechnique 23, No.2,pp.233-244.

CASTIGLIANO A. Cited in TIMOSHENKO S. and GOODIER J.pp. 254-58.

COOK N.G.W. (1966) The design of underground excavations,
Proc. of the Eighth Symp. on Rock Mechanics held at the Univ. of Minnessota, 1966,
pp.167-197.

COOLING L. and SKEMPTON A. (1940) A laboratory study of London Clay,
Journal of Institution of Civil Engineers,
vol.17, 1940-41, pp.251-276.

DENKHAUS H.G. (1965) Strength of Rock Material and rock systems,
Int. J.R.Mech. Min. Sci., Vol.2, pp.III-121.

FAIRHURST C. (1963) Rock Mechanics,
Proc. of the Fifth Symp. on Rock Mech. held at the Univ. of Minnesota, May 1962.

FAIRHURST C. and COOK N. (1966)
The Phenomenon of Rock Splitting Parallel to a Free Surface Under Compressive Stress,
Chamber of Mines Research Report No.105/65,
First Congress of the International Society of Rock Mechanics, Lisbon, 1966.

FAIRHURST C. (1967) Failure and breakage of Rock,
Proc. of the Eighth Symp. on Rock Mech. held at the Univ. of Minnesota, 1966.

FLINN D. (1958) On tests of significance of preferred orientation in three-dimensional fabric diagram, J. of Geol.,Vol.66, pp.526-539.

FOOKES P.G. and PARRISH D.G. (1969) Observations on small-scale structural discontinuities in the London Clay and their relationship to regional Geology, Q. Eng. G., Vol.1, 1969, pp.217-240.

GAY N.C. (1973) Fracture growth around openings in thick-walled cylinders of rock subjected to hydro-static compression, Int. J.Rock Mech.Min.Sci., Vol.10, pp.209-233.

GLOUGH R.W. (1960) The finite element method in plane stress analysis, Proc. 2nd.A.S.C.E. Conf. on Electronic Computation, Pittsburg Pa., Sept. 1960.

GOODMAN R.E. (1963) The resolution of stresses in rock using stereographic projection, Int. J.Rock Mech. Min.Sci., Vol.I, pp.93-103.

GOODMAN R.E. (1966) On the distribution of stresses around circular tunnels in non-homogeneous rocks, Proc. of the first congr. of the Int.Soc. of Rock Mech., Lisbon 1966, Vol. 2, pp.249-255.

GRIFFITH A.A. (1924) The theory of Rupture, Proc. of the first Int. Congress for Applied Mechanics, Delft. 1924, pp.55-63.

HOEK E. (1964) Rock fracture around mining excavations, Strata Control and Rock Mech.,1964, Columbia Univ., New York, pp.334-348.

HORVATH J. (1964) Formation of axially symmetrical limit loads around mine roadways of circular section,
Int. J.Rock Mech. Mining Sci., Vol.I, pp.505-518.

HOYAUX B. and LADANYI B. (1969) Gravitational stress field around a tunnel in soft ground,
Canadian Geotechnical Journal, Vol.7, 1970, pp.54-61.

INGLIS C.E. (1913) Stresses in a Plate due to the Presence of Cracks and Sharp Corners,
London: Institution of Naval Architects, 1913, pp.219-230.

JAEGER J.C. (1969) Elasticity, fracture and flow with Engineering and Geological applications,
Science Paperbacks, 1971.

JAEGER J.C. and COOK N.G. (1971) Fundamentals of Rock Mechanics,
Chapman and Hall, London.

KEY P.L. (1969) A relation between Crack Surface. Displacements and the Strain Energy release rate,
Int. J. of Fracture Mech., Vol.5, No.4, pp.287-296.

KIRSCH G. (1898) Theory of elasticity and the requirements for a theory of the strength of materials,
Z. Ver dent Ing, vol 42, N29, 1898.

LAJTAI E.Z. (1969) Strength of discontinuous rocks in direct shear,
Geotechnique 19, pp.218-233.

LAJTAI E.Z. (1969) Shear strength of weakness planes in rock,
Int. J.Rock Mech. Min.Sci.,Vol.6, pp.499-515.

LO K.Y. (1970) The operational strength of fissured clays,
Geotechnique, Vol.20, pp.57-73.

LOMBARDI G. (1968) The influence of rock characteristics on the stability of rock cavities,
Part 2, Tunnels and Tunneling, March 1970,
pp. 104-110.

McCLINTOCK F.A. and WALSH J.B.(1962) Friction on Griffith Cracks in Rock under Pressure,
Int. Congress on Applied Mech,
Berkeley 1962, pp.1015-1023.

MARSLAND A. (1971) The shear strength of stiff fissured clays,
B.R.S. Current paper CP June, pp.59-69.

MINDLIN R.D. (1940) Stress distribution around a tunnel,
Trans. A.C.S.E. 105, pp.1117-1153.

MOGI K. (1967) Effect of the Intermediate Principal Stress on Rock Failure,
J. of Geophysical Research, Vol.72, No.20,
pp.5117-5131.

MORGAN H.D. (1961) A contribution to the analysis of stress in a circular tunnel,
Geotechnique, Vol.II, 1961, pp.37-46.

OBERT L. and DUVALL W.I. (1967) Rock Mechanics and the Design of structures in Rock,
John Wiley and Sons, New York, 1967.

OROWAN E. (1949) Fracture and Strength of Solids,
Rep. Progr. Phys., vol.12, pp.185-235.

PASSARIS E.K.S. Personal Communication.

PETLEY (1966) The shear strength of soils at large strains, Ph.D. Thesis, Univ. of London.

POULOS H.G. and DAVIS E.H. Elastic solution for soil and Rock Mechanics, John Wiley and Sons.

PRICE N. (1966) Fault and joint developed in brittle and semi-brittle rock, Oxford, Pergamon, 1966.

PRIEST S. (1973) Data from Ph.D. thesis to be published, University of Durham, England.

PROTODYAKONOV M. (1958) (Cited in K.SZECHY, pp.213-217).

RABCEWICZ L. (1944) (Cited in K.SZECHY, p. 135).

RILEY W. (1964) Stresses at tunnel intersections, J. of the Engineering Mechanics Division, Vol. 90, pp.167-179.

SACK R.C. (1946) Extention of Griffith Theory of Rupture to three Dimensions, Proc. of Physics Soc.,1946, Vol.58, pp.729-736.

SCHMIED (1926) (Cited in K.Szechy, pp.167-169).

SINGH B. (1972) Continuum characterization of jointed rock masses, Int. J.Rock Mech. Min. Sci. and Geomech. Abstr., Vol.10, pp.311-349, 1973.

SKEMPTON A.W. and HENKEL D.J. (1957) Tests on London Clay from deep borings at Paddington, Victoria, and the South Bank, Proc. 4th.Int. Conf. Soil Mech., London, pp.100-106.

SKEMPTON A.(1961) Horizontal stresses in an over-consolidated Eocene clay,
Proc. 5th.Int.Conf. Soil Mech., vol.1, pp.351-57, Paris 1961.

SKEMPTON A.W. (1964) Long-term stability of clay slopes, Geotechnique, vol.14, pp.77-101.

SKEMPTON A.W. and PETLEY D.J. (1967) The strength along structural discontinuities in Stiff Clays, Proc. of Geotechn. Conf.,Oslo 1967,Vol.2, pp.29-46.

STINI J. (1950) Tunnelbaugeologie, Springer, Vienna.

SZECHY K. (1967) The art of tunnelling, Publ. Akademiai Kiado, Budapest 1967.

TCHALENKO J. (1967) The influence of shear and consolidation on the microscopic structure of some clays, Ph.D. Thesis, Univ.of London, 2 vol., 1967.

TERZAGHI (1946) Introduction to tunnel Geology, Commercial Shearing and Stamping Co., Youngstown, Ohio.

TERZAGHI K. and RICHARD F.E. (1952) Stresses in rock about cavities, Geotechnique, Vol.3, 1952-53, pp.57-90.

THEOCARIS P.S. and KORONEOS E. (1971) Stress distribution around a tunnel situated in a Layer under the action of gravity, Rock Mechanics, Vol.4, pp.139-154, 1972.

TIMOSHENKO S. and GOODIER J.N. (1951) Theory of elasticity, New York, McGRAW-HILL, London.

TROLLOPE D.H. and BROWN E.T. (1966) Effective stress criteria of failure of rock masses,
Proc. of the first congr. of Int.Soc.of Rock Mech., Lisbon, 1966, pp.515-519.

WALSH J. (1965) The effect of Cracks on the Uniaxial Elastic Compression of Rock,
J. of Geophysics Res.,Vol.70, 1965,pp.399-411.

WARDS W.H., SAMUELS S.G. and BATLER M.E. (1959) Further studies of the properties of London Clay,
Geotechnique, Vol.9, No.2, pp.33-58.

WIEBOLS G.A. and COOK N.G. (1968) An energy criterion for the strength of rock in polyaxial compression,
Int. J.Rock Mech. Min.Sci.,
Vol.5, pp.529-549.

WILLMANN (cited in K.SZECHY, pp.163-165).

ZIENKIEWICZ O.C. (1971) The Finite Element Method in Engineering Science,
McGRAW-HILL, London.